Arctic Report Card: *Update for 2011*

Tracking recent environmental changes

Home | About | Printouts | Previous Report Cards | NOAA Arctic Theme Page | Contacts

What's new in 2011?

Persistent warming has caused dramatic changes in the Arctic Ocean and the ecosystem it supports.

Ocean changes include reduced sea ice and freshening of the upper ocean, and impacts such as increased biological productivity at the base of the food chain and loss of habit for walrus and polar bears.

2011 by Chapter

Atmosphere

Higher temperatures in the Arctic and unusually lower temperatures in some low latitude regions are linked to global shifts in atmospheric wind patterns.

Marine Ecosystems

Since 1998, biological productivity at the base of the food chain has increased by 20%. Polar bears and walrus continue to lose habitat in Alaskan waters.

Hydrology & Terrestrial Cryosphere

Continued dramatic loss of ice sheet and glacier mass, reduced snow extent and duration, and increasing permafrost temperatures are linked to higher Arctic air temperatures.

Sea Ice & Ocean

A shift in the Arctic Ocean system since 2007 is indicated by the decline in ice age and summer extent, and the warmer, fresher upper ocean.

Terrestrial Ecosystems

Increased "greenness" of tundra vegetation in Eurasia and North America linked to increase in open water and warmer land temperatures in coastal regions.

Status

Significant change
Some change
Little or no change

December 2011

www.arctic.noaa.gov/reportcard

Citing the complete report:
Richter-Menge, J., M.O. Jeffries and J.E. Overland, Eds., 2011: Arctic Report Card 2011, http://www.arctic.noaa.gov/reportcard.

Citing an essay (example):
Derksen, C. and R. Brown, 2011: Snow [in Arctic Report Card 2011], http://www.arctic.noaa.gov/reportcard.

Authors and Affiliations

K. R. Arrigo, Department of Environmental Earth System Science, Stanford University, Stanford, CA, USA

I. Ashik, Arctic and Antarctic Research Institute, St. Petersburg, Russia

G. Bernhard, Biospherical Instruments, San Diego, CA

A. Beszczynska-Moeller, Alfred Wegener Institute, Bremerhaven, Germany

U. S. Bhatt, Geophysical Institute, University of Alaska Fairbanks, Fairbanks, AK, USA

B. A. Bluhm, School of Fisheries and Ocean Sciences, University of Alaska Fairbanks, Fairbanks, AK, USA

J. E. Box, Byrd Polar Research Center, The Ohio State University, Columbus, Ohio, USA

L. Brown, Interdisciplinary Centre on Climate Change and Department of Geography & Environmental Management University of Waterloo, Canada

R. Brown, Climate Research Division, Environment Canada

L. Bruhwiler, NOAA, Earth System Research Laboratory (ESRL), Global Monitoring Division, Boulder, CO

T. V. Callaghan, Royal Swedish Academy of Sciences, Abisko Naturvetenskapliga Station, Abisko, Sweden

J. Cappelen, Danish Meteorological Institute, Copenhagen, Denmark

E. Carmack, Institute of Ocean Sciences, Fisheries and Oceans Canada, Sidney, British Columbia, Canada

C. Chen, Byrd Polar Research Center, The Ohio State University, Columbus, Ohio, USA

H. H. Christiansen, Geology Department, University Centre in Svalbard, UNIS, Norway and Department of Geosciences, University of Oslo, Norway

J. C. Comiso, NASA Goddard Space Flight Center, Greenbelt, MD, USA

L. W. Cooper, Chesapeake Biological Laboratory, University of Maryland Center for Environmental Science, Solomons, Maryland, 20688 USA

D. Decker, Byrd Polar Research Center, The Ohio State University, Columbus, Ohio, USA

C. Derksen, Climate Research Division, Environment Canada

E. Dlugokencky, NOAA, Earth System Research Laboratory (ESRL), Global Monitoring Division, Boulder, CO

D. S. Drozdov, Earth Cryosphere Institute, Tyumen, Russia

C. Duguay, Interdisciplinary Centre on Climate Change and Department of Geography & Environmental Management University of Waterloo, Canada

J. Eert, Institute of Ocean Sciences, Fisheries and Oceans Canada, Sidney, British Columbia, Canada

H. E. Epstein, Department of Environmental Sciences, University of Virginia, Charlottesville, VA, USA
X. Fettweis, Department of Geography, University of Liège, Liège, Belgium

V. Fioletov, Environment Canada, Toronto, Ontario, Canada

B. C. Forbes, Arctic Centre, University of Lapland, Rovaniemi, Finland

K. E. Frey, Graduate School of Geography, Clark University, Worcester, MA, USA

I. Frolov, Arctic and Antarctic Research Institute, St. Petersburg, Russia

M. Gill, Environment Canada, Whitehorse, Canada

W. A. Gould, USDA Forest Service, International Institute of Tropical Forestry, San Juan, PR

R. R. Gradinger, School of Fisheries and Ocean Sciences, University of Alaska Fairbanks, Fairbanks, AK, USA

J. M. Grebmeier, Center for Environmental Science, University of Maryland, Solomons, MD, USA; Chesapeake Biological Laboratory, University of Maryland Center for Environmental Science, Solomons, Maryland, 20688 USA

J. -U. Grooß, Forschungszentrum Jülich, Jülich, Germany

A. Gunn, 368 Roland Road, Salt Spring Island, BC, Canada V8K 1V1

D. Hall, Department of Geology, Aarhus University, 8000 Aarhus, Denmark

E. Hanna, Department of Geography, University of Sheffield, UK

A. Heikkilä, Finnish Meteorological Institute, Helsinki, Finland

G. H. R. Henry, Geography Department, University of British Columbia, Vancouver, BC, Canada

R. M. Holmes, Woods Hole Research Center, Falmouth, MA

M. Itoh, Japan Agency for Marine-Earth Science and Technology, Tokyo, Japan

G. J. Jia, RCE-TEA, CAS, Chinese Academy of Sciences, Institute for Atmospheric Physics, Beijing, China

B. Johnsen, Norwegian Radiation Protection Authority, Østerås, Norway

B. V. Jørgensen, Danish Meteorological Institute, Copenhagen, Denmark

K. -K. Kang, Interdisciplinary Centre on Climate Change and Department of Geography & Environmental Management University of Waterloo, Canada

J. Key, Center for Satellite Applications and Research, NOAA/NESDIS, Madison, WI

H. Kheyrollah Pour, Interdisciplinary Centre on Climate Change and Department of Geography & Environmental Management University of Waterloo, Canada

A. L. Kholodov, Geophysical Institute, University of Alaska Fairbanks, Fairbanks, Alaska, USA

T. Kikuchi, Japan Agency for Marine-Earth Science and Technology, Tokyo, Japan

N. T. Knudsen, Department of Geology, Aarhus University, 8000 Aarhus, Denmark

S. V. Kokelj, Water Resources Division, Indian and Northern Affairs Canada, Yellowknife, NWT, Canada

T. Koskela, Finnish Meteorological Institute, Helsinki, Finland

R. Krishfield, Woods Hole Oceanographic Institution, Woods Hole, MA, USA

K. L. Laidre, Polar Science Center, Applied Physics Laboratory, University of Washington, Seattle WA USA

K. Lakkala, Finnish Meteorological Institute, Arctic Research Centre, Sodankylä, Finland

R. B. Lammers, Water Systems Analysis Group, Institute for the Study of Earth, Oceans, and Space, University of New Hampshire, Durham, NH 03824

T. C. Lantz, University of Victoria, British Columbia, Canada

W. H. Lipscomb, Los Alamos National Laboratory, Los Alamos, New Mexico 87545, USA

Y. Liu, Cooperative Institute of Meteorological Satellite Studies, University of Wisconsin, Madison, WI

C. Lund Myhre, Norwegian Institute for Air Research, Kjeller, Norway

G. Manney, Jet Propulsion Laboratory, California Institute of Technology, Pasadena, CA; New Mexico Institute of Mining and Technology, Socorro, NM

S. S. Marchenko, Geophysical Institute, University of Alaska Fairbanks, Fairbanks, Alaska, USA

J. Maslanik, Aerospace Engineering Sciences, University of Colorado, Boulder, CO 80309

J. T. Mathis, School of Fisheries and Ocean Science & Institute of Marine Science, University of Alaska Fairbanks, Fairbanks AK 99709

J. W. McClelland, University of Texas at Austin, Marine Science Institute, Port Aransas, TX

F. McLaughlin, Institute of Ocean Sciences, Fisheries and Oceans Canada, Sidney, British Columbia, Canada

W. Meier, National Snow and Ice Data Center, University of Colorado, Boulder, CO 80309

S. H. Mernild, Los Alamos National Laboratory, Los Alamos, New Mexico 87545, USA

S. E. Moore, NOAA/Fisheries, Office of Science & Technology, Seattle, Washington, 98115 USA

T. Mote, Department of Geography, University of Georgia, Athens, Georgia, USA

R. Müller, Forschungszentrum Jülich, Jülich, Germany

S. Nishino, Japan Agency for Marine-Earth Science and Technology, Tokyo, Japan

S. F. Oberbauer, Department of Biological Sciences, Florida International University, Miami, FL, USA

N. G. Oberman, MIRECO Mining Company, Syktyvkar, Russia

J. Overland, NOAA, Pacific Marine Environmental Laboratory, Seattle, WA
D. Perovich, ERDC - CRREL, 72 Lyme Road, Hanover, NH 03755; Thayer School of Engineering, Dartmouth College, Hanover NH 03755

B. J. Peterson, Marine Biological Laboratory, Woods Hole, MA

J. E. Pinzon, NASA Goddard Space Flight Center, Greenbelt, MD, USA

A. Proshutinsky, Woods Hole Oceanographic Institution, Woods Hole, MA, USA

B. Rabe, Institute of Ocean Sciences, Fisheries and Oceans Canada, Sidney, British Columbia, Canada

P. A. Raymond, Yale University, New Haven, CT

M. K. Raynolds, Institute of Arctic Biology, University of Alaska, Fairbanks, Fairbanks, AK, USA

M. Rex, Alfred Wegener Institute for Polar and Marine Research, Potsdam, Germany

E. Richardson, Science and Technology Branch, Environment Canada, Edmonton, Alberta, Canada

J. Richter-Menge, ERDC - CRREL, 72 Lyme Road, Hanover, NH 03755

V. E. Romanovsky, Geophysical Institute, University of Alaska Fairbanks, Fairbanks, Alaska, USA

D. Russell, Yukon College, Box 10038 Whitehorse YT, Canada Y1A 7A1

U. Schauer, Alfred Wegener Institute, Bremerhaven, Germany

M. Sharp, University of Alberta, Department of Earth and Atmospheric Sciences

G. R. Shaver, Ecosystem Center, Marine Biological Laboratory, Woods Hole, MA, USA

A. I. Shiklomanov, Water Systems Analysis Group, Institute for the Study of Earth, Oceans, and Space, University of New Hampshire, Durham, NH 03824

N. I. Shiklomanov, Department of Geography, George Washington University, Washington, DC, USA

K. Shimada, Alfred Wegener Institute, Bremerhaven, Germany

S. L. Smith, Geological Survey of Canada, Natural Resources Canada, Ottawa, Ontario, Canada

V. Sokolov, Arctic and Antarctic Research Institute, St. Petersburg, Russia

M. Steele, University of Washington, Seattle, WA, USA

N. Steiner, City College of New York, New York, NY, USA

S. E. Tank, Marine Biological Laboratory, Woods Hole, MA

M. Tedesco, City College of New York, New York, NY, USA

P. O. Thomas, US Marine Mammal Commission, Bethesda, MD USA

M. -L. Timmermans, Yale University, New Haven, CT, USA

J. Toole, Woods Hole Oceanographic Institution, Woods Hole, MA, USA

C. J. Tucker, NASA Goddard Space Flight Center, Greenbelt, MD, USA

C. E. Tweedie, Department of Biology, The University of Texas at El Paso, El Paso, Texas, USA

R. S. W. van de Wal, Institute for Marine and Atmospheric Research Utrecht, Utrecht University, Utrecht, The Netherlands

D. Vongraven, Norwegian Polar Institute, Fram Center, Tromso, Norway

J. Wahr, Cooperative Institute for Research in Environmental Sciences, University of Colorado Boulder, Boulder, Colorado, USA

D. A. Walker, Institute of Arctic Biology, University of Alaska, Fairbanks, Fairbanks, AK, USA

J. Walsh, International Arctic Research Center, Fairbanks, AK

M. Wang, Joint Institute for the Study of the Atmosphere and Ocean, University of Washington, Seattle, WA

P. J. Webber, Department of Plant Biology, Michigan State University, East Lansing, MI, USA

W. Williams, Institute of Ocean Sciences, Fisheries and Oceans Canada, Sidney, British Columbia, Canada

G. Wolken, Alaska Division of Geological & Geophysical Surveys

R. Woodgate, University of Washington, Seattle, WA, USA

M. Yamamoto-Kawai, Tokyo University of Marine Science and Technology, Tokyo, Japan

A. V. Zhulidov, South Russia Center for Preparation and Implementation of International Projects, Rostov-on-Don, Russia

S. Zimmermann, Institute of Ocean Sciences, Fisheries and Oceans Canada, Sidney, British Columbia, Canada

Executive Summary

November 23, 2011

Overview

The Arctic Report Card (www.arctic.noaa.gov/reportcard/) considers a wide range of environmental observations throughout the Arctic, and is updated annually. A major conclusion of the 2011 Report is that there are now a sufficient number of years of data to indicate a shift in the Arctic Ocean system since 2006. This shifted is characterized by the persistent decline in the thickness and summer extent of the sea ice cover, and a warmer, fresher upper ocean. As a result of increased open water area, biological productivity at the base of the marine food chain has increased and sea ice-dependent marine mammals continue to lose habitat. Increases in the greenness of tundra vegetation and permafrost temperatures are linked to warmer land temperatures in coastal regions, often adjacent to the areas of greatest sea ice retreat. A second key point in the 2011 Report is the repeated occurrence of 2010 Arctic winter wind patterns that mark a departure from the norm. These changes resulted in higher than normal temperatures in the Arctic, with record ice sheet mass loss, record low late spring snow cover in Eurasia, shorter lake ice duration, and unusually lower temperatures and snow storms in some low latitude regions. A potential indicator of recent atmospheric changes was record low ozone concentrations in March 2011. The 2011 Report Card shows that record-setting changes are occurring throughout the Arctic environmental system. Given the projection of continued global warming, it is very likely that major Arctic changes will continue in years to come, with increasing climatic, biological and social impacts.

Highlights for 2011

Sea ice and ocean observations over the past decade (2001-2011) suggest that the Arctic Ocean climate has reached a new state, with characteristics different than those observed previously. The new ocean climate has less sea ice (both thickness and summer extent) and, as a result, a warmer and fresher upper ocean. A clockwise ocean circulation regime has dominated the Arctic Ocean for at least 14 years (1997-2011), in contrast to the typical duration of a 5-8 year pattern of circulation shifts observed from 1948-1996. In the Bering Sea, aragonite undersaturation, i.e., ocean acidification, throughout the water column is causing seasonal calcium carbonate mineral suppression in some areas.

The September 2011 Arctic sea ice extent was the second lowest of the past 30 years. The five lowest September ice extents having occurred in the past five years, suggesting that a shift to a new sea ice state continues. The amount of older, thicker multiyear ice continues to decrease and both the Northern Sea Route and the Northwest Passage were ice-free in September.

Observations of the Arctic marine ecosystems provide a glimpse of what can only be described as profound and continuing changes. For example, primary production by phytoplankton in the Arctic Ocean increased ~20% between 1998 and 2009, mainly as a result of increasing open water extent and duration of the open water season. Changes in Arctic Ocean bottom communities include shifts in composition, geographical ranges, and biomass. While polar bears and walrus are experiencing negative impacts due to loss of habitat, whales now have greater access to the Northwest Passage and other northern feeding areas.

There is a direct link between increases and earlier peaks in Arctic tundra vegetation in many parts of the Arctic and increasing duration of the open water season due to decreasing summer sea ice extent. Vegetation productivity ranged from a 26% increase adjacent to the Beaufort Sea to a small decline in several areas. On the North Slope of Alaska, immediately south of the Beaufort Sea, new record high temperatures at 20 m depth were recorded at all permafrost observatories, where measurements began in the late 1970s. River discharge into the Arctic Ocean during 2010 was close to the long-term mean. Despite changes in tundra biomass, migratory barren-ground caribou appear to be within known ranges of natural variation.

In 2011 there was continued widespread warming in the Arctic, where deviations from historical air temperatures are amplified by a factor of two or more relative to lower latitudes. This phenomenon, called *Arctic Amplification*, is primarily a consequence of increased summer sea ice loss and northward transport of heat by the atmosphere and ocean. December 2010 to January 2011, and summer 2011, repeated the shift in wind patterns observed in December 2009 and February 2010 that resulted in relatively warm Arctic temperatures and severe cold weather in eastern North America, northern Europe and eastern Asia. Related to these shifts, the western slope of the Greenland ice sheet in particular experienced an increase in surface melting in summer 2011, amplified by albedo feedback and below-normal summer snowfall. Satellite gravity measurements show that the mass loss from the entire Greenland ice sheet during 2010-2011 was the largest annual loss in the satellite record of 2002-present. Lake ice cover duration, largely influenced by air temperature changes, was shorter by as much as 4-5 weeks in 2010-2011 compared to the 1997-2010 average in the eastern Canadian Arctic.

Acknowledgments

The Arctic Report Card reflects the work of an international team of 121 researchers in 14 countries and is based upon published and ongoing scientific research. Peer-review of the scientific content of the report card was facilitated by the Arctic Monitoring and Assessment (AMAP) Program. The Circumpolar Biodiversity Monitoring Program (CBMP), the cornerstone program of the Arctic Council's Conservation of Arctic Flora and Fauna (CAFF) Working Group, provides leadership on the biodiversity elements of the report card. The Report Card is lead by an inter-agency team from NOAA, the Cold Regions Research and Engineering Laboratory and the Office of Naval Research. Support for the Arctic Report Card is provided by the NOAA Climate Program Office through the Arctic Research Program.

Baselines and Trends

October 20, 2011

When scientists make statements about changes in climate they compare the magnitude of recent observations to conditions in the past. In the early 1970s, the the World Meteorological Organization (WMO) defined a climatological baseline as a 30-year "normal" period. It was believed that 30 years was a long enough period for the natural variability of the atmosphere to be averaged out, and thus whichever 30 year period was selected would not make a substantial difference.

This has not been the case for the Arctic. Large natural changes can occur over 30-year periods and there is a recent persistent upward trend in temperature and downward trend in sea ice extent (Fig. A2 in the *Temperature and Clouds* essay). Several plots in the Arctic Report Card are for the first time calculated from a new baseline period of 1981 through 2010. The magnitude of these temperature anomalies over the Arctic are about 1.0 °C less than those calculated from a baseline of data from 1971 through 2000.

Thus, readers of all sections of the Report Card should be aware of what baseline period or trend interval is used to assess the magnitude of recent changes. Figure A2 shows that even if recent years are included in the baseline, the year 2011 remains a warm year. More information can be found at http://www.ncdc.noaa.gov/oa/climate/normals/usnormals.html.

Atmosphere Summary

Section Coordinator: James E. Overland

NOAA Pacific Marine Environmental Laboratory, Seattle, WA, USA

November 10, 2011

In 2011, annual near-surface air temperatures over much of the ocean were approximately +1.5 °C greater than the 1981-2010 baseline period and land temperatures were also above their baseline values. This continued a decade-long warm-bias of the Arctic relative to mid-latitudes. The wintertime increase and the summertime decrease in cloudiness resulted in greater energy flux to the surface, potentially contributing to the near record low sea ice extent this year (see the essay on *Sea Ice*). Similar to winter 2009-2010, winter 2010-2011 and summer 2011 had increased linkages of wind patterns between the Arctic and the sub-Arctic. This pattern is responsible for sending cold air from the Arctic southward into eastern North America and northern Europe, and warm air from the sub-Arctic northward into western Greenland and east Asia. Possibly linked to recent changes in wind patterns, ozone concentrations in the Arctic stratosphere during March 2011 were the lowest ever recorded during the period beginning in 1979. While the global increase of human sources of greenhouse gases continues, there is no direct evidence that Arctic emissions of methane are changing.

Temperature and Clouds

J. Overland[1], U. Bhatt[2], J. Key[3], Y. Liu[4], J. Walsh[5], M. Wang[6]

[1]NOAA, Pacific Marine Environmental Laboratory, Seattle, WA
[2]Geophysical Institute, University of Alaska Fairbanks, Fairbanks, AK
[3]Center for Satellite Applications and Research, NOAA/NESDIS, Madison, WI
[4]Cooperative Institute of Meteorological Satellite Studies, University of Wisconsin, Madison, WI
[5]International Arctic Research Center, Fairbanks, AK
[6]Joint Institute for the Study of the Atmosphere and Ocean, University of Washington, Seattle, WA

November 10, 2011

Highlights

- Annual average temperature anomalies over the Arctic continued to be positive (warm) for October 2010 through September 2011 relative to temperatures in the 20th Century.
- Unusually strong north and south winds in fall and winter resulted in an Arctic-wide pattern of impacts, with warmer than normal temperatures of several °C over Baffin Bay/west Greenland and Bering Strait, and cooler temperatures over NW Canada and northern Europe. A new record low snow cover extent occurred over Eurasia due to persistent warm spring air temperatures. Summer also had vigorous wind patterns, with warmer than normal temperatures over NW Greenland and cooler temperatures in the Bering Sea.
- Slight decreases in cloud amount were observed in winter and slight increases were observed in summer.

The annual mean air temperature for 2010 over Arctic land areas mirrored 2009, with slightly cooler temperatures than in recent years, although the average temperature for the last decade remained the warmest in the record beginning in 1900 (Fig. A1). The lower values in 2009 and 2010 reflect relatively cold continents in winter. In 2009 there was a coincident circum-Arctic decrease in Arctic greenness (see Fig. TE2 in the essay on *Vegetation*). However, the Arctic in 2011 continues to exhibit area-wide positive temperature anomalies which, together with other indicators discussed in this Report Card, suggest systematic changes since the end of the 20th Century. The past six years have been the warmest such period in the instrumental record for the region poleward of 60°N (SWIPA, 2011). There were notable local manifestations of the recent warming. Beginning on June 30, Barrow in northwesternmost Alaska had a record run of 86 consecutive summer days with minimum temperatures at or above freezing. The previous record, set in 2009, was 68 days. For the sixth consecutive year, the first freeze of autumn in Fairbanks in central Alaska occurred more than two weeks later than its long-term average.

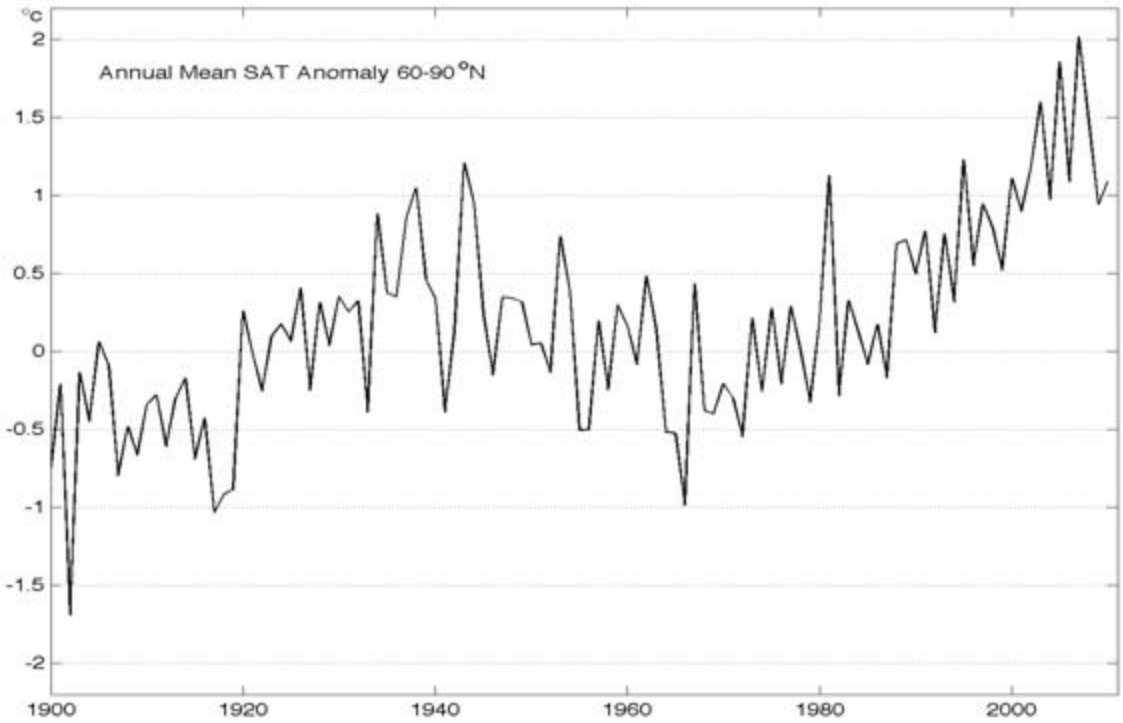

Fig. A1. Arctic-wide annual average surface air temperature anomalies relative to the 1961-90 mean, based on land stations north of 60°N. Data are from the CRUTEM 3v dataset, available online at www.cru.uea.ac.uk/cru/data/temperature/. Note this curve does not include marine observations.

It should be noted that this year this essay uses a new baseline interval for temperature anomaly departures using an average over the years 1981 through 2010. These include the recent warm years in the baseline average. In previous Report Cards the baseline average years were 1961 through 1990. The new baseline average is 0.77°C higher than the old baseline.

A key indicator of change is termed "Arctic Amplification". It notes that the Arctic is warming faster than more southerly latitudes and that temperature increases will be Arctic-wide. This is in contrast to more regional warming patterns typical at lower latitudes, which are associated with internal climate variability due to changes in wind patterns. This amplification effect is seen in data for 2011 (Fig. A2) and has been a prediction of climate models for 30 years (Manabe and Stouffer, 1980). Twelve-month average near-surface air temperature anomalies for October 2010 through September 2011 are above 1.5 °C for most of the Arctic Ocean area. While the cause of Arctic temperature amplification is mostly associated with current local loss of sea ice and terrestrial snow cover, Arctic amplification also results from the process of poleward movement of heat and moisture from mid-latitudes as part of the required overall global heat transport from equatorial regions to polar regions (Döscher et al., 2010, Serreze et al., 2008, Langen and Alexeev, 2007, Graversen and Wang, 2009).

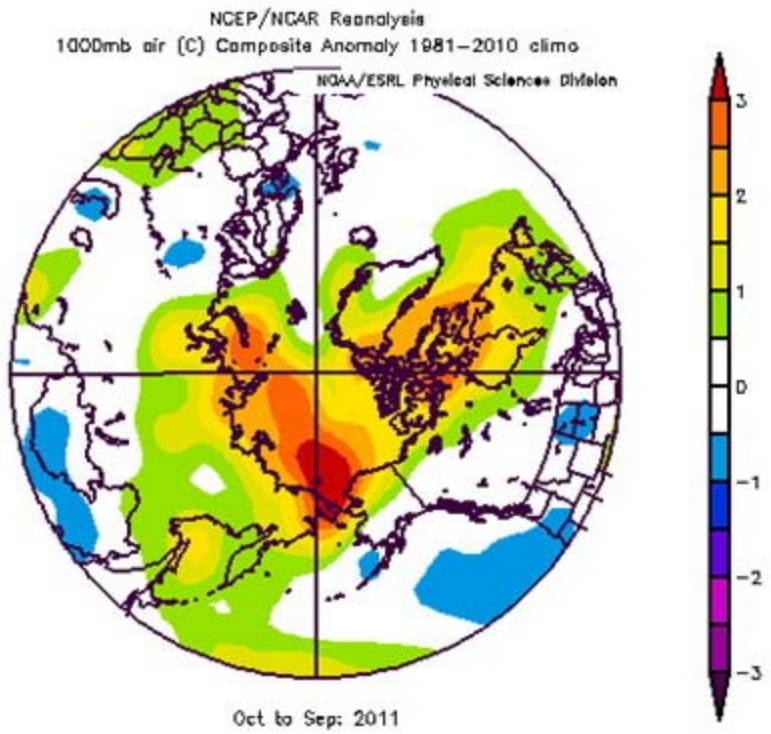

Fig A2. Annual average (October 2010 through September 2011) near-surface air temperature anomalies relative to the period 1981-2010. Image provided by the NOAA/ESRL Physical Sciences Division, Boulder, CO, from its Web site at http://www.esrl.noaa.gov/psd/.

Seasonal Air Temperatures

Seasonal anomaly distributions for near-surface temperatures in late 2010 and 2011 are shown in Fig. A3. Relative hot spots in autumn and winter are seen in regions of low sea ice concentrations for the previous summer (2010), lying north of far eastern Siberia and Alaska, in the vicinity of greater Baffin Bay and far northeastern Canada, and to some extent in the Kara Sea (see Fig. SIO4 in the essay on *Sea Ice*). A new record low June snow cover extent (since satellite observations began in 1966) occurred over Eurasia in 2011, due to persistent warm spring air temperature anomalies over almost the entire Eurasian sector of the Arctic (see the essay on *Snow*). In summer, unusual warm temperature anomalies again returned to northern Canada with cool temperature anomalies in northern Siberia and the Bering Sea (see Fig. HTC7 in the essay on *Glaciers and Ice Caps*).

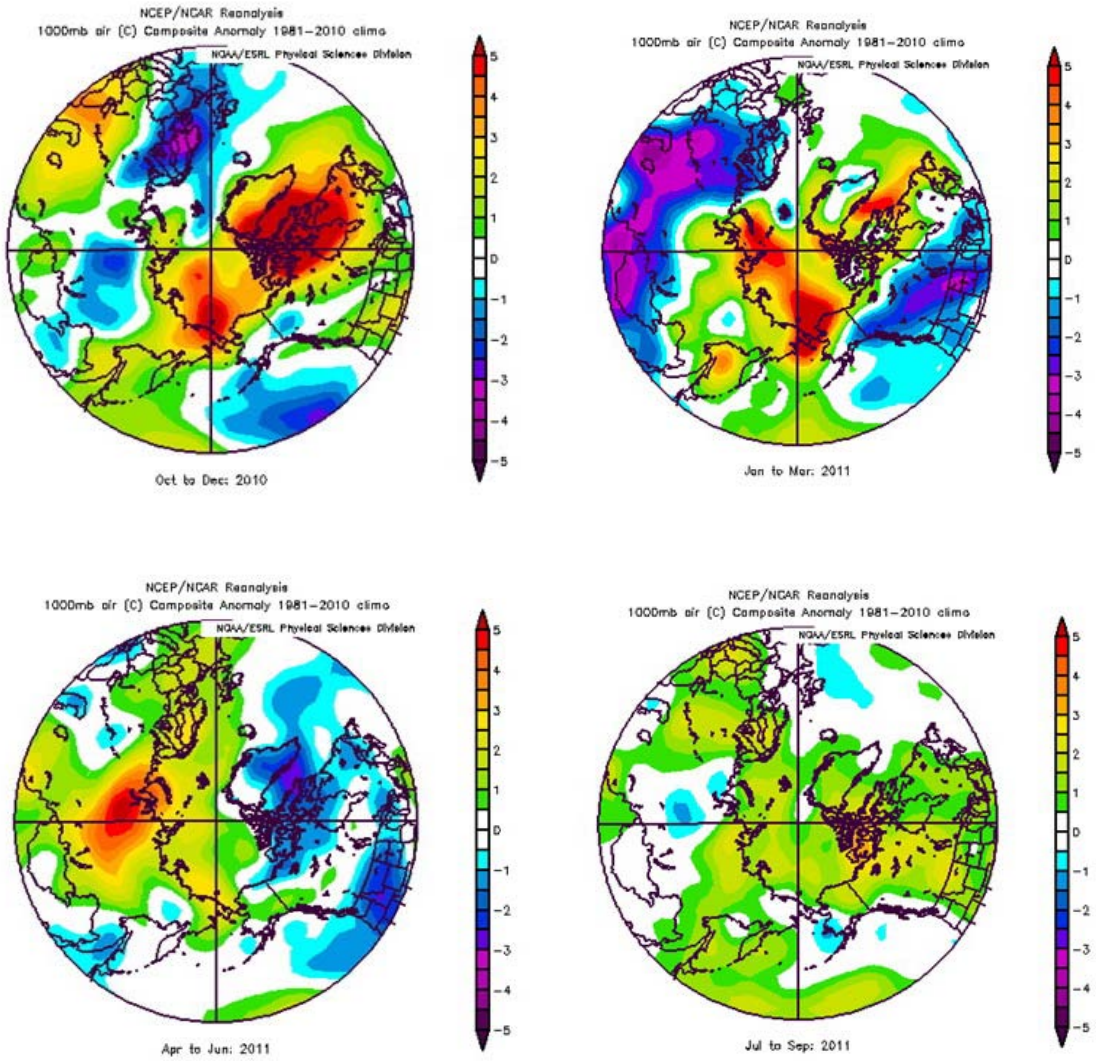

Fig. A3. Seasonal anomaly patterns for near surface air temperatures relative to the baseline period 1981-2010.

In late autumn 2010 and early winter 2011 there was a continuation of the "warm Arctic-cold Continent" climate pattern that first appeared in winter 2009-2010, when an increased linkage between Arctic climate and mid-latitude severe weather occurred. This was due to changing wind patterns, which resulted in both warmer and colder regions in the sub-Arctic. Figure A4a illustrates normal early-winter atmospheric winds. Meteorologists investigate wind fields by examining the heights of constant pressure surfaces; winds tend to blow counter-clockwise around the centers of low heights (purple), parallel to the height contours. In Fig. A4a, for example, climatological average Arctic winds in December tend to blow from west to east, thus separating cold Arctic air masses from the regions further south. In December 2009 there was a reversal of this climate pattern, with higher heights over the Arctic that eliminated the normal west-to-east winds (see the 2010 Report Card). This allowed cold air from the Arctic to penetrate into Europe, eastern China and the north-eastern USA. December 2010 also exhibited extremes in both warm and cold temperatures, with record-setting snowfall across lower latitudes as a result of changing wind patterns, as shown in the geopotential height field

for that month (Fig. A4b). While the sub-Arctic temperature extremes in December 2010 tended to be similar to those in 2009, the height pattern is different. In December 2010, the normal polar height pattern separated into multiple centers (purple regions in Fig. A4b) and expanded southward over the sub-Arctic. Winds were from the south along west Greenland and in East Asia, and out of the north over eastern North America and northern Europe. What is of particular interest is that this pattern of Arctic/sub-Arctic linkage simultaneously occurs in all northern regions rather than occurring as discrete local events. The cause for the increased exchange in the last two winters is a subject for further research into whether recent changes in the Arctic are involved, whether they are the result of extreme but random events, or a combination of these and other mechanisms.

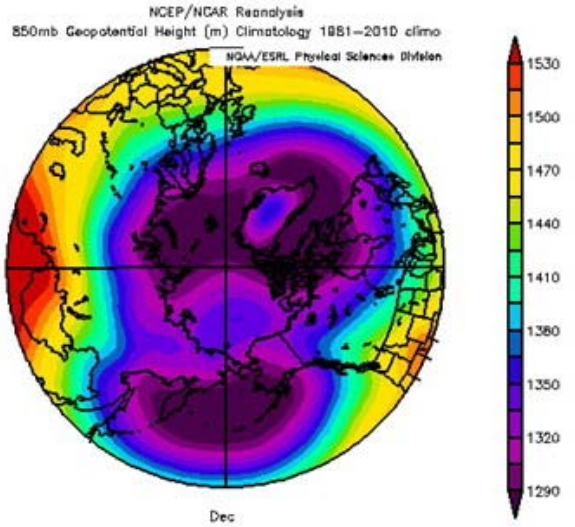

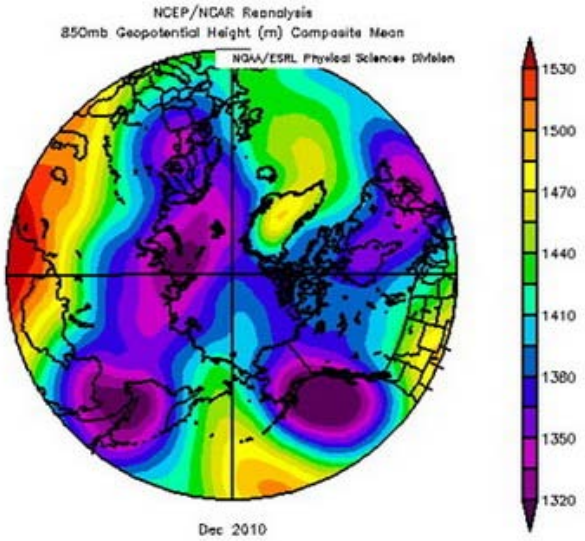

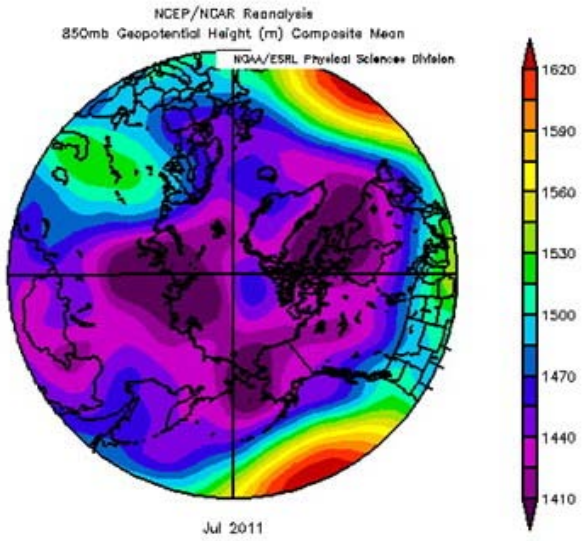

Fig. A4. (a, top) The climatological 850 mb geopotential height field for December, over the period 1981-2010. Low heights over the Arctic are representative of westerly winds centered over the Arctic. (b, centre) Observed 850 mb geopotential height field in December 2010. Note the southern locations of the multiple low height centers (purple). Air streamlines follow the height contours, bringing cold air into the eastern United States and northern Europe. (c, bottom) Observed 850 mb geopotential height field in July 2011. Data are from the NCEP-NCAR Reanalysis through the NOAA /ESRL/PSD on-line tool.

A further unusual event was the change in the wind pattern for summer 2011 (Fig. A4c for July). Unlike summer climatology, which has generally weak winds confined to the Arctic, July 2011 had a southward location of multiple low height centers not unlike December 2010. This continued the unusual warming in west Greenland (see Fig. HTC7 in the essay on *Glaciers and Ice Caps* and Fig. HTC10 in the essay on the *Greenland Ice Sheet*), the warm temperatures in Barrow mentioned in the Introduction, the cold temperatures in western Siberia, and kept warm storms from entering the Bering Sea.

The climate of the Arctic represents a unique system of interacting changes in sea ice, upper ocean temperatures, the atmosphere (including clouds), land surfaces, and linkages to lower latitudes. Many Arctic changes mentioned in the Reportcard can be related to increases in near surface atmospheric temperatures. Arctic temperature changes in turn result from a combination of gradual global warming, warm anomalies in internal climate variability in individual years, and impacts from multiple feedbacks processes. Nearly unique to the poles, however, is that once multi-year sea ice and glacial mass is gone, it is difficult to return to return to previous conditions.

Cloud Cover

Cloud optical properties have an important role in climate change as well as being significant in their own right. Clouds reflect sunlight, but also trap longwave radiation near the surface. With the decrease in sea ice cover, there is now an increased moisture source in newly opened sea ice-free ocean areas of the Arctic (see Fig. SIO4 in the essay on *Sea Ice*). Thus, scientists expect new interactions and modified feedbacks between sea ice loss and clouds. In 2011, Arctic cloud cover was somewhat higher than the average of the last ten years (2002-2011) in

winter and lower than average in the summer, particularly over the western Arctic Ocean (Fig. A5). The magnitude and timing of the anomalies varied on the regional scale. On an annual average over the Arctic Ocean, however, cloud cover was not significantly different from recent years. The 2011 wintertime increase and summertime decrease in cloud amount resulted in greater downward energy flux and surface warming, potentially contributing to the near record low sea ice extent this year (see the essay on *Sea Ice*). This is in contrast to the general trend over the period 1982-2004, when a decrease in wintertime clouds and increase in springtime clouds over parts of the Arctic acted to dampen surface warming (Wang and Key, 2003,2005).

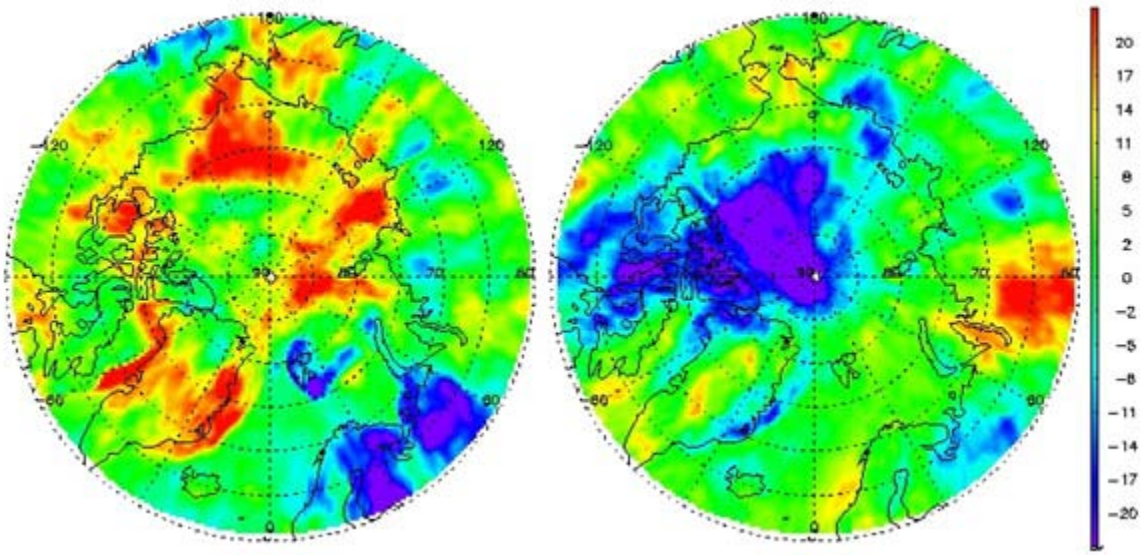

Fig. A5. Cloud cover anomalies (%) in February (left) and July (right) 2011 relative to the corresponding monthly means over the period 2002-2011 based on data from the Moderate Resolution Imaging Spectroradiometer (MODIS) on the Aqua satellite.

While clouds influence the surface energy budget (Liu et al., 2009) and thus sea ice growth and melt, they also respond to changes in the sea ice cover. This was particularly evident in September-October 2007 (not shown) at the time of the record minimum ice extent, and is also evident in 2011. Figure A6 shows the cloud cover anomaly for the first half of September 2011, with higher than normal cloud amounts in the poleward portions of the Beaufort, Chukchi, and Laptev seas. Sea ice concentration was lower than normal in these same areas (see the essay on *Sea Ice*). This is not coincidental, as a feedback analysis of data from 2000 to 2010 indicates that a 1% decrease in ice concentration leads to a 0.3-0.4% increase in cloud amount. There are, of course, other processes that influence cloud amount, in particular large-scale advection of heat and moisture and the frequency of synoptic scale systems (Liu et al., 2007).

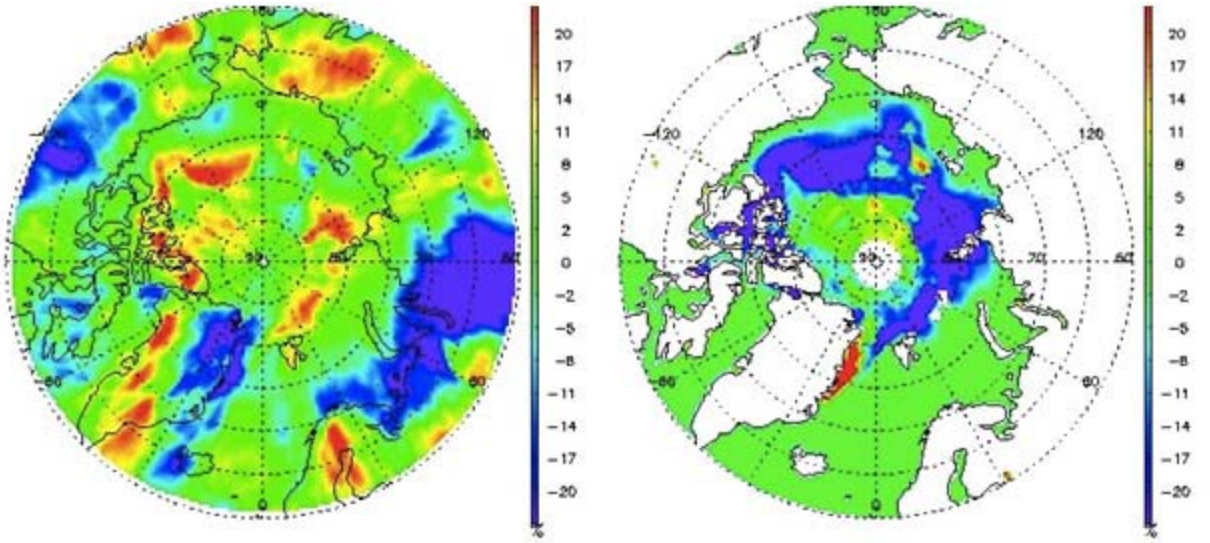

Fig. A6. Cloud cover anomalies (left) and sea ice anomalies (right) in September 2011 (1-17 September) relative to the 2002-2011 September mean. Cloud cover (%) is based on Aqua MODIS data. Sea ice concentration (%) is from the Special Sensor Microwave/Imager (SSM/I) using the NASA Team algorithm.

References

Döscher, R., K. Wyser, M. Meier, R. Qian, and G. Redler. 2009. Quantifying Arctic contributions to climate predictability in a regional coupled ocean-ice-atmosphere model. Climate Dynamics 34:1,157-1,176.

Gascard, J.-C., J. Festy, H. le Goff, M. Weber, B. Bruemmer, M. Offermann, M. Doble, P. Wadhams, R. Forsberg, S. Hanson, and others. 2008. Exploring Arctic transpolar drift during dramatic sea ice retreat. Eos, Transactions American Geophysical Union 89:21-22.

Graversen, R.G., and M. Wang. 2009. Polar amplification in a coupled climate model with locked albedo. Climate Dynamics 33:629-643.

Langen, P.L., and V.A. Alexeev. 2007. Polar amplification as a preferred response in an idealized aquaplanet GCM. Climate Dynamics 29:305-317.

Liu, Y., J. Key, and X. Wang, 2009. Influence of changes in sea ice concentration and cloud cover on recent Arctic surface temperature trends, Geophys. Research Lett., 36, L20710, doi:10.1029/2009GL040708.

Liu, Y., J. Key, J. Francis, and X. Wang, 2007. Possible causes of decreasing cloud cover in the Arctic winter, 1982-2000, Geophys. Res. Letters, 34, L14705, doi:10.1029/2007GL030042.

Manabe S., and R.J. Stouffer. 1980. Sensitivity of a global climate model to an increase of CO2 concentration in the atmosphere. Journal of Geophysical Research 85:5,529-5,554.

Przybylak, R. 2002. Variability of Air Temperature and Atmospheric Precipitation in the Arctic. Kluwer Academic Publishers, Dordrecht, 330 pp.

Quadrelli, R., and J.M. Wallace. 2004. A simplified linear framework for interpreting patterns of Northern Hemisphere wintertime climate variability. Journal of Climate 17:3,728-3,744.

Screen, J.A., and I. Simmonds. 2010. Increasing fall-winter energy loss from the Arctic Ocean and its role in Arctic temperature amplification. Geophysical Research Letters 37, L16707, doi:10.1029/2010GL044136.

Serreze, M.C., A.P. Barrett, J.C. Stroeve, D.N. Kindig, and M.M. Holland. 2008. The emergence of surface-based Arctic amplification. The Cryosphere Discussions 2:601-622.

Shupe, M. D., and J. M. Intrieri, 2004. Cloud radiative forcing of the Arctic surface: The influence of cloud properties, surface albedo, and solar zenith angle. J. Climate, 17, 616-628.

Snow, Water, Ice and Permafrost in the Arctic (SWIPA). 2011. AMAP, Oslo, Norway.

Wang, X. and J. Key, 2005. Arctic surface, cloud, and radiation properties based on the AVHRR Polar Pathfinder data set. Part II: Recent trends, J. Climate, 18(14), 2575-2593.

Wang, X. and J. Key, 2003. Recent trends in Arctic surface, cloud, and radiation properties from space, Science, 299(5613), 1725-1728.

Wood, K.R., and J.E. Overland. 2010. Early 20th century Arctic warming in retrospect. International Journal of Climatology doi:10.1002/joc.1973.

Carbon Dioxide (CO_2) and Methane (CH_4)

L. Bruhwiler and E. Dlugokencky

NOAA, Earth System Research Laboratory (ESRL),
Global Monitoring Division, Boulder, CO

November 10, 2011

Highlights

- Global increases in greenhouse gases from human sources continue.
- NOAA ESRL weekly air samples from 8 Arctic sites (north of 53°N) show that, as yet, there is no direct atmospheric evidence either that Arctic emissions of CH_4, or the net balance of C from CO_2, are changing.

In addition to solar radiation that makes its way to the Earth's surface, carbon dioxide (CO_2) and methane (CH_4) are the two largest contributors to radiative forcing by long-lived greenhouse gases, accounting for about 80% of the total (2.29 out of 2.81 W m^{-2} in 2010; see: http://www.esrl.noaa.gov/gmd/aggi/). In contrast to short-lived species like black carbon, whose Arctic emissions only affect Arctic climate, CO_2 and CH_4 emissions from anywhere on Earth will impact Arctic climate. Both these greenhouse gases have long atmospheric residence times; the residence time of CH_4 is about a decade due to photochemical loss (Forster et al., 2007), and for CO_2, whose loss from the atmosphere is controlled by many processes with different time scales, it is much longer (Tans, 2010). CO_2 released in the past and future decade will remain a global warming driver for most of the century.

The Arctic has great potential to influence climate through positive feedbacks. The topmost 3 m of ice-rich permafrost is estimated to hold an amount of carbon about equal to the carbon in known coal reserves, i.e., ~1000 PgC (where 1 Pg [petagram] = 10^{15} g) (Tarnocai et al., 2009). If that permafrost were to melt and become water-saturated soil, microbes could convert the carbon into CH_4. If the soils drain, the carbon will be respired as CO_2 into the atmosphere. Currently, however, peat formation at high northern latitudes takes up an estimated 0 to 0.8 PgC yr^{-1} (McGuire et al., 2009). A major uncertainty is whether continued Arctic warming and permafrost thawing could cause these high latitude ecosystems to become a net source of CO_2. See the essay on *Permafrost* for more information about permafrost warming and thawing.

The NOAA ESRL measures atmospheric CO_2 and CH_4 in weekly air samples from 8 Arctic sites (north of 53°N, Table A1). Figure A7 shows the inter-polar difference (IPD, defined as the difference in zonally-averaged CH_4 and CO_2 annual mean abundances for polar zones covering 53° to 90° in each hemisphere) for CO_2 and CH_4. The IPD is a potential indicator of changes in Arctic emissions of CO_2 and CH_4 since there are no significant sources of either gas in southern polar latitudes. The IPD of CO_2 increases with time because increasing CO_2 emissions from fossil fuel combustion at northern mid-latitudes are transported to the Arctic. Independent evidence from model analyses (not shown) suggests that Arctic biogenic emissions of CO_2 are not increasing (see: http://www.esrl.noaa.gov/gmd/ccgg/carbontracker/). Trends in mid-latitude anthropogenic emissions of CH_4 are likely small; therefore, trends in IPD mainly reflect changes in Arctic emissions. No trend in IPD is seen for CH_4, which is also supported by model analyses.

The economic collapse of the former Soviet Union from 1991 to 1992 shows the sensitivity of IPD to changing emissions of CH_4. During this period, high northern latitude CH_4 emissions (typically expressed in teragrams, Tg, where 1 Tg = 10^{12} g) are estimated to have decreased by ~10 Tg CH_4 yr^{-1}, and IPD decreased by ~10 ppb (parts per billion) (Dlugokencky et al., 2003), but has not recovered. As yet, there is no direct atmospheric evidence that either Arctic emissions of CH_4, or the net balance of C from CO_2, are changing.

Table A1. NOAA ESRL measures CO_2 and CH_4 in air samples taken at these eight sites. All are classified as Arctic, i.e, north of 53°N.

Site	**Latitude (°N)**	**Longitude (°)***
ALT: Alert, Nunavut, Canada	82.45	-62.51
BAL: Baltic Sea, Poland	55.35	17.22
BRW: Barrow, Alaska, USA	71.32	-156.61
CBA: Cold Bay, Alaska, USA	55.21	-162.72
ICE: Storhofdi, Vestmannaeyjar, Iceland	63.40	-20.29
STM: Ocean Station M, Norway	66.00	2.00
SUM: Summit, Greenland	72.58	-38.48
ZEP: Ny Ålesund, Svalbard, Norway	78.90	11.88

*Positive and negative values are east and west of the Greenwich meridian, respectively.

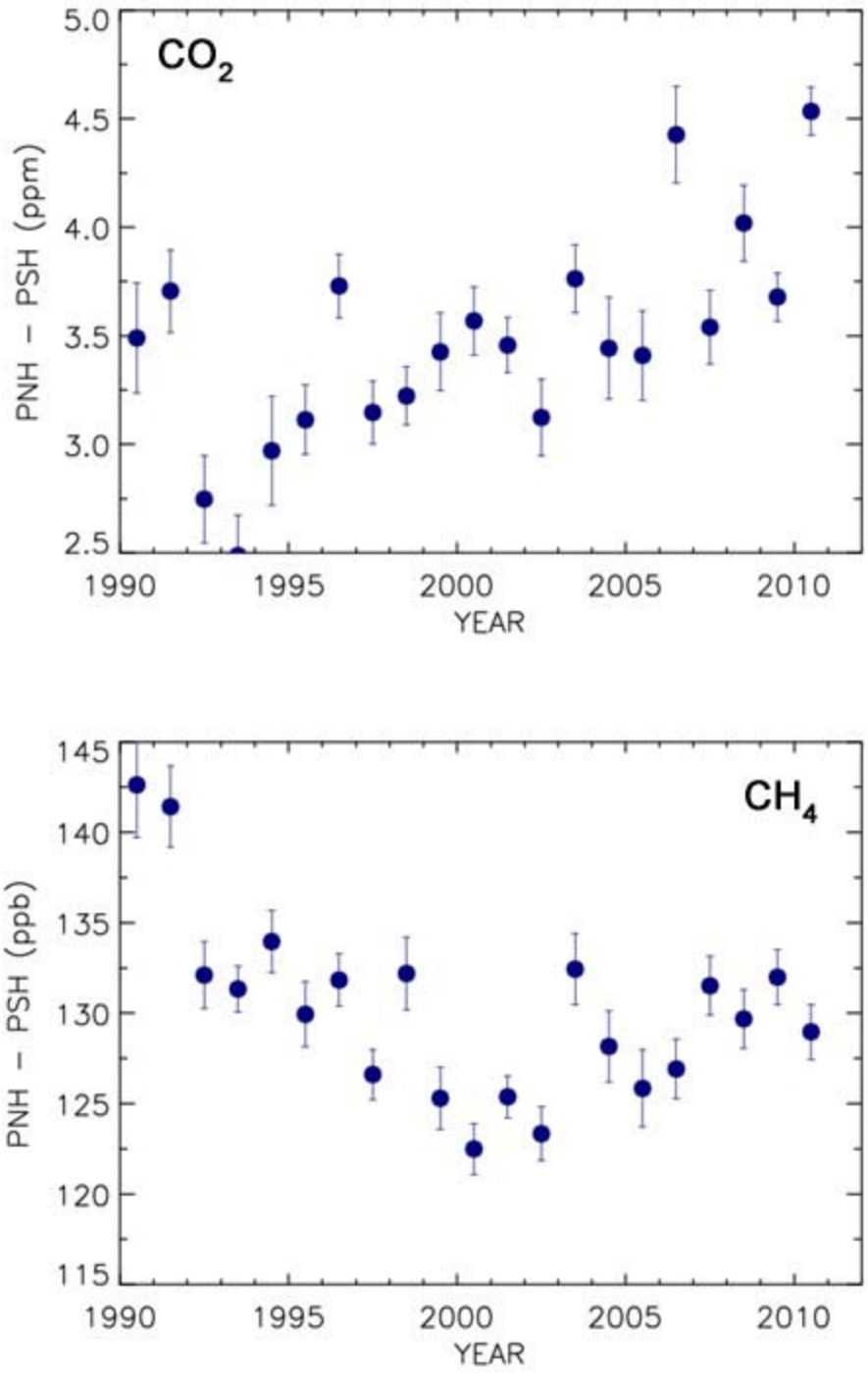

Fig. A7. Differences in annual mean abundances of CO_2 (top) and CH_4 (bottom) in parts per billion (ppb) for polar northern (53° to 90°N, PNH) and polar southern (53° to 90°S, PSH) regions determined from the NOAA ESRL global cooperative air sampling network. Data are available at http://www.esrl.noaa.gov/gmd/dv/iadv/.

References

Dlugokencky, E. J., S. Houweling, L. Bruhwiler, K. A. Masarie, P. M. Lang, J. B. Miller, and P. P. Tans (2003), Atmospheric methane levels off: Temporary pause or a new steady-state?, Geophys. Res. Lett., 30, 1992, doi:10.1029/2003GL018126.

Forster, P., V. Ramaswamy, P. Artaxo, T. Berntsen, R. Betts, D.W. Fahey, J. Haywood, J. Lean, D.C. Lowe, G. Myhre, J. Nganga, R. Prinn, G. Raga, M. Schulz and R. Van Dorland, 2007: Changes in Atmospheric Constituents and in Radiative Forcing. In: Climate Change 2007: The Physical Science Basis. Contribution of Working Group I to the Fourth Assessment Report of the Intergovernmental Panel on Climate Change [Solomon, S., D. Qin, M. Manning, Z. Chen, M. Marquis, K.B. Averyt, M.Tignor and H.L. Miller (eds.)]. Cambridge University Press, Cambridge, United Kingdom and New York, NY, USA.

McGuire, D. A., L. G. Anderson, T. R. Christensen, S. Dallimore, L. Guo, D. J. Hayes, M. Heimann, T. D. Lorenson, R. W. Macdonald, and N. Roulet (2009), Sensitivity of the carbon cycle in the Arctic to climate change, Ecol. Monogr., 79(4), 523-555.

Tans, P. (2009), An Accounting of the Observed Increase in Oceanic and Atmospheric CO_2 and an Outlook for the Future, Oceanography, 26-35.

Tarnocai, C., J. G. Canadell, E. A. G. Schuur, P. Kuhry, G. Mazhitova, and S. Zimov (2009), Soil organic carbon pools in the northern circumpolar permafrost region, Global Biogeochem. Cycles, 23, GB2023, doi:10.1029/2008GB003327.

Ozone and UV Radiation

G. Bernhard[1], G. Manney[2,3], V. Fioletov[4], J.-U. Grooß[5], A. Heikkilä[6], B. Johnsen[7], T. Koskela[6], K. Lakkala[8], R. Müller[5], C. Lund Myhre[9], M. Rex[10]

[1]Biospherical Instruments, San Diego, CA
[2]Jet Propulsion Laboratory, California Institute of Technology, Pasadena, CA
[3]New Mexico Institute of Mining and Technology, Socorro, NM
[4]Environment Canada, Toronto, Ontario, Canada
[5]Forschungszentrum Jülich, Jülich, Germany
[6]Finnish Meteorological Institute, Helsinki, Finland
[7]Norwegian Radiation Protection Authority, Østerås, Norway
[8]Finnish Meteorological Institute, Arctic Research Centre, Sodankylä, Finland
[9]Norwegian Institute for Air Research, Kjeller, Norway
[10]Alfred Wegener Institute for Polar and Marine Research, Potsdam, Germany

November 23, 2011

Highlights

- Ozone concentrations in the Arctic stratosphere during March 2011 were the lowest ever recorded during the period beginning in 1979; they were 6% below the previous record-low observed in 2000.
- The low levels of total ozone in March and April of 2011 led to elevated UV levels throughout the Arctic and sub-Arctic.

Introduction

Ozone molecules in the Earth's atmosphere greatly attenuate the part of the Sun's ultraviolet (UV) radiation that is harmful to life. Reductions in the atmospheric ozone amount will always lead to increased UV levels, but other factors such as the height of the Sun above the horizon play an important role. This chapter discusses the large ozone loss observed over the Arctic in the spring of 2011 and the resulting increase in UV radiation. UV radiation at some Arctic locations spiked by more than 100% relative to the long-term mean; however, absolute changes remained modest because the ozone loss occurred early in spring when the Sun was still low in the sky.

Ozone

Stratospheric ozone loss in spring 2011 reached a level never observed before in the northern hemisphere (Schiermeier, 2011, Manney et al., 2011). The minimum total ozone column[1] for March 2011, averaged over the "equivalent latitude[2]" band 63°-90° N, was 297 Dobson Units (DU[3]). The previous record-low was 315 DU in 2000 (Fig. A8). The ozone loss in spring 2011 was comparable to that observed during the annually-recurring "ozone hole" over the Antarctic. The record loss was mostly caused by chemical destruction of ozone, attributed to the existing stratospheric burden of ozone-depleting halogens and favored by an unusually prolonged cold period in the lower stratosphere in 2011. These low temperatures facilitate the formation of polar

stratospheric clouds (PSC), which provide surfaces for heterogeneous reactions that activate stratospheric chlorine. The activated chlorine, in turn, destroys ozone rapidly in catalytic cycles.

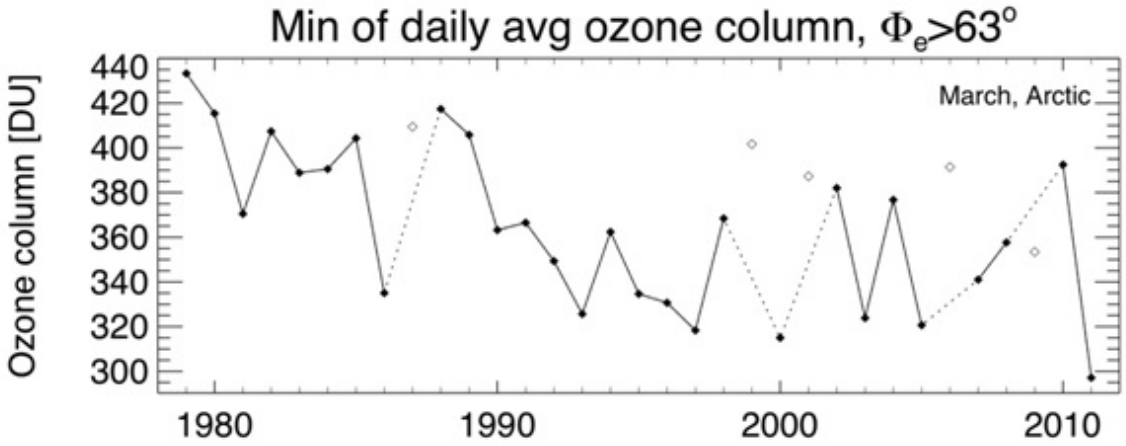

Fig. A8. Time series of minimum total ozone over for March in the Arctic, calculated as the minimum of daily average column ozone poleward of 63° equivalent latitude. Winters in which the vortex broke up before March (1987, 1999, 2001, 2006, and 2009) are shown as circles. Polar ozone in those years was relatively high because of mixing with air from lower latitudes. Figure adapted from Müller et al. (2008), updated using the combined total column ozone database of the New Zealand National Institute of Water and Atmospheric Research (NIWA), Version 2.7, provided by Hamish Chisholm of NIWA and Greg Bodeker of Bodeker Scientific.

The extraordinary situation in 2011 is further illustrated in Fig. A9, which compares satellite measurements of total ozone column on 3 April 1981 (a year with a long-lasting and cold Arctic vortex, and relatively low stratospheric chlorine concentrations), 3 April 2002 (long-lasting warm vortex, high total chlorine loading), and 3 April 2011 (long-lasting cold vortex, high chlorine). The figure emphasizes that chemical ozone loss resulting from chlorine activation is most effective in years such as 2011, when there was a long-lasting, cold vortex.

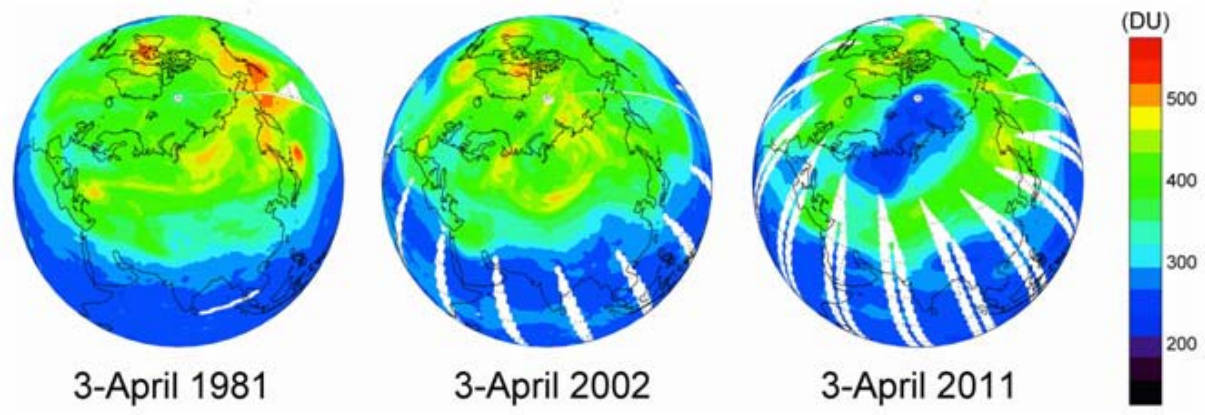

Fig. A9. Comparison of total ozone column measured by satellites on 3 April 1981, 2002 and 2011. Data are from the Total Ozone Mapping Spectrometer (TOMS) onboard the Nimbus-7 (1981) and Earth Probe (2002) satellites, and the Ozone Monitoring Instrument (OMI) onboard of the AURA spacecraft (2011).

The fraction of the Arctic vortex with total ozone below 275 DU is typically near zero for March, but reached nearly 45% in March 2011 (Fig. A10). Minimum total ozone in spring 2011 was continuously below 250 DU for about 27 days, with a maximum area below that level of about two million square kilometers. Values between 220 and 230 DU were reached for about one week in late March 2011.

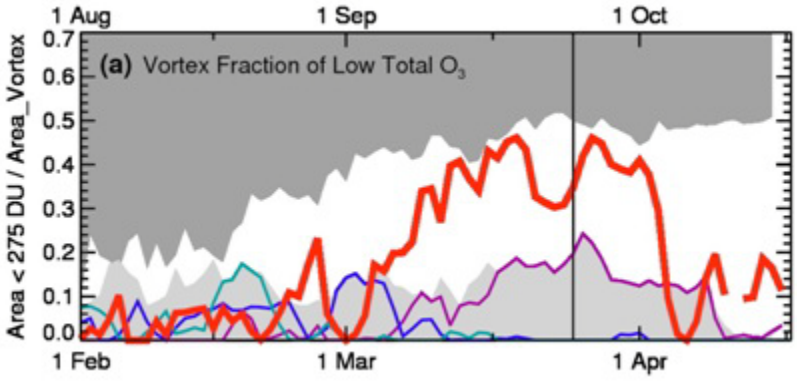

Fig. A10. Fraction of vortex area with total ozone below 275 Dobson units (DU) in February-April in the Arctic (August-October in the Antarctic). Light gray shading shows the range of Arctic values for 1979-2010. Dark gray shading shows the range of Antarctic values for the same period. Because Antarctic ozone is so much lower, only the bottom of the range is apparent here; that is, the dark grey shading begins at the minimum value for that area in any of the years. Red, purple, blue and green lines show the 2010/2011, 1996/1997, 2004/2005 and 2007/2008 Arctic winters, respectively. 2005-2011 values are from Ozone Monitoring Instrument (OMI); earlier values are from the Total Ozone Mapping Spectrometer (TOMS) instruments, available at http://ozoneaq.gsfc.nasa.gov/.

Many aspects of the 2011 Arctic ozone depletion event resemble those of the annually reoccurring ozone hole over Antarctica. For example, ozone profiles in late March 2011 look more like typical Antarctic late-winter profiles than average Arctic profiles (Fig. A11).

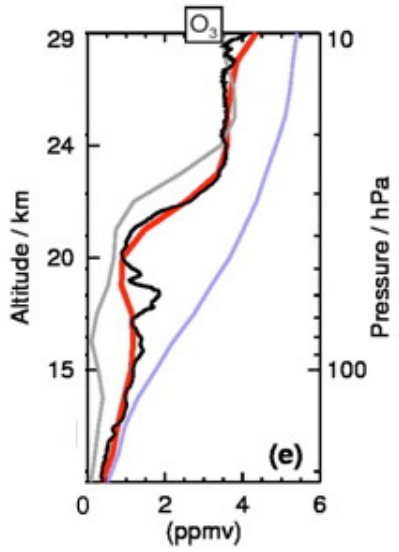

Fig. A11. Comparison of vertical ozone profiles. Red: ozone profiles for a 4°×15° latitude×longitude box around 79°N, 12°E measured on 26 March 2011 by the Earth Observing System Microwave Limb Sounder (MLS); lavender: the MLS 7-day average for 2005-2010 centered on the same location and date; grey: average MLS profiles in a similar box around 79°S, 12°E measured on 26 September; black: a high-resolution ozonesonde profile measured at Ny Ålesund (79°N, 12°E) on 26-March 2011.

The low total ozone in March 2011 resulted primarily from chemical loss (Manney et al., 2011). Chemical destruction was severe between 16 and 22 km, with the largest loss exceeding 2.5 ppmv (parts per million by volume) by March 26. From about 18 to 20 km, over 80% of the ozone present in January had been chemically destroyed by late March (Manney et al., 2011).

Chemical destruction was facilitated by an unusually strong, cold and long-lasting stratospheric polar vortex. During February and March 2011, the vortex was the strongest throughout the lower stratosphere in either hemisphere in the last 30 years (Manney et al., 2011). The strong vortex led to the existence of PSCs over extended areas. Temperatures below the threshold temperature for PSC formation of about 196 K (-77°C) existed between December 2010 and early April 2011 (Fig. A12). Temperatures allowing PSC formation after early March were observed only once before (in 1997).

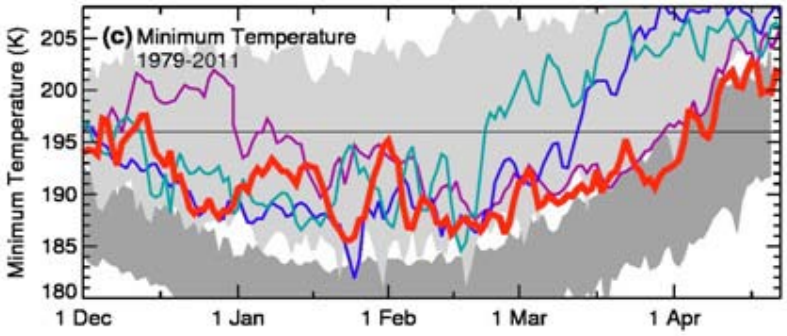

Fig. A12. Minimum temperatures at approximately 18 km altitude poleward of 40° latitude. Line colors and shading are as in Figure A10. The threshold temperature of about 196 K below which PSCs can exist is indicated by the horizontal line. Data are from the Goddard Earth Observing System Version 5.2.0 MERRA reanalyses.

PSCs are important because these clouds provide surfaces for heterogeneous conversion of chlorine into reactive (ozone-destroying) forms such as chlorine monoxide (ClO). ClO enhancement in March 2011 vastly exceeded the range from all previous Arctic winters (Manney et al., 2011). The volume of air, V_{PSC}, with temperatures below the PSC occurrence threshold is a good indicator of the potential for chlorine activation and ozone loss (Rex et al., 2004). V_{PSC} reached a value of 48 million km^3 in 2011 (Fig. A13), similar to the previous records of 2000 and 2005. Since the polar vortex was smaller in 2011 compared to those years, the fraction of vortex air that had been exposed to PSC conditions was larger in 2011 than in any other year shown in Fig. A13. This, and the persistence of low temperatures, and hence the occurrence PSCs, into April 2011 (Fig. A12), led to much more chemical ozone loss in 2011.

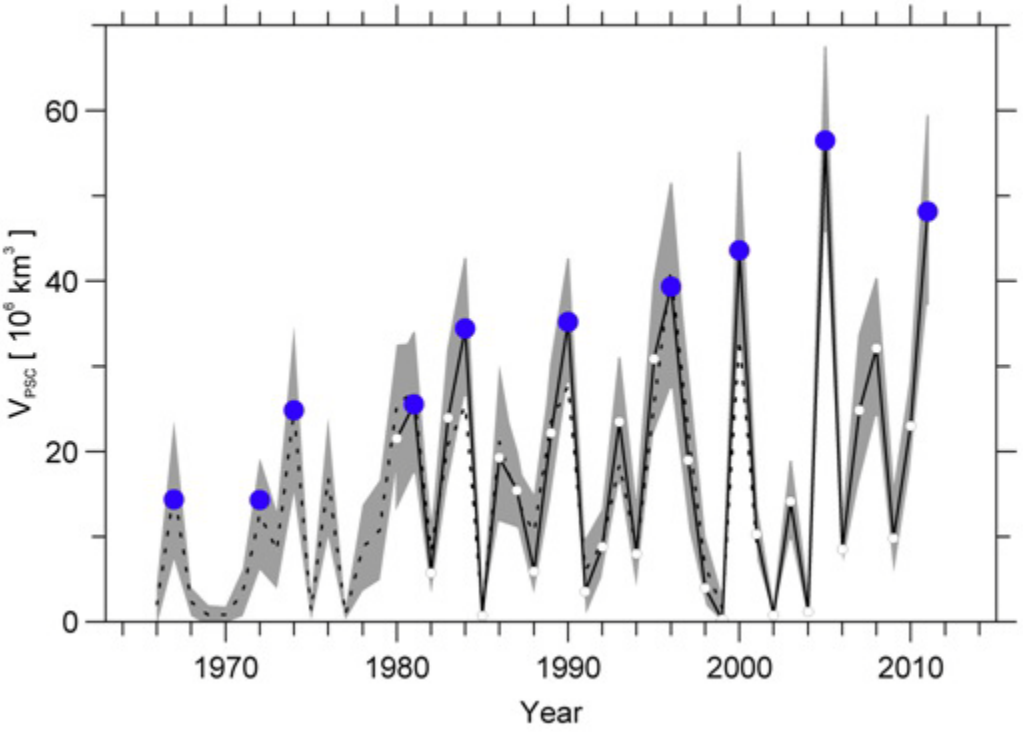

Fig. A13. Evolution of the volume of air with temperatures below the PSC formation threshold (V_{PSC}) for the Arctic. Data are from the European Centre for Medium-Range Weather Forecasts (ECMWF; solid black line) and Free University of Berlin (FUB; dashed line) data. Blue dots represent the maximum values of V_{PSC} during five-year intervals. The gray shading represents the uncertainty of V_{PSC} assuming a 1 K uncertainty in the long-term stability of radiosonde temperatures. Updated from Figure 3 of Rex et al. (2004).

UV Radiation

The low levels of total ozone in March and April of 2011 led to elevated UV levels throughout the Arctic and sub-Arctic, as shown in Fig. A14 and explained in more detail below. Note that the UV Index is a measure of the ability of UV radiation to cause erythema (sunburn) in human skin. It is calculated by weighting UV spectra with the CIE action spectrum for erythema (McKinlay and Diffey, 1987) and multiplying the result by 40 m^2/W.

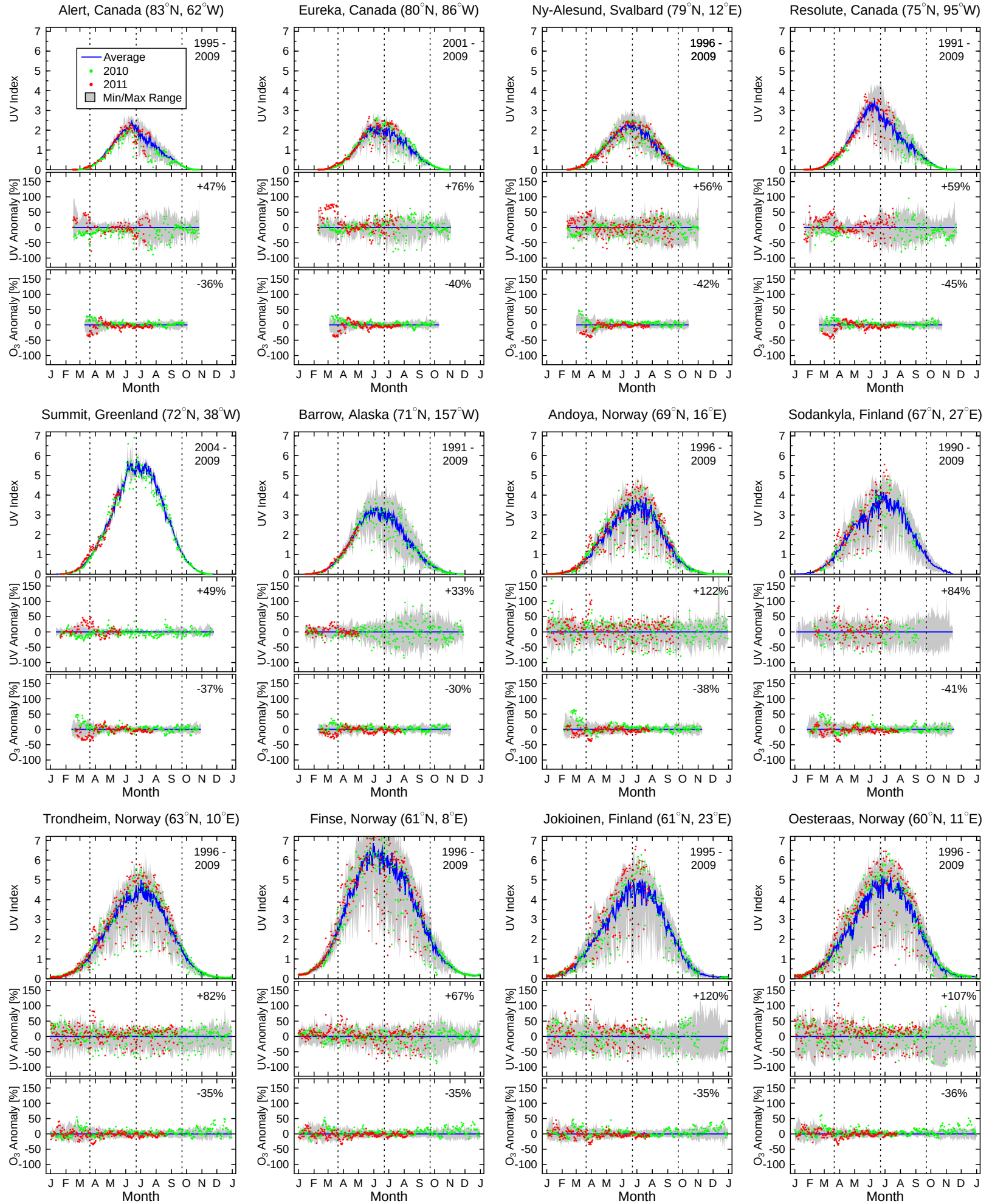
Alert, Canada (83°N, 62°W)
Eureka, Canada (80°N, 86°W)
Ny-Alesund, Svalbard (79°N, 12°E)
Resolute, Canada (75°N, 95°W)
Summit, Greenland (72°N, 38°W)
Barrow, Alaska (71°N, 157°W)
Andoya, Norway (69°N, 16°E)
Sodankyla, Finland (67°N, 27°E)
Trondheim, Norway (63°N, 10°E)
Finse, Norway (61°N, 8°E)
Jokioinen, Finland (61°N, 23°E)
Oesteraas, Norway (60°N, 11°E)
Average
2010
2011
Min/Max Range
1995 - 2009
2001 - 2009
1996 - 2009
1991 - 2009
2004 - 2009
1990 - 2009
+47%
+76%
+56%
+59%
+49%
+33%
+122%
+84%
+82%
+67%
+120%
+107%
-36%
-40%
-42%
-45%
-37%
-30%
-38%
-41%
-35%
-35%
-35%
-36%
UV Index
UV Anomaly [%]
O3 Anomaly [%]
J F M A M J J A S O N D J
Month

Fig. A14. Seasonal variation of the noontime UV Index for 12 Arctic and sub-Arctic sites measured by ground-based radiometers. The upper panel for each site compares the climatological average (blue line) with the measurements in 2010 (green dots) and 2011 (red dots), and historical minima and maxima (shaded range). The latter were calculated from measurements of the periods indicated in the top-right corner of the panel. The center panel shows the anomaly in the UV Index, calculated as the percental departure from the climatological average. The numbers indicate the maximum anomalies for March and April 2011. The bottom panel shows a similar anomaly analysis for total ozone derived from measurements of the following satellites: TOMS/Nimbus7 (1991-1992), TOMS/Meteor3 (1993-1994), TOMS/EarthProbe (1996-2004), and OMI (2005-2011). The shaded range for the ozone data set is based on data of the years 1991–2009 (1996-2009 for Trondheim and Finse). Ozone data are available at http://toms.gsfc.nasa.gov and http://ozoneaq.gsfc.nasa.gov/. Vertical broken lines indicate the times of the vernal and autumnal equinoxes, and the summer solstice.

In addition to atmospheric ozone concentrations, UV radiation is affected by the height of the Sun above the horizon (the solar elevation), clouds, aerosols (liquid and solid particles suspended in air), the reflectivity of the surface (high, when snow or ice covered), and other factors (Weatherhead et al., 2005). The main driver of the annual cycle is the solar elevation. Sites closest to the North Pole (Alert, Eureka and Ny-Alesund in Fig. A14) have the smallest peak radiation. Clouds lead to a large variability in UV levels on time scales from minutes to days, but their effect is largely reduced when the ground is covered by fresh snow. (Bernhard et al. 2008). Measurements at Barrow, and to a lesser extent at Alert and Eureka, show a large asymmetry between spring (low variability) and fall (high variability) because the surface at these sites is covered by snow until about June and free of snow thereafter until the beginning of winter. In particular, during summer and fall the variability introduced by clouds is substantially larger than that related to ozone variations (compare shaded ranges in center and bottom panels of Fig. A14).

The abnormally low stratospheric ozone concentrations in the spring 2011 led to substantially elevated UV Indices at all sites shown in Fig. A14. Changes in the UV Index anti-correlate with changes in total ozone (compare 2011 data in center and bottom panels of Fig. A14). Noontime UV Indices of March 2011 exceeded historical measurements for this month at all sites. Enhancements of the UV Index relative to the climatological average (the "UV anomaly" shown in the center panels of Fig. A14) were most pronounced at Andoya (122%), Jokioinen (120%) and Oesteraas (107%). The relative enhancement at the northernmost sites is somewhat smaller because changes in UV are less sensitive to changes in ozone when the solar elevation is small (Douglas et al., 2011). At all sites, the relative increase in the UV Index is outside the range defined by measurements of earlier years, and at many sites the anomaly is outside the envelope defined by the variability introduced by clouds. While these large relative increases are unprecedented, the absolute increases in UV levels were modest at all sites because the low-ozone event occurred early in spring when the solar elevation was still small. For example, at Andoya, the large relative increase of 122% changed the UV Index from 0.8 (average for 28-March) to 1.9. This value is less than half as large as the peak UV Index of 5.1 measured in July at this site. Although UV Indices below 2 are considered low (WHO, 2002), people involved in certain outdoor activities may receive higher-than-expected UV doses if their faces and eyes are oriented perpendicular to the low Sun or if they are exposed to UV radiation reflected off snow.

Larger absolute increases of UV Indices occurred at lower latitudes during excursions of the polar vortex in April. For example, on April 22, the clear-sky UV Index over parts of Mongolia (48°N, 98°E) estimated by TEMIS (Tropospheric Emission Monitoring Internet Service (TEMIS) at http://www.temis.nl/uvradiation/UVindex.html) was 8.6 when a lobe of the vortex extended to central Asia. The long-term average for this day at this location is 5.4 with a 1-σ standard deviation of 0.5, i.e., the anomaly was more than six standard deviations larger than the climatological mean. A similar situation occurred in central Europe on April 17 when a tongue of the vortex extended over the Alps. The noontime UV Index at Arosa, Switzerland (46.8°N, 9.7°E), was 7.4 on that day, which is four standard deviations larger than the long-term average of 5.3.

Figure A14 also highlights measurements made in 2010. In March 2010, UV Indices were abnormally small due to larger-than-normal stratospheric ozone concentrations in that year. The variability in the second half of 2010 was within the range of previous years.

[1]Total ozone column is the height of a hypothetical layer which would result if all ozone molecules in a vertical column above the Earth's surface were brought to standard pressure (1013.25 hPa) and temperature (273.15 K).
[2]Equivalent latitude is a latitude-like coordinate aligned with the polar vortex (Butchart and Remsberg, 1986).

[3]Dobson Unit, the standard unit for measuring the total ozone column. 1 DU equals a column height of 0.01 mm and corresponds to
2.69×10^{16} molecules / cm^2.

References

Bernhard, G., C. R. Booth, and J. C. Ehramjian (2008): Comparison of UV irradiance measurements at Summit, Greenland; Barrow, Alaska; and South Pole, Antarctica, Atmos. Chem. Phys., 8, 4799-4810. Available at: http://www.atmos-chem-phys.net/8/4799/2008/acp-8-4799-2008.html.

Butchart, N. and E. E. Remsberg (1986): The area of the stratospheric polar vortex as a diagnostic for tracer transport on an isentropic surface, J. Atmos. Sci., 43, 1319-1339.

Douglas, A., and V. Fioletov (Coordinating Lead Authors), S. Godin-Beekmann, R. Müller, R.S. Stolarski, A. Webb, A. Arola, J.B. Burkholder, J.P. Burrows, M.P. Chipperfield, R. Cordero, C. David, P.N. den Outer, S.B. Diaz, L.E. Flynn, M. Hegglin, J.R. Herman, P. Huck, S. Janjai, I.M. Jánosi, J.W. Krzyścin, Y. Liu, J. Logan, K. Matthes, R.L. McKenzie, N.J. Muthama, I. Petropavlovskikh, M. Pitts, S. Ramachandran, M. Rex, R.J. Salawitch, B.-M. Sinnhuber, J. Staehelin, S. Strahan, K. Tourpali, J. Valverde-Canossa, C. Vigouroux (2011): Stratospheric changes and climate, Chapter 4 in Scientific Assessment of Ozone Depletion: 2010, Global Ozone Research and Monitoring Project-Report No. 52, 516 pp., World Meteorological Organization, Geneva, Switzerland. Available at: http://ozone.unep.org/Assessment_Panels/SAP/Scientific_Assessment_2010/04-Chapter_2.pdf.

Manney, G. L., M. L. Santee, M. Rex., N. J. Livesey, M. C. Pitts, P. Veefkind, E. R. Nash, I. Wohltmann, R. Lehmann, L. Froidevaux, L. R. Poole, M. R. Schoeberl, D. P. Haffner, J. Davies, V. Dorokhov, H. Gernandt, B. Johnson, R. Kivi, E. Kyrö, N. Larsen, P. F. Levelt, A. Makshtas, C. T. McElroy, H. Nakajima, M. C. Parrondo, D. W. Tarasick, P. von der Gathen, K. A. Walker, and N. S. Zinoviev (2011): Unprecedented Arctic ozone loss in 2011 echoed the Antarctic ozone hole, Nature, 478, 469-475. Available at: http://www.nature.com/nature/journal/v478/n7370/full/nature10556.html.

McKinlay, A. F., and B. L. Diffey (1987): A reference action spectrum for ultraviolet induced erythema in human skin, CIE Res. Note, 6(1), 17- 22.

Müller, R., J.-U. Grooß, C. Lemmen, D. Heinze, M. Dameris, and G. Bodeker (2008): Simple measures of ozone depletion in the polar stratosphere, Atmos. Chem. Phys., 8, 251-264. Available at: http://www.atmos-chem-phys.org/8/251/2008/acp-8-251-2008.pdf.

Rex, M., R. J. Salawitch, P. von der Gathen, N. R. P. Harris, M. P. Chipperfield, and B. Naujokat (2004):Arctic ozone loss and climate change, Geophys. Res. Lett., 31, L04116, doi:10.1029/2003GL018844.

Schiermeier, Q. (2011): Arctic ozone hole causes concern - April 05, 2011, http://blogs.nature.com/news/2011/04/arctic_ozone_hole_causes_conce.html.

Weatherhead B., A. Tanskanen, and A. Stevermer (2005): Ozone and Ultraviolet Radiation, Chapter 5 in: Arctic Climate Impact Assessment, 1042 pp, Cambridge University Press, New York. Available at: http://www.acia.uaf.edu/PDFs/ACIA_Science_Chapters_Final/ACIA_Ch05_Final.pdf.

WHO (2002): Global Solar UV Index: A Practical Guide, 28 pp., published by World Health Organization (WHO), World Meteorological Organization (WMO), United Nations Environment Programme (UNEP), and the International Commission on Non-Ionizing Radiation Protection (ICNIRP), WHO, Geneva, Switzerland, ISBN 9241590076. Available at: http://www.who.int/uv/publications/en/GlobalUVI.pdf.

Sea Ice and Ocean Summary

Section Coordinator: Andrey Proshutinsky

Woods Hole Oceanographic Institution, MA, USA

November 9, 2011

Sea ice and ocean observations over the past decade (2001-2011) suggest that the Arctic Ocean climate has reached a new state with characteristics different than those observed previously. The new ocean climate is characterized by less sea ice (both extent and thickness) and a warmer and fresher upper ocean than in 1979-2000. The persistence of these changes is having a measureable impact on Arctic marine and terrestrial ecosystems (see the essays on *Marine Ecosystems* and *Terrestrial Ecosystems*).

An anticyclonic (clockwise) wind-driven circulation regime has dominated the Arctic Ocean for at least 14 years (1997-2011), in contrast to the typical 5-8 year pattern of anticylonic/cyclonic circulation shifts observed from 1948-1996. Under the recent persistent anticyclonic circulation regime with relatively warm air temperatures (see the essay on *Temperature and Clouds*) the summer extent of the sea ice cover has been at least 15-20% below the 1979-2000 average. The decline in total sea ice extent has been accompanied by an unprecedented loss of old, thick multiyear ice. Melting sea ice has released additional fresh water into the upper ocean. Influenced by strong anticyclonic winds, fresh water has accumulated in the Beaufort Gyre region, where the fresh water content has increased by approximately 5,000 km^3 relative to 1970s climatology. The loss of sea ice has also resulted in the warming of the upper ocean and ocean expansion, leading to an increase in the rate of sea level rise.

In the Bering Sea, aragonite undersaturation, i.e., acidification, throughout the water column is causing seasonal $CaCO_3$ mineral suppression in some areas. The effects of ocean acidification in the Chukchi Sea, induced by the uptake of anthropogenic CO_2 over the last century, are amplified by high rates of summertime phytoplankton primary production, which leads to increased seawater pCO_2 and decreased pH of sub-surface waters, which become more corrosive to $CaCO_3$.

Sea Ice

D. Perovich[1,2], W. Meier[3], J. Maslanik[4], J. Richter-Menge[1]

[1]ERDC - CRREL, 72 Lyme Road, Hanover, NH 03755
[2]Thayer School of Engineering, Dartmouth College, Hanover NH 03755
[3]National Snow and Ice Data Center, University of Colorado, Boulder, CO 80309
[4]Aerospace Engineering Sciences, University of Colorado, Boulder, CO 80309

November 9, 2011

Highlights

- Minimum Arctic sea ice extent in September 2011 was the second lowest recorded by satellite since 1979.
- Based on passive microwave remote sensing data, the Northwest Passage (both the northern and southern routes) and the Northern Sea Route were open in 2011 for the second consecutive year.

Sea ice extent

Sea ice extent is the primary variable for summarizing the state of the Arctic sea ice cover. Passive microwave instruments on satellites have routinely and accurately monitored the extent since 1979. There are two periods that define the annual cycle and thus are of particular interest: September, at the end of summer, when the ice reaches its annual minimum extent, and March, at the end of winter, when the ice is at its maximum extent. Maps of ice extent in September 2011 and March 2011 are presented in Fig. SIO1.

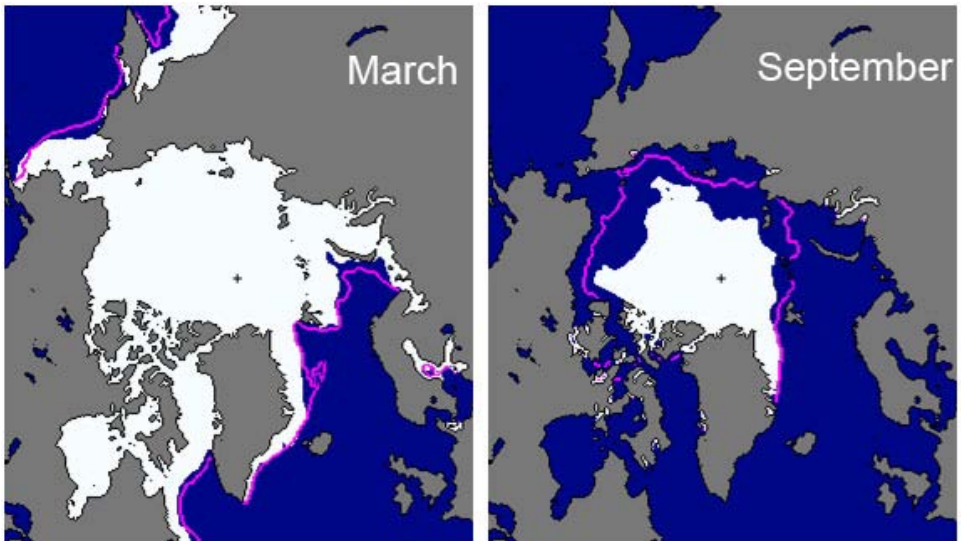

Fig. SIO1. Sea ice extent in March 2011 (left) and September 2011 (right), illustrating the respective monthly winter maximum and summer minimum extents. The magenta line indicates the median maximum and minimum ice extents in the given month for the period 1979-2000. Maps are from the National Snow and Ice Data Center Sea Ice Index: nsidc.org/data/seaice_index.

On September 9, 2011, sea ice extent reached a minimum for the year of 4.33 million km^2. The 2011 minimum is the second lowest, only 0.16 million km^2 greater than the 2007 record minimum. Overall, the 2011 minimum was 31% (2.08 million km^2) smaller than the 1979-2000 average. The last five summers (2007-2011) have experienced the five lowest minima in the satellite record, and the past decade (2002-2011) has experienced nine of the ten lowest minima.

The March 2011 maximum ice extent was 14.64 million km^2, 7.7% less than the 1979-2000 average of 15.86 million km^2. The yearly maximum sea ice extent occurred on March 7. This was about normal compared to the 1979-2000 average. As in 2010, the extent around the maximum data tended to be flat, undulating up and down in response to weather-induced variations in the ice edge.

The time series of the anomalies in monthly average sea ice extent in March and September for the period 1979-2011 are shown in Fig. SIO2. The anomalies are computed with respect to the average from 1979 to 2000. The large inter-annual variability in September ice extent is evident. Both winter and summer ice extent exhibit a negative trend, with values of -2.7 % per decade for March and -12.0% per decade for September over the period 1979-2011.

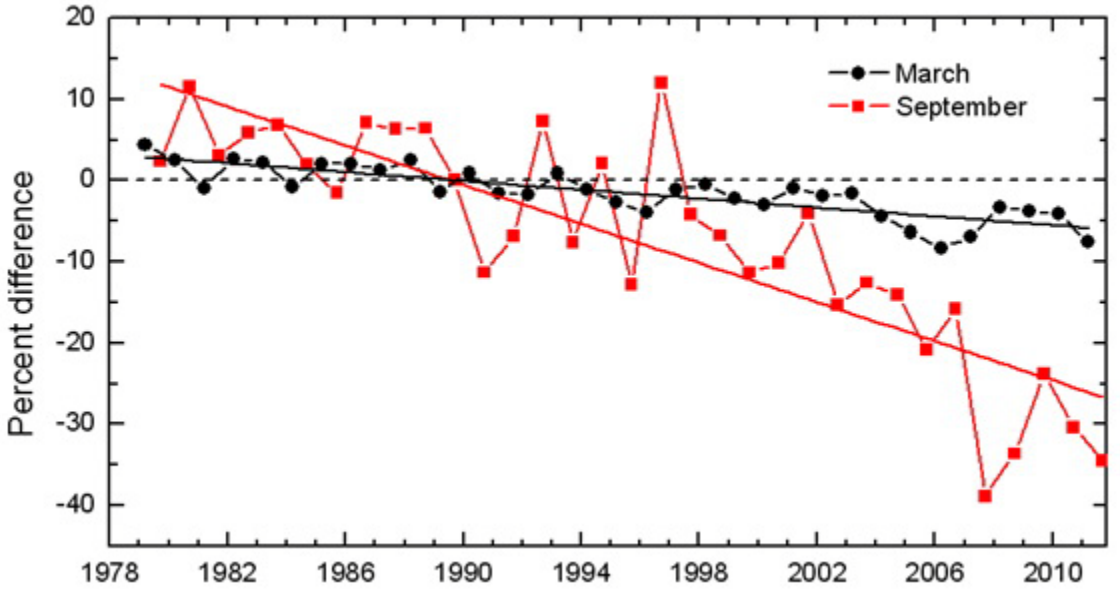

Fig. SIO2. Time series of the percentage difference in ice extent in March (the month of ice extent maximum) and September (the month of ice extent minimum) relative to the mean values for the period 1979-2000. Based on a least squares linear regression for the period 1979-2011, the rate of decrease for the March and September ice extents is -2.7% and -12.0% per decade, respectively.

Monthly ice extents averaged for the periods 1979-2000 and 2001-2011 are plotted in Fig. SIO3. Ice extents for the period 2001-2011 are smaller than 1979-2000 for all months. For most months, the ice extent curves are more than a standard deviation apart. The decline in ice extent is greatest in August, September, and October. Those months also show an increase in inter-annual variability for the 2001-2011 period. The difference in ice extent between these two periods suggests a shift to a new regime of reduced sea ice.

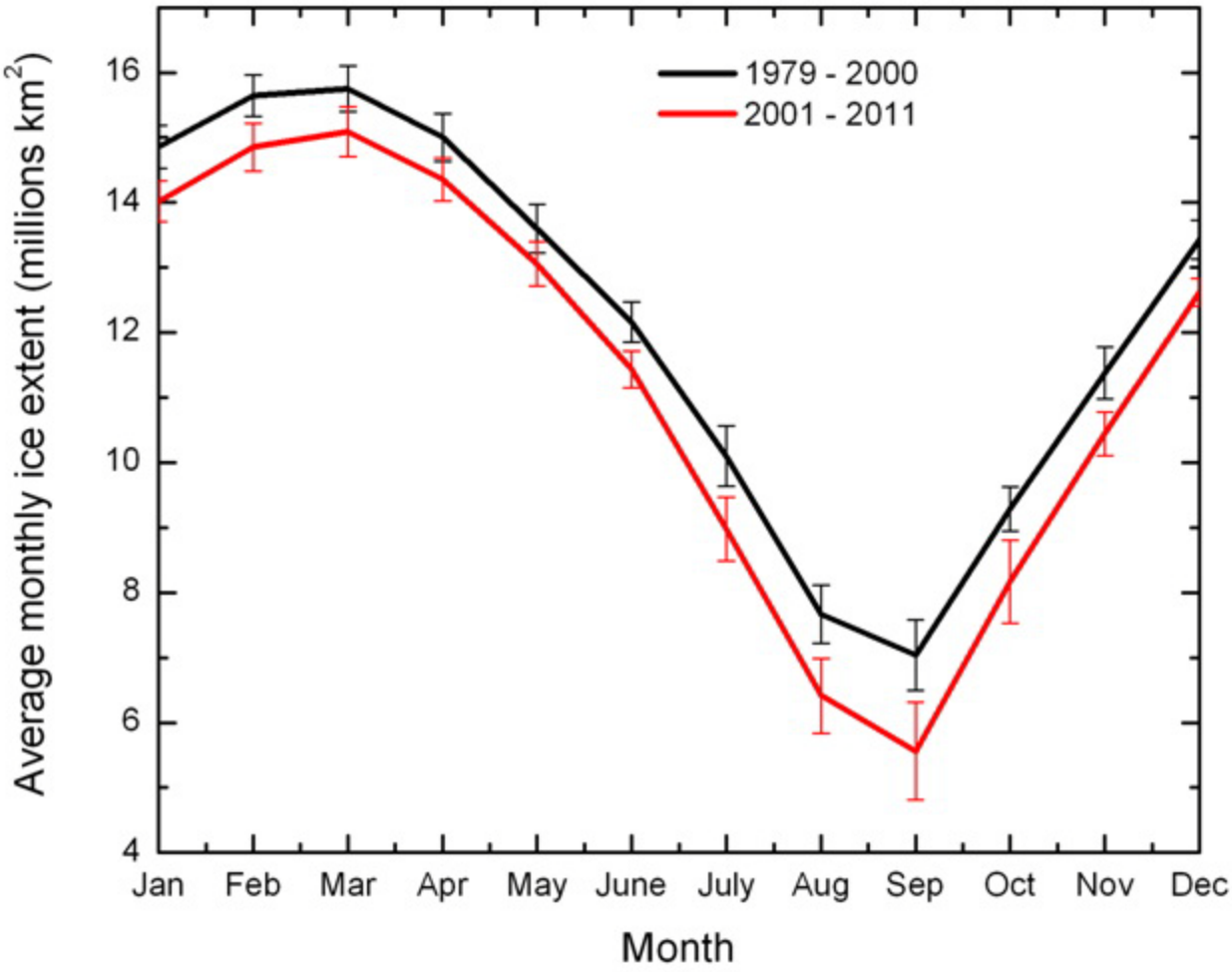

Fig. SIO3. Mean monthly sea ice extent for the period 1979-2000 (thick black line) and for the period 2001-2011 (thick red line). The vertical bars represent one standard deviation about the mean.

Ice spatial distribution

The spatial distribution of September sea ice extent for the past five years is shown in Fig. SIO4. For reference, the ice extent for September 1980 is also shown. Large changes from 1980 are evident, with a pronounced retreat of ice around the periphery of the Arctic Basin and ice loss in the Canadian Archipelago. There is a similar pattern to ice distribution in the past three years. Ice remains in the central Arctic, along northeast Greenland, and adjacent to the northern edge of the Canadian Arctic Archipelago. North of Alaska and Siberian the ice edge forms an arc with lobes of ice extending from both edges. These lobes consist of a mixture of dispersed floes of first-year and multiyear ice amid considerable amounts of open water. This contrasts with many earlier years, including 2007, when the ice edge at the end of summer was compact and most of the remaining ice was a consolidated pack.

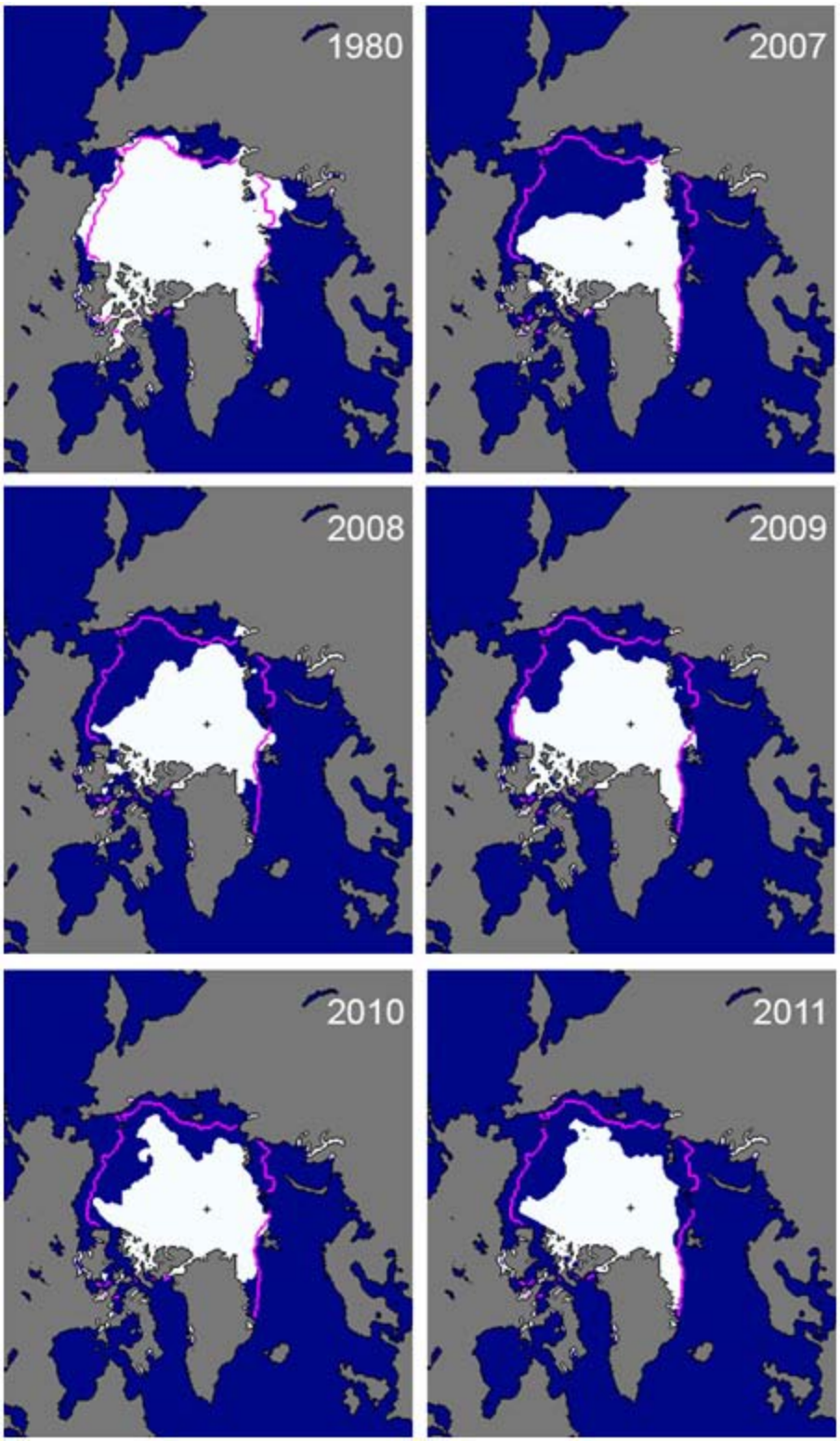

Fig. SIO4. Maps of September ice extent for 1980, 2007, 2008, 2009, 2010 and 2011. The magenta line indicates the median September ice extent for the period 1979-2000. Maps are from the National Snow and Ice Data Center Sea Ice Index: nsidc.org/data/seaice_index.

Table SIO1 summarizes ice conditions in the southern and northern routes of the Northwest Passage and the Siberian Coast passage of the Northern Sea Route. Ice conditions were determined using passive microwave satellites. Open means the route appeared ice-free in the passive microwave imagery and closed means ice blocked passage somewhere along the route. Due to resolution limitations, passive microwave imagery may miss small pieces of ice and areas that appear "open" in satellite images may have ice covering as much as 15% of their surface (IICWG, 2011). All three routes have been open the past two years and the Northwest Passage southern route has been open every year since 2007. Additional information on the routes and on sea ice in the Greenland and Baltic Seas is available from the International Ice Charting Working Group news release (IICWG, 2011).

Table SIO1. Status of September ice conditions in the Northwest Passage and Northern Sea Route as determined from passive microwave satellite data.

Year	Northwest Passage	Northwest Passage	Northern Sea Route
2011	Open	Open	Open
2010	Open	Open	Open
2009	Open	Closed	Open
2008	Open	Closed	Open
2007	Open	Open	Closed

Sea ice age

The age of the ice is another key descriptor of the state of the sea ice cover. Older ice tends to be thicker and thus more resilient than younger ice. The age of the ice is determined using satellites observations to track ice parcels over several years. This method has been used to provide a record of ice age since the early 1980s. Fig. SIO5 shows sea ice age derived from tracking ice parcels for 1979 through 2011. The distribution of ice of different ages illustrates the extensive loss in recent years of the older ice types (Maslanik et al., 2011). Analysis of the time series of areal coverage by age category indicates some recovery of 3rd-year ice coverage. However, the loss of the older (4+ year ice) that began in earnest in 2005 (Maslanik et al., 2011) has continued, reaching a record minimum in summer 2011, or 19% of the 1982-2005 mean. The net increase in 3rd year ice from 2010 to 2011 (0.36 million sq. km) is greater than the decrease in 4+ year ice (-0.11 million sq. km), which suggests a potential gain in ice mass within the multiyear ice coverage. However, given that the older ice types tend to be thicker (e.g., Maslanik et al., 2007a), this increase might be relatively slight.

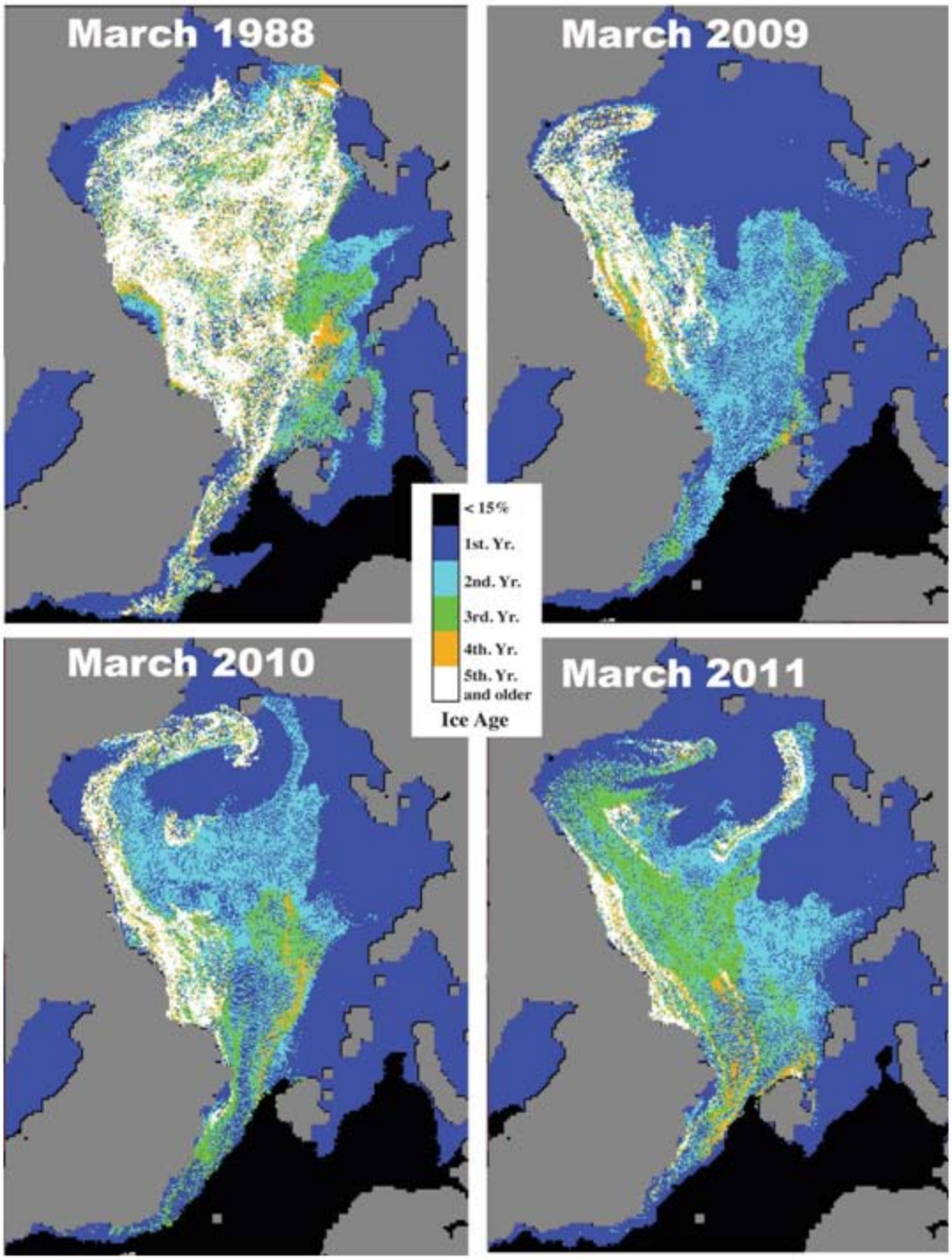

Fig. SIO5. Sea ice age in the first week of March derived from tracking the drift of ice floes in 1988, 2009, 2010 and 2011. Figure courtesy of J. Maslanik and C. Fowler.

References

International Ice Charting Working Group (IICWG). 2011. News Release: International Ice Services Caution that "Open" Does Not Mean Ice-free. http://nsidc.org/noaa/iicwg

Maslanik J. A., C. Fowler, J. Stroeve, S. Drobot, J. Zwally, D. Yi, W. Emery, A younger, thinner Arctic ice cover: Increased potential for rapid, extensive sea-ice loss, Geophys. Res. Lett., 34, L24501, doi:10.1029/2007GL032043, 2007.

Maslanik, J., J. Stroeve, C. Fowler, and W. Emery. 2011. Distribution and trends in Arctic sea ice age through spring 2011. Geophysical Research Letters 38, L13502, doi:10.1029/2011GL047735.

National Snow and Ice Data Center, Web Site, http://nsidc.org/arcticseaicenews/2010/100410.html.

Stroeve, J. C., J. Maslanik, M. C. Serreze, I. Rigor, W. Meier, and C. Fowler. 2011. Sea ice response to an extreme negative phase of the Arctic Oscillation during winter 2009/2010. Geophysical Research Letter 38, L02502, doi:10.1029/2010GL045662.

Ocean

A. Proshutinsky[1], M.-L. Timmermans[2], I. Ashik[3], A. Beszczynska-Moeller[4], E. Carmack[5], J. Eert[5], I. Frolov[3], M. Itoh[6], T. Kikuchi[6], R. Krishfield[1], F. McLaughlin[5], B. Rabe[4], U. Schauer[4], K. Shimada[7], V. Sokolov[3], M. Steele[8], J. Toole[1], W. Williams[5], R. Woodgate[8], S. Zimmermann[5]

[1]Woods Hole Oceanographic Institution, Woods Hole, MA, USA
[2]Yale University, New Haven, CT, USA
[3]Arctic and Antarctic Research Institute, St. Petersburg, Russia
[4]Alfred Wegener Institute, Bremerhaven, Germany
[5]Institute of Ocean Sciences, Fisheries and Oceans Canada, Sidney, British Columbia, Canada
[6]Japan Agency for Marine-Earth Science and Technology, Tokyo, Japan
[7]Tokyo University of Marine Science and Technology, Tokyo, Japan
[8]University of Washington, Seattle, WA, USA

November 9, 2011

Highlights

- The wind-driven circulation regime was anticyclonic, supporting a high volume of freshwater in the Beaufort Gyre region.
- Upper ocean temperature and salinity were comparable with previous years, indicating some stabilization in warming and consistent with sea ice conditions described in the *Sea Ice* essay.
- The state of the deep ocean layers also shows some stabilization without pronounced inter-annual changes.
- Rates of sea level rise did not change significantly, following previously observed patterns of decadal variability in which multiyear periods of significant sea level rise alternate with periods of sea level decrease.

Wind driven circulation

In 2010, the annual wind-driven circulation regime was anticyclonic (clockwise) with a well-organized Beaufort Gyre and relatively weak Transpolar Drift (Fig. SIO6a). In 2011 (January-August), the anticyclonic wind-driven circulation intensified (Fig. SIO6b) relative to conditions in 2010, and the Transpolar Drift was much stronger than in 2010. Circulation in 2011 (January - August) more closely resembled 2007 conditions, although a stronger Arctic High and anticyclonic circulation was observed in 2007 (Fig. SIO6c). The anticyclonic circulation regime similar to that shown in Fig. SIO6a-c has persisted between 1997 and 2011, with only one short-lived reversal to a cyclonic regime in 2009, the consequences of which were important, as discussed below. The anticyclonic regime has dominated for at least 14 years instead of the typical 5-8 year pattern (as reported in Proshutinsky and Johnson [1997, 2010], who analyzed statistics of Arctic circulation regimes between 1948 and 2010). It may be that after the anomalous 2007 conditions (a historical minimum of September sea-ice extent, and maximum upper-ocean warming and freshening) the Arctic climate system bifurcated towards a new state characterized by a more persistent anticyclonic regime and with relatively small changes from year to year.

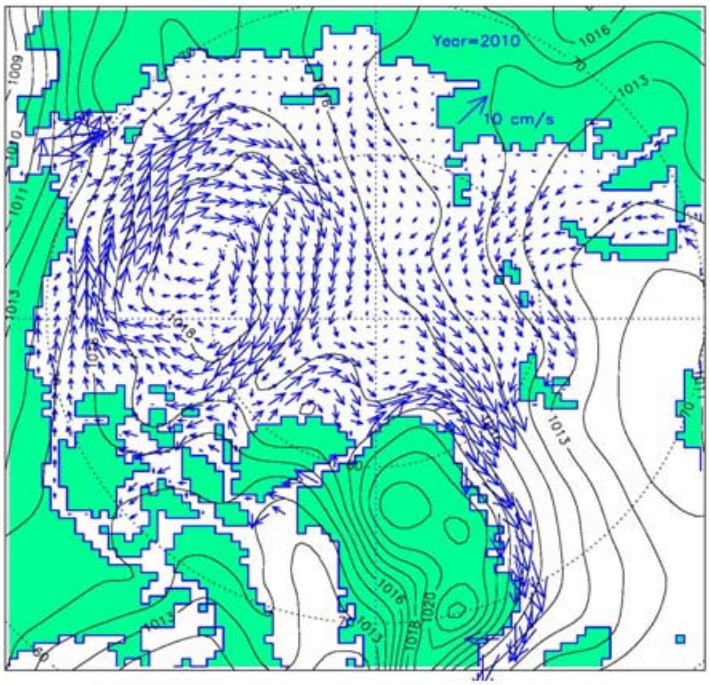

Fig. SIO6a. Simulated wind-driven ice motion (arrows) and observed sea level atmospheric pressure (hPa, black lines) for 2010. Results are from a 2-D coupled ice-ocean model (Proshutinsky and Johnson, 1997; 2011) forced by wind stresses derived from 2010 NCEP/NCAR reanalysis 6-hourly sea level pressure fields.

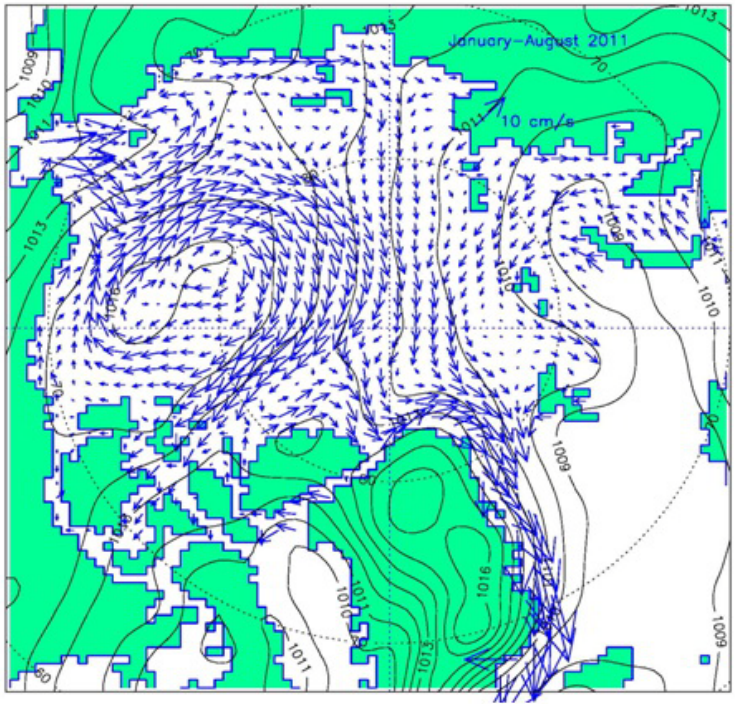

Fig. SIO6b. Simulated wind-driven ice motion (arrows) and observed sea level atmospheric pressure (hPa, black lines) for January-August 2011. Results are from a 2-D coupled ice-ocean model (Proshutinsky and Johnson, 1997; 2011) forced by wind stresses derived from 2011 NCEP/NCAR reanalysis 6-hourly sea level pressure fields.

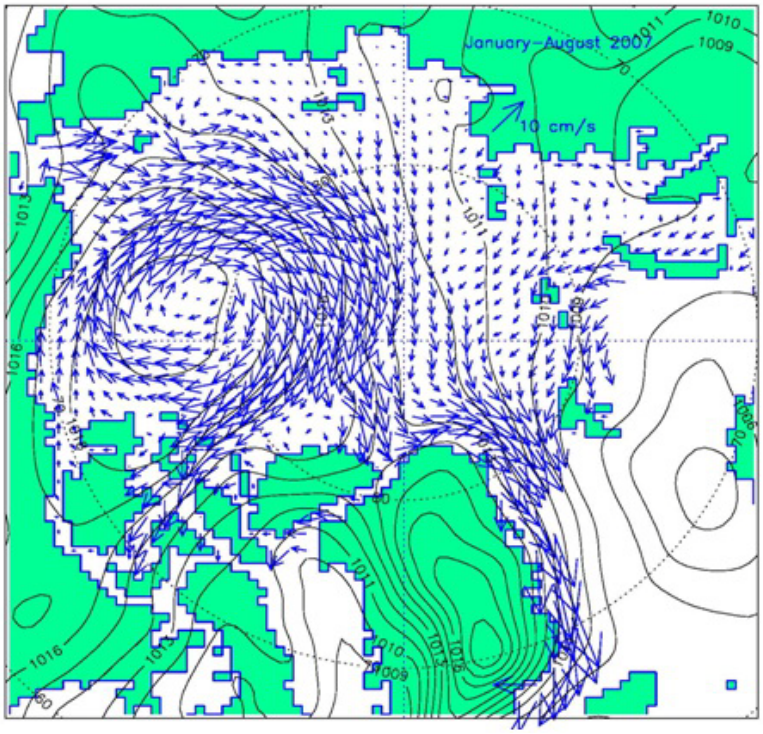

Fig. SIO6c. Simulated wind-driven ice motion (arrows) and observed sea level atmospheric pressure (hPa, black lines) for January-August 2007. Results are from a 2-D coupled ice-ocean model (Proshutinsky and Johnson, 1997; 2011) forced by wind stresses derived from 2007 NCEP/NCAR reanalysis 6-hourly sea level pressure fields.

Ocean temperature and salinity

Upper-ocean temperature

Upper ocean temperature anomalies in summer 2010 (Fig. SIO7 were comparable to those in 2009 (not shown) but remained lower than the record set in 2007, with no significant inter-annual changes in summer warming since 2008. In August 2011, there is a wide area of anomalously warm SSTs (sea surface temperature) in the western Arctic Ocean (north of NW Canada, Alaska and eastern Siberia), although maximum values do not reach those seen in 2007 (Fig. SIO7). Much of the eastern Arctic Ocean (north of western Russia and Europe) is also anomalously warm, with the exception of Fram Strait. For more information about water temperatures in Fram Strait, and the adjacent Greenland and Norwegian seas, see the essay on *Cetaceans and Pinnipeds*.

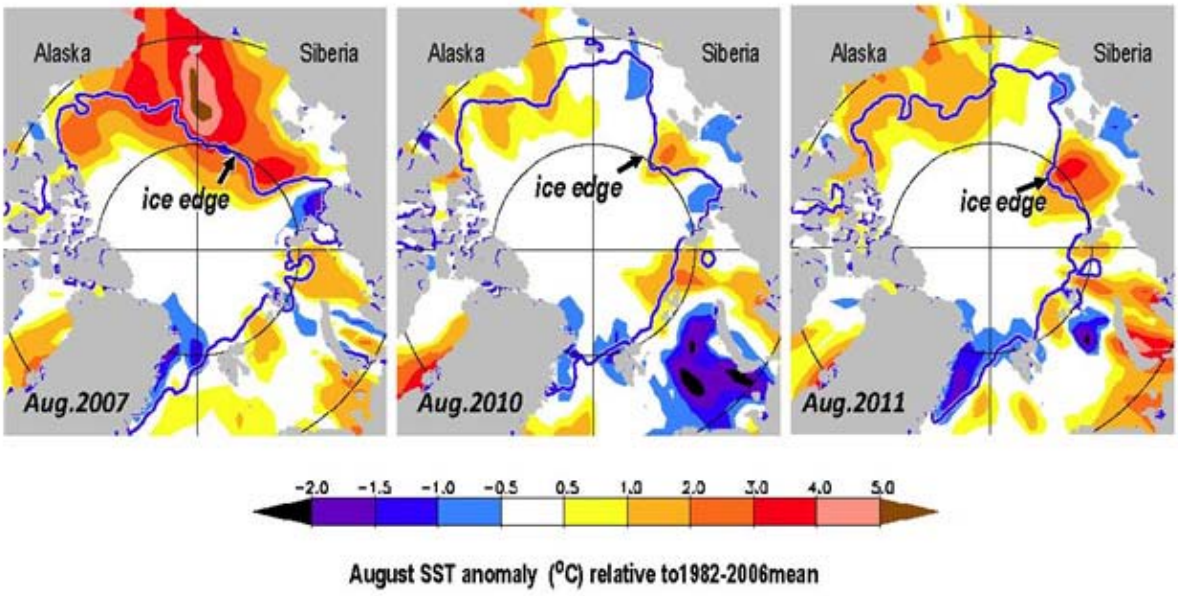

Fig. SIO7. SST anomalies in August of 2007 (left), 2010 (middle) and 2011 (right) relative to the August mean of 1982-2006. The anomalies are derived from satellite data according to Reynolds et al. (2002). The August mean ice edge (thick blue line) is also shown.

Inter-annual variations in SST anomalies reflect differences in the pace of sea ice retreat (see the essay on *Sea Ice*), as well as changing advection of warm ocean currents from the south (Steele et al. 2011). In recent years, solar radiation has penetrated more easily into the upper ocean under thinning and retreating ice cover to create warm near-surface temperature maxima (Jackson et al., 2010). In the Canada Basin, this maximum has descended to depths around 30 m because of increased downwelling in the convergent Beaufort Gyre during recent strongly-anticyclonic years (Yang et al. 2009), while surface mixing is decreasing as stratification increases (Toole et al. 2010; McPhee et al. 2009). Outside of the Beaufort Gyre, the temperature maximum does not survive through the winter (Steele et al. 2010).

Upper-ocean salinity

Relative to the 1970s, surface waters in 2009-10 (Fig. SIO8 were generally saltier in the Eurasian Basin and fresher in the Canada Basin, with the maximum freshwater anomaly centered in the Beaufort Gyre. Several key changes in salinity distribution of the upper layers occurred between 2007-08 and 2009-10 (not shown). The western Canada Basin surface waters were fresher in the latter two years, with saltier surface waters in the eastern Canada Basin in 2010-09 compared to 2007-08. The region between Greenland and the North Pole was generally fresher in 2009-10 than in 2007-08, while the upper ocean was saltier in the western Makarov Basin in the latter two years. These changes in upper-ocean salinity possibly result from a 2009 shift in the large-scale wind-driven circulation to some reduction in strength of the anticyclonic Beaufort Gyre and the Transpolar Drift (Timmermans et al. 2011).

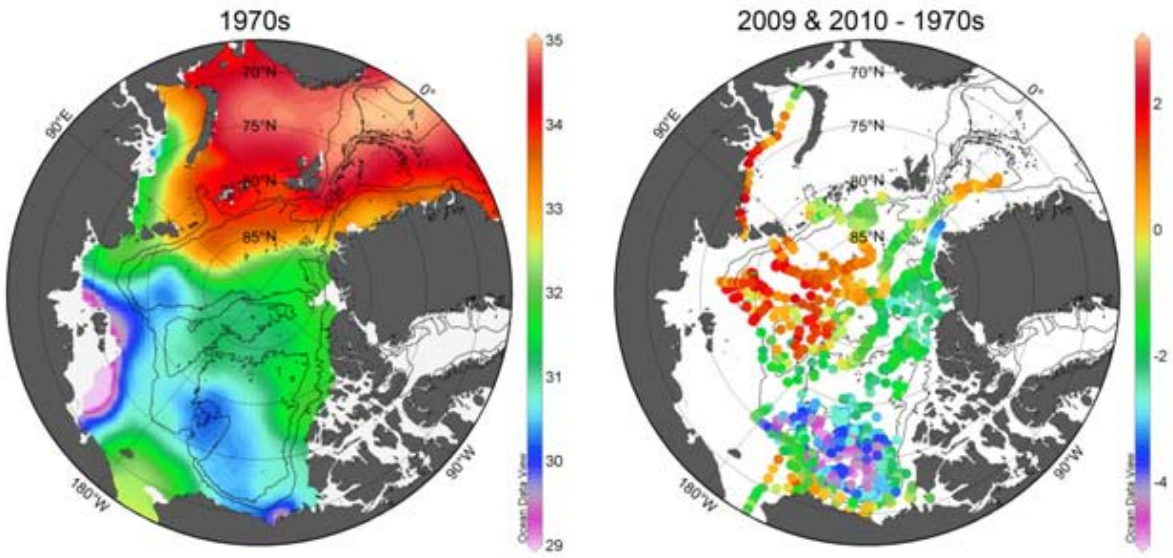

Fig. SIO8. Salinity anomalies at 20 m depth in 2009-2010 (right) relative to 1970s climatology (left). The 500 and 2500 m isobaths have been plotted using the IBCAO grid.

Beaufort Gyre freshwater and heat content

The Beaufort Gyre is the largest reservoir of freshwater in the Arctic Ocean. In 2010, the magnitude of the freshwater content was comparable to 2008 and 2009 conditions, with the exception that freshwater tended to spread out from the 2007-2009 center (Fig. SIO9). In total, during 2003-2010 the Beaufort Gyre accumulated more than 5000 km^3 of freshwater, a gain of approximately 25 percent (update to Proshutinsky et al. 2009) relative to climatology of the 1970s.

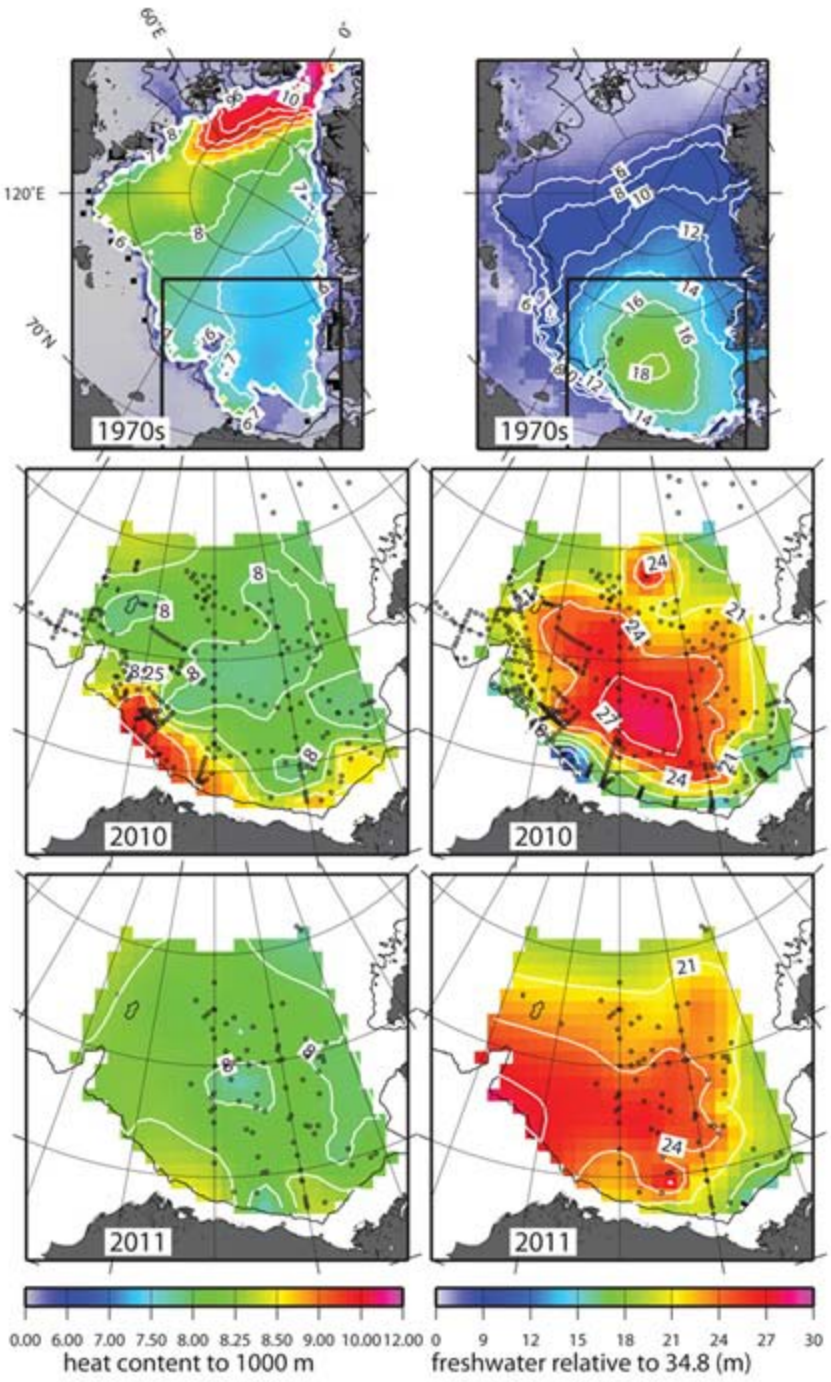

Fig. SIO9. Summer heat content (1×10^{10} J m^{-2}) and freshwater content (m). The top row shows heat and freshwater content in the Arctic Ocean based on 1970s climatology (Timokhov and Tanis 1997, 1998). The centre and bottom rows show heat and freshwater content in the Beaufort Gyre based on hydrographic surveys (black dots depict hydrographic station locations) in 2010 and 2011, respectively. The Beaufort Gyre region is shown by black boxes in the top row. Heat content is calculated relative to freezing temperature in the upper 1000 m of the water column. Freshwater content is calculated relative to a reference salinity of 34.8.

Note that freshwater increases in recent years have not been limited to the Beaufort Gyre. Relatively recent changes in upper ocean freshwater content (Fig. SIO10) in all Arctic Ocean basins were reported by Rabe et al. (2011). They showed that between 1992-1999 and 2006-2008, the freshwater content in Arctic basins increased by 8400 ± 2000 km^3, and suggested that this was largely due to enhanced advection of river water from the shelves and net melting of sea ice.

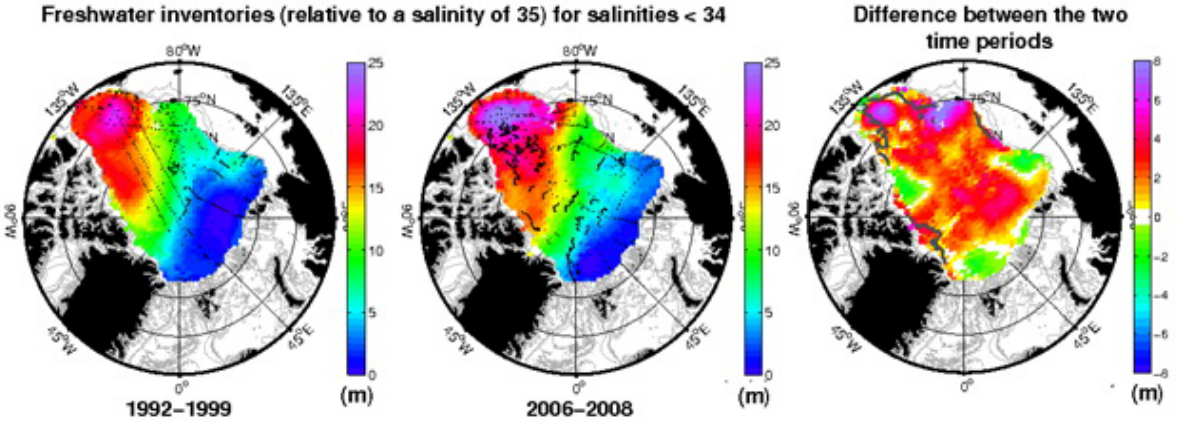

Fig. SIO10. Objectively-mapped observed freshwater inventory (meters) from the surface to the depth of the 34 isohaline for the deep Arctic Ocean during July, August and September: (left) 1992-1999, (center) 2006-2008 and (right) difference between the 2006-2008 and 1992-1999 periods. Positive differences mean freshening. The locations of measured salinity profiles used for mapping are shown as black dots. The thick gray line represents the 1 m contour of the combined (maximum) statistical error estimate for both mapping time periods. Figures were modified from Rabe et al. (2011).

The Beaufort Gyre heat content in 2010 increased relative to 2009 primarily due to surface heating by direct penetration of solar radiation into ice-free coastal regions (Fig. SIO9, left panels; and see the essay on *Sea Ice*). In August 2011, freshwater and heat conditions similar to 2010 were emerging (Fig. SIO9), although insufficient data were available to constrain the 2011 estimates at the time of this writing.

The Atlantic Water Layer

Warm water of North Atlantic origin, the Atlantic Water Layer (AWL), resides between approximately 200 and 900 meters and is characterized by temperatures >0°C and salinities >34.5. In 2009-2010, AWL maximum temperature anomalies were generally highest on the Eurasian side of the Lomonosov Ridge, with maximum values about 1°C along the boundaries of the Eurasian Basin (Fig. SIO11). Warming was less pronounced in the Canada Basin than in the Eurasian Basin. There was little to no temperature anomaly (<0.1°C) at the south-east boundary of the Canada Basin or in the basin boundary regions adjacent to Greenland and the Canadian Arctic Archipelago. Negative (cooling) temperature anomalies were detected in the vicinity of Nares Strait.

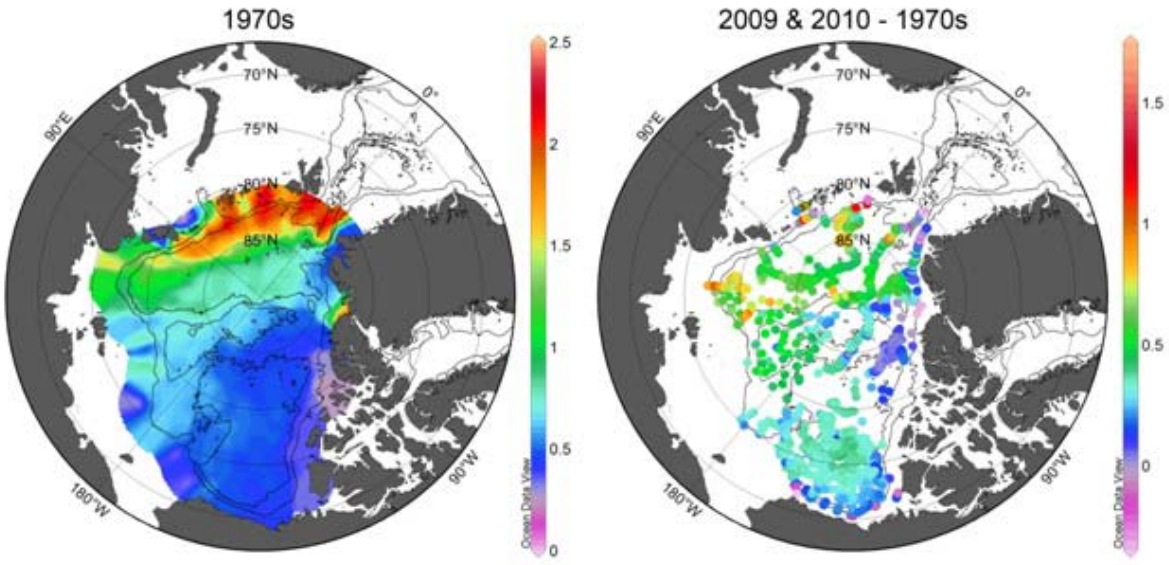

Fig. SIO11. Atlantic Water layer temperature maximum anomalies (right) relative to 1970s climatology (left). The 500 and 2500 m isobaths have been plotted using the IBCAO grid.

The characteristics of the AWL are regulated by the Atlantic Water (AW) properties and transport at the inflow in Fram Strait. After reaching a maximum in 2006, AW temperature in Fram Strait decreased until 2008 (Fig. SIO12). In 2009, AW temperature and salinity in northern Fram Strait increased, returning in summer 2010 to the long-term mean. The autumn and winter AW temperatures were slightly higher in 2009/2010 than the previous year, while in summer 2010 the mean temperature remained close to that observed in summer 2009, with typical substantial seasonal variability. With the exception of one strong event in December, the AW inflow with the West Spitsbergen Current was lower in 2009-2010 compared to the somewhat stronger inflows observed in winter 2008-2009. However, in summer 2010 the AW volume transport was relatively high and the typical seasonal summer minimum was not well pronounced (Fig. SIO12); this is the case at least for the months for which data are available. For more information about water temperatures in Fram Strait, and the adjacent Greenland and Norwegian seas, see the essay on *Cetaceans and Pinnipeds*.

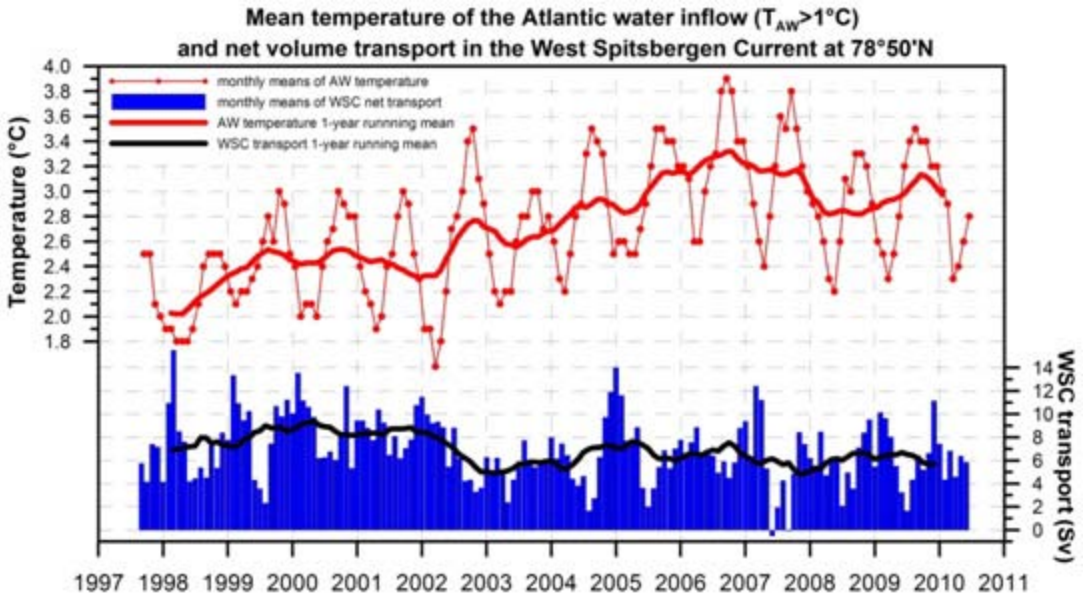

Fig. SIO12. Atlantic water (defined by T >1°C) mean temperature and the volume inflow in the West Spitsbergen Current, northern Fram Strait, measured by moorings at 78°50'N. A mooring array has been maintained in the Fram Strait since 1997 as a joint effort of the Norwegian Polar Institute and the Alfred Wegener Institute for Polar and Marine Research.

The Pacific Water Layer

The Pacific Water Layer (PWL) is located in the Canada Basin at depths between approximately 50 and 150 meters (Steele et al. 2004) and originates from the Bering Strait inflow. The relatively warm and fresh PWL (S <33.5) comprises about two thirds of the Canada Basin halocline by thickness and about half by freshwater content (e.g., Aagaard and Carmack 1989). Some component of this water carries high nutrient content throughout the Arctic Ocean and even downstream into, for example, Baffin Bay (Tremblay et al. 2002). The freshwater flux from the North Pacific Ocean into the North Atlantic Ocean provides a "short circuit" for the global thermohaline ocean circulation (e.g., Wijffels et al. 1992). Important changes in Pacific Winter water spreading between 2002-2006 and 2007-2010 are shown in Fig. SIO13 In the period 2002-2006, this water penetrated into the Beaufort Sea from the southern end of the Northwind Ridge. In 2007-2010, it took a different path, spreading northward along the Chukchi Plateau directly from the Herald Canyon. The pathway change was possibly associated with changes in strength and spatial pattern of the wind-driven sea-ice motion (Fig. SIO13, bottom panels). While the extent to which the Pacific Winter water is influenced by wind forcing is unclear, it may be that in recent years the increased westward wind forcing (and increased westward ice transport) prevents the Pacific Winter water from spreading directly east. These changes in the physical environment cause changes in the biogeochemical environment in the Pacific sector of the Arctic Ocean (see the essay on *Ocean Biogeophysical Conditions*).

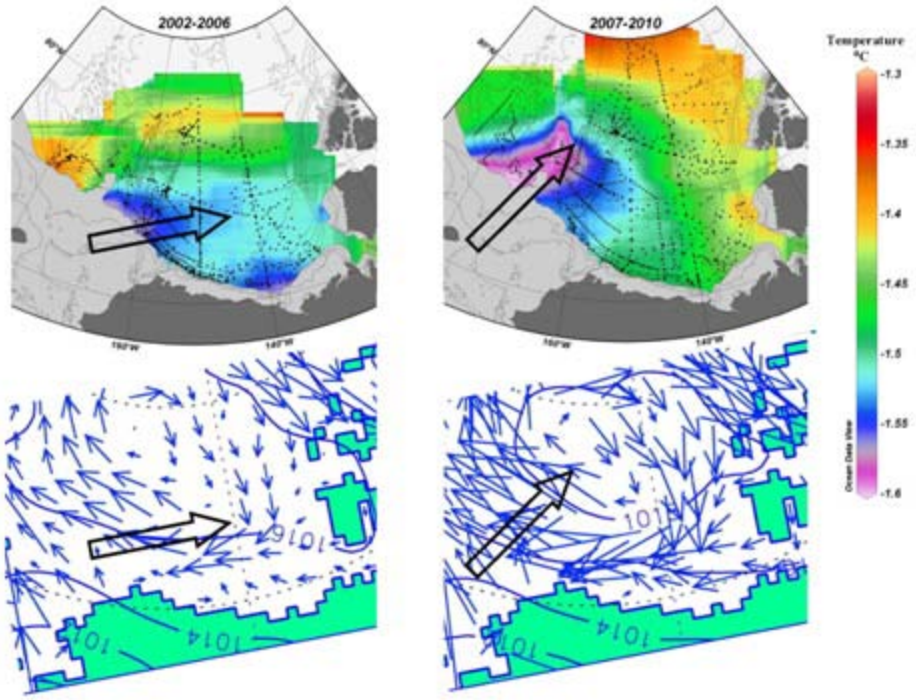

Fig. SIO13. Top row: potential temperature (°C) in the Canada Basin at the S=33.1 isohaline. Bottom row: sea level atmospheric pressure (hPa) and simulated wind-driven component of ice drift. Left and right columns are for 2002-2006 and 2007-2010, respectively. Large arrows show suggested spreading of Pacific Winter waters.

The characteristics of Pacific waters depend on water properties and transport in Bering Strait and on atmospheric conditions which modify these waters during their propagation over the shallow Chukchi Sea region. At this time, preliminary annual mean values (not shown) of the Bering Strait volume flux, temperature and salinity are available through 2009. The values suggest that 2008 and 2009 were slightly cooler than the period 2002-2007, but still warmer than measurements made between 1999 and 2001. The 2009 volume transport (~0.9Sv) was slightly higher than in 2008, but still less than the 2007 transport (>1Sv) which was the highest in the available record (spanning 1991-95 and 1998-2009). The 2009 heat flux was close to the long-term mean value, while the freshwater flux in 2009 was somewhat higher than the mean (due in part to the higher than average transports), but still less than previous maxima in 2004 and 2007. Mooring data are only available up to the summer of 2010. Temperatures in August 2010 were somewhat warmer than in August 2009, but the impact of this on the annual mean can only be assessed when an entire year of data is available. Similarly, the first half of 2010 was somewhat saltier than in 2009, although it is too soon to reach conclusions about annual mean freshwater flux.

Sea level

Sea level (SL) is a natural integral indicator of climate variability. It reflects changes in practically all dynamic and thermodynamic processes of terrestrial, oceanic, atmospheric and cryospheric origin. SL time series are available from nine coastal stations in the Siberian seas that have representative records for the period of 1954-2010 (Arctic and Antarctic Research Institute data archives). In 2010, SL along the Siberian coastline continued to decrease relative to 2008 and

2009 (Fig. SIO14). This caused a reduction in the estimated rate of SL rise for the nine stations since 1954 to 2.49 ± 0.45 mm yr^{-1} (after correction for glacial isostatic adjustment, GIA; Proshutinsky et al., 2004). Until the late 1990s, the SL time series correlates relatively well with the Arctic Oscillation (AO, Thompson and Wallace, 1998) index and with the inverse of the sea level atmospheric pressure (SLP) at the North Pole. Consistent with these influences, sea level declined significantly after 1990 and reached a minimum in 1996-1997, when the atmospheric circulation regime changed from cyclonic to anticyclonic. In contrast, from 1997 to 2006, mean SL has generally increased while the AO and SLP have remained more or less stable. After 2008, SL has tended to decrease and shown no apparent correlation with the AO or SLP at the North Pole. Since SL change exhibits large inter-annual variability and is the net result of many individual effects of environmental forcing, it is difficult to evaluate the significance of the change in relative terms. Although not statistically robust, the tendency toward decreasing SL rise may be due to steric effects associated with some reduction of surface ocean warming and stabilization of ocean freshwater content and/or with the wind regime shift over the Siberian seas.

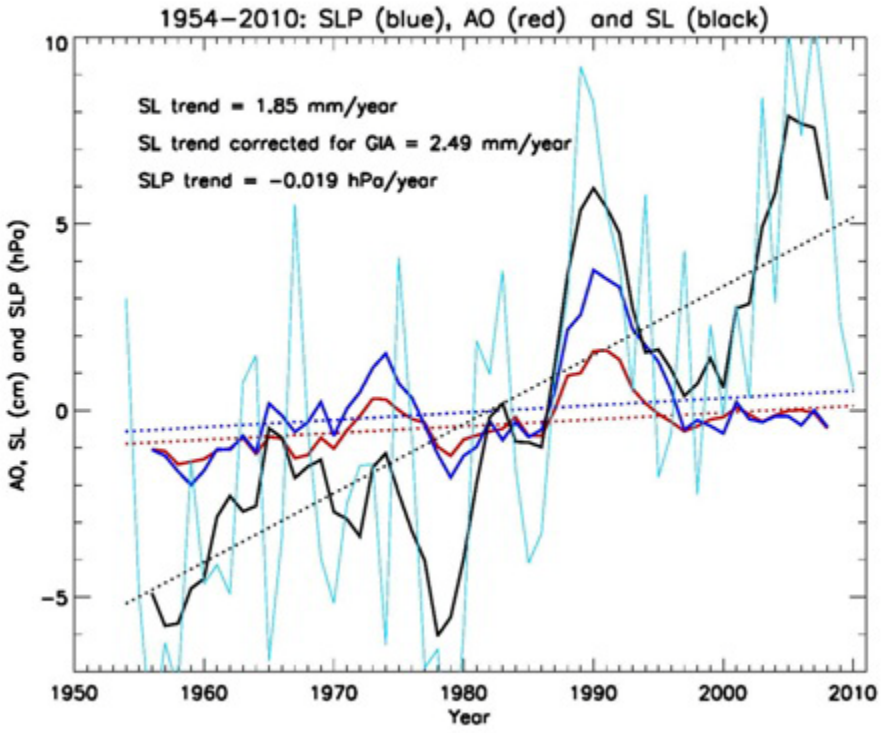

Fig. SIO14. Five-year running mean time series of: annual mean sea level at nine tide gauge stations located along the coasts of the Kara, Laptev, east Siberian, and Chukchi seas (black line); anomalies of the annual mean Arctic Oscillation index (AO, Thompson and Wallace, 1998) multiplied by 3 for better visual comparison with other factors (red line); sea surface atmospheric pressure at the North Pole (from NCAR-NCEP reanalysis data) multiplied by -1 (inverted barometer effect, dark blue line); and annual sea level variability (light blue line). Dotted lines depict trends for SL, AO and SLP.

References

Aagaard, K., and E. C. Carmack (1989), The role of sea ice and other freshwater in the Arctic circulation, J. Geophys. Res., 94, 14,485- 14,498.

Jackson, J. M., E. C. Carmack, F. A. McLaughlin, S. E. Allen, and R. G. Ingram, 2010: Identification, characterization, and change of the near-surface temperature maximum in the Canada Basin, 1993-2008, J. Geophys. Res., 115, C05021, doi:10.1029/2009JC005265.

McPhee M. G., A. Proshutinsky, J. H. Morison, M. Steele, M. B. Alkire, 2009: Rapid change in freshwater content of the Arctic Ocean, Geophys. Res. Lett., 36, L10602, doi:10.1029/2009GL037525.

Proshutinsky, A.Y. and M.A. Johnson. 1997: Two circulation regimes of the wind-driven Arctic Ocean. J. Geophys. Res. 102(C9 June 15): 12493-12514.

Proshutinsky A., and M. Johnson, 2011: Arctic Ocean Oscillation Index (AOO): interannual and decadal changes of the Arctic climate, Geophysical Research Abstracts Vol. 13, EGU2011-7850, 2011, EGU General Assembly 2011.

Proshutinsky, A., I. M. Ashik, E. N. Dvorkin, S. Hakkinen, R. A. Krishfield, and W. R. Peltier, 2004: Secular sea level change in the Russian sector of the Arctic Ocean, J. Geophys. Res., 109, C03042, doi:10.1029/2003JC002007.

Proshutinsky, A., R. Krishfield, M.-L. Timmermans, J. Toole, E. Carmack, F. McLaughlin, W. J. Williams, S. Zimmermann, M. Itoh, and K. Shimada, 2009: Beaufort Gyre freshwater reservoir: State and variability from observations J. Geophys. Res., doi:10.1029/2008JC005104.

Rabe, B., M. Karcher, U. Schauer, J. Toole, R. Krishfield, S. Pisarev, F. Kauker, R. Gerdes and T. Kikuchi, 2011: An assessment of Arctic Ocean freshwater content changes from the 1990s to 2006-2008", Deep-Sea Res. I, 58, p. 173-185, doi:10.1016/j.dsr.2010.12.002.

Reynolds, R. W., et al., 2002: An improved in situ and satellite SST analysis for climate, J. Clim., 15, 1609-1625.

Steele, M., J. Zhang, and W. Ermold, 2010: Mechanisms of summertime upper Arctic Ocean warming and the effect on sea ice melt, J. Geophys. Res., 115, C11004, doi:10.1029/2009JC005849.

Steele, M., W. S. Ermold, and J. Zhang, 2011: Modeling the formation and fate of the near-surface temperature maximum in the Canadian Basin of the Arctic Ocean, J. Geophys. Res., doi:10.1029/2010JC006803, in press.

Steele, M., J. Morison, W. Ermold, I. Rigor, M. Ortmeyer, and K. Shimada, 2004: Circulation of summer Pacific halocline water in the Arctic Ocean, J. Geophys. Res., 109, C02027, doi:10.1029/2003JC002009.

Timmermans, M-L., A. Proshutinsky, R. Krishfield, D. Perovich, J. Richter-Menge and J. Toole 2011: Surface freshening in the Arctic Ocean's Eurasian Basin: an apparent consequence of recent change in the wind-driven circulation, Geophysical Research Abstracts Vol. 13, EGU2011-1455, 2011, EGU General Assembly 2011.

Timokhov, L., and F. Tanis, Eds., 1997: Environmental Working Group Joint U.S.-Russian Atlas of the Arctic Ocean-Winter Period. Environmental Research Institute of Michigan in association with the National Snow and Ice Data Center, Arctic Climatology Project, CD-ROM.

Timokhov, L., and F. Tanis, Eds., 1998: Environmental Working Group Joint U.S.-Russian Atlas of the Arctic Ocean-Summer Period. Environmental Research Institute of Michigan in association with the National Snow and Ice Data Center, Arctic Climatology Project, CD-ROM.

Thompson, D. W. J., and J. M. Wallace, 1998: The Arctic oscillation signature in the wintertime geopotential height and temperature fields, Geophys. Res. Lett., 25(9), 1297-1300.

Toole, J. M., M.-L. Timmermans, D. K. Perovich, R. A. Krishfield, A. Proshutinsky, and J. A. Richter-Menge (2010), Influences of the ocean surface mixed layer and thermohaline stratification on Arctic Sea ice in the central Canada Basin , J. Geophys. Res. , 115 , C10018, doi:10.1029/2009JC005660.

Tremblay, J.-E., Y. Gratton, E. C. Carmack, C. D. Payne, and N. M. Price, 2002: Impact of the large-scale Arctic circulation and the North Water Polynya on nutrient inventories in Baffin Bay, J. Geophys. Res., 107(C8), 3112, doi:10.1029/2000JC00595.

Wijffels, S. E., R. W. Schmitt, H. L. Bryden, and A. Stigebrandt, 1992: Transport of freshwater by the oceans, J. Phys. Oceanogr., 22, 155- 162.

Yang, J., 2009: Seasonal and interannual variability of downwelling in the Beaufort Sea, J. Geophys. Res. , 114 , C00A14, doi:10.1029/2008JC005084.

The Extent and Controls on Ocean Acidification in the Western Arctic Ocean and Adjacent Continental Shelf Seas

J. T. Mathis

School of Fisheries and Ocean Science & Institute of Marine Science,
University of Alaska Fairbanks, Fairbanks, AK, 99709

November 9, 2011

Highlights

- Observations in the eastern Bering Sea have revealed aragonite undersaturation throughout the water column and areas of seasonal $CaCO_3$ mineral suppression.
- The effects of ocean acidification in the Chukchi Sea, induced by the uptake of anthropogenic CO_2 over the last century, are amplified by high rates of summertime phytoplankton primary production, which leads to increased seawater pCO_2 and decreased pH of sub-surface waters, which become more corrosive to $CaCO_3$.

Ocean acidification

It has been widely shown that the uptake of anthropogenic CO_2 by the oceans (e.g. Sabine et al., 2004; Sabine et al., 2007) has a significant effect on marine biogeochemistry by reducing seawater pH (Feely et al., 2009; Caldiera et al., 2003) and the saturation states (Ω) of important calcium carbonate ($CaCO_3$) minerals (Feely et al., 2004; Orr et al., 2005; Caldiera and Wickett, 2005) through a process termed "ocean acidification". Seawater exhibiting undersaturated conditions (i.e., $\Omega < 1$) are potentially corrosive for biogenic $CaCO_3$ minerals such as aragonite, calcite and high-Mg calcite. The reduction of $CaCO_3$ mineral saturation states in the surface ocean and along continental margins could have potentially negative consequences for benthic and pelagic calcifying organisms, and entire marine ecosystems (Fabry et al., 2008). Of even greater concern is the rate at which ocean acidification and $CaCO_3$ mineral saturation state suppression are progressing, particularly in the high latitude Pacific-Arctic Region (PAR) (Fig. SIO15) (Byrne et al., 2010; Fabry et al., 2009), where mixing processes and colder temperatures naturally precondition the water column to have lower pH and Ω values compared to more temperate ocean environments (Fig. SIO16).

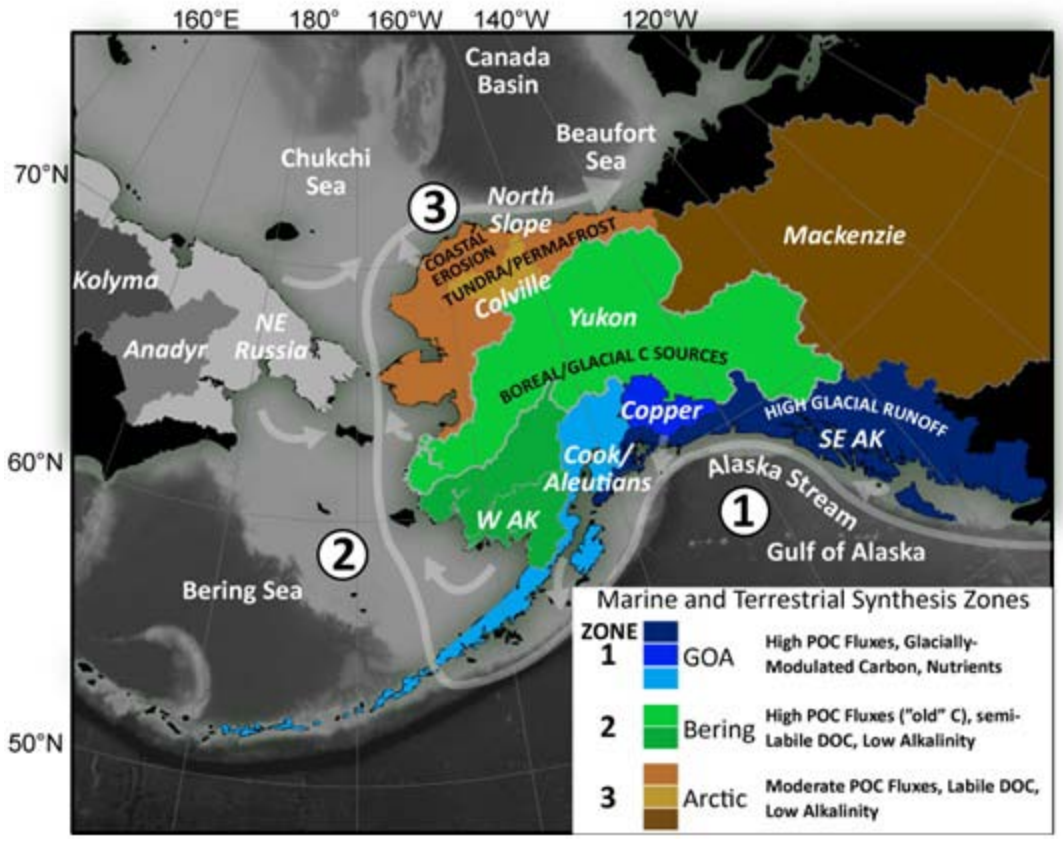

Fig. SIO15. Map of the Pacific Arctic Region (PAR) showing the major drainage basins and the associated biogeochemical properties that affect the carbon cycle. (1) Gulf of Alaska; (2) Bering Sea; and (3) Chukchi Sea. The color bars in the inset illustrate the various terrestrial drainage basins around North America and their predominant biogeochemical characteristics.

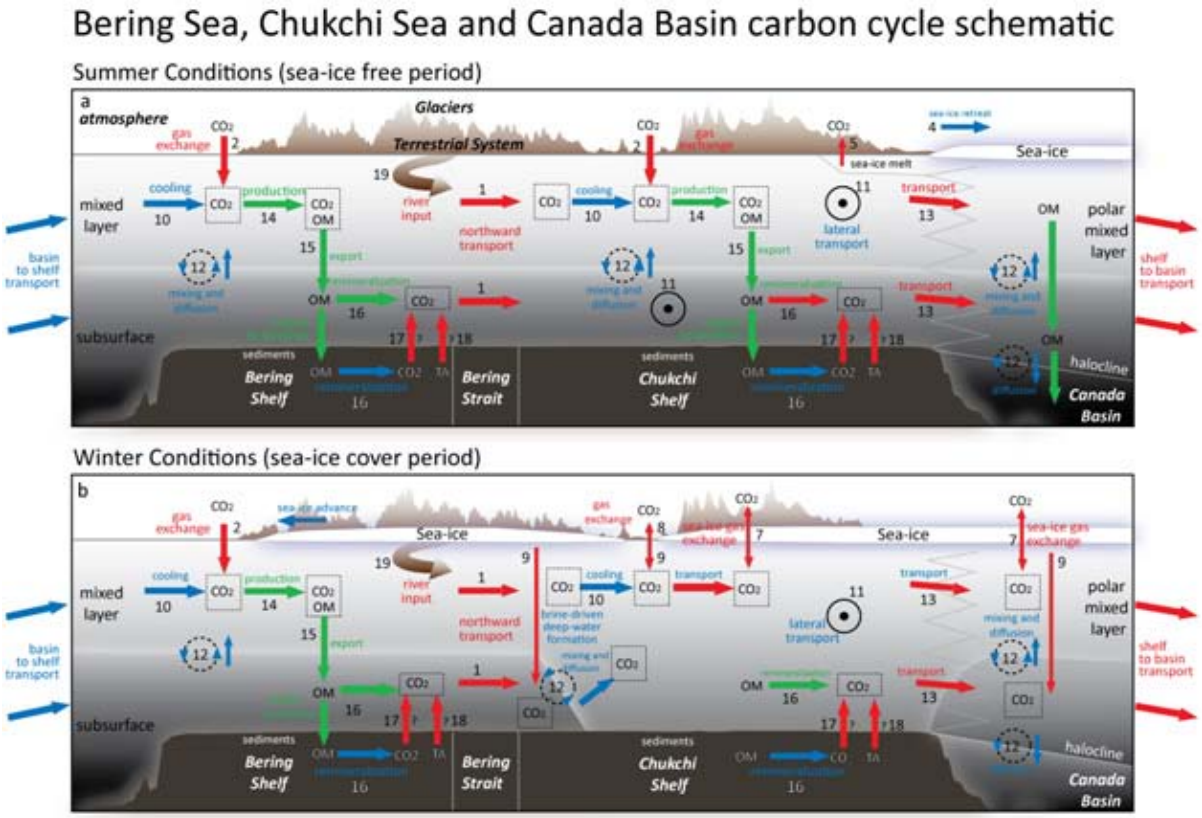

Fig. SIO16. Schematic of processes potentially influencing the inorganic carbon cycle and air-sea CO2 gas exchange in the western Arctic Ocean from the Bering Sea shelf through the Bering Strait, across the Chukchi Sea and northwards into the Canada Basin (from left to right) on "inflow" shelves of the Arctic (e.g., Barents and Chukchi seas). The two panels represent physical and biological processes likely operating during the summertime sea-ice free period (Panel a, top), and during the wintertime sea-ice covered period (Panel b, bottom). The processes are denoted by numeral with the caveat that the size of arrow does not necessarily reflect magnitude of flux, transport or transformation of CO2. The processes include: 1. northward transport of DIC; 2. air-sea gas exchange; 3. warming; 4. exposure of surface water to the atmosphere due to sea-ice retreat and melting; 5. localized air-sea gas exchange from surface water highly influenced by sea-ice melt; 7. air-sea gas exchange through sea-ice; 8. winter air-sea gas exchange in leads and polynyas; 9. inorganic carbon flux due to brine rejection during deep-water formation in fall and winter. 10. cooling of surface waters during northward transport of Atlantic or Pacific Ocean waters into the Arctic Ocean; 11. between-shelf transport of water and carbon; 12. redistribution of inorganic carbon between mixed layer and subsurface due to vertical diffusion and vertical entrainment/detrainment due to mixing; 13. shelf-basin exchanges of inorganic carbon (i.e., DIC) and organic carbon due to generalized circulation and eddy-mediated transport; 14. net uptake of CO_2 due to phytoplankton photosynthesis or new production; 15. export flux of organic matter (OM) or export production; 16. remineralization of organic matter back to CO_2 either in sub-surface waters or in sediments; 17. release of CO2 from sediments; 18. release of alkalinity from sediments due to anaerobic processes in sediments, and; 19. river runoff input. Adapted from Bates and Mathis, 2009.

Recent observations in the sub-Arctic north Pacific Ocean (Mathis et al., 2011) have already revealed areas of seasonal $CaCO_3$ mineral Ω suppression. Aragonite undersaturation has been observed throughout the water column, while models project widening areas of aragonite undersaturation in the region during the next several decades (Steinacher et al., 2009). Undersaturation has potentially negative consequences for the region because the expansive

continental shelf of the eastern Bering Sea sustains a commercially valuable fishery (Cooley and Doney, 2009; Cooley et al., 2009) that produces approximately 47% of the US fish catch by weight. This marine ecosystem is critical to both the regional and national economy as well as subsistence communities in Alaska that rely heavily on the seasonal fish catch as their primary source of protein. These new findings show that the eastern Bering Sea will likely be one of the first ocean acidification impact zones for US national interests. Therefore, it is critical to gain a better understanding of both the natural and anthropogenic controls on $CaCO_3$ mineral suppression in the region.

As observed in several open-ocean time-series, the uptake of anthropogenic CO_2 has already decreased surface water pH by 0.1 units. IPCC scenarios, based on present-day CO_2 emissions, predict a further decrease in seawater pH by 0.3 to 0.5 units over the next century and beyond (Caldeira and Wickett, 2003). Ocean acidification and decreased pH reduces the saturation states of calcium carbonate minerals such as aragonite and calcite, with many studies showing decreased $CaCO_3$ production by calcifying fauna (Buddemeier et al., 2004; Fabry et al., 2008) and increased $CaCO_3$ dissolution. The PAR is particularly vulnerable to ocean acidification due to relatively low pH and low temperature of polar waters compared to other waters (Orr et al., 2005; Steinacher et al., 2009) and low buffer capacity of sea-ice melt waters (Yamamoto-Kawai et al., 2009).

In the high latitude PAR, the uncoupling of primary production and grazing leads to high export rates of organic matter to the bottom waters and the sediments. When this organic matter is remineralized back into CO_2, it naturally decreases pH and suppresses carbonate mineral saturation states. However, the presence of anthropogenic CO_2 in the water column has caused bottom waters over some parts of the PAR shelves to become undersaturated in carbonate minerals (mostly aragonite, but in some locations calcite undersaturations have been observed).

The Bering Sea

The eastern shelf of the Bering Sea (Fig. SIO15) is a highly dynamic area that is influenced by a number of terrestrial and marine processes (Fig. SIO17) that affect seawater carbonate chemistry with considerable spatial, seasonal and inter-annual variability in the saturation states of the two most biogenically important $CaCO_3$ minerals: aragonite ($\Omega_{aragonite}$) and calcite ($\Omega_{calcite}$) (Mathis et al., 2011). The springtime retreat of sea ice, coupled with warming and seasonally high rates of freshwater discharge create distinctive horizontal and vertical zones over the shelf, each with their own unique characteristics (Stabeno et al., 1999). The onset of stratification in surface waters stimulates an intense period of phytoplankton primary production (PP), particularly over the middle region of the shelf where the confluence of macronutrient-rich Bering Sea water and coastal water replete in micronutrients is highest (Agular-Islas et al., 2007). In this region, historically referred to as the "*green belt*", rates of PP or net community production (NCP) can exceed 480 mg C m^{-2} d^{-1} while average rates across the shelf are ~330 mg C m^{-2} d^{-1}, making the eastern Bering Sea shelf one the most productive regions in the global ocean (Sambrotto et al., 2008; Mathis et al., 2010).

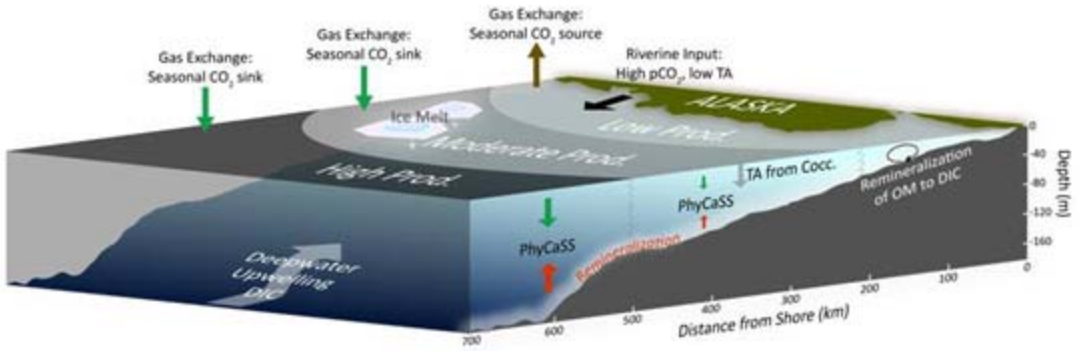

Fig. SIO17. Generalized description of the processes affecting the carbonate chemistry of the eastern Bering Sea shelf. The influx of runoff from the coast delivers water with high pCO_2, low TA, and moderate concentrations of dissolved organic matter (OM). The high pCO_2 of the water creates a seasonal source of CO_2 to the atmosphere while reducing carbonate mineral saturation states. Offshore, the upper water column is dominated by sea ice melt in late spring and summer that creates a highly stratified surface layer where primary production is controlled by the confluence of coastal waters rich in micronutrients and basin water replete in macronutrients. Seasonally high rates of NCP lead to a rapid drawdown of CO_2 at the surface creating a strong seasonal sink for atmospheric CO_2. In 2009, coccolithophore (Cocc.) blooms were observed in the intermediate shelf waters and lowered TA concentrations at the surface. The varying degree of export production at the surface determined the amount of remineralization that occurred at depth, which ultimately controlled saturation states. This PhyCaSS interaction can be observed to varying degrees across the shelf (adapted from Mathis et al., in press).

On the eastern Bering Sea shelf, a seasonal divergence in pH and Ω is observed between surface and sub-surface waters, driven primarily by the biology of the system (Mathis et al., 2010). During the spring phytoplankton bloom, high rates of NCP effectively remove CO_2 from the surface waters creating a strong seasonal disequilibrium with the atmosphere (Bates et al., 2010), but also increasing pH and Ω values by ~0.1 and ~1, respectively (Mathis et al., 2011). However, in sub-surface waters the opposite is observed, with pH and Ω values decreasing significantly (~0.3 and ~0.2, respectively) (Mathis et al., 2011). Much of the organic matter that is produced during the spring phytoplankton bloom is exported vertically out of the mixed layer. By mid-summer, the water-column becomes highly stratified and bottom waters are effectively isolated from surface waters over much of the shelf. The vertical export of organic matter and its subsequent seasonal remineralization at depth induces a significant build-up of CO_2 in bottom waters (i.e. pCO_2 increases) and concurrent suppression of $CaCO_3$ mineral Ω values (Mathis et al., 2010; Mathis et al., 2011). The seasonal divergence of pH and Ω in surface and sub-surface waters has been described in terms of a "Phytoplankton-Carbonate Saturation State" (PhyCaSS) (Bates et al., 2009). In 2008, sub-surface waters of the eastern Bering Sea shelf became undersaturated with respect to aragonite (but not calcite) (Mathis et al., 2011). It has also been shown that the addition of anthropogenic CO_2 to the ocean augments this natural seasonal interaction between ocean biology and seawater carbonate chemistry, tipping sub-surface waters below the saturation state threshold ($\Omega_{aragonite} = 1$) for aragonite. Increasing levels of atmospheric CO_2 could push the Bering Sea closer to a tipping point that could be detrimental for calcifying organisms.

The Western Arctic Ocean

In the Arctic Ocean, potentially corrosive waters are found in the sub-surface layer of the central basin (Jutterstrom and Anderson, 2005; Yamamoto-Kawai et al., 2009; Cheirici and Fransson, 2009), on the Chukchi Sea shelf (Bates et al., 2009) and in outflow waters of the Arctic found on the Canadian Arctic Archipelago shelf (Azetsu-Scott et al., 2010). In the Chukchi Sea, waters corrosive to $CaCO_3$ occur seasonally in the bottom waters, with unknown impacts on benthic organisms. The seasonally high rates of summertime phytoplankton primary production in the Chukchi Sea (see the essay on *Arctic Ocean Primary Productivity*) drives a downward export of organic carbon, which is remineralized back to CO_2, which in turn increases seawater pCO_2 (and decreasing pH) of sub-surface waters. Such a seasonal biological influence on the pH of sub-surface waters amplifies existing effects of ocean acidification induced by the uptake of anthropogenic CO_2 over the last century (Bates et al., 2009). Given the scenarios for pH changes in the Arctic, the Arctic Ocean and adjacent Arctic shelves, including the western Arctic, will be increasingly affected by ocean acidification, with potentially negative implications for shelled benthic organisms as well as those animals that rely on the shelf seafloor ecosystem.

Note: Acidification in the Canada Basin of the Arctic Ocean is described in the essay on *Ocean Biogeophysical Conditions*.

References

Aguilar-Islas, A.M., Hurst, M.P., Buck, K.N., Sohst, B., Smith, G.J., Lohan, M.C., and Bruland, K.W., 2007. Micro- and macronutrients in the southeastern Bering Sea: Insight into iron-replete and iron-depleted regimes. Progress in Oceanography, 73, 99-126.

Azetsu-Scott, K., Clarke, A., Falkner, K., Hamilton, J., Jones, E.P., Lee, C., Petrie, B., Prinsenberg, S., Starr, M., and, Yeats, P., 2010. Calcium carbonate saturation states in the waters of the Canadian Arctic Archipelago and the Labrador Sea. Journal of Geophysical Research-Oceans, 115, C11021, doi:10.1029/2009JC005917.

Bates, N.R., and Mathis, J.T., (2009). The Arctic Ocean marine carbon cycle: evaluation of air-sea CO_2 exchanges, ocean acidification impacts and potential feedbacks. Biogeosciences, 6, 2433-2459.

Bates, N.R., Mathis, J.T., Jefferies, M.A., (2010). Air-Sea CO2 fluxes on the Bering Sea Shelf. (Biogeosciences Discuss., 7, 1-44, 2010).

Buddemeier, R.W., Keypas, J.A., and Aronson, R.B., 2004. Coral reefs and global climate change: Potential contributions of climate change to stresses on coral reef ecosystems, report, 44 pp., Pew Center on Climate Change, Arlington, Va. (Available at http://www.pewclimate.org/global-warming-in-depth/all_reports/coral_reefs/)

Byrne, R.H., Mecking, S., Feely, R.A., and Liu, Z., 2010. Direct observations of basin-wide acidification of the North Pacific Ocean. Geophysical Research Letters, 37, L02601, doi:10.1029/2009GL040999.

Caldiera, K. and Wickett, M.E., 2003. Anthropogenic carbon and ocean pH. Nature, 425(6956), 365.

Caldiera, K., and Wickett, M.E., 2005. Ocean model predictions of chemistry changes from carbon dioxide emissions to the atmosphere and ocean. Journal of Geophysical Research - Oceans, 110(C9), C09S04.

Chierici, M., and Fransson, A., 2009. Calcium carbonate saturation in the surface water of the Arctic Ocean: undersaturation in freshwater influenced shelves. Biogeosciences, 6, 2421-2432, www.biogeosciences.net/6/2421/2009/.

Cooley, S.R., and Doney, S.C., 2009. Anticipating ocean acidification's economic consequences for commercial fisheries. Environmental Research Letters, 4, 024007, doi:10.1088/1748-9326/4/2/024007.

Cooley, S.R., Kite-Powell, H.L., and Doney, S.C., 2009. Ocean Acidification's potential to alter global marine ecosystem services. Oceanography, 22(4), 172-181.

Fabry, V.J., Seibel, B.A., Feely, R A., and Orr, J.C., 2008. Impacts of ocean acidification on marine fauna and ecosystem processes. ICES Journal of Marine Science, 65, 414-432.

Fabry, V.J., McClintock, J.B., Mathis, J.T., and Grebmeier, J.M., 2009. Ocean Acidification at high latitudes: the Bellwether. Oceanography, 22(4), 160-171.

Feely, R.A., Doney, S.C., and Cooley S.R., 2009. Ocean acidification: Present conditions and future changes in a high-CO_2 world. Oceanography 22(4), 36-47.

Feely, R.A., Sabine, C.L., Lee, K., Berelson, W., Keypas, J., Fabry, V J., and Millero, F. J., 2004. Impact of anthropogenic CO_2 on the $CaCO_3$ system in the oceans. Science, 305(5682), 362-266.

Jutterström, S., and Anderson, L.G., 2005. The saturation of calcite and aragonite in the Arctic Ocean. Marine Chemistry, 94, 101-110.

Mathis, J.T., Cross, J.N., Bates, N.R., (2011) Coupling Primary Production and Terrestrial Runoff to Ocean Acidification and Carbonate Mineral Suppression in the Eastern Bering Sea J. Geophys. Res., 116, C02030, doi:10.1029/2010JC006453, 2011.

Mathis, J.T., Cross, J.N., Bates, N.R., Lomas, M.L., Moran, S.B., Mordy, C.W., Stabeno, P., (2010). Seasonal Distribution of Dissolved Inorganic Carbon and Net Community Production on the Bering Sea Shelf (Biogeosciences, 7, 1769-1787, doi:10.5194/bg-7-1769-2010).

Orr, J.C., Fabry, V.J., Aumont, O., Bopp, L., Doney, S.C., Feely, R.A., Gnanadesikan, A., Gruber, N., Ishida, A., Joos, F., Key, R.M., Lindsay, K., Maier-Reimer, E., Matear, R., Monfray, P., Mouchet, A., Najjar, R.G., Plattner, G.K., Rodgers, K. B., Sabine, C.L., Sarmiento, J.L., Schlitzer, R., Slater, R.D., Totterdell, I J., Weirig, M.F., Yamanaka, Y., and Yool, A., 2005. Anthropogenic ocean acidification over the twenty-first century and its impact on calcifying organisms. Nature, 437(7059), 681-686.

Sabine, C.L., Feely, R.A., Gruber, N., Key, R. M., Lee, K., Bullister, J.L., Wanninkhof, R., Wong, C.S., Wallace, D.W.R., Tilbrook, B., Millero, F. J., Peng, T.-H., Kozyr, A., Ono, T., and Rios, A.F., 2004. The Oceanic Sink for Anthropogenic CO2. Science, 305(5682), 367-371.

Sabine, C.L. and Feely, R A., 2007. The oceanic sink for carbon dioxide. In D. Reay, N. Hewitt, J. Grace and K. Smith, Eds. Greenhouse Gas Sinks. pp. 31-49. CABI Publishing, Oxfordshire, UK.

Sambrotto, R.N., Mordy, C., Zeeman, S.I., Stabeno, P.J., and Macklin, S.A., 2008. Physical forcing and nutrient conditions associated with patterns of Chl a and phytoplankton productivity in the southeastern Bering Sea during summer. Deep Sea Research, II, 55, 1745-1760.

Stabeno, P. J., Schumacher, J.D., and Ohtani, K., 1999. The physical oceanography of the Bering Sea. In: T.R. Loughlin and K. Ohtani, Eds. Dynamics of the Bering Sea: A Summary of Physical, Chemical, and Biological Characteristics, and a Synopsis of Research on the Bering Sea. AK-SG-99-03, 1-28. North Pacific Marine Science Organization (PICES), University of Alaska Sea Grant, Fairbanks, AK.

Steinacher, M., Joos, F., Frolicher, T. L., Platter, G.-K., and Doney, S.C., 2009. Imminent ocean acidification of the Arctic projected with the NCAR global coupled carbon-cycle climate model. Biogeosciences, 6, 515-533.

Yamamoto-Kawai, M., McLaughlin, F.A., Carmack, E.C., Nishino, S., Shimada, K., (2009). Aragonite Undersaturation in the Arctic Ocean: Effects of Ocean Acidification and Sea Ice Melt. Science, Vol. 326. no. 5956, pp. 1098-1100.

Marine Ecosystems Summary

Section Coordinators: Sue Moore[1] and Mike Gill[2]

[1]NOAA Pacific Marine Environmental Laboratory, Seattle, WA, USA
[2]Canadian Wildlife Service, Environment Canada, Whitehorse, YT, Canada
& Conservation of Arctic Flora and Fauna (CAFF)/
Circumpolar Biodiversity Monitoring Programme

November 7, 2011

The Marine Ecosystem section of the 2012 Arctic Report Card highlights the highly variable nature of Arctic ecosystems and provides some insight into how the marine ecosystem and the biodiversity it supports are responding to changing environmental conditions. Recent changes in the marine ecosystem, from primary and secondary productivity to responses by some marine mammals species, are summarized in six essays. These essays provide a glimpse of what can only be described as profound, continuing changes in the Arctic marine ecosystem. For example, primary production by phytoplankton in the Arctic Ocean increased ~20% between 1998 and 2009, mainly as a result of increasing open water extent and duration of the open water season (see the essay on *Sea Ice*). Increases in primary production were geographically heterogeneous, with greatest increases found in the Kara (+70%) and Siberian (+135%) sectors. In addition to shifts in the total amount of production, recent observations indicate an earlier timing of phytoplankton blooms in the Arctic Ocean (advancing up to 50 days over the period 1997-2009), as well as community composition shifts towards a dominance of smaller phytoplankton species. These changes in production were accompanied by biogeochemical shifts in the system, including profound freshening of waters in the Canadian Basin (see the essay on *Ocean Temperature and Salinity*) and an undersaturation of the surface waters with respect to aragonite, a relatively soluble form of calcium carbonate found in plankton and invertebrates (see the essays on *Ocean Biogeophysical Conditions* and *Ocean Acidification*).

Shifts in primary and secondary production have direct impacts on benthic communities. Organic carbon supply to the benthos in regions of the northern Bering Sea has declined ~30-50%, as has the infaunal biomass of bivalves that are winter prey for the World population of the threatened spectacled eider. Recent changes in Arctic benthic biodiversity include shifts in community composition and biomass, which might be related to climate warming. In several cases, switches from longer-lived and slow-growing Arctic species and/or communities to faster-growing temperate species and/or communities reflect increasing water temperatures. Similarly, northern range extensions of several sea floor dwellers likely are tied to the warming habitat. In the Atlantic Arctic, this process is anticipated to result in the 'Atlantification' of the benthos, i.e., the replacement of Arctic communities with those endemic to the North Atlantic Ocean. New research on sediment-associated microbes, including bacteria, archaea, viruses and microscopic fungi, are currently expanding our knowledge of this topic.

Changes in the Marine Ecosystem are affecting higher-trophic species including seabirds and marine mammals. For example, 7 of 19 of the world's polar bear sub-populations are declining in number, with trends in two populations linked to reductions in sea ice. Thousands of walruses had hauled out on the NW coast of Alaska by mid-August 2011, the fourth time in the past five years for a behavior thought to be triggered by a lack of sea ice in the Chukchi Sea (see the essay on *Sea Ice*). These unprecedented haul-outs result in pup mortality by crushing and a switch in foraging by walrus from moving sea ice to static shore sites. Conversely, the decline in sea ice extends access to waters north of Bering Strait for feeding by seasonally-migrant baleen

whales. Sea ice reductions in the Northwest Passage also provided the opportunity for overlap between bowhead whales from the West Greenland and the Alaska populations, suggesting that reduced summer sea ice may facilitate exchange between the two populations.

Ocean Biogeophysical Conditions

M. Yamamoto-Kawai[1], W. Williams[2], S. Nishino[3], F. McLaughlin[2]

[1]Tokyo University of Marine Science and Technology, Tokyo, Japan
[2]Institute of Ocean Sciences, Fisheries and Oceans Canada, Sidney, British Columbia, Canada
[3]Japan Agency for Marine-Earth Science and Technology, Tokyo, Japan

November 8, 2011

Highlights

- In 2010 and 2011, the nutricline and associated chlorophyll maximum were slightly less deep than in 2009, but still significantly deeper than in 2003-2007. This is consistent with the slight relaxation of the Beaufort Gyre since 2009 (see the essay on *Ocean*).
- Undersaturation of the surface waters of the Canada Basin with respect to aragonite, a form of calcium carbonate found in plankton and invertebrates, was first observed in 2008. The areal extent of undersaturated surface water in 2011 was similar to that in 2010 (see the essay on *Ocean Acidification*).

As described in the *Ocean* essay, the quantity of fresh water stored in the Beaufort Gyre increased substantially in 2004-2005, 2006-2007 and 2007-2008, and has remained at high levels since 2008. These increases in freshwater content are due to inputs of sea-ice melt water (Yamamoto-Kawai et al. 2009) and strong Ekman pumping conditions (updates to Proshutinsky et al. 2009 and Yang 2009), and have increased the depth of the upper halocline in the interior of the Canada Basin (Fig. ME1a), freshened the surface waters (Fig. ME1b) and increased surface layer stratification (Fig ME1c). Consequently, there is a deeper nutricline and a deeper subsurface chlorophyll maximum, a feature that is closely associated with the top of the nutricline in summer and fall (Fig. ME1d; McLaughlin and Carmack 2010). In 2010 and 2011, the chlorophyll maximum and nutricline were slightly shallower than in 2009, but still significantly deeper than in 2003-2007. This is consistent with the slight relaxation of the Beaufort Gyre since 2009.

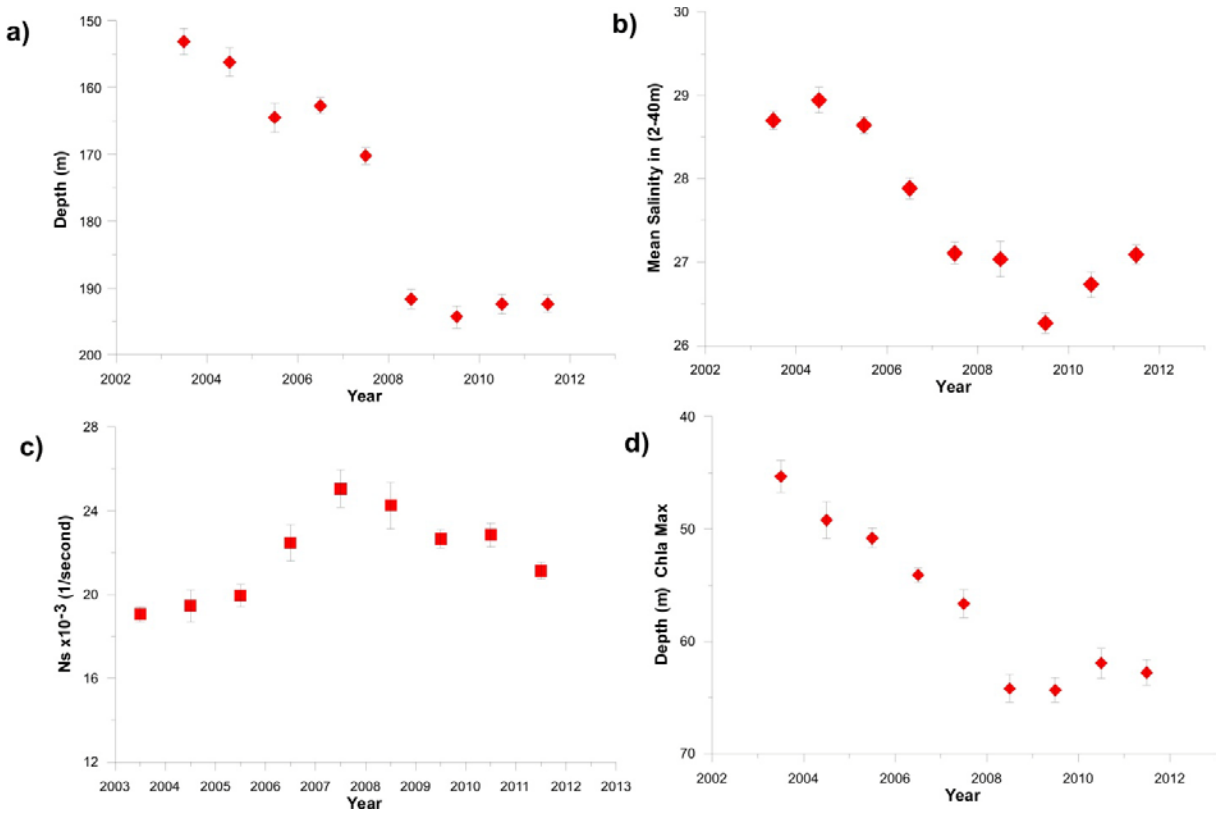

Fig. ME1. Average properties in the Beaufort Gyre region of the Canada Basin as observed by the Joint Ocean Ice Studies Expeditions: (a) average depth of the 33.1 isohaline; (b) mean salinity at 2-40 m depth; (c) average salinity stratification between 5-100m; (d) depth of the sub-surface chlorophyll maximum at the top of the nutricline.

These changes in the Beaufort Gyre are expected to stress biological production. Increased stratification is thought to lead to a reduction of overall nitrate fluxes into the mixed layer, a condition that limits new biological production and favors smaller organisms at the base of the food web (Li et al. 2009), while a deeper upper halocline further removes the nutricline and chlorophyll maximum from sunlight increasing the importance of light limitation.

In 2010, a large warm-core eddy was observed in the southwestern Canada Basin. This eddy carried ammonium from the shelf to the basin to sustain a higher biomass of picophytoplankton within the eddy (Nishino et al., 2011a). Such episodic transport of nutrients from the shelf to the Canada Basin by eddies is likely now more important to biological production as the nutricline is now deeper and those nutrients less available.

Biological productivity may be enhanced outside of the Beaufort Gyre in the Arctic Ocean. In the basins (e.g., Makarov Basin), this could be due to the nutrient supply from the shelves and greater light penetration for photosynthesis caused by the sea ice loss (see the essay on *Sea Ice*) (Nishino et al., 2011b). Over the Canadian and Alaskan Beaufort shelves, the same wind-forcing that drives Ekman convergence in the Beaufort Gyre is responsible for shelfbreak upwelling, which can act to bring nutrient-rich Pacific-origin water from depth into the euphotic zone (Carmack and Chapman 2003; Williams and Carmack 2008; Tremblay et al., 2011). Waters along these continental shelves are thus expected to become more productive because of increased exposure to upwelling favorable wind enhanced by reduced ice extent and a more

mobile ice pack that is more responsive to wind forcing (Yang 2009; Carmack and Chapman 2003).

Undersaturation of the surface waters of the Canada Basin with respect to aragonite, a form of calcium carbonate found in plankton and invertebrates, was first observed in 2008 (Yamamoto-Kawai et al., 2009). This rapid and large decrease in aragonite saturation state was caused by a combination of increased atmospheric CO_2 and melting of sea ice. The increased amount of open water (see the essay on *Sea Ice*) enhanced the uptake of CO_2 from the atmosphere and the freshening of the upper ocean (see the essay on *Ocean*) decreased alkalinity, inorganic carbon and calcium ion concentrations (Yamamoto-Kawai et al., 2011). Although CO_2 concentration in surface waters in 2010 and 2011 was not as high as in 2008 (Cai et al., 2009), these waters have continued to be undersaturated with respect to aragonite. The areal extent of undersaturated surface water in 2011 was similar to that in 2010. For more information on ocean acidification, see the essay on *The Extent and Controls on Ocean Acidification in the Western Arctic Ocean and Adjacent Continental Shelf Seas*.

References

Cai, W.-J., et al., 2010, Decrease in the CO2 uptake capacity in an ice-free Arctic Ocean Basin, Science, 329, 556-559, doi:10.1126/science.1189338.

Carmack, E. C. and D. C. Chapman, 2003, Wind-driven shelf/basin exchange on an Arctic shelf: The joint roles of ice cover extent and shelf-break bathymetry, Geophys. Res. Lett., 30, 1778 doi:10.10.1029/2003GL017526.

Li W.K., F.A. McLaughlin, C. Lovejoy, E.C. Carmack, 2009: Smallest Algae Thrive As the Arctic Ocean Freshens, Science, Vol. 326. no. 5952, p. 539, doi:10.1126/science.1179798.

McLaughlin, F. A. and E. C. Carmack, 2010: Deepening of the nutricline and chlorophyll maximum in the Canada Basin interior, 2003-2009, Geophys. Res. Lett., 37, L24602, doi:10.1029/2010GL045459.

Nishino, S., M. Itoh, Y. Kawaguchi, T. Kikuchi, and M. Aoyama, 2011a; Impact of an unusually largewarm-core eddy on distributions of nutrients and phytoplankton in the southwestern Canada Basin during late summer/early fall 2010, Geophys. Res. Lett., 38, L16602, doi:10.1029/2011GL047885.

Nishino, S., T. Kikuchi, M. Yamamoto-Kawai, Y. Kawaguchi, T. Hirawake, and M. Itoh, 2011b; Enhancement/reduction of biological pump depends on ocean circulation in the sea-ice reduction regions of the Arctic Ocean, J. Oceanogr., 67, 305-314, doi:10.1007/s10872-011-0030-7.

Proshutinsky, A., R. Krishfield, M.-L. Timmermans, J. Toole, E. Carmack, F. McLaughlin, W. J. Williams, S. Zimmermann, M. Itoh, and K. Shimada, 2009: Beaufort Gyre freshwater reservoir: State and variability from observations J. Geophys. Res., doi:10.1029/2008JC005104.

Tremblay, J.-É., S. Bélanger, D. G. Barber, M. Asplin, J. Martin, G. Darnis, L. Fortier, Y. Gratton, H. Link, P. Archambault, A. Sallon, C. Michel, W. J. Williams, B. Philippe, and M. Gosselin, 2011; Climate forcing multiplies biological productivity in the coastal Arctic Ocean, Geophys. Res. Lett., 38, L18604, doi:10.1029/2011GL048825.

Williams, W. J. and E. C. Carmack, 2008: Combined effect of wind-forcing and isobath divergence on upwelling at Cape Bathurst, Beaufort Sea, Journal of Marine Research, 66, 645-663.

Yamamoto-Kawai, M., F. A. McLaughlin, E. C. Carmack, S. Nishino, K. Shimada, 2009: Aragonite Undersaturation in the Arctic Ocean: Effects of Ocean Acidification and Sea Ice Melt, Science, Vol. 326. no. 5956, pp. 1098-1100. doi: 10.1126/science.1174190

Yamamoto-Kawai, M., F. A. McLaughlin, and E. C. Carmack (2011), Effects of ocean acidification, warming and melting of sea ice on aragonite saturation of the Canada Basin surface water, Geophys. Res. Lett., 38, L03601, doi:10.1029/2010GL045501.

Yang, J., 2009: Seasonal and interannual variability of downwelling in the Beaufort Sea, J. Geophys. Res., 114 , C00A14, doi:10.1029/2008JC005084.

Arctic Ocean Primary Productivity

K. E. Frey[1], K. R. Arrigo[2], R. R. Gradinger[3]

[1]Graduate School of Geography, Clark University, Worcester, MA, USA
[2]Department of Environmental Earth System Science, Stanford University, Stanford, CA, USA
[3]School of Fisheries and Ocean Sciences, University of Alaska Fairbanks, Fairbanks, AK, USA

November 8, 2011

Highlights

- Phytoplankton primary production in the Arctic Ocean increased ~20% from 1998-2009, mainly as a result of increasing open water extent and duration of the open water season. Increases in primary production were greatest in the eastern Arctic Ocean, particularly in the Kara (+70%) and Siberian (+135%) sectors.
- In addition to shifts in the total amount of production, new observations indicate an earlier timing of phytoplankton blooms in the Arctic Ocean (advancing up to 50 days over the 1997-2009 period) as well as community composition shifts towards a dominance of smaller phytoplankton species.

Sea ice melt and break-up during spring strongly drive primary production in the Arctic Ocean and its adjacent shelf seas by enhancing light availability as well as increasing stratification and stabilization of the water column. Recently observed dramatic declines in sea ice extent, thickness and annual persistence (see the essay on *Sea Ice*) should, therefore, have profound consequences for primary production throughout the region. Recent studies indeed document significant increases in primary production in several sectors of the Arctic Ocean, in addition to significant shifts in the timing and species composition of phytoplankton blooms.

Newly compiled satellite observations of primary production in the Arctic Ocean over a 12-year period (1998-2009) reveal a ~20% overall increase, resulting primarily from increases in open water extent (+27%) and duration of the open water season (+45 days) (Arrigo and van Dijken, 2011). However, no statistically significant secular trend in net primary production per unit area was found, stressing the overall importance of sea ice decline in driving these observed trends. Of the eight geographic sectors of the Arctic Ocean investigated (Fig. ME2, four exhibited statistically significant trends in primary production over the 12-year time period: Greenland (-13%), Kara (+70%), Siberian (+135%), and Chukchi (+48%). For the Arctic Ocean as a whole, annual phytoplankton primary production averaged 493 ± 41.7 Tg C yr^{-1} over the 1998-2009 period (based on direct satellite observations), as opposed to an estimate of 438 ± 21.5 Tg Cyr^{-1} over the 1979-1998 period (based on linear relationships with open water extent). However, these overall estimates are likely conservative, as they do not account for potential productivity that may occur within or beneath sea ice cover.

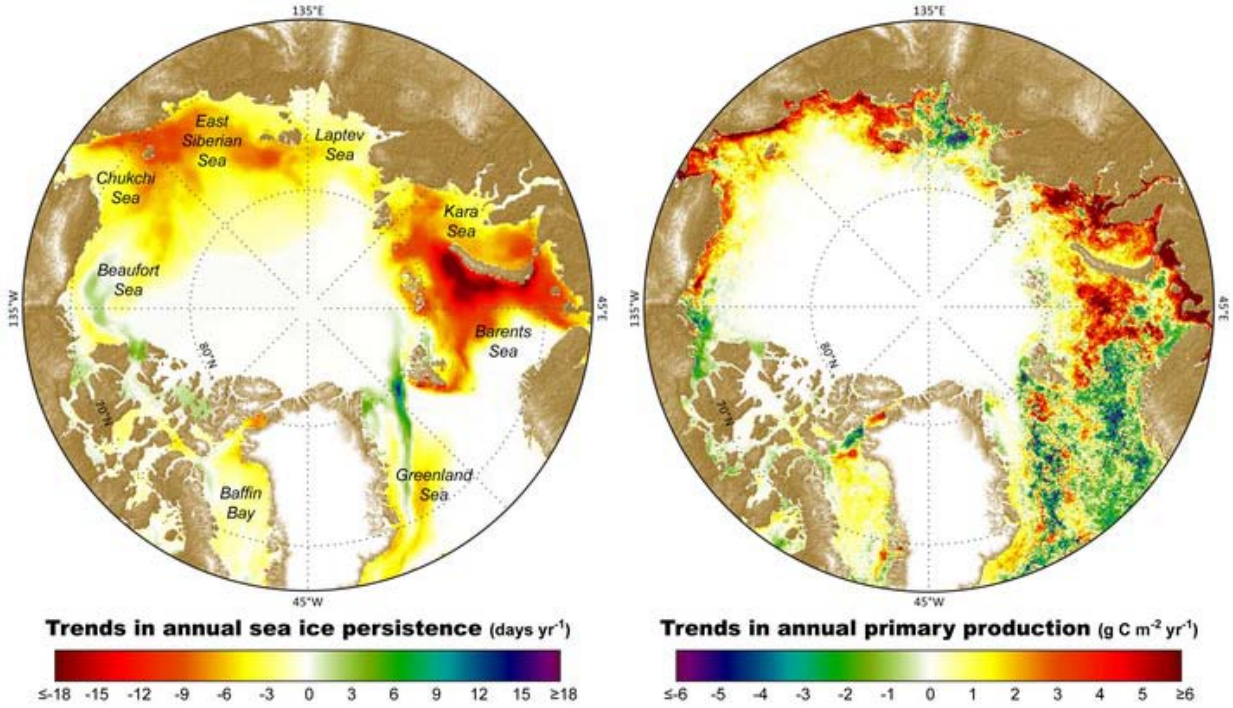

Fig. ME2. Trends in annual sea ice persistence (left) and total annual net primary production (right) across the Arctic Ocean and its adjacent shelf seas from 1998-2009. Sea ice persistence data (based on a 15% sea ice concentration threshold) are derived from Special Sensor Microwave/Imager passive microwave radiances (Cavalieri et al., 2008) and primary production data are from Arrigo and van Dijken (2011).

In addition to phytoplankton primary production, sea ice algal production is also important to consider in the overall Arctic Ocean system. During periods of sea ice cover, total primary productivity is generally relatively small compared to estimates in open seas. As such, the central Arctic Ocean (with its historically multi-year ice cover) is one of the least productive marine regions on Earth, with annual primary production rates estimated at ~14 g C m^{-2} yr^{-1}. During periods of ice cover, primary production by sea ice algae can be an important contributor to these overall production rates. Furthermore, release of ice algal material not only can act as a seed for phytoplankton blooms, but also may provide important food for pelagic and benthic biota (Leu et al., 2011). Annual estimates of the contribution of sea ice algal production to total production varies, with lowest contributions in the shelf seas (<10%) and highest contributions in the central Arctic Ocean (>50%) (Gosselin et al., 1997).

New observations of the timing of phytoplankton blooms in the Arctic Ocean show significant changes. Kahru et al. (2010) report significant trends towards earlier phytoplankton blooms for 11% of the area of the Arctic Ocean that is observable with satellite imagery over the 1997-2009 period. Areas experiencing earlier blooms in particular include those in the Hudson Bay, Foxe Basin, Baffin Sea, Greenland coasts, Kara Sea and near Novaya Zemlya, which are also areas roughly coincident with trends towards earlier sea ice break-up during early summer. In some of these regions, peak blooms in phytoplankton production have advanced from September to early July (a shift of up to ~50 days). Wassmann (2011) suggests that earlier sea ice retreats also cause earlier onset of the pelagic bloom, thus shortening the growth season of ice algae (which in turn is restricted to occur earlier because of critical limitations of available sunlight). The timing of phytoplankton and/or sea ice algal production is critical for the quantity and quality of primary production and associated grazers and therefore also the transfer of carbon and

energy to higher trophic levels in both pelagic and benthic communities (Grebmeier et al., 2010, Tremblay et al., 2011; also see the essay on *Marine Ecology: Biological Responses to Changing Sea Ice and Hydrographic Conditions in the Pacific Arctic Region*).

The community composition of phytoplankton blooms in the Arctic has also shown measurable trends, with recent observations revealing shifts towards a dominance of smaller sized phytoplankton. With a freshening of the Arctic Ocean and associated reduction in the supply of nutrients, trends towards a dominance of smaller picophytoplankton over larger nanophytoplankton have been observed (Li et al., 2009). Even though the total amount of production may not change, a smaller community size structure of primary producers generally may not allow for large transfers of carbon up the food chain.

References

Arrigo, K. R., and G. L. van Dijken (2011), Secular trends in Arctic Ocean net primary production. Journal of Geophysical Research 116, C09011, doi:10.1029/2011JC007151.

Cavalieri, D., C. Parkinson, P. Gloersen, and H. J. Zwally (2008), Sea Ice Concentrations from Nimbus-7 SMMR and DMSP SSM/I Passive Microwave Data. Boulder, Colorado USA: National Snow and Ice Data Center. Digital media.

Gosselin, M., M. Levasseur, P. A. Wheeler, R. A. Horner, and B. C. Booth (1997), New measurements of phytoplankton and ice algal production in the Arctic Ocean. Deep-Sea Research-II 44, 1623-1644.

Grebmeier, J. M., S. E. Moore, J. E. Overland, K. E. Frey, and R. R. Gradinger (2010), Biological response to recent Pacific Arctic sea ice retreats. Eos, Transactions, American Geophysical Union 91, 161-162.

Kahru, M., V. Brotas, M. Manzano-Sarabia, and B. G. Mitchell (2010), Are phytoplankton blooms occurring earlier in the Arctic? Global Change Biology, doi: 10.1111/j.1365-2486.2010.02312.x.

Leu, E., J. E. Søreide, D. O. Hessen, S. Falk-Petersen, and J. Berge (2011), Consequences of changing sea-ice cover for primary and secondary producers in the European Arctic shelf seas: Timing, quantity, and quality. Progress in Oceanography 90, 18-32.

Li, W. K. W., F. A. McLaughlin, C. Lovejoy, and E. C. Carmack (2009), Smallest algae thrive as the Arctic Ocean freshens. Science 326, 539.

Tremblay, J.-É., S. Bélanger, D. G. Barber, M. Asplin, J. Martin, G. Darnis, L. Fortier, Y. Gratton, H. Link, P. Archambault, A. Sallon, C. Michel, W. J. Williams, B. Philippe, and M. Gosselin (2011), Climate forcing multiplies biological productivity in the coastal Arctic Ocean, Geophys. Res. Lett., 38, L18604, doi:10.1029/2011GL048825.

Wassmann, P. (2011), Arctic marine ecosystems in an era of rapid climate change. Progress in Oceanography 90, 1-17.

Biodiversity - Status and Trends of Benthic Organisms

B. A. Bluhm[1] and J. M. Grebmeier[2]

[1]School of Fisheries and Ocean Sciences, University of Alaska Fairbanks, Fairbanks, AK, USA
[2]Center for Environmental Science, University of Maryland, Solomons, MD, USA

November 21, 2011

Highlights

- A recent (2010-2011) inventory documented the occurrence of at least 4600 benthic animal species in the Arctic, with at least hundreds of species yet to be discovered.
- Recent studies indicate changes in benthic community composition and biomass in relation to climate warming in both the Pacific and Atlantic sectors.
- Changes in the benthic biomass in some Arctic seas, or parts thereof, likely reflect shifts in energy flux patterns related to regional sea ice loss.
- Snow crab populations have expanded northward and commercially-harvestable size specimens have been observed in both the Barents Sea and on the Beaufort Sea slope.

The newest estimate of Arctic benthic faunal species indicates at least 4600 species inhabit the Arctic sea floor (Bluhm et al. 2011). Several hundred species, if not thousands, are estimated to still be discovered (Piepenburg et al. 2011), in particular in the Arctic deep sea and within small size classes. As a result of concentrated efforts related primarily to the International Polar Year and the Census of Marine Life, several dozen benthic species were newly described in the past few years (of at least 100 discovered). Taxa included a broad range of groups such as bristle worms, moss animals, snails and crustaceans, and were discovered in poorly-charted territory such as the Canada Basin as well as well-sampled areas such as Svalbard's Hornsund Fjord.

A good 10% of all known Arctic benthic species now have part of their genetic make-up, the so-called COI (cytochrome c oxidase sub-unit 1 mitochondrial region) 'barcode' gene, archived in publicly-accessible online databases. These and other new sequence data confirm past morphological analyses in documenting high population connectivity of the Arctic fauna to Atlantic and Pacific faunas.

A gradually increasing body of literature documents recent changes in Arctic benthic biodiversity, community composition and biomass, interpreted in the light of climate warming (Grebmeier 2012). In several cases, switches from longer-lived and slow-growing Arctic species and/or communities to faster-growing temperate species and/or communities reflect increasing water temperatures. Similarly, northern range extensions of several sea floor dwellers likely are tied to the warming habitat. In the Atlantic Arctic, this process is anticipated to result in the 'Atlantification' of the benthos. New research on sediment-associated microbes, including bacteria, archaea, viruses and microscopic fungi, are currently expanding our knowledge of this topic.

An example species of high interest is the snow crab, a crustacean commercially harvested in the southeastern Bering Sea and Canadian north Atlantic Ocean. A self-sustaining population of

snow crab has recently established itself in the Barents Sea, and specimens of harvestable size were recently found on the western Beaufort Sea slope.

A new data-rich estimate of global benthic biomass distribution confirms historic data documenting comparatively high biomass on Arctic shelves compared to lower latitudes. Recent changes in benthic biomass in some Arctic seas, or parts thereof, probably reflect shifts in energy flux patterns, regionally related to sea ice loss. Biomass changes over the past one to three decades include decreases in infaunal biomass in parts of the Bering Sea, increase in epifaunal biomass in parts of the Bering and Chukchi seas, decrease in epifaunal biomass in deep Fram Strait, and no changes in a Svalbard fjord system.

Examples of the sparse but much-needed long-term observations that are documenting changes in the benthos include those from: (1) the HAUSGARTEN deep sea observatory, which has been in operation since 1999 in Fram Strait; and (2) the Pacific Arctic shelves (Fig. ME3 where observations have been made for almost 30 years (see the essay on *Marine Ecology: Biological Responses to Changing Sea Ice and Hydrographic Conditions in the Pacific Arctic Region*).

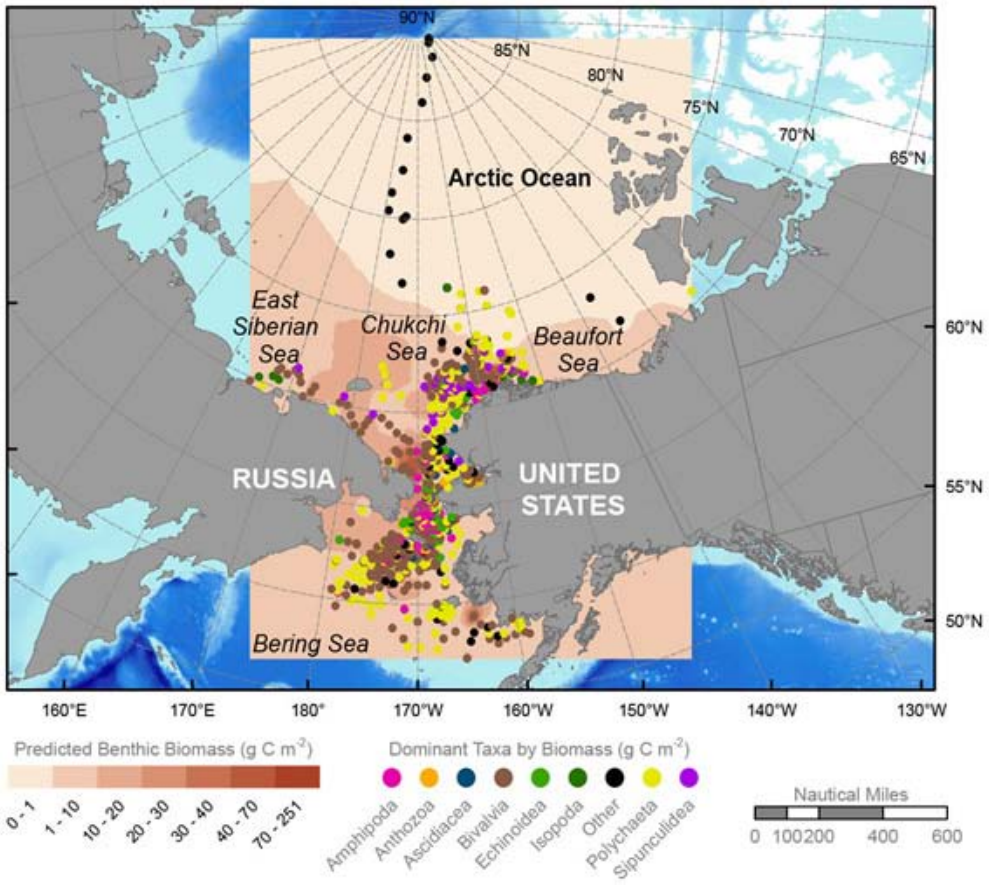

Fig. ME3. Dominant benthic infaunal taxa and biomass for stations sampled in the northern Bering and Chukchi seas and into the Canada Basin from 1973-2010 (updated from Grebmeier et al. 2006, plus unpublished data through 2010, and data from Bluhm et al. 2011).

References

Bluhm B. A., Gebruk A.V., Gradinger R., Hopcroft R. R., Huettmann F., Kosobokova K. N., Sirenko S. I., Weslawski J. M. (2011) Arctic marine biodiversity - an update of species richness and examples of biodiversity change. Oceanography 24:232-248.

Grebmeier J. M. (2012) Shifting patterns of life in the Pacific Arctic and Sub-Arctic seas. Ann Rev Mar Sci 4:16.1-16.16 (in press, doi: 10.1146/annurev-marine-120710-100926.

Piepenburg D., Archambault P., Ambrose W. G. Jr., Blanchard A., Bluhm B. A., Carroll M. L., Conlan K., Cusson M., Feder H. M., Grebmeier J. M., Jewett S. C., Lévesque M., Petryashev V. V., Sejr M. K., Sirenko B., Włodarska-Kowalczuk M. (2011) Towards a pan-Arctic inventory of the species diversity of the macro- and megabenthic fauna of the Arctic shelf seas. Marine Biodiversity 41:51-70.

Biodiversity - Status and Trends of Polar Bears

D. Vongraven[1] and E. Richardson[2]

[1]Norwegian Polar Institute, Fram Center, Tromso, Norway
[2]Science and Technology Branch, Environment Canada, Edmonton, Alberta, Canada

November 8, 2011

Highlights

- The status of polar bear populations has been assessed at both national (5 national assessments) and international level, and 7 of 19 of the World's polar bear sub-populations are found to declining in number, with trends in two linked to reductions in sea ice.

Introduction

Polar bears (*Ursus maritimus*) have a circumpolar distribution that is influenced by the distribution and availability of sea ice. Sea ice provides the primary platform on which polar bears travel, hunt, mate and, in some areas, den. Polar bears prey primarily on ice associate seals (ringed seals, bearded seals, harp seals, hooded seals) and to a lesser extent on other marine mammals (e.g., walrus and whales). As a result, climate-mediated changes in the availability of sea ice (see the essay on *Sea Ice*) have the potential to significantly influence the availability of prey for bears, potentially affecting individual growth, reproduction and survival.

Status and trends

The world's polar bear population is estimated to be between 20,000-25,000 bears occurring in 19 relatively discrete sub-populations around the Arctic (Fig. ME4 Of these 19 sub-populations, eight were classified as data deficient due to a lack of recent information by the IUCN/Polar Bear Specialist Group (PBSG) in 2009 (Obbard et al. 2010). Since then the trend assessment of the Davis Strait sub-population has been updated, from declining to stable, and there is a new abundance estimate for the Foxe Basin sub-population from 2010, changing the status assessment of that sub-population from being data deficient to being not reduced (Table ME1). However, of the 12 sub-populations currently considered as having sufficient data to assess a population trend, only three have good trend data (western Hudson Bay, northern Beaufort and southern Beaufort).

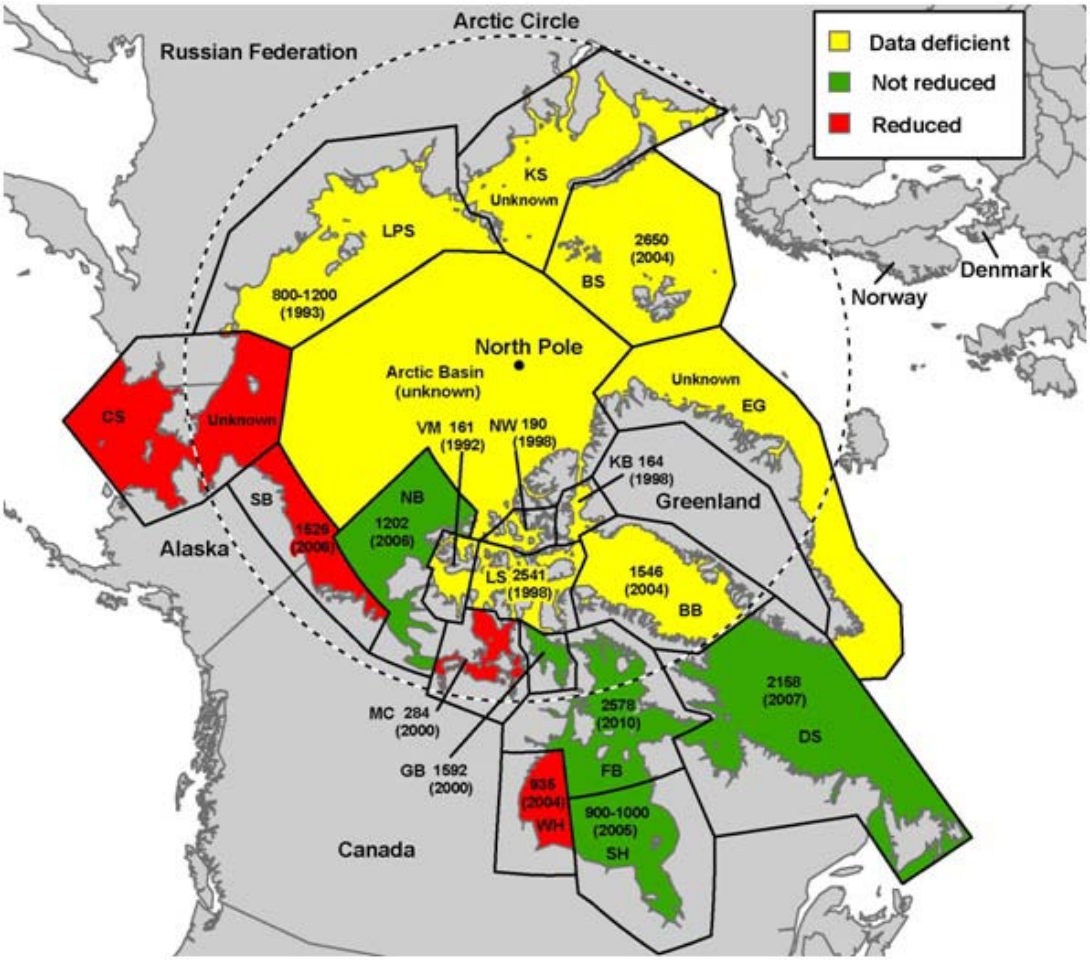

Fig. ME4. Status assessments and the best or most recent abundance estimates for the world's 19 polar bear sub-populations (updated from Obbard et al. 2010, see Table ME1).

Table ME1. Abundance estimates and assessments of status and trends for the 19 acknowledged sub-populations of polar bears (based on Obbard et al. 2010).

Subpopulation	Abundance estimate (year of estimate)	Trend	Status
Arctic Basin	unknown	Data deficient	Data deficient
Baffin Bay	1546 (2004)	Decline [1]	Data deficient
Barents Sea	2650 (2004)	Data deficient	Data deficient
Chukchi Sea	unknown	Decline	Reduced
Davis Strait	2158 (2007)	Stable[2]	Not reduced
East Greenland	unknown	Data deficient	Data deficient
Foxe Basin	2578 (2010)[3]	Data deficient	Not reduced
Gulf of Boothia	1592 (2000)	Stable	Not reduced
Kane Basin	164 (1998)	Decline	Data deficient
Kara Sea	unknown	Data deficient	Data deficient
Lancaster Sound	2541 (1998)	Decline	Data deficient
Laptev Sea	800-1200 (1993)	Data deficient	Data deficient
M'Clintock Channel	284 (2000)	Increase	Reduced
Northern Beaufort Sea	1202 (2006)	Stable	Not reduced
Norwegian Bay	190 (1998)	Decline	Data deficient
Southern Beaufort Sea	1526 (2006)	Decline	Reduced
Southern Hudson Bay	900-1000 (2005)	Stable	Not reduced
Viscount Melville	161 (1992)	Data deficient	Data deficient
Western Hudson Bay	935 (2004)	Decline	Reduced

[1] On-going study to validate status assessment

[2] Elizabeth Peacock (pers.comm.)

[3] Seth Stapleton (pers. comm.)

There are still seven sub-populations showing a declining trend, and it is expected that, if sea ice conditions continue to degrade across the Arctic, several other sub-populations may be threatened as a result of habitat loss and decreased access to prey, i.e., ice-associated seals. There have been criticisms that, except for the long data series on body condition related to sea ice break-up in spring in Western Hudson Bay, there have been little hard data to support any effect of climate warming on polar bears. This is clearly changing, and at this point in time two of these sub-populations are believed to be in decline (western Hudson Bay and southern Beaufort Sea) as a result of climate-mediated changes in the availability of sea ice. Specifically, changes in the seasonal availability of sea ice have been shown to influence polar bear survival in western Hudson Bay (Regehr et al. 2007) and survival and breeding rates in the southern Beaufort Sea (Regehr et al. 2010).

There is still little or no knowledge on status and trends for the East Greenland sub-population or the two sub-populations under exclusive Russian jurisdiction (Laptev Sea and Kara Sea).

Formal status assessments

The status of polar bears has been assessed at both the international and national level resulting in the following assessments:

- International Union on the Conservation of Nature (IUCN Red List): *Vulnerable*
- (http://www.iucnredlist.org/apps/redlist/details/22823/0)
- Norway (Norwegian Red List): *Vulnerable*
- (http://www.biodiversity.no)
- Russia (The Red Data Book): *Uncertain, Rare, and Rehabilitated/Rehabilitating* (a specific Russian classification for the Russian sub-populations; Russia acknowledges three sub-populations within its territory while PBSG acknowledges four).
- United States (Endangered Species Act): *Threatened*
- (http://ecos.fws.gov/speciesProfile/SpeciesReport.do?spcode=A0IJ)
- Greenland: *Vulnerable*
- (http://www.artsdatabanken.no/Grønlands_Rødliste_2007_DK_IiZsU.pdf.file)
- Canada (COSEWIC): *Species of Special Concern*
- (http://www.sararegistry.gc.ca/virtual_sara/files/cosewic/sr_polar_bear_0808_e.pdf)

Knowledge gaps

Despite substantial research and monitoring of polar bears in some areas of the Arctic there is a general lack of knowledge in regards to how the cumulative effects of climate warming, contaminants, disease, harvest, industrial development and other human activities are likely to interact to influence the status of the world's polar bear sub-populations. In an effort to address both the individual and cumulative effects of these stressors, the Conservation of Arctic Flora and Fauna Working Group of the Arctic Council (CAFF) has facilitated the development of a Circumpolar Polar Bear Monitoring Plan that will provide advice on approaches for the coordinated collection and synthesis of the data required to effectively manage and mitigate existing threats to polar bear conservation.

References

Obbard, M.E., Thiemann, G.W., Peacock, E., and DeBruyn, T.D. (eds) (2010). Polar Bears: Proceedings of the 15th Working Meeting of the IUCN/SSC Polar Bear Specialist Group, Copenhagen, Denmark, 29 June-3 July 2009. Gland, Switzerland and Cambridge, UK: IUCN. vii + 235 pp.

Regehr, E.V., Lunn, N.J., Amstrup, S.C. & Stirling, I. 2007. Effects of earlier sea ice breakup on survival and population size of polar bears in western Hudson Bay. Journal of Wildlife Management 71:2673-2683.

Regehr, E.V., Hunter, C.M., Caswell, H., Amstrup, S.C. and Stirling, I. 2010. Survival and breeding of polar bears in the southern Beaufort Sea in relation to sea ice. Journal of Animal Ecology 79: 117-127.

Biodiversity - Cetaceans and Pinnipeds (Whales and Seals)

P. O. Thomas[1] and K. L. Laidre[2]

[1]US Marine Mammal Commission, Bethesda, MD USA
[2]Polar Science Center, Applied Physics Laboratory,
University of Washington, Seattle WA USA

November 23, 2011

Highlights

- Thousands of walruses hauled out on the NW coast of Alaska by mid-August 2011, the fourth time this has been observed in the past five years. The behavior is thought to be triggered by reduced sea ice in the Chukchi Sea.
- Observations of overlap between bowhead whales from the Baffin Bay and the Bering-Chukchi-Beaufort populations in the Northwest Passage indicate that reduced summer sea ice may facilitate exchange between the two populations.

Arctic biodiversity assessment

Over the past several years, the Arctic Report Card for Marine Mammals has presented available information on the population status of Arctic marine mammals. In 2011, the "Arctic Biodiversity Assessment - Status and Trends" (ABA) was launched by the Arctic Council's Working Group on Conservation of Arctic Flora and Fauna (CAFF) to synthesize and assess the status and trends of biological diversity in the Arctic. The report, due out in 2013, will inventory and update the status and trends of all stocks of Arctic marine mammals, and will be presented in the next Arctic Report Card.

Arctic marine mammal movements and distribution relative to ice

Pacific walruses: Diminishing Arctic sea-ice, and specifically the retreat of the pack-ice beyond the continental shelf of the Chukchi Sea, has resulted in Pacific walruses (*Odobenus rosmarus divergens*) hauling out on land by the thousands along the Alaskan coast of the Chukchi Sea in the summer. While fall migratory aggregations (October-November) have been seen on the Alaskan coast in the past (notably at Cape Lisburne) the summer haul-outs are new and occur primarily north of Point Lay (Garlich-Miller et al. 2011). Radio-tagging studies conducted in the Chukchi Sea by the U.S. Geological Survey since 2007 have demonstrated that walruses remain offshore over the continental shelf feeding grounds for as long as possible, hauling out on sparse marginal ice. When suitable ice disappears, some animals move west toward Russia but the majority move to land haul-outs on the Alaska coast (http://alaska.usgs.gov/science/biology/walrus/index.html). Jay et al. (2010) showed that walruses prefer to stay in particular areas of the Chukchi Sea rather than remain with specific ice floes as they drift. This indicates their dependence on shallow bottom feeding areas in the summer months. Bayesian network models, designed to integrate potential effects of changing environmental conditions and anthropogenic stressors on Pacific walruses demonstrate a clear future trend of worsening conditions for the sub-species (Jay et al. 2011). Also see the essay on

Marine Ecology: Biological Responses to Changing Sea Ice and Hydrographic Conditions in the Pacific Arctic Region.

Bowhead whales: Satellite tagging studies of bowhead whales (*Balaena mysticetus*) shed light on how this large baleen whale species uses sea ice habitat. In the Pacific Arctic, bowhead whales undertake their spring migration, north along the Alaskan Chukchi Sea coast and eastward across the Beaufort Sea, through 80-100% ice cover (Quakenbush et al. 2010). After feeding in the Canadian Beaufort Sea they move westward in late summer, often feeding along the way, especially near Barrow, Alaska, and along the Russian Chukotka coast. http://www.adfg.alaska.gov/index.cfm?adfg=marinemammalprogram.bowheadmovements

In August 2010, two satellite tagged bowhead whales, one from Disko Bay, West Greenland and one from Alaska, entered the Northwest Passage from opposite directions and spent approximately 10 days in the same area. This is the first time distributional overlap between the two populations, which have been assumed to be separated by sea ice, has been documented. Reduced summer sea ice in the Northwest passage may remove this geographic barrier and facilitate exchange between the populations (Heide-Jørgensen et al. 2011). In East Greenland, Lydersen et al. (2011) reported the first satellite-tagged bowhead whale from the critically endangered Spitsbergen stock, and found movements consistent with the patterns described for bowhead whales in this region by the early whalers in the 16th and 17th century.

Beluga whales and narwhals: In West Greenland, a clear relationship between decreasing annual sea ice cover in Baffin Bay and increasing offshore distance of beluga (*Delphinapterus leucas*) sightings was established based on 30 years of aerial survey data, suggesting belugas expand their distribution westward as new areas on the banks of West Greenland open up earlier in spring with reduced sea-ice coverage (Heide-Jørgensen et al. 2011). Recent analysis of sea ice trends in autumn on narwhal (*Monodon monoceros*) summering grounds has documented freeze-up occurring roughly 2 to 4 weeks later since 1979. Four ice entrapments occurred in the summering areas between 2008 and 2011; however, it is not clear if the entrapments are due to random variation in narwhal residence time in summer areas, or whether there is a trend in prolonged summer residence time as narwhals adapt to a longer open water season (Laidre et al. 2011).

Tagged marine mammals as environmental sensors

Marine mammals are increasingly becoming sources of information on conditions around Arctic Seas, building oceanographic baselines and allowing observations of changing conditions beyond what is practical with ship-borne or aerially-deployed instruments. In Baffin Bay, 14 narwhals equipped with satellite-linked time-depth-temperature recorders provided wintertime temperature data for Baffin Bay. These animal-borne instruments confirmed earlier measurements of warming winter water temperatures in Baffin Bay associated with a warming West Greenland Current (Laidre et al. 2010). Hooded seals (*Cristophora cristata*) carrying similar instruments provided detailed oceanographic data for a significant portion of the northeast Atlantic Ocean, which have allowed scientists to study how freshwater moves from the Arctic Ocean into the North Atlantic through the Fram Strait (Fig. ME5) (Lydersen et al. 2010). For more information on ocean temperature and freshwater content, see the essay on *Ocean*.

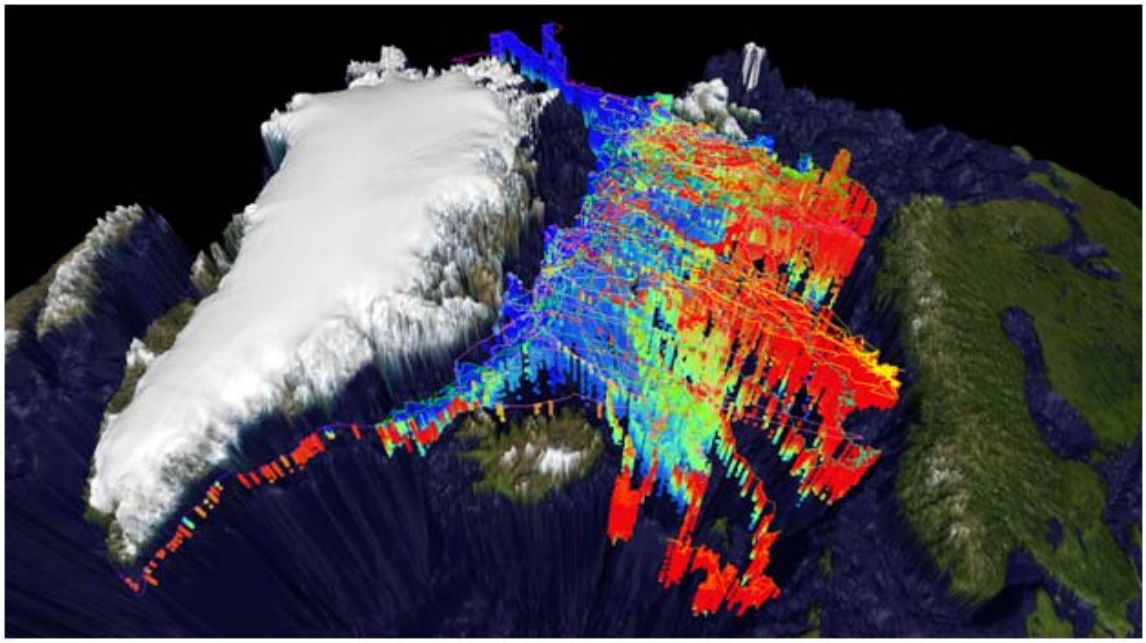

Fig. ME5. Tagged hooded seals provided water temperature profiles from an area of over 3 million km2 in the Greenland and Norwegian Seas, from south of the Faroe Islands almost to the North Pole, and from the surface to over 1,000 m depth (Kovacs et al., 2011). Water temperatures recorded are from -2 °C (dark blue) to +9 °C (red).

Marine mammals and changes in prey

Changing sea-ice formation, extent and concentration are the most visible manifestations of climate change in the Arctic. The impacts of these changes on the timing and location of primary and secondary production are just now starting to be understood (see the essay on *Arctic Ocean Primary Productivity*). Uncertainty about how changes in production will affect trophic structure leads to concerns whether Arctic marine mammal species will continue to find adequate food and be able to compete with more temperate species in a warmer, more seasonally ice-free environment (Kovacs et al. 2010). Early loss of sea-ice over the continental shelf is predicted to reduce the productivity of the benthic communities marine mammals such as walruses and gray whales (*Eschrichtius robustus*) feed upon (see the essay on *Marine Ecology: Biological Responses to Changing Sea Ice and Hydrographic Conditions in the Pacific Arctic Region*).

Patterns of seasonal ice cover likely influence the availability of bowhead prey by affecting light penetration and wind-driven upwelling (Ashjian et al. 2010). Extreme sea-ice retreats in the Pacific Arctic sector (see the essay on *Sea Ice*) may actually improve foraging opportunities for bowheads (Moore et al. 2010, Tremblay et al. 2011). As temperature changes lead to changing prey species assemblages, some hypothesize that lipid-rich arctic prey species will be replaced by leaner temperate species, reducing the ability of the most arctic-adapted marine mammals (e.g., bowheads, narwhals, ringed seals) to replenish essential blubber stores in the short summer season (Kovacs et al. 2010).

In winter, narwhals feed intensively in dense pack ice over the continental slope in central Baffin Bay and Davis Strait, selecting areas of nearly 100% ice cover in order to remain above the highest densities of their preferred Greenland halibut prey. Narwhal winter distribution appears

to be dictated by optimal foraging areas rather than sea ice density or the presence of open water, and a recent study has documented densities of over 70 narwhals/km^2 in preferred pack ice foraging areas with <3% open water (Laidre and Heide-Jørgensen 2011).

References

Ashjian, C. J., S. R. Braund, R. G. Campbell, J. C. George, J. Kruse, W. Maslowski, S. E. Moore, C. R. Nicolson, S. R. Okkonen, B. F. Sherr, E. B. Sherr, and Y. H. Spitz, 2010: Climate Variability, Oceanography, Bowhead Whale Distribution, and Iñupiat Subsistence Whaling near Barrow, Alaska. Arctic, 63, 179-194.

Garlich-Miller, J. L., J. G. MacCracken, J. Snyder, R. Meehan, M. J. Myers, J. M. Wilder, E. Lance, and A. Matz, 2011: Status review of the Pacific walrus (*Odobenus rosmarus divergens*). U.S. Fish and Wildlife Service, Marine Mammals Management, January 2011, Anchorage, AK, 155 pp.

Heide-Jørgensen M. P., K.L. Laidre, L. T. Quakenbush, and J. Citta, 2011: Northwest Passage opens for bowhead whales. Biology Letters, in press.

Heide-Jørgensen M. P., K. L. Laidre, D. Borchers, T. A. Marques, H. Stern, and M. J. Simon, 2010: The effect of sea ice loss on beluga whales (*Delphinapterus leucas*) in West Greenland. Polar Research, 29, 198-208.

Jay C. V., M. S. Udevitz, R. Kwok, A. S. Fischbach, D. C. Douglas, 2010: Divergent movements of walrus and sea ice in the northern Bering Sea. MEPS 407, 293-302.

Jay, C. V., B. G. Marcot, D. C. Douglas, 2011: Projected status of the Pacific walrus (*Odobenus rosmarus divergens*) in the twenty-first century. Polar Biol., doi:10.1007/s00300-011-0967-4.

Kovacs, K.M., M. Biuw, O.A. Nøst, P. Dodd, E. Hansen, Q. Zhou, M. Fedak, and C. Lydersen, 2011: Seals used as "research assistants" in the polar oceans. International Polar Year 2007-2008: The Norwegian Contribution, O. Orheim and K. Ulstein, Eds., Research Council of Norway, 100-103.

Kovacs, K. M., C. Lydersen, J. E. Overland, and S. E. Moore, 2010: Impacts of changing sea-ice conditions on Arctic marine mammals. Mar. Biodiv., doi:10.1007/s12526-010-0061-0.

Laidre, K. L., M. P. Heide-Jørgensen, W. Ermold, and M. Steele, 2010: Narwhals document continued warming of southern Baffin Bay. Journal of Geophysical Research., 115, doi:10.1029/2009JC005820.

Laidre, K. L. and M. P. Heide-Jørgensen, 2011: Life in the lead: extreme densities of narwhals *Monodon monoceros* in the offshore pack ice. Mar Ecol Prog Ser., 423, 269-278.

Laidre K. L., M. P. Heide-Jørgensen, H. Stern, P. Richard, 2011: Unusual sea ice entrapments and delayed autumn ice-up timing reinforce narwhal vulnerability to climate change. Polar Biology, doi:10.1007/s00300-011-1036-8.

Lydersen, C., M. Biuw, O.A. Nøst, P. Dodd, E. Hansen, Q. Zhou, M.A. Fedak, T. Haug, and K.M. Kovacs, 2010: Satellite tracking of hooded seals (*Cystophora cristata*) in the Greenland Sea using CTD-tags: oceanography and biology. Marine Mammals of the Holarctic: Collection of

Scientific Papers after the Sixth International Conference, Kaliningrad, Russia, 11-15 October 2010. pp. 325-327.

Lydersen, C., C. Freitas, Ø. Wiig, L. Bachmann, M. P Heide-Jørgensen, R. Swift, and K. Kovacs, 2011: Lost highway not forgotten: satellite tracking of a bowhead whale (*Balaena mysticetus*) from the critically endangered Spitsbergen stock. Endangered Species Research, in press.

Moore, S. E., J. C. George, G. Sheffield, J. Bacon, and C. J. Ashjian, 2010: Bowhead Whale Distribution and Feeding near Barrow, Alaska, in Late Summer 2005-06. Arctic, 63, 195-205.

Quakenbush, L. T., J. J. Citta, J. C. George, R. J. Small, and M .P. Heide-Jørgensen, 2010: Fall and winter movements of bowhead whales (*Balaena mysticetus*) in the Chukchi Sea and within a petroleum development area. Arctic, 63, 289-307.

Tremblay, J.-É., S. Bélanger, D. G. Barber, M. Asplin, J. Martin, G. Darnis, L. Fortier, Y. Gratton, H. Link, P. Archambault, A. Sallon, C. Michel, W. J. Williams, B. Philippe, and M. Gosselin, 2011; Climate forcing multiplies biological productivity in the coastal Arctic Ocean, Geophys. Res. Lett., 38, L18604, doi:10.1029/2011GL048825.

Marine Ecology: Biological Responses to Changing Sea Ice and Hydrographic Conditions in the Pacific Arctic Region

J. M. Grebmeier[1], L. W. Cooper[1], S. E. Moore[2]

[1]Chesapeake Biological Laboratory, University of Maryland Center for Environmental Science, Solomons, Maryland, 20688 USA
[2]NOAA/Fisheries, Office of Science & Technology, Seattle, Washington, 98115 USA

November 21, 2011

Highlights

- Organic carbon supply to the benthos in regions of the northern Bering Sea has declined ~30-50%, as has the infaunal biomass of bivalves that are winter prey for the world population of the threatened spectacled eider.
- Changes in the distribution and biomass of some plankton and benthic prey are being observed in the Pacific Arctic with corresponding shifts in higher trophic predator feeding and migration patterns.

Seasonal sea ice duration and extent are critical factors driving biological processes and marine ecosystem structure. The seasonal ice zones have a direct influence on sea ice algal biomass and productivity and also provide early stabilization of the water column following sea ice melt, which can lead to intense phytoplankton blooms (see the essay on *Arctic Ocean Primary Productivity*). The timing and location of this primary production and associated grazing by zooplankton has a direct influence on the energy pathways connecting the water column to the underlying sediments. Recent studies indicate that increasing seawater temperature can have a positive impact on zooplankton growth rates (see the essay on *Status and Trends of Benthic Organisms*) and grazing rates. However, these changes will have the potential to diminish export production of carbon that currently supports globally significant soft-bottom infaunal populations on the shallow shelves of many areas of the Pacific Arctic (citations in Grebmeier et al. 2012). The short food chains characteristic of polar regions can have immediate cascading impacts on higher trophic organisms, including diving seaducks, seals, walruses, and whales. This is particularly the case when many of these apex predators require ice as a moving offshore feeding and resting platform that provides access to offshore foraging areas. In light of the changing dynamics of Arctic seasonal sea-ice (see the essay on *Sea Ice*), the marine ecosystems in polar regions will likely respond to both short-term population changes and long-term restructuring as sea ice retreat continues.

Some of the best-documented examples of biological response to physical forcing in the Pacific Arctic sector are prey-predator response to hydrographic shifts. For example, a reduction in sea ice provides access for seasonally-migrant baleen whales to feed north of Bering Strait (Moore and Huntington 2008). Gray whales now feeding north of the Bering Strait are likely responding to declines in benthic amphipod populations in the historical northern Bering Sea feeding grounds (citations in Grebmeier et al. 2012). Another change is in dominant clam populations in the northern Bering Sea, which have declined in abundance and biomass, as have Spectacled Eiders that preferentially consume these clams as prey. Modeling by Lovvorn et al. (2009) indicates that these diving birds lose more energy resting in the water between feeding bouts

than when standing on ice. Thus, both the shift to more open-water conditions and the observed clam population declines are likely key factors creating energy stress for these diving seaducks. The recent observations of thousands of walrus coming ashore on both the US and Russia Chukchi coastlines are another indication of biological response to rapid sea ice retreat in the Chukchi Sea (see the essay on *Biodiversity - Cetaceans and Pinnipeds*). In addition to the increased mortalities for young walruses on beaches in close proximity to much larger adults, all of these shore-based populations have increased energetic requirements to access the productive offshore waters with higher benthic infaunal prey (citations in Grebmeier et al. 2012).

Over the last two decades specific marine sites have been occupied and re-occupied during both national and international ship-based projects. The data collected by these projects is forming a growing biologically-oriented time-series ranging geographically from the northern Bering Sea to Barrow Canyon. One of the most complete times-series is in the northern Bering Sea and includes sediment community oxygen consumption (Fig. ME6 upper panel), which is used as an indicator of carbon supply to the benthos. These data indicate a 30-50% decline over the last two decades coincident with ~30% decline in total infaunal biomass (Fig. ME6 lower panel). Other related evidence indicates a spatial shift northward in some fish distributions and marine mammal migrations, with direct impacts on habitat for ice-dependent species, such as walrus (citations in Grebmeier et al. 2012).

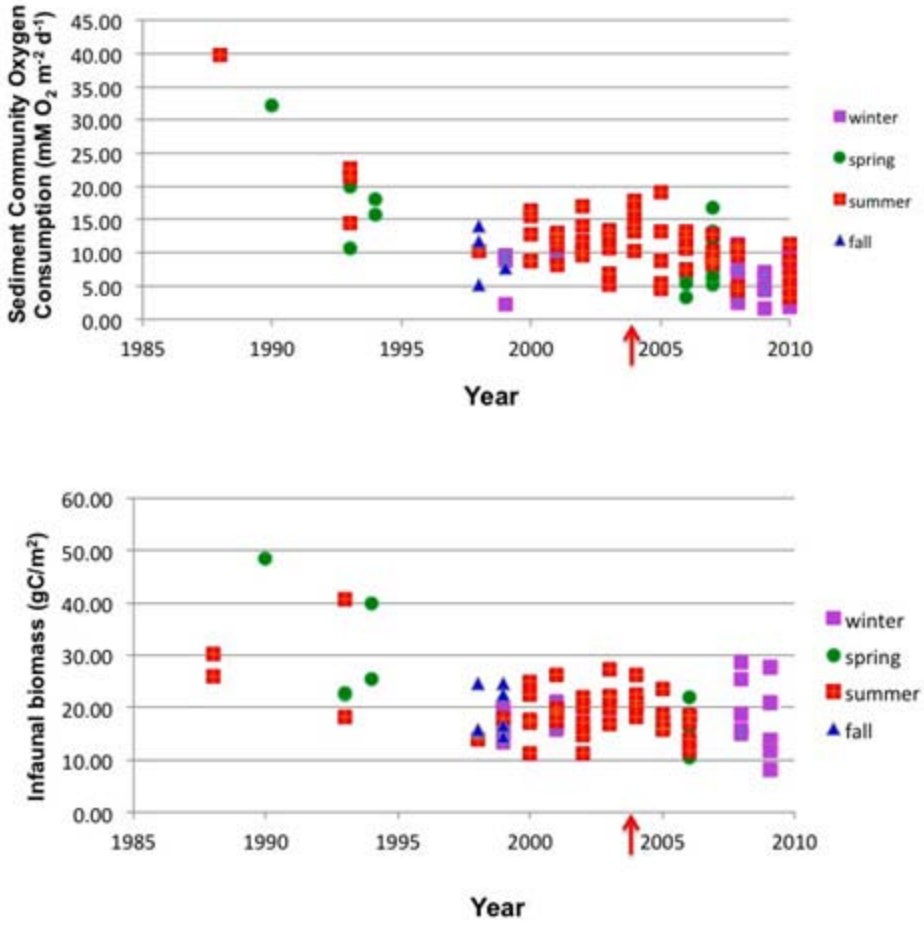

Fig. ME6. Decline in sediment community oxygen consumption (SCOC; upper panel), which indicates a reduced carbon supply to the benthos and macroinfaunal biomass (lower panel) at sites southwest of St. Lawrence Island in the northern Bering Sea. Data updated from Grebmeier et al. 2006; red arrow indicates the start of those new data. Most benthic data illustrated are available at: http://www.eol.ucar.edu/projects/sbi (phase I, Dunton, Grebmeier & Maidment component; and phase II, Grebmeier & Cooper component) and http://www.eol.ucar.edu/projects/best (Grebmeier & Cooper component).

The biological response to sea ice retreat and environmental change is being tracked through coordination among scientists in the Pacific Arctic Group (http://pag.arcticportal.org/). This voluntary international interest and working group has initiated a "Distributed Biological Observatory (DBO)" that includes select biological measurements of lower trophic level species that are tied to higher trophic level species, as well as undertaking coordinated hydrographic measurements. The DBO is developing as a change detection array for the identification and consistent monitoring of biophysical responses. Data sets from 2010-2011 pilot studies, along with other biological time series results, and information are available at http://www.arctic.noaa.gov/dbo/. Efforts are also underway to network the DBO with biological observatories in the Eurasian Arctic, e.g., the "HAUSGARTEN" deep water biological observatory, and developing transect-based biodiversity sampling on behalf of the CBMP (Circumpolar Biodiversity Monitoring Program) of the Arctic Council (http://caff.is/monitoring).

References

Grebmeier, J. M. 2012: Shifting patterns of life in the Pacific Arctic and Sub-Arctic seas. Ann. Rev. Mar. Sci., 4: 16.1-16.16 (in press, doi: 10.1146/annurev-marine-120710-100926).

Grebmeier, J. M, J. E. Overland, S. E. Moore, E. V. Farley, E. C. Carmack, L. W. Cooper, K. E. Frey, J. H. Helle, F. A. McLaughlin, and L. McNutt, 2006b: A major ecosystem shift in the northern Bering Sea. Science, 311: 1461-1464.

Lovvorn, J. R., J.M. Grebmeier, L.W. Cooper, J.K. Bump, and J.G. Richman, 2009: Modeling marine protected areas for threatened eiders in a climatically shifting Bering Sea, Ecol. Applic., 19(6), 1596-1613.

Moore, S.E. and H.P. Huntington. 2008. Arctic marine mammals and climate change: impacts and resilience. Ecological Applications 18(2): S157-S165.

Terrestrial Ecosystems Summary

Section Coordinators: D. A. "Skip" Walker[1] and Mike Gill[2]

[1]University of Alaska Fairbanks, Fairbanks, AK, USA
[2]Canadian Wildlife Service, Environment Canada, Whitehorse, YT, Canada
& Conservation of Arctic Flora and Fauna (CAFF) / Circumpolar Biodiversity Monitoring Programme

November 10, 2011

The Terrestrial Ecosystem section of the 2012 Arctic Report Card illustrates the interconnections between the Arctic marine and terrestrial ecosystems. An example is the direct link between increases in Arctic tundra vegetation productivity and earlier peak productivity in many parts of the Arctic on one hand and increasing duration of the open water season and decreasing summer sea ice extent on the other (see the essay on *Sea Ice*).

The Normalized Difference Vegetation Index (NDVI) shows that there is a long-term trend of increased biomass production in many parts of the Arctic. Over the whole Arctic from 1982 to 2010, the maximum summer NDVI increased by an average of 8%. However, there is considerable spatial variability, ranging from a 26% increase in lands adjacent to the Beaufort Sea to a small decline in several areas. The areas of greatest increase appear to be correlated with adjacent coastal areas that have experienced dramatic retreats in summer sea ice extent (see the essay on *Sea Ice*). Despite these long-term trends, annual variation is significant. In 2009, circumpolar NDVI showed a dip that corresponded to elevated atmospheric aerosols and generally cooler summer temperatures over the Arctic. Then, in 2010, NDVI rebounded strongly in North America, but less so in Eurasia. Information from long-term ground-based observations shows that, in addition to increasing air temperatures and loss of summer sea ice, widespread greening is also occurring in response to other factors. These include landslides and other erosion features related to warming permafrost, tundra fires and factors related to increased human presence in the Arctic.

The impacts of increased biomass production in Arctic tundra ecosystems on arctic wildlife are unclear. Despite changes in tundra biomass, migratory barren-ground caribou appear to be within known ranges of natural variation, with many herds that have experienced declines in the past decade beginning to increase or stabilize. Despite this, rapid environmental and social changes in the Arctic are a concern.

Vegetation

D. A. Walker[1], U. S. Bhatt[2], T. V. Callaghan[3], J. C. Comiso[4], H. E. Epstein[5], B. C. Forbes[6], M. Gill[7], W. A. Gould[8], G. H. R. Henry[9], G. J. Jia[10], S. V. Kokelj[11], T. C. Lantz[12], S. F. Oberbauer[13], J. E. Pinzon[4], M. K. Raynolds[1], G. R. Shaver[14], C. J. Tucker[4], C. E. Tweedie[15], P. J. Webber[16]

[1]Institute of Arctic Biology, University of Alaska, Fairbanks, Fairbanks, AK, USA
[2]Geophysical Institute, University of Alaska Fairbanks, Fairbanks, AK, USA
[3]Royal Swedish Academy of Sciences, Abisko Naturvetenskapliga Station, Abisko, Sweden
[4]NASA Goddard Space Flight Center, Greenbelt, MD, USA
[5]Department of Environmental Sciences, University of Virginia, Charlottesville, VA, USA
[6]Arctic Centre, University of Lapland, Rovaniemi, Finland
[7]Environment Canada, Whitehorse, Canada
[8]USDA Forest Service, International Institute of Tropical Forestry, San Juan, PR
[9]Geography Department, University of British Columbia, Vancouver, BC, Canada
[10]RCE-TEA, CAS, Chinese Academy of Sciences, Institute for Atmospheric Physics, Beijing, China
[11]Water Resources Division, Indian and Northern Affairs Canada, Yellowknife, NWT, Canada
[12]University of Victoria, British Columbia, Canada
[13]Department of Biological Sciences, Florida International University, Miami, FL, USA
[14]Ecosystem Center, Marine Biological Laboratory, Woods Hole, MA, USA
[15]Department of Biology, The University of Texas at El Paso, El Paso, Texas, USA
[16]Department of Plant Biology, Michigan State University, East Lansing, MI, USA

November 10, 2011

Highlights

- The "greenness" of tundra vegetation has increased during the period of satellite observations (1982-2010) in Eurasia and North America.
- Increasing "greenness" is positively and significantly correlated with more abundant ice-free coastal waters and higher land temperatures over most of the Arctic region.
- A circum-Arctic dip in "greenness" in 2009 was a response to elevated atmospheric aerosols, including volcanic dust, and generally cooler summer temperatures across the Arctic. A circumpolar recovery occurred in 2010, and the mean NDVI for North America and the Northern Hemisphere overall was the greatest on record.
- In Eurasia, green-up is more rapid than in North America, and peak "greenness" in Eurasia occurred about 2 weeks earlier during 2000-2009 than in the 1980s.

Introduction

Circumpolar changes to tundra vegetation are currently being monitored from space using the Normalized Difference Vegetation Index (NDVI), an index of vegetation greenness. Maximum NDVI (MaxNDVI) was obtained each year from a 29-year (1982-2010) record of NDVI in a new NDVI dataset derived from the AVHRR sensors on NOAA weather satellites (Bhatt et al. 2010, Raynolds et al. 2012). In tundra regions the annual MaxNDVI usually occurs in early August and is correlated with above-ground biomass, gross ecosystem production, CO_2 fluxes and numerous other biophysical properties of tundra vegetation (Tucker et al. 1986; Stow et al. 2004). This essay describes MaxNDVI through to the end of 2010, the last complete year for which data are available.

Long-term circumpolar change in NDVI

MaxNDVI has increased during the period of satellite observations (1982-2010) in Eurasia and North America (Fig. TE1a), supporting model predictions that primary production of arctic tundra ecosystems will respond positively to increased summer warmth (Bhatt et al. 2008; Lawrence et al. 2008). Despite considerable spatial variation in the magnitude of change in each of the three variables (MaxNDVI, open water, summer warmth) examined, annual MaxNDVI patterns were also positively and significantly correlated with more abundant ice-free coastal waters (Fig. TE1a in this essay and Fig. SIO3 in the essay on *Sea Ice*) and higher tundra land temperatures (Fig. TE1b) over most of the Arctic region (Bhatt et al. 2010). However, some areas are showing negative trends in NDVI. The negative trends in NDVI in northern North America (e.g., northern Greenland and the Queen Elizabeth Islands of Canada) correspond to the areas with persistent summer-long coastal sea ice, while the areas of northern Russia with negative NDVI trends generally have decreasing land temperatures (Fig. TE1b).

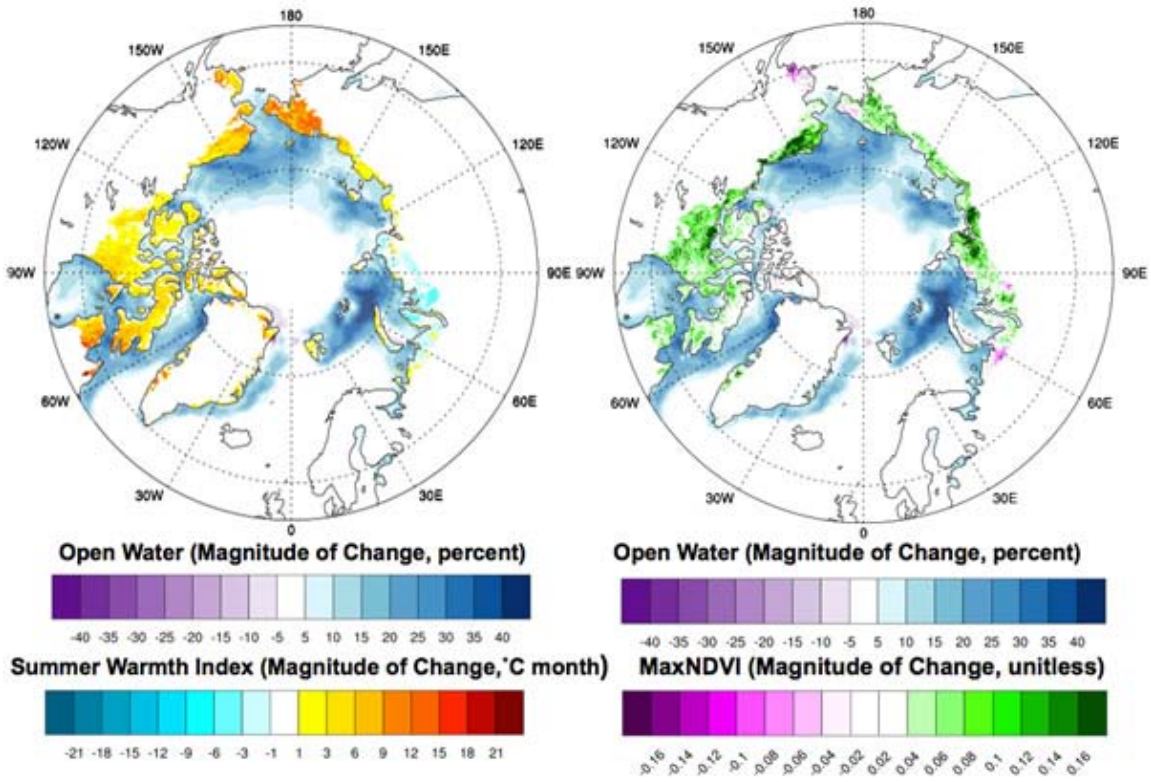

Fig. TE1. Trends for (a, right) summer (May-August) open water and annual MaxNDVI and (b, left) summer (May-August) open water and land-surface summer warmth index (SWI, the annual sum of the monthly mean temperatures >0 °C) derived from AVHRR thermal channels 3 (3.5-3.9 μm), 4 (10.3-11.3 μm) and 5 (11.5-12.5 μm). Trends were calculated using a least squares fit (regression) at each pixel. The total trend magnitude (regression times 29 years) over the 1982-2010 period is displayed.

Long-term, regional change in NDVI

Temporal changes in MaxNDVI for Arctic areas in Eurasia and North America show positive and nearly parallel increases amounting to a MaxNDVI increase of 0.02 NDVI units per decade (Fig. TE2a). However, there is considerable variability in the rate of increase in different regions of

the Arctic. For example, the MaxNDVI increase adjacent to the Beaufort Sea (+26%) is the most rapid in the Arctic and corresponds to large changes in open water (+31%) and summer warmth index (17%). On the other hand, the MaxNDVI change in the western Kara Sea is among the smallest (+4.4%). corresponding to smaller changes in sea ice (+20%) and land temperatures (-6%) (Fig. TE2b). The sea-ice changes occurring in the eastern Kara Sea far exceed those elsewhere, but have not caused warming over adjacent lands or a major increase in MaxNDVI, as would have been expected. Instead, the adjacent land areas have cooled slightly and there is only a modest increase in NDVI. The causes are unknown, but might include greater summer cloudiness.

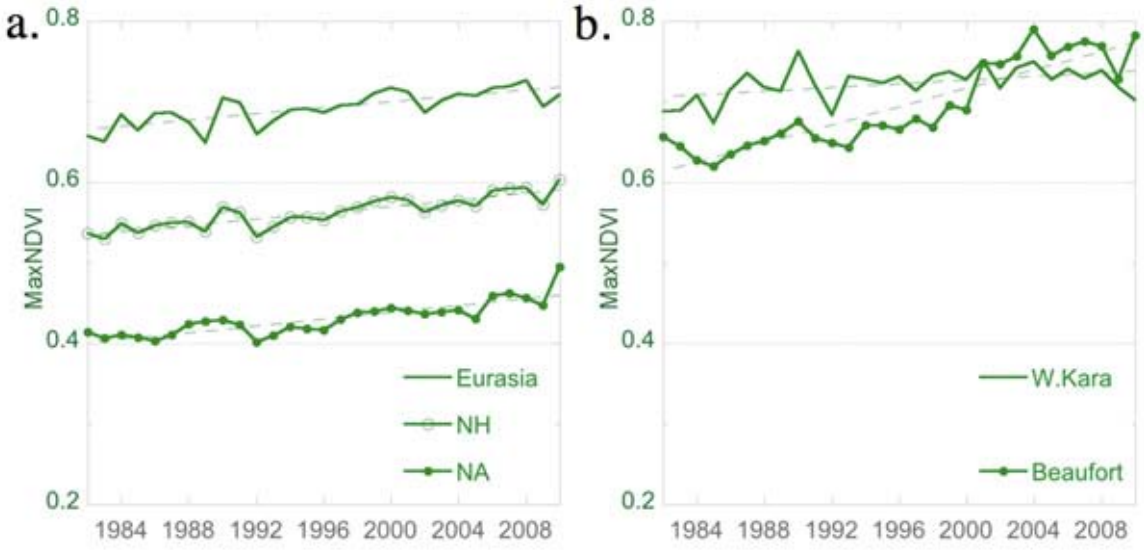

Fig. TE2. Time series of MaxNDVI during 1982-2010 for coastal tundra in (a) the Northern Hemisphere (NH) as a whole, Eurasia and North America, and (b) the western Kara Sea and Beaufort Sea.

In 2009 there was a circum-Arctic dip in NDVI (Fig. TE2) that corresponded to elevated atmospheric aerosols over the Arctic in the same year (Stone et al. 2010). This coincided with generally lower temperatures across the Arctic in 2009 and 2010. The elevated aerosols were attributed to an accumulation of pollutants from Eurasian industrial centers in the upper troposphere in combination with volcanic plumes from the eruption of Mt. Redoubt in Alaska. The enhanced Arctic haze in 2009 was estimated to reduce net shortwave irradiance by about 2-5 W m^{-2} (Stone et al., 2010).

NDVI and phenology

Bi-weekly NDVI data are used to show the yearly progression of the magnitude and timing of the photosynthetically-active period for the vegetation (Fig. TE3). Clear differences in phenological patterns occur in Eurasia and North America. Both areas show a ~0.06 unit MaxNDVI increase during the 29-yr record. In North America the curves show the increase in the MaxNDVI but no significant shift in timing of peak greenness. In Eurasia there is a somewhat more rapid green-up, and peak NDVI was reached about 2 weeks earlier during 2000-2009 than in the 1980s. This is consistent with Eurasian snow cover duration, which was stable during the 1980s and 1990s, but has declined rapidly since the early 2000s (see Fig. HTC3 in the essay on *Snow*). Neither North America nor Eurasia show a significant trend

toward a longer growing season. However, whole-continent data appear to mask changes along latitudinal gradients and in different regions. For example, during 1982-2003, MaxNDVI along the Canadian Arctic climate gradient showed a ~1-week shift in the initiation of green-up and a somewhat higher NDVI late in the growing season in the Low Arctic (Jia et al. 2009). The High Arctic in Canada did not show earlier initiation of greenness, but did show a ~1-2 week shift toward earlier MaxNDVI.

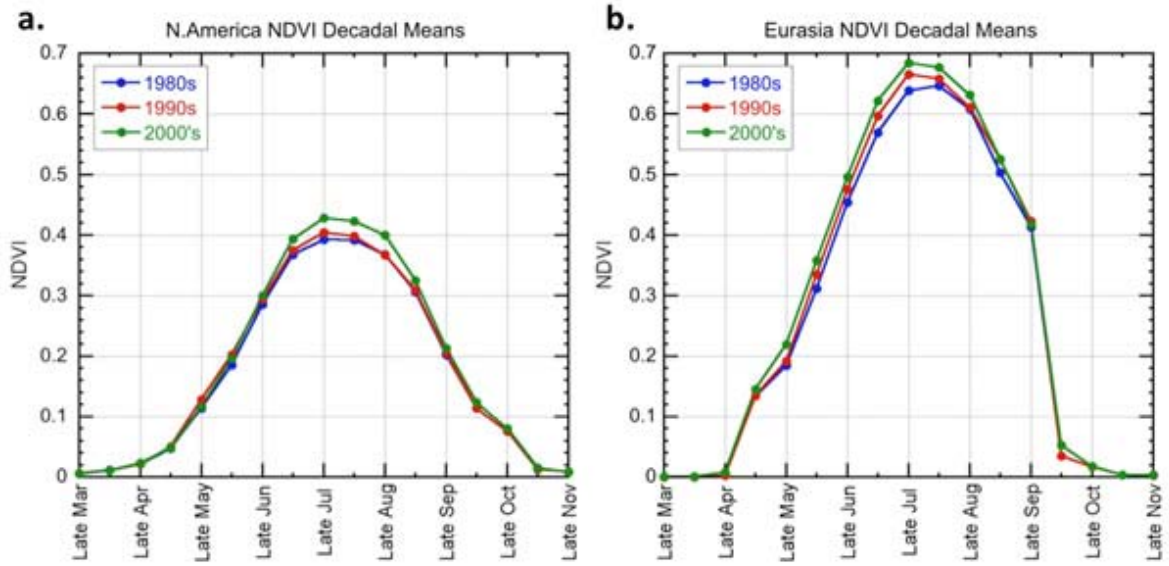

Fig. TE3. Decadal changes in NDVI-derived phenology in (a) Eurasia and (b) North America.

Field observations

The increased Arctic greening observed in the satellite data is also observed in long-term *in situ* vegetation measurements. For example, the International Tundra Experiment (ITEX), established in 1990, has made annual measurements of plant growth and phenology for up to 20 years using standardized protocols (Henry and Molau 1997). A recent synthesis of the long-term ITEX warming experiments has shown that effects on plant phenology differ by trait, community, and functional types (Elmendorf and Henry 2010). Some of these results indicate there have been increases in productivity consistent with warming (e.g. Hill and Henry 2011). In others, the links between local climate warming and vegetation change found in the NDVI data were not supported at the plot scale. There is a need for more careful evaluation of the causes of the observed changes, which may be driven by local, long-term, non-equilibrium factors other than climate warming, such as recovery from glaciation or changes in snow cover or precipitation (Troxler et al. 2010; Mercado and Gould 2010).

The Back to the Future (BTF) International Polar Year project, which revisited numerous Arctic research sites that were established between 15 to 60 years ago, is revealing decadal-scale changes. These include vegetation change and increases in plant cover at Barrow, Alaska, on Baffin Island and at multiple sites throughout Beringia (Tweedie et al. 2010). Advanced phenological development and species shifts associated with drying occurred on Disko Island, Greenland. Warming of permafrost was documented in sub-Arctic Sweden, and dramatic changes in pond water column nutrients, macrophyte cover and chironomid assemblages have been noted near Barrow. NDVI, gross ecosystem production, and methane efflux from wet

vegetation types have increased at sites near Barrow, on Baffin Island and at the Stordalen mire in sub-Arctic Sweden. In most cases, air and ground warming appear to be the primary causes of change, but disturbances of various types are causing change at some sites. For example, at herbivore exclosures established at Barrow in the 1950s and 1970s it has been found that lemmings and other herbivores outside the exclosures had reduced the relative cover of lichens and graminoids and increased the relative cover of deciduous shrubs. Consequently, a wide variety of ecosystem properties, including thaw depth, soil moisture, albedo, NDVI, net ecosystem exchange and methane efflux were affected (Johnson et al. 2010). A warming Arctic will cause changes in species distributions and biodiversity in the Arctic. In response to these expected changes, the Circumpolar Biodiversity Monitoring Program is launching an integrated biodiversity monitoring plan for Arctic land, marine, coastal and freshwater ecosystems (Gill et al. 2008).

Other Arctic vegetation changes that are indirectly related to climate include those associated with landslides, thermokarst and fires, which are increasing in frequency in several regions of the Arctic (e.g., Goosef et al. 2009; Lantz et al. 2010a,b; Mack et al. 2011 in revision; Rocha and Shaver 2011). Higher soil temperatures, thawing permafrost, more abundant water and increased nutrients due to such disturbances result in pronounced greening often associated with more abundant shrub growth. Increasing air and ground temperatures are predicted to increase shrub growth in much of the Arctic, with major consequences for ecosystems (Lantz et al. 2010b). Several studies have observed increased shrub growth due to artificial warming, although the increases are small and frequently not statistically significant (e.g., Bret-Harte et al. 2003). On the other hand, there is growing evidence for increased shrub abundance at climatically- and anthropogenically-disturbed sites (Lantz et al. 2010a, b; Walker et al. 2011). In the Russian Arctic, erect deciduous shrub growth is closely associated with both the recent summer warming of ~2°C over more than half a century and a trend of increasing NDVI since 1981 (Forbes et al. 2010).

References

Bhatt, U. S, and co-authors, 2008: The atmospheric response to realistic reduced summer arctic sea ice anomalies. Geophysical Monograph Series 180, Arctic Sea Ice Decline: Observations, Projections, Mechanisms, and Implications, 91-110.

Bhatt, U. S. and co-authors, 2010: Circumpolar Arctic tundra vegetation change is linked to sea-ice decline. Earth Interactions, 14, 1-20.

Bret-Harte, M.S., G.R. Shaver, F.S. Chapin III. 2002: Primary and secondary stem growth in arctic shrubs: implications for community response to environmental change. Journal of Ecology 90: 251-267.

Elmendorf, S., G. Henry, and co-authors 2010: Assessments of recent tundra change based on repeated vegetation surveys. Abstract GC3B-05 presented at the 2010 Fall Meeting, AGU San Francisco CA, 13-17 Dec 2010.

Forbes, B.C., M. M. Fauria, and P. Zetterberg, 2010: Russian Arctic warming and 'greening' are closely tracked by tundra shrub willows. Global Change Biology, 16, 1542-1554.

Gill, M.J., M.C. Raillard, C. Zockler and R.B. Smith. 2008: Developing an Integrated and Sustained Arctic Biodiversity Monitoring Network: The Circumpolar Biodiversity Monitoring

Program Five Year Implementation Plan. CAFF CBMP Report No. 14, CAFF International Secretariat, Akureyri, Iceland.

Gooseff, M. N., A. Balser, W. B. Bowden, and J. B. Jones, 2009: Effects of hillslope thermokarst in Northern Alaska. EOS, 90, 29-36.

Henry, G. H. R., and U. Molau, 1997: Tundra plants and climate change: the International Tundra Experiment (ITEX). Global Change Biology, 3 (Suppl. 1), 1-9.

Hill, G. B., and G. H. R. Henry, 2011: Responses of High Arctic wet sedge tundra to climate warming since 1980. Global Change Biology, 17, 276-287.

Hudson, J. M. G., and G. H. R. Henry, 2009: Increased plant biomass in a High Arctic heath community from 1981 to 2008. Ecology, 90, 2657-2663.

Jia, G. J., H. E. Epstein, and D. A. Walker, 2009: Vegetation greening in the Canadian Arctic related to decadal warming. Journal of Environmental Monitoring, 11, 2231-2238.

Johnson, D. R., M. J. Lara, G. R. Shaver, and C. Tweedie, 2010: Herbivory and soil moisture drive long-term patterns of vegetation structure and function in Alaskan coastal tundra: results from resampling historic exclosures at Barrow. Abstract GC43B-0908 presented at 2010 Fall Meeting, AGU, San Francisco, CA, 13-17 Dec 2010.

Lantz, T. C., S. E. Gergel, and G. H. R. Henry, 2010a: Response of green alder (*Alnus viridis subsp fruticosa*) patch dynamics and plant community composition to fire and regional temperature in north-western Canada. Journal of Biogeography, 37, 1597-1610.

Lantz, T. C, S. E. Gergel, and S. V. Kokelj. 2010b. Spatial heterogeneity in the shrub tundra ecotone in the Mackenzie Delta region, Northwest Territories: Implications for Arctic environmental change. Ecosystems, 13, 194-204.

Lawrence, D. M., A. G. Slater, R. A. Tomas, M. M. Holland, and C. Deser, 2008: Accelerated Arctic land warming and permafrost degradation during rapid sea ice loss. Geophysical Research Letters, 35: L11506, doi:10.1029/2008GL033985.

Mack, M. C., M. S. Bret-Harte, T. N. Hollingsworth, R. R. Jandt, E. A. G. Schuur, G. R. Shaver, D. L. Verbyla. Novel wildfire disturbance and carbon loss from arctic tundra. Nature, in revision.

Mercado-Diaz, J. A., and W. A. Gould, 2010: Landscape- and decadal scale changes in the composition and structure of plant communities in the northern foothills of the Brooks Range of Arctic Alaska. Abstract GC43B-0982 presented at 2010 Fall Meeting, AGU, San Francisco, Calif., 13-17 Dec.

Overland, J., M. Wang, and J. Walsh, 2011: Atmosphere. 2010, BAMS Report This volume.

Raynolds, M.K., D.A. Walker, H.E. Epstein, J.E. Pinzon and C.J. Tucker. 2012. A new estimate of tundra-biome phytomass from trans-Arctic field data and AVHRR NDVI. Remote Sensing Letters, 3, 403-411.

Rocha, A., and G. R. Shaver. 2011. Burn severity influences post-fire CO2 exchange in arctic tundra. Ecological Applications, doi:10.1890/10-0255.1.

Stone, R. S., and co-authors, 2010: A three-dimensional characterization of Arctic aerosols from airborne Sun photometer observations PAM-ARCMIP, April 2009. Journal of Geophysical Research, 115, D13203, doi:10.1029/2009JD013605.

Stow, D. A., and coauthors. 2004: Remote sensing of vegetation and land-cover change in arctic tundra ecosystems. Remote Sensing of Environment, 89: 281-308.

Tucker, C. J., I. Y. Fung, D. C. Kealing, and R. H. Gammon, 1986: Relationship between atmospheric CO_2 variations and a satellite derived vegetation index. Nature, 319, 195-199.

Troxler, T. G., and co-authors. 2010: Long-term phenological changes in tundra plants in response to experimental warming using the International Tundra Experiment (ITEX) Network. Abstract COS 93-10, 95th ESA Annual Meeting, Pittsburg, PA, 1-6 Aug 2010.

Tweedie, C.E., and co-authors, 2010: Decadal time scale change in terrestrial plant communities in North America arctic and alpine tundra: A contribution to the International Polar Year Back to the Future project. Abstract GC53B-03 presented at 2010 Fall Meeting, AGU, San Francisco, CA, 13-17 Dec 2010.

Walker, D.A., and co-authors, 2010: Vegetation: Special Supplement to Bulletin of the American Meteorological Society, 91, S115-S116.

Walker. D. A., and co-authors, 2011: Cumulative effects of rapid land-cover and land-use changes on the Yamal Peninsula, Russia. Eurasian Arctic Land Cover and Land Use in a Changing Climate, Gutman, G., and Reissel, A., Eds., Springer, 206-236.

Caribou and Reindeer (Rangifer)

D. Russell[1] and A. Gunn[2]

[1]Yukon College, Box 10038 Whitehorse YT, Canada Y1A 7A1
[2]368 Roland Road, Salt Spring Island, BC, Canada V8K 1V1

November 15, 2011

Highlights

- The total, pan-Arctic population of Arctic reindeer and caribou (Rangifer) may have ceased to decline, thus ending a ~40-year cycle.
- There is strong regional variation in Rangifer populations; some are declining, but most are either increasing or stable.

Geographic variation of Rangifer

The most recent population estimates for migratory tundra reindeer and caribou herds indicate that many are either increasing or stable (Porcupine, Central Arctic, Teshekpuk Lake, Cape Bathurst, Bluenose West, Bluenose East, Lena-Olenyk, Kangerlussuaq-Sisimiut), with a few herds starting or continuing to decline (George River, Leaf River, Chokotka, Taimyr, Akia-Maniitsoq, Western Arctic). The current status of the 23 herds updated by the CircumArctic Monitoring and Assessment (CARMA) Network is illustrated in Fig. TE4. Numbers in the map are referenced to specific herds in the text below.

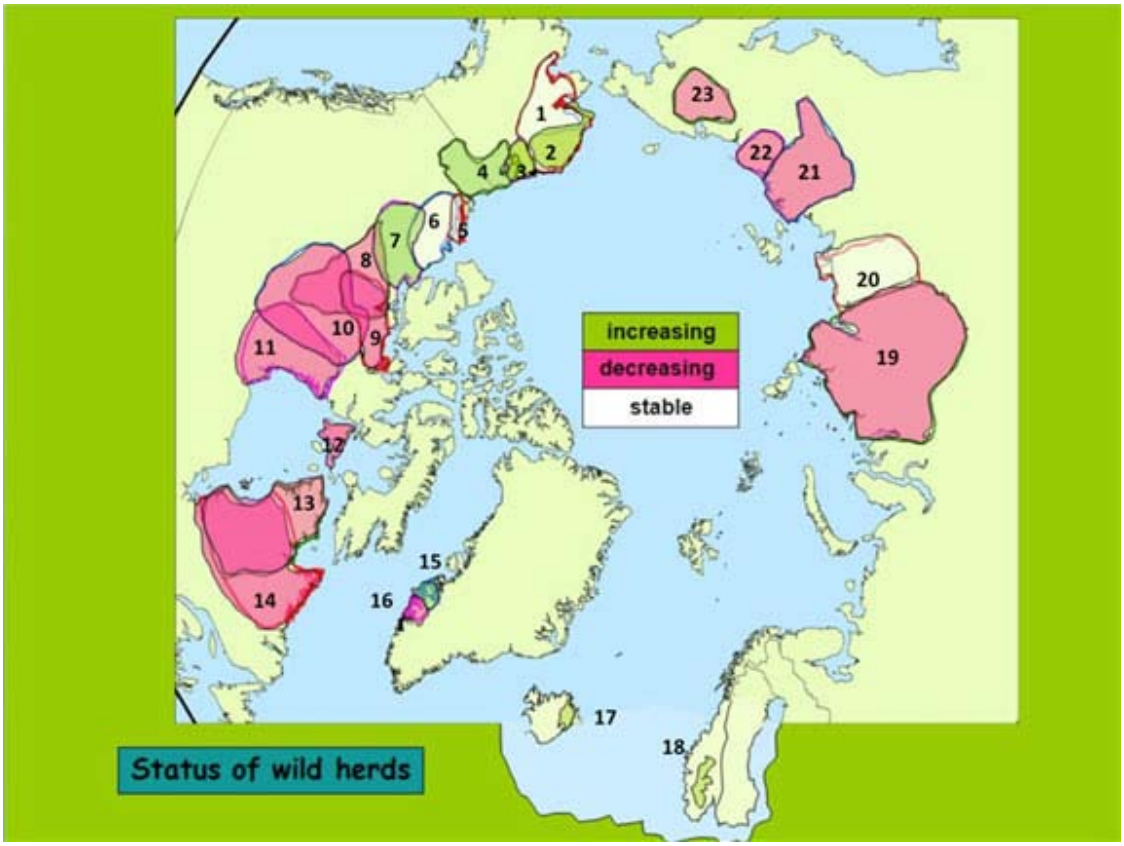

Fig. TE4. Current status of the world's migratory tundra reindeer and caribou herds. 1: Western Arctic; 2: Teshekpuk Lake; 3: Central Arctic; 4: Porcupine; 5: Cape Bathurst; 6: Bluenose West; 7: Bluenose East; 8: Bathurst; 9: Ahiak; 10: Beverly; 11: Qamanirjuaq; 12: Southampton; 13: Leaf River; 14: George River; 15: Kangerlussuaq-Sisimiut; 16: Akia-Maniitsoq; 17: Snoefells; 18: Norwegian; 19: Taimyr; 20: Lena-Olenyk; 21: Yana-Indigurka; 22: Sundrunskya; 23: Chokotka. Descriptions of the herds in the text are cross-referenced to the numbers above.

Temporal variation in migratory tundra Rangifer

Local and traditional knowledge has indicated that caribou go through periods of abundance and scarcity every 40-60 years. However, relatively objective population estimates have only been employed since the late 1960s and early 1970s. These estimates have shown one single "cycle" over the last 40 years. This cycle is "somewhat" synchronous around the Arctic, although there is a lot of individual herd variation (Fig. TE5).

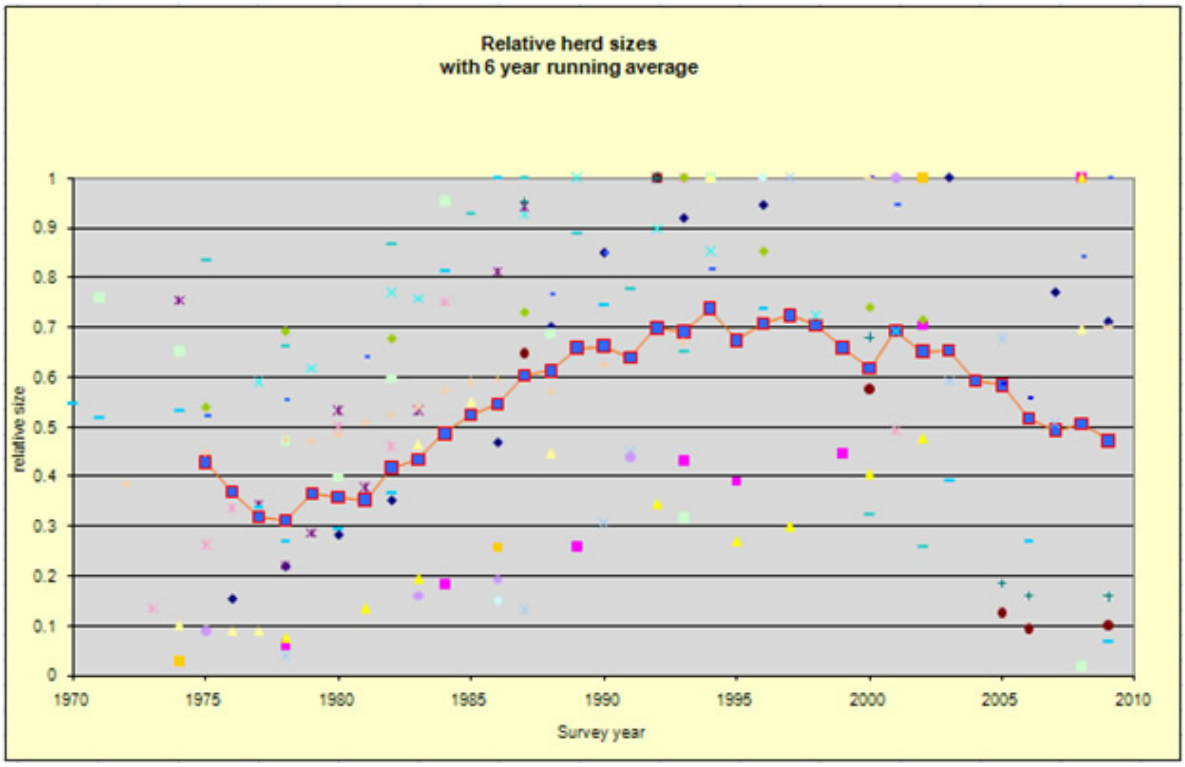

Fig. TE5. The relative population size (proportion of maximum estimate) for migratory tundra Rangifer herds (1970-2010). The red line is a 6-year running average. Data are from the CARMA Web site www.carmanetwork.com).

There has been considerable concern that declining numbers of caribou in the last decade were associated with global warming (Vors and Boyce 2009); however, no clear link between individual herd declines and climate was ever established. In the last 3 years, population estimates indicate that we may now be seeing a halt to the declines, and recovery for some of the herds, particularly in western Canada (Fig. TE4). At the same time, herds that have not declined since estimates began have started to decline. Increased development, more efficient harvesting methods and regional climate trends, however, are still a concern that may affect speed, timing and magnitude of the recovery (Gunn et al. 2010).

In the last 20-30 years, methods of counting have become more standardized, which improves the statistical reliability of trend information. Herd size is estimated from photographs taken either when the cows aggregate on the calving ground, or during summer when the insect harassment drives the animals into aggregations. In Russia, the methods include photography of summer aggregations, but without the use of radio- or satellite-collared individuals to ensure that all aggregations are found. Since 1970, for the 23 circum-Arctic herds whose size is tracked through aerial surveys, the numbers of caribou and wild reindeer have declined from a recorded peak of about 5.5 million to 2.7 million (CARMA 2011).

In Alaska, the Western Arctic herd (**1**, Fig. TE4) was at a low (75,000) in the mid 1970s then increased during the 1980s and 1990s, and reached a peak of 490,000 in 2003. The herd then declined to 348,000 caribou in 2009 (Alaska Department of Fish and Game 2011a). Both the Teshekpuk Lake **(2)** and Central Arctic **(3)** herds were recognized as distinct herds in the 1970s, and were estimated to number 4000-5000. Both herds increased, and continued to increase, during the 1990s. By 2008, the Teshekpuk Lake herd had reached 64,107 and the Central

Arctic herd 67,000 ((Parrett, 2009; Lenart 2009). The Porcupine herd **(4)** reached a peak in 1989 (178,000), declined to 123,000 by 2001, before recovering and increasing to 169,000 by 2010 (Alaska Department of Fish and Game 2011b).

In Canada, there is considerable variation in the timing of increases and decreases, and changes in survey techniques likely contributed to differences in estimated herd size. The ten herds have declined since peak sizes, and the Bathurst **(8)**, Beverly **(10)** and Ahiak **(9)** herds are currently (2010) considered to be in decline. The Qamanirjuaq **(11)**, was estimated to have decreased from 496,000 in 1994 to 345,000 in 2008 (Campbell et al. 2011). However, these estimates were not significantly different and, because there were 14 years between counts, any intervening trends could not be determined. The Cape Bathurst **(5)** and Bluenose-West **(6)** herds stabilized between 2006 and 2009 after sharp declines (Davison, pers. comm. 2010; CARMA 2011); the 2010 census of the Bluenose-East **(7)** showed that the herd has increased from 66,700 in 2006 to 98,600 in 2010 (Government of NWT 2010). Caribou were re-introduced on Southampton Island **(12)** in 1967, followed the extirpation of caribou on the island. The initial re-introduction increased to a peak of 30,381 animals in 1997. Disease and parasites have been implicated in the subsequent decline of the herd to a 2009 estimate of 13,953 (Campbell et al. in press). Since the mid-1980s, the George River Herd **(14)** sharply declined, based on the 2010 census, and the Leaf River Herd **(13)** has not been counted since 2001, although it is thought to be declining as well. The George River herd increased dramatically from about 5000 animals in the 1950s to 750,000 in the mid-1990s (Couturier et al. 2004). The herd then declined to about 385,000 individuals in 2001, and declined further to 74,131 based on the 2010 post-calving photo-census (Ressources naturelles et Faune 2010).

There are two major herds in Greenland. Recent surveys indicate that the largest herd, the Kangerlussuaq-Sisimiut **(15)** has increased from under 60,000 in 2001 to 98,000 in 2010. In contrast, the smaller Akia-Maniitsoq **(16)** herd declined from 46,000 in 2001 to 31,000 in 2010 (Cuyler 2007; CARMA 2011).

Reindeer were introduced to Iceland **(17)** in the late 1700s (Thórisson, 1984). In the absence of predators and with active harvesting the number was estimated at approximately 6,500 animals in fall 2009 (Thorarinsdottir, pers. comm. 2010; CARMA 2011).

Wild mountain reindeer in Norway **(18)** consist of 23 separate herds that in 2004 numbered from 22,000 to 29,000 animals. Herds are largely regulated by hunting and the degree of infrastructure, range fragmentation and forage conditions largely determine individual herd status (Lund 2004).

In Russia, the Taimyr Herd **(19)** is one of the largest in the world. Between the 1950s and 1970s, the herd increased from 110,000 to 450,000 in 1975. Commercial hunting increased and held the herd at about 600,000 animals. Then subsidies to commercial hunters were removed, hunting declined, and the herd grew rapidly to 1 million animals by the year 2000. Currently, the herd is assumed to be declining, although a population estimate has not been conducted since 2000 (Klovov 2004, Kolpashikov et al, in press). East of the Taimyr is the central Siberian region of Yakutia where three large herds of migratory tundra wild reindeer currently exist. The Lena-Olenek herd **(20)** in 2009 numbered over 95,000 reindeer, a slight increase from 90,000 estimated in 2001. The Yana-Indigirka **(21)** population declined from 130,000 reindeer in 1987 to 34,000 by 2002. The Sundrun **(22)** population declined from about 40,000 reindeer in 1993 to about 28,500 by 2002. East of Yakutia, the Chukotka herd **(23)** increased following the collapse of the domestic reindeer industry. The domestic reindeer industry rapidly collapsed from 587,000 in 1971 to about 92,000 by 2001 (Klokov 2004). Consequently, the wild reindeer

recovered and numbered 32,200 individuals by 1986, and 120-130,000 in 2002, then declined to less than 70,000 by 2009.

References

Alaska Department of Fish and Game. 2011a. Press release - Western Arctic caribou Herd count revised. http://www.adfg.alaska.gov/index.cfm?adfg=pressreleases.pr03242011.

Alaska Department of Fish and Game. 2011b. Press release - Porcupine Caribou Herd shows growth. http://www.adfg.alaska.gov/index.cfm?adfg=pressreleases.pr03022011.

Campbell, M. Boulanger, J. and Lee, D. in press. Demographic Effects of an Outbreak of *Brucella suis* On Island Bound Barren-Ground Caribou (*Rangifer tarandus groenlandicus*) Southampton Island Nunavut. Presented at the 13th Arctic Ungulate Conference, Yellowknife, Northwest Territories, Canada, August, 2011.

Campbell, M., Nishi, J. and Boulanger, J. 2010. A calving ground photo survey of the Qamanirjuaq migratory barren-ground caribou (*Rangifer tarandus groenlandicus*) population -- June 2008. Technical Report Series 2010 No. 1-10. Government of Nunavut. 129 p.

CARMA. 2011. Circumarctic Monitoring and Assessment (CARMA) Network Web site www.carmanetwork.com.

Couturier, S., Jean, D., Otto, R. and Rivard, S. 2004. Demography of the migratory tundra caribou (Rangifer tarandus) of the Nord-du-québec region and Labrador. Ministère des Ressources Naturelles, de la Faune et des Parcs, Québec, and Direction de la recherche sur la faune. Québec. 68 p.

Cuyler C. 2007. West Greenland caribou explosion: What happened? What about the future? Proceedings of the 11th North American Caribou Workshop, Jasper, Alberta, Canada, 23-27 April 2006. Rangifer, Special Issue No. 17: 219-226.

Government of NWT. 2010. Press release - Survey results of Bluenose East caribou herd released. Website:
http://www.enr.gov.nt.ca/_live/documents/content/Survey_Results_Bluenose-East_Caribou_Herd.pdf.

Gunn, A. and Russell, D.R. 2011. Northern Caribou Population Trends. Canadian Biodiversity: Ecosystem Status and Trends, 2010 Technical Thematic Report Series No. 10. Canadian Councils of Resource Ministers. Ottawa, iv+55 p.

Gunn A., Russell, D., White, R. & Kofinas, G. 2009. Facing a Future of Change: Migratory caribou and reindeer. Arctic 62(3): 3-4.

Klokov. K. 2004. Russia. Chapter Family-Based Reindeer Herding and Hunting Economies, and the Status and Management of Wild Reindeer/Caribou Populations. Sustainable Development Program, Arctic Council, Published by Centre for Saami Studies, University of Tromsø.

Kolpashikov, L., V. Makhailov, and D. Russell. In press. The role of harvest in the dynamics of the Taimyr wild reindeer herd: Lessons for North America.

Lenart, E. A. 2009. Units 26B and 26Ccaribou. Pages 299-325 in P. Harper. Editor. Caribou Management report of survey and inventory activities 1 July 2006 - 30 June 2008. Alaska Department of Fish and game. Project 3.0 Juneau, Alaska, USA.

Lund, E. 2004. Wild reindeer in Norway. In: (B. Ulvevadet and K. Klokov eds.) Family-Based Reindeer Herding and Hunting Economies, and the Status and Management of Wild Reindeer/Caribou Populations. Sustainable Development Program, Arctic Council, Published by Centre for Saami Studies, University of Tromsø.

Parrett, L. S. 2009. Unit 26A. Teshekpuk caribou herd. Pages 271-298 in P. Harper. Editor. Caribou Management report of survey and inventory activities 1 July 2006 - 30 June 2008. Alaska Department of Fisg and game. Project 3.0 Juneau, Alaska, USA.

Ressources naturelles et Faune. 2010. Results of the George River Caribou Herd census [online]. Government of Quebec. http://www.mrn.gouv.qc.ca/english/press/press-release-detail.jsp?id=8713 (accessed 23 December, 2010). Press release.

Thórisson, S. 1984. The history of reindeer in Iceland and reindeer study 1979-1981. Rangifer 4 (2): 22-38.

Vors, L. S. and Boyce, M. S. (2009), Global declines of caribou and reindeer. Global Change Biology 15: 2626-2633.

Hydrology and Terrestrial Cryosphere Summary

Section Coordinator: Marco Tedesco

The City College of New York, New York, NY, USA

November 15, 2011

The Hydrology & Terrestrial Cryosphere section of the 2012 Arctic Report Card documents consistent and widespread evidence for continuing change in snow cover, glaciers and ice caps, the Greenland ice sheet, permafrost, lake ice, river discharge and river biogeochemistry. On the Greenland ice sheet and on most glaciers and ice caps elsewhere in the Arctic, the period 2010-2011 was characterized by a negative mass balance, i.e., more snow and ice was lost, primarily by surface melting and runoff, than snow was gained. The western slope of the Greenland ice sheet in particular experienced a significant increase in surface melting, amplified by albedo feedback and, in 2011 and 2010, by below-normal summer snowfall. GRACE satellite gravity solutions show that the mass loss from the entire ice sheet during the 2010-2011 balance year was -430 Gt, the largest annual loss in the GRACE record (2002-present) and equivalent to a eustatic sea level rise of 1.1 mm. Mass losses in summer 2011 are linked to positive surface and upper air temperature anomalies similar to those observed in 2007 and 2005.

Below-average snow extent during spring 2011 is consistent with a decline observed since the 1970s, and continues an accelerated decrease since 2006. June snow cover extent in Eurasia was the lowest since the start of the satellite record in 1966. Positive snow water equivalent (SWE) anomalies in the North American Arctic in 2011 were the third highest since the start of the time series in 1980. Despite this, spring snow cover extent and duration were below-average across both the North American and Eurasian sectors of the Arctic due to positive air temperature anomalies in May and June, the two primary months for snow melt. A general increase in permafrost temperatures observed in Alaska, northwest Canada, Nordic countries, and in Siberia during the last several decades continued in 2010-2011. New record high permafrost temperatures at 20 m depth were measured in 2011 at all observatories on the North Slope of Alaska, where measurements began in the late 1970s. However, a slight decrease (by as much as 0.3°C) in Interior Alaska has been observed during the last three years.

Lake ice cover duration, largely influenced by air temperature changes, was shorter by as much as 4-5 weeks in 2010-2011 compared to the 1997-2010 average for the eastern Canadian Arctic. River discharge into the Arctic Ocean during 2010 was close to the long-term (1936-2009) mean for the six largest Eurasian Arctic rivers and the four large North American Arctic rivers. Preliminary estimates for 2011, based on modeling and some observations, indicate river flows to the Arctic Ocean during January to July were significantly lower than the long-term mean. In 2010, dissolved organic carbon (DOC) flux from five of the six largest Arctic rivers was less than the 2003-2009 average. Combined DOC flux from all six rivers peaked in 2007, but has been lower each year since, closely tracking the downward trend in their combined discharge.

Snow

C. Derksen and R. Brown

Climate Research Division, Environment Canada

November 21, 2011

Highlights

- Although snow water equivalent (SWE; the product of the snow depth and density, or the total water stored in the snowpack) was close to average for the Eurasian Arctic and well above average for the North American Arctic, spring snow cover extent and duration during 2011 were below average across the Arctic.
- Persistent warm temperature anomalies in May and June created new record lows for snow extent and spring snow cover duration (for the satellite record dating from 1967) across the Eurasian sector of the Arctic.
- The time series of snow cover duration anomalies (1966 through 2011) identifies a marked seasonal asymmetry: in contrast to a strong trend towards less snow in the spring period (as a result of earlier melt), the start date of snow cover over the Arctic has remained stable during the satellite era.

Arctic snow cover exhibits a high degree of spatial variability due to the pronounced topographic and vegetative controls on snow catchment, redistribution and metamorphosis in high latitude environments. In turn, this heterogeneity introduces uncertainty into the gridded datasets utilized to identify the response of Arctic snow cover to climate variability and change. The use of multiple datasets can mitigate this uncertainty by allowing the calculation of statistical uncertainty in time series data, and through comprehensive characterization of Arctic snow cover changes by considering snow cover extent (SCE), snow cover duration (SCD), and snow water equivalent (SWE).

Northern Hemisphere spring SCE anomalies (relative to a 1988-2007 reference period), computed from the weekly NOAA snow chart Climate Data Record (CDR; maintained at Rutgers University and described in Brown and Robinson, 2011) for months when snow cover is confined largely to the Arctic showed a reduction in SCE **in 2011**, continuing the trend identified from multiple datasets by Brown et al. (2010) (Fig. HTC1). This spring season trend to less snow cover becomes stronger from April through June because of the poleward amplification of SCE sensitivity to warming air temperatures (Dery and Brown, 2007). Variability in SCE across high latitudes is primarily controlled by surface temperature anomalies during the snow melt period (Brown et al., 2007). In April 2011, cold surface temperature anomalies extended over the Canadian high Arctic, while warm air temperature anomalies covered almost the entire Eurasian sector of the Arctic (see the essay on *Temperature and Clouds*). These warm anomalies persisted through May and June, driving a new record low June snow cover extent over Eurasia since satellite observations began in 1966. The cold anomaly over Arctic Canada subsided in May and June. Because these are the two primary months for snow melt in this region, SCE anomalies over the North American (NA) sector of the Arctic were strongly negative by June, in spite of the cold start to the spring season.

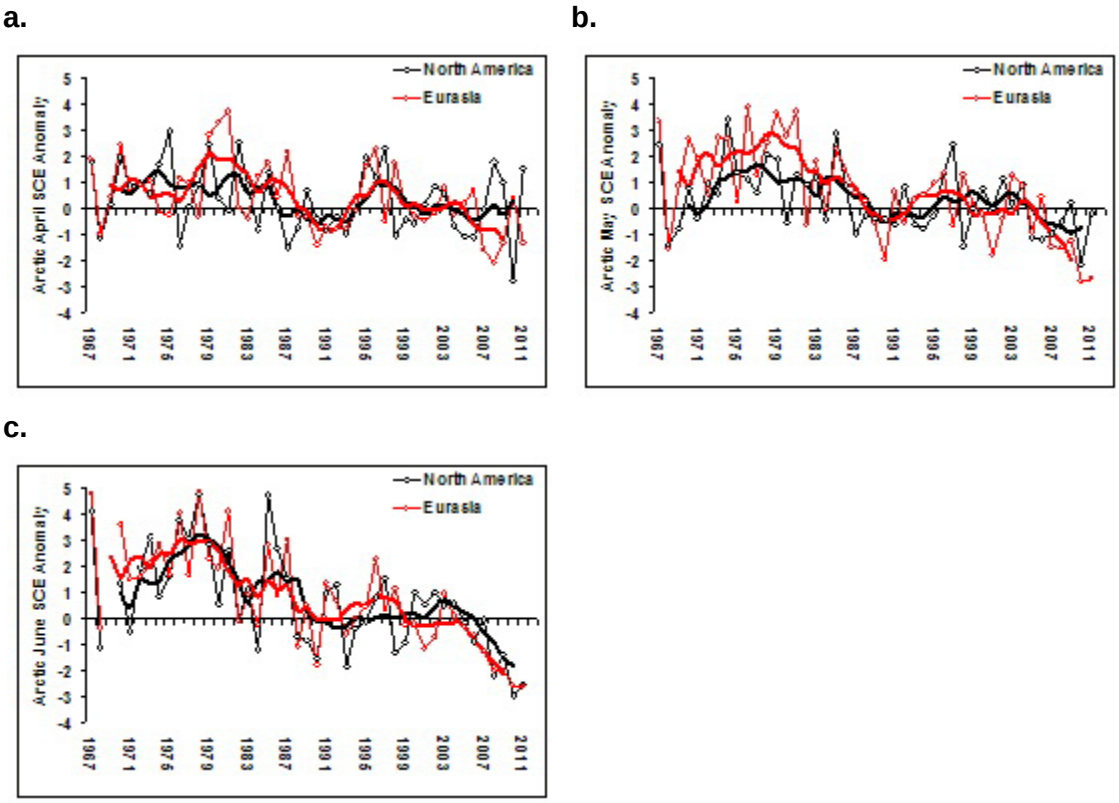

Fig. HTC1. Monthly Arctic snow cover extent (SCE) anomaly time series (with respect to 1988-2007) from the NOAA snow chart CDR for (a) April (b) May and (c) June. Anomalies for each year (the difference between the time series mean and each individual monthly value) were standardized by the monthly standard deviation through the time series and are, therefore, unitless. Solid line depicts 5-yr running mean.

Spatial patterns of fall, spring and seasonal SCD anomalies derived from the NOAA CDR for 2010/11 (Fig. HTC2) show little evidence of fall SCD anomalies over the Arctic, while the early spring melt anomaly in Eurasia located over the Ob and Yenisey basins contributed to the shortest spring SCD for Eurasia in the NOAA snow chart record (Fig. HTC3). A striking feature in the SCD anomaly time series is the seasonal asymmetry of the trends through the data record. In contrast to the trend towards less snow in the spring period (as a result of earlier melt), the start date of snow cover over the Arctic has remained stable during the satellite era. When Arctic and mid-latitude regions are compared, the SCD anomalies are consistent with the "warm Arctic-cold Continent" climate pattern noted in the *Temperature and Clouds* essay.

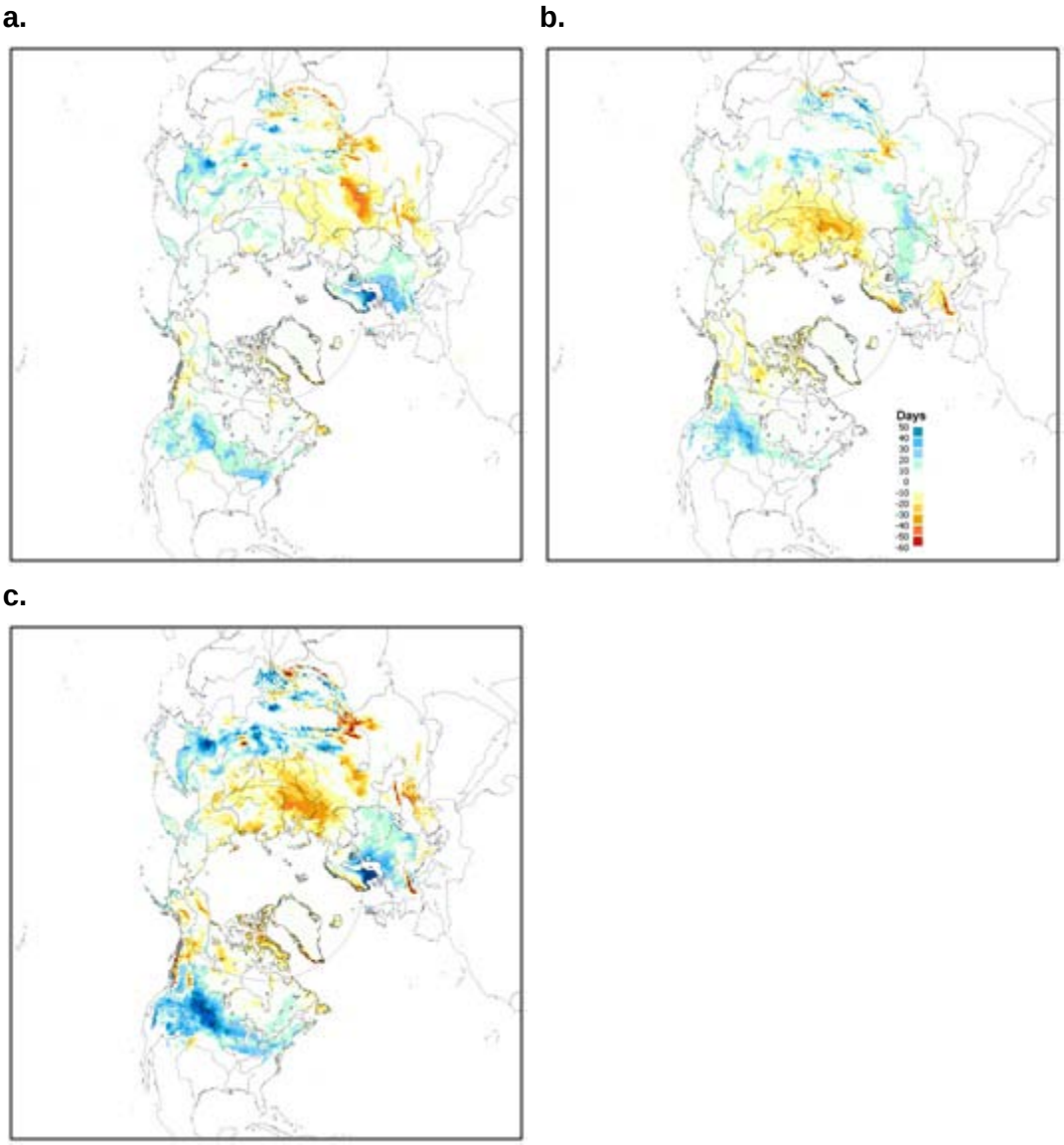

Fig. HTC2. Snow cover duration (SCD) departures (with respect to 1998-2010) from the NOAA IMS data record for the 2010/11 snow year: (a) fall; (b) spring; (c) complete snow season.

a.

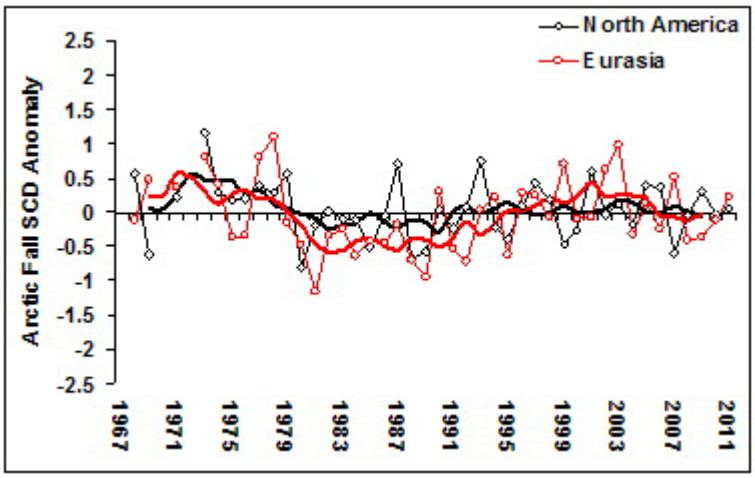

b.

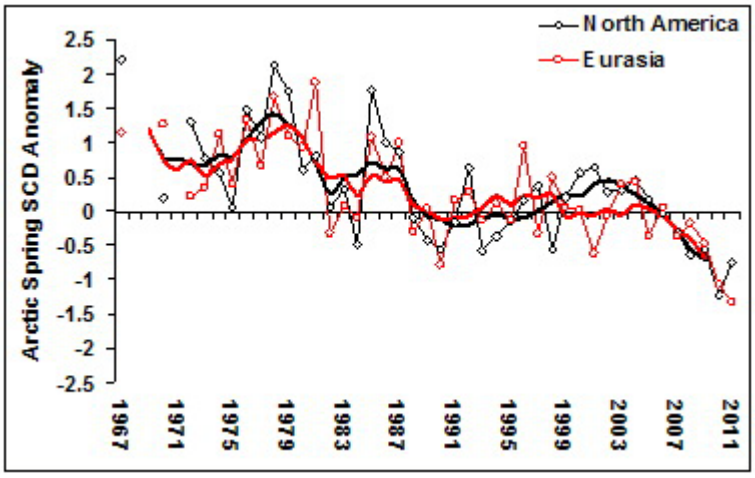

Fig. HTC3. Arctic seasonal snow cover duration (SCD) standardized anomaly time series (with respect to 1988-2007) from the NOAA record for (a) the first (fall) and (b) second (spring) halves of the snow season. Solid lines denote 5-yr moving average.

Three pan-Arctic SWE datasets were compiled for 1980 through 2011: an assimilation of surface observations of snow depth and satellite passive microwave measurements recently developed within the European Space Agency GlobSnow project (www.globsnow.info) and described in Takala et al. (2011), the Canadian Meteorological Centre (CMC) daily gridded global snow depth analysis (Brasnett, 1999), and the ERA-interim atmospheric reanalysis (Dee et al., 2011). While the CMC analysis was utilized in previous Arctic Report Cards, the recent release of ERA-interim data back to 1980 combined with the first release of the GlobSnow data record (also available from 1980) allowed all 3 datasets to be available for each season since 1980, ten years longer than the previously considered time series. The multi-dataset Arctic SWE anomaly series (with respect to 1988-2007) for the month of April is shown in Fig. HTC4. Across the NA Arctic, 2011 was characterized by the third highest peak pre-melt SWE anomaly in the record. This is also reflected in mean April snow depth analysis from CMC (Fig. HTC5), which shows predominantly positive snow depth anomalies over the North American Arctic. While a

negative SWE trend was evident between 1980 and 2003 (r=-0.56), the strong positive anomaly in 2011 continues a short-term positive trend apparent since 2004 (r=0.60). Across Eurasia, the 2011 April SWE anomaly was near normal, with the time series exhibiting a weak positive trend since 1980 (r=0.40).

a.

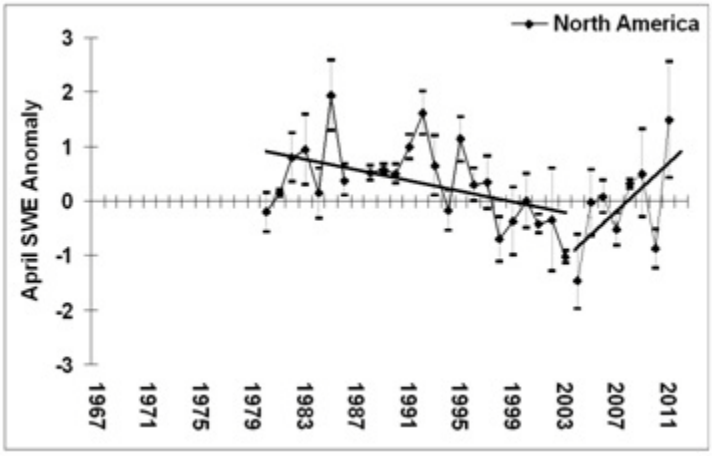

b.

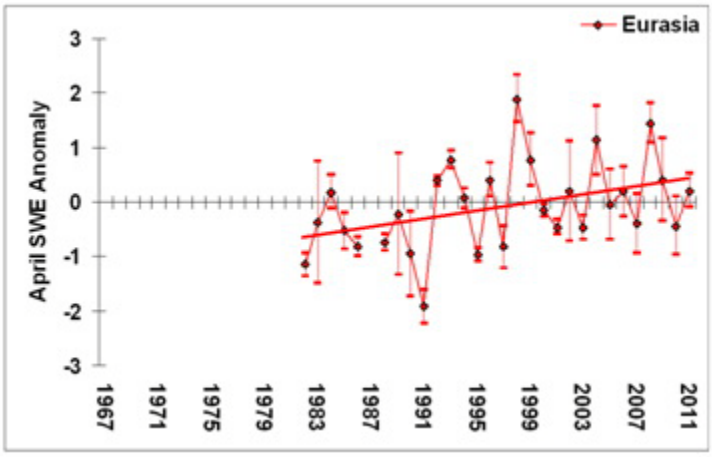

Fig. HTC4. Time series of multi-dataset average monthly April SWE standardized anomalies (+/- the standard error) relative to 1988-2007 for (a) North America and (b) Eurasia. Solid lines denote the linear trend. The break point in the NA best fit line is 2004.

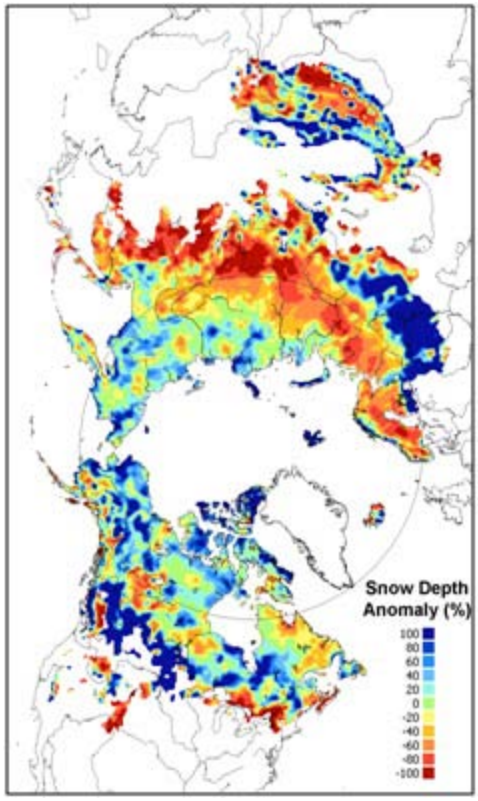

Fig. HTC5. April 2011 snow depth anomaly (% of 1999-2010 average) from the CMC snow depth analysis.

Variability in Arctic SWE is more difficult to interpret than SCE because it responds to both temperature and precipitation anomalies, and varies with snow climate regime and elevation (Brown and Mote, 2009). The overall positive pan-Arctic SWE trend observed over the past decade is consistent with documented trends of increasing precipitation over high latitudes (Zhang et al., 2007; Mekis and Vincent, 2011) and climate model predictions of increased high latitude precipitation across a warming Arctic (Min et al., 2008). The combination of continent-wide increases in SWE coupled with reduced spring SCD over the past 10 years is consistent with earlier peak stream flow, a more rapid recessional limb and higher peak runoff volume (Shiklomanov and Lammers, 2009). The recent reductions in Arctic spring snow cover extent and duration (due to earlier spring snow melt) are consistent with phenological changes in Arctic vegetation (Jia et al., 2009, and see the essay on *Vegetation*). Changing Arctic snow cover can also be linked to observed changes in wildlife (e.g., Drever et al., 2011).

References

Brasnett, B. 1999. A global analysis of snow depth for numerical weather prediction. Journal of Applied Meteorology. 38: 726-740.

Brown, R., C. Derksen, and L. Wang. 2007. Assessment of spring snow cover duration variability over northern Canada from satellite datasets. Remote Sensing of Environment. 111: 367-381.

Brown, R., and Mote, P. 2009. The response of Northern Hemisphere snow cover to a changing climate. Journal of Climate. 22: 2124-2145.

Brown, R., C. Derksen, and L. Wang. 2010. A multi-dataset analysis of variability and change in Arctic spring snow cover extent, 1967-2008. Journal of Geophysical Research. doi:10.1029/2010JD013975.

Brown, R., and Robinson, D. 2011 Northern Hemisphere spring snow cover variability and change over 1922-2010 including an assessment of uncertainty. The Cryosphere. 5: 219-229.

Dee, D. P., Uppala, S. M., Simmons, A. J., Berrisford, P., Poli, P., Kobayashi, S., Andrae, U., Balmaseda, M. A., Balsamo, G., Bauer, P., Bechtold, P., Beljaars, A. C. M., van de Berg, L., Bidlot, J., Bormann, N., Delsol, C., Dragani, R., Fuentes, M., Geer, A. J., Haimberger, L., Healy, S. B., Hersbach, H., Hólm, E. V., Isaksen, L., Kållberg, P., Köhler, M., Matricardi, M., McNally, A. P., Monge-Sanz, B. M., Morcrette, J.-J., Park, B.-K., Peubey, C., de Rosnay, P., Tavolato, C., Thépaut, J.-N. and Vitart, F. 2011 The ERA-Interim reanalysis: configuration and performance of the data assimilation system. Quarterly Journal of the Royal Meteorological Society. 137: 553-597. doi: 10.1002/qj.828.

Dery, S., and R. Brown. 2007. Recent Northern Hemisphere snow cover extent trends and implications for the snow-albedo feedback. Geophysical Research Letters. 34: L22504, doi:10.1029/2007GL031474.

Drever, M., R. Clark, C. Derksen, P. Toose, T. Nudds, and S. Slattery. 2011. Population vulnerability to climate change linked to timing of breeding in boreal ducks. Global Change Biology. doi: 10.1111/j.1365-2486.2011.02541.x.

Jia, G. Epstein, H. and Walker, D. 2009 Vegetation greening in the Canadian Arctic related to decadal warming. Journal of Environmental Monitoring. 11: 2231-2238.

Mekis, E., and L. Vincent. 2011. An overview of the second generation adjusted daily precipitation dataset for trend analysis in Canada. Atmosphere-Ocean. 49: 163 - 177.

Min, S-K., X. Zhang, and F. Zwiers. 2008. Human-induced Arctic moistening. Science. 320: 518-520.

Shiklomanov, A. and Lammers, R. 2009 Record Russian river discharge in 2007 and the limits of analysis. Environmental Research Letters. 4: 045015, doi:10.1088/1748-9326/4/4/045015.

Takala, M., K. Luojus, J. Pulliainen, C. Derksen, J. Lemmetyinen, J-P Kärnä, and J. Koskinen. 2011. Estimating northern hemisphere snow water equivalent for climate research through assimilation of space-borne radiometer data and ground-based measurements. Remote Sensing of Environment. doi:10.1016/j.rse.2011.08.014.

Zhang, X., F. W. Zwiers, G. C. Hagerl, F.H. Lambert, N. P. Gillet, S. Solomon, P. A. Stott and T. Nozawa, 2007: Detection of human influences on twentieth-century precipitation trends. Nature doi:10.1038/nature06025.

Glaciers and Ice Caps (outside Greenland)

M. Sharp[1] and G. Wolken[2]

[1]University of Alberta, Department of Earth and Atmospheric Sciences
[2]Alaska Division of Geological & Geophysical Surveys
With data contributions from
D. Burgess, A. Arendt, S. Luthcke, L. Copland, and D. Mueller

November 23, 2011

Highlights

- Warm summer temperatures caused negative mass balances on glaciers in Arctic Canada in the 2009-2010 balance year, extending a period of extremely negative balances in the region that began in 2005. These are nested in a longer period of very negative balances that began in 1987.
- The recent series of warm summers in Arctic Canada has also been associated with continued break-up of the floating ice shelves that fringe northern Ellesmere Island. They are now 54% of their 2005 total area.
- Climatic conditions during the 2010-2011 balance year suggest negative balances on most glaciers and ice caps in the Arctic, and especially on those within a broad region extending from southwest Greenland, the Canadian Arctic Islands and the eastern Russian Arctic.

Mountain glaciers and ice caps in the Arctic, with an area of over 400,000 km^2, are a significant contributor to global sea level change (Meier et al. 2007; Gardner et al. 2011). They lose mass by iceberg calving, and by surface melt and runoff. The net surface mass balance (B_n, the difference between annual snow accumulation and annual runoff) is a widely used measure of how they respond to climate variability and change. Variability in mean summer temperature accounts for much of the inter-annual variability in B_n in cold, dry regions like the Canadian high Arctic while, in more maritime regions like Iceland and southern Alaska, variability in winter precipitation is also a factor.

Measurements of B_n of 20 Arctic glaciers have been published for 2008-2009 (World Glacier Monitoring Service 2011). These are located in Alaska (three glaciers), Arctic Canada (four glaciers), Iceland (nine glaciers) and Svalbard (four glaciers) (Table HTC1). All but one of these glaciers (Dyngjujokull in Iceland) had a negative annual balance. The measured mass balances of the Alaskan glaciers for 2008-2009 were all very negative, and the 2008-2009 regional annual B_n for all glaciers in the Gulf of Alaska region (measured by GRACE satellite gravimetry) was -151±17 Gt yr^{-1}, the most negative annual value in the GRACE record for this region (A. Arendt and S. Luthcke, pers. comm.). Mass balances of glaciers in Iceland were less negative than in 2007-2008, while those of Svalbard glaciers were more negative.

Table HTC1. Measured annual net surface mass balance of glaciers in Alaska, the Canadian Arctic, Iceland and Svalbard for 2008-2009 and 2009-2010. Mass balance data for glaciers in Alaska, Svalbard and Iceland are from the World Glacier Monitoring Service (2011); those for the Canadian Arctic were supplied by D. Burgess and J. G. Cogley. The mass balance of all Gulf of Alaska glaciers is derived from GRACE satellite gravity measurements (S. Luthcke and A. Arendt, pers. comm.).

Region	Glacier	Net Balance 2008-9 (kg m^{-2} yr^{-1})	Net Balance 2009-10 (kg m^{-2} yr^{-1})	GRACE 2008-2009 (Gt yr^{-1})
Alaska				
	Gulf of Alaska glaciers			-151± 17
	Wolverine	-1780		
	Lemon Creek	-700		
	Gulkana	-720		
Arctic Canada				
	Devon Ice Cap	-523	-112	
	Meighen Ice Cap	-676	-118	
	Melville S. Ice Cap	-351	-211	
	White	-580	-188	
Iceland				
	Langjökull S. Dome	-362		
	Hofsjökull E	-170		
	Hofsjökull N	-350		
	Hofsjökull SW	-350		
	Köldukvislarjökull	-134		
	Tungnaarjökull	-809		
	Dyngjujökull	227		
	Brúarjökull	-122		
	Eyjabakkajökull	-507		
Svalbard				
	Midre Lovenbreen	-138		
	Austre Broggerbreen	-246		
	Kongsvegen	-78		
	Hansbreen	-138		

Measurements of B_n for the 2009-2010 balance year for the 4 glaciers in Arctic Canada were all negative (Table HTC1; D. Burgess and J.G. Cogley, pers. comm.), though less so than the 2008-2009 net balances. Nevertheless, they extend a period of very negative balances in the region that began in 1987. Of the total mass lost from the 4 glaciers monitored since 1963, 30-48% has occurred since 2005. The mean rate of mass loss from these 4 glaciers between 2005 and 2009 (-493 kg m^{-2} yr^{-1}) was nearly 5 times greater than the 1963-2004 average. In 2007 and 2008, it was 7 times greater (-698 kg m^{-2} yr^{-1}) (Sharp et al. 2011).

This recent series of warm summers in Arctic Canada (Sharp et al. 2011) has also been associated with the break-up of the floating ice shelves that fringe northern Ellesmere Island. The total area of these ice shelves is now 563 km^2, 54% of what it was in August 2005 (L. Copland and D. Mueller, pers. comm.). In summer 2011, the areas of the two remaining sections of the Serson Ice Shelf (which in 2008 were 42 km^2 (Serson A) and 35 km^2 (Serson B)) were reduced to 25 km^2 and 7 km^2 respectively. The Ward Hunt Ice Shelf, which had an area of 340 km^2 in 2010, split into two separate pieces with areas of 227 km^2 and 74 km^2.

To provide a direct measure of summer conditions over glaciers across the Arctic in summer 2011, we use the MODIS MOD11A2 land surface temperature (LST) product (2000-2011; ORNL DAAC 2010) (Table HTC2; Fig. HTC6). In the Canadian Arctic, summer mean 2011 LST anomalies ranged from -0.12°C in South Baffin to +2.68°C on the Agassiz Ice Cap, Ellesmere Island. Summer mean LSTs in 2011 were the warmest in the 12 year record on northern Ellesmere and Axel Heiberg islands, and the second warmest on the Devon, Sydkap (southern Ellesmere Island), and Barnes (northern Baffin Island) ice caps. Elsewhere in the Arctic, 2011 summer mean LSTs were also the warmest on record on Severnaya Zemlya and Franz Josef Land (anomalies of +1.74°C and +1.14°C respectively), and the second warmest in Svalbard and southwest Alaska (Table HTC1). Data for Novaya Zemlya and Iceland were not available at the time of writing as the melt season had not ended in those regions. By contrast, 2011 summer mean LSTs were only the 8th warmest on record on the Penny ice cap (southern Baffin Island; anomaly of -0.12°C) and the 9th warmest in southeast Alaska (anomaly of -0.11°C).

Table HTC2. Anomalies of summer (June-August) 2011 700 hPa air temperature, winter (September 2010-May 2011) precipitation, and summer 2011 MODIS MOD11A2 Land Surface Temperature (LST) for major glaciated regions of the Arctic (excluding Greenland). Air temperature and precipitation anomalies are relative to 1948-2008 climatology from the NCEP/NCAR R1 Reanalysis. LST anomalies are relative to the mean LST for the period 2000-2010. For ranks, 1 = year with highest summer air or land surface temperature and winter precipitation. Mean summer LST values are calculated from 8 day averages of daytime, clear sky values for a period centered on July 15 of each year. The length of the measurement period varies between regions and is equal to the mean (+ 4 standard deviations) annual melt duration in each region during the period 2000-2009 derived using microwave backscatter measurements from the Seawinds scatterometer on QuikScat. LST is measured for blocks of 1km by 1km cells containing only glacier ice centered on high elevation regions of major ice caps in each region. Block size varies with the size of the ice cap, but is consistent between years.

Region	Sub-Region	Latitude (N)	Longitude (E)	2011 JJA 700 hPa T Anomaly	2011 Rank	2010-11 Sep-May Ppt Anomaly	2010-11 Rank	2011 MODIS LST Anomaly	2011 Rank
				(°C)	(/64)	(mm)	(/63)	(°C)	(/12)
Arctic Canada	N. Ellesmere Island	80.6 - 83.1	267.7 - 294.1	2.72	2	-6.8	38	1.52	1
	Axel Heiberg Island	78.4 - 80.6	265.5 - 271.5	2.57	1	2.4	29	2.56	1
	Agassiz Ice Cap	79.2 - 81.1	278.9 - 290.4	2.43	2	15.7	9	2.68	1
	Prince of Wales Icefield	77.3 - 79.1	278 - 284.9	1.96	4	161.0	1	1.94	1
	Sydkap	76.5 - 77.1	270.7 - 275.8	2.01	3	58.1	8	1.39	2
	Manson Icefield	76.2 - 77.2	278.7 - 282.1	1.95	4	144.6	2	0.75	4
	Devon Ice Cap	74.5 - 75.8	273.4 - 280.3	1.50	6	-14.5	40	0.95	2
	North Baffin	68 - 74	278 - 295	1.42	7	-9.6	38	0.47	2
	South Baffin	65 - 68	290 - 300	1.76	3	60.9	14	-0.12	8
Eurasian Arctic	Severnaya Zemlya	76.25 - 81.25	88.75 - 111.25	1.46	7	47.6	8	1.74	1
	Novaya Zemlya	68.75 - 78.75	48.75 - 71.25	-0.32	40	36.8	16		
	Franz Josef Land	80 - 83	45 - 65	0.78	15	10.2	21	1.14	1
	Svalbard	76.25 - 81.25	8.75 - 31.25	0.62	15	13.3	25	0.51	2
	Iceland	63 - 66	338 - 346	-0.70	51	-3.3	32		
Alaska	SW Alaska	60 - 65	210 - 220	0.30	22	-33.2	37	0.40	2
	SE Alaska	55 - 60	220 - 230	-0.79	51	-196.5	56	-0.11	9

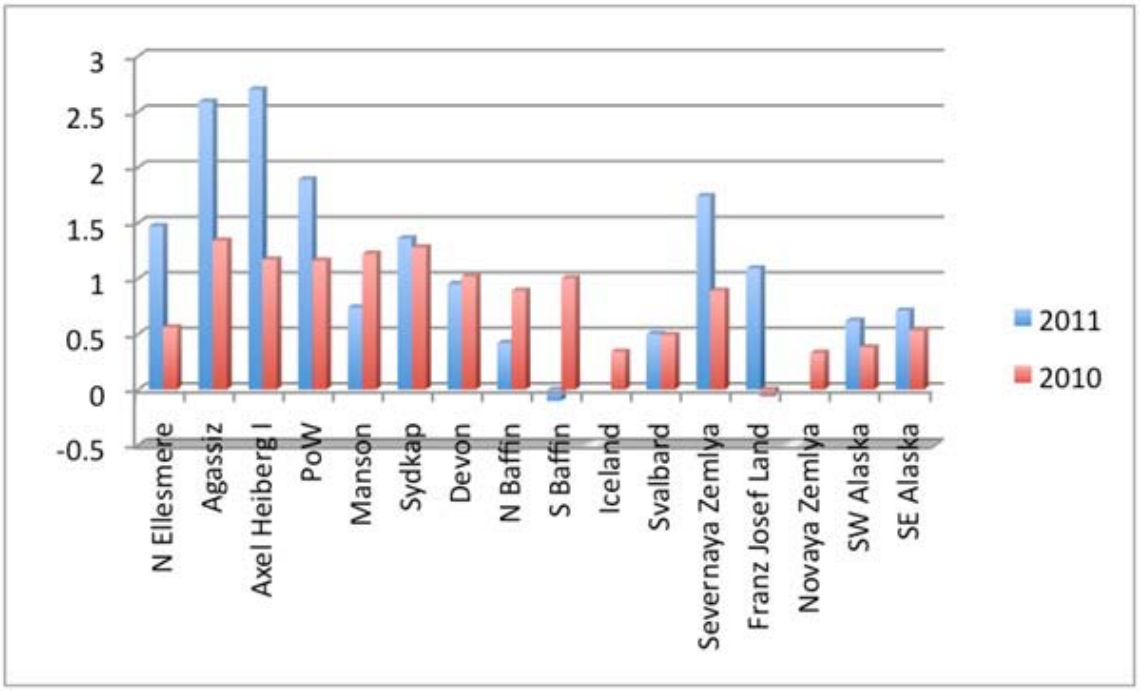

Fig. HTC6. Comparison of 2010 (red) and 2011 (blue) summer mean land surface temperature (LST) anomalies (relative to 2000-2010 climatology) for 16 glaciated regions of the Arctic based on the MODIS MOD11A2 LST product.

Data from the NCEP/NCAR R1 Reanalysis were also used as indicators of climatic conditions over the major glaciated regions of the Arctic during the 2010-2011 mass balance year. Relative to the 1948-2008 mean, winter precipitation (September 2010-May 2011) was significantly above normal in southeastern Ellesmere Island (anomalies of +145 to +161 mm) and in Novaya Zemlya and Severnaya Zemlya (+37 to +48 mm), and below normal in south eastern Alaska (-196.5 mm; Table HTC2; Fig. HTC7e). Summer temperature anomalies (JJA 2011 mean at 700 hPa geopotential height, relative to the 1948-2008 mean) were strongly positive over the Canadian Arctic Islands (including Baffin Island) and Severnaya Zemlya (+1.4 to +2.7°C; Table HTC2, Fig. HTC7d), moderately positive in Svalbard and Franz Josef Land (+0.6 to +0.8°C), and negative over Iceland (-0.7°C) and southeast Alaska (-0.79°C). These patterns of summer air temperature anomalies are broadly consistent with the pattern of summer LST anomalies.

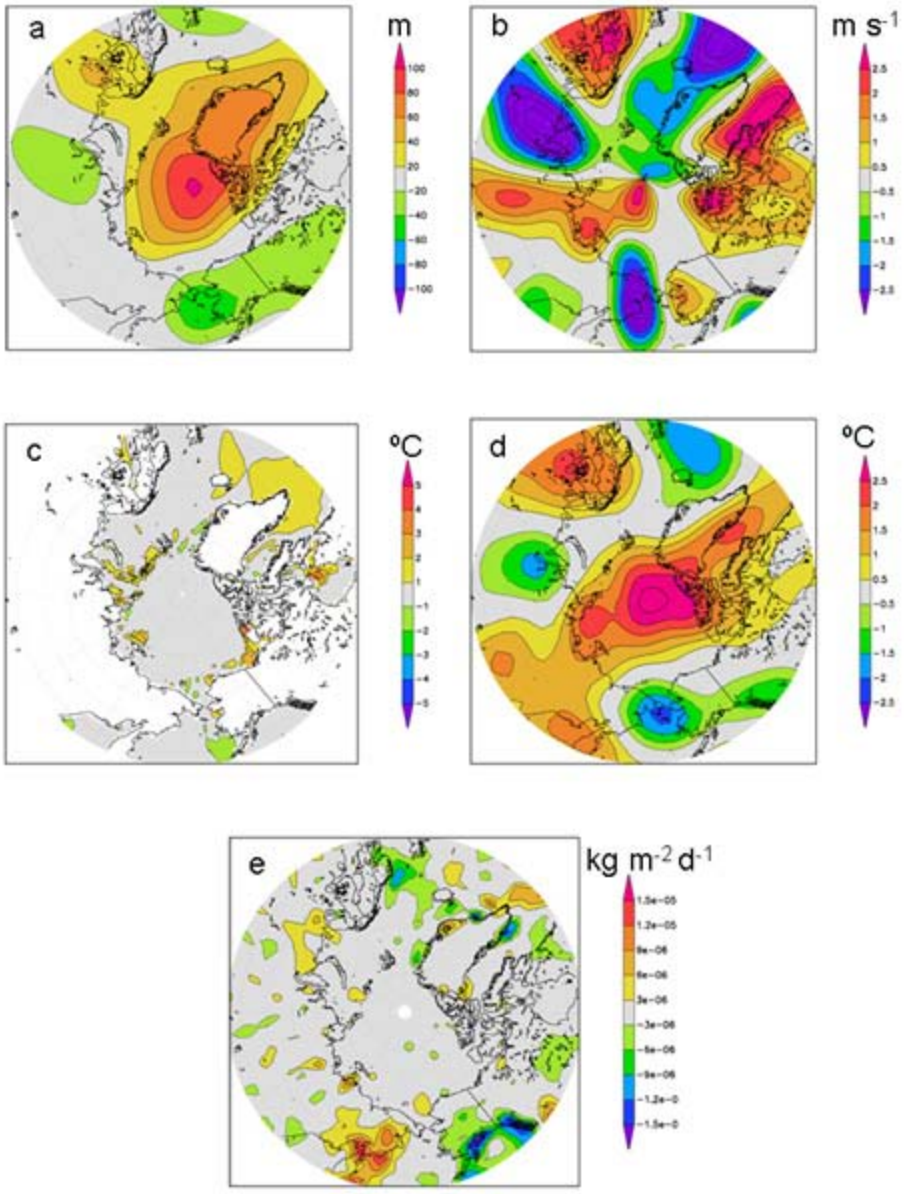

Fig. HTC7. (a) Summer (JJA) 2011 700 hPa geopotential height anomalies (relative to 1980-2010) over the Arctic from the NCEP/NCAR R1 Reanalysis; (b) Summer (JJA 2011) 700 hPa meridional wind speed anomalies over the Arctic (yellow/red = northward directed anomaly; blue/green = southward directed anomaly) from the NCEP/NCAR R1 Reanalysis; (c) Summer (JJ) 2011 sea surface temperature anomalies over the Arctic from the HADSST1 dataset; (d) Summer (JJA) 2011 700 hPa air temperature anomalies over the Arctic from the NCEP/NCAR R1 Reanalysis; (e) Winter (September 2010-May 2011) precipitation anomalies from the NCEP/NCAR R1 reanalysis.

The region of strongly positive summer 700 hPa air temperature anomalies in 2011 over west Greenland, Arctic Canada, Svalbard, Franz Josef Land and Severnaya Zemlya (Fig. HTC7d) was associated with a region of anomalously high 700 hPa geopotential height that was centred over the North Pole and extended across the Canadian Arctic Islands, Greenland, Iceland and the Eurasian Arctic Islands (excluding Novaya Zemlya) (Fig. HTC7a). Anomalous air flow

associated with this feature resulted in anomalous poleward-directed meridional winds at 700 hPa over Davis Strait, Baffin Bay and northeastern Canada (Fig. HTC7b). These seem to play an important role in transporting heat to west Greenland, the Canadian Arctic Islands and the more northerly of the Eurasian Arctic archipelagos from a region around southern Greenland and eastern Baffin Bay, where sea surface temperature anomalies in June and July 2011 were +1-2°C (Fig. HTC7c). Atmospheric circulation and air temperature are also described in the essay on *Temperature & Clouds* and *Greenland Ice Sheet*.

By comparing the 2010-11 winter precipitation and 2011 summer temperature anomaly patterns with the anomaly patterns and measured mass balances from previous years, we predict negative annual mass balances in most regions in 2010-2011. It seems likely that balances will be less negative than 2009-10 in southern Ellesmere and Devon islands, Iceland and southern Alaska, and more negative in northern Ellesmere and Axel Heiberg islands, Svalbard, Franz Josef Land and Severnaya Zemlya.

References

Gardner, A. S., G. Moholdt, B. Wouters, G. J. Wolken, J. G. Cogley, D. O. Burgess, M. J. Sharp, C. Braun, and C. Labine, 2011: Sharply increased mass loss from glaciers and ice caps in the Canadian Arctic Archipelago. Nature, 473, 357-360.

Meier, M. F., M. B. Dyurgerov, U. K. Rick, S. O'Neel, W. T. Pfeffer, R. S. Anderson, S. P. Anderson and A. F. Glazovsky, 2007: Glaciers dominate eustatic sea level rise in the 21st century. Science, 317, 1064-1067.

Oak Ridge National Laboratory Distributed Active Archive Center (ORNL DAAC), 2010: MODIS subsetted land products, Collection 5. Available on-line [http://daac.ornl.gov/MODIS/modis.html] from ORNL DAAC, Oak Ridge, Tennessee, U.S.A. Accessed September 26, 2011.

Sharp, M., D. O. Burgess, J. G. Cogley, M. Ecclestone, C. Labine, and G. J. Wolken, 2011: Extreme melt on Canada's Arctic ice caps in the 21st century. Geophysical Research Letters, 38, L11501, doi:10.1029/2011GL047381.

World Glacier Monitoring Service, 2011: Glacier mass balance data 2008 and 2009. http://www.geo.uzh.ch/microsite/wgms/mbb/sum09.html. Accessed 2 October 2011.

Greenland Ice Sheet

J. E. Box[1], J. Cappelen[2], C. Chen[1], D. Decker[1], X. Fettweis[3], D. Hall[5], E. Hanna[4], B. V. Jørgensen[2], N. T. Knudsen[6], W. H. Lipscomb[7], S. H. Mernild[7], T. Mote[8], N. Steiner[9], M. Tedesco[9], R. S. W. van de Wal[10], J. Wahr[11]

[1]Byrd Polar Research Center, The Ohio State University, Columbus, Ohio, USA
[2]Danish Meteorological Institute, Copenhagen, Denmark
[3]Department of Geography, University of Liège, Liège, Belgium
[4]Department of Geography, University of Sheffield, UK
[5]NASA Goddard Space Flight Center, Greenbelt, MD
[6]Department of Geology, Aarhus University, 8000 Aarhus, Denmark
[7]Los Alamos National Laboratory, Los Alamos, New Mexico 87545, USA
[8]Department of Geography, University of Georgia, Athens, Georgia, USA
[9]City College of New York, New York, NY, USA
[10]Institute for Marine and Atmospheric Research Utrecht, Utrecht University, Utrecht, The Netherlands
[11]Cooperative Institute for Research in Environmental Sciences, University of Colorado Boulder, Boulder, Colorado, USA

November 29, 2011

Highlights

- A persistent and strong negative North Atlantic Oscillation (NAO) index was responsible for southerly air flow along the west of Greenland, which caused anomalously warm weather in winter 2010-11 and summer 2011.
- The area and duration of melting at the surface of the ice sheet in summer 2011 were the third highest since 1979.
- The lowest surface albedo observed in 12 years of satellite observations (2000-2011) was a consequence of enhanced surface melting and below normal summer snowfall.
- The area of marine-terminating glaciers continued to decrease, though at less than half the rate of the previous 10 years.
- *In situ* measurements revealed near record-setting mass losses concentrated at higher elevations on the western slope of the ice sheet, and at an isolated glacier in southeastern Greenland.
- Total ice sheet mass loss in 2011 was 70% larger than the 2003-09 average annual loss rate of -250 Gt y^{-1}. According to satellite gravity data obtained since 2002, ice sheet mass loss is accelerating.

Meteorological station records (J. E. Box and J. Cappelen)

Surface air temperatures from Greenland long-term meteorological stations are characterized by a record-setting warm winter, unusually cold spring (March-May) and a record-setting warm late summer in the northwest of the island (Table HTC3). At Upernavik, summer 2011 was the warmest since the Beginning of Records (BR) in 1873. Similarly, at Thule AFB, July 2011 and the summer season (June-August) was the warmest on record since BR 1961. At Kangerlussuaq, April 2011 was the coldest on record since BR 1949. April 2011 cold anomalies exceeding 2 standard deviations below the 1971-2000 normal were observed at west Greenland

stations Nuuk and Paamiut. Surface air temperatures at the ice sheet Summit station since BR 1987 were below normal during March-June.

Table HTC3. Greenland station air temperature anomalies in the 12-month period before September 2011 relative to 1981-2010.

Station (Region), Latitude, Longitude	First Year	Statistic	SEP	OCT	NOV	Autumn	DEC	JAN	FEB	Winter	MAR	APR	MAY	Spring	JUN	JUL	AUG	Summer
Eureka	1948	Anomaly	-0.1	-0.6	3.8	1.1	**7.4**	5.6	-1.4	**4.0**	4.4	-3.5	1.8	0.9	**2.5**	**3.5**	0.0	**3.1**
80.0		Rank	24	30	5	13	**1**	5	44	**1**	3	49	14	14	**1**	**1**	0	**1**
85.9		Z-score	0.4	0.0	1.5	0.9	**2.3**	1.7	-0.3	**2.1**	1.8	-0.9	0.7	0.6	1.9	**3.3**	0.0	**3.2**
		warmest year	1998	2006	2009	1998	**2010**	1977	1978	**2011**	1962	1953	1967	2010	**2011**	**2011**	1960	**2011**
		coldest year	1979	1978	1982	1978	1972	1975	1979	1973	1977	1987	1995	1987	1974	1964	2000	1979
Pituffik/Thule AFB	1961	Anomaly	0.8	-0.1	**4.6**	2.8	5.3	5.9	-1.8	4.6	-1.1	**-5.0**	-0.5	-1.2	0.8	**3.5**	2.0	2.1
76.5		Rank	12	18	**1**	3	4	3	22	2	19	**33**	16	37	3	**1**	3	**1**
68.8		Z-score	0.4	0.0	**2.0**	1.4	1.2	1.5	-0.4	1.4	-0.2	**-2.0**	0.1	-0.7	1.2	**2.6**	1.4	**2.2**
		warmest year	1978	2004	**2010**	2000	1978	1977	1963	1963	1980	1968	1965	2010	1996	**2011**	2009	**2011**
		coldest year	1997	1964	1978	1986	2007	2004	1979	1984	1961	**2011**	1999	1992	1980	1972	1996	1972
Upernavik	1873	Anomaly	1.3	2.1	5.8	**3.1**	6.9	10.5	7.0	8.2	1.4	-4.1	-0.6	-1.1	1.8	3.7	1.8	2.4
72.8		Rank	20	18	2	**1**	3	4	13	3	52	132	94	98	5	**1**	11	**1**
56.2		Z-score	1.1	1.3	**2.4**	**2.3**	1.9	**2.1**	1.4	**2.3**	0.3	-1.4	-0.4	-0.6	1.9	**3.0**	1.5	**2.7**
		warmest year	1928	1960	1878	**2010**	1873	1929	1947	1947	1916	1905	1932	1932	2008	**2011**	1960	**2011**
		coldest year	1997	1986	1917	1917	1898	1983	1984	1983	1887	1896	1964	1896	1894	1916	1873	1873
Kangerlussuaq	1949	Anomaly	2.7	2.8	6.9	4.1	10.5	5.2	2.9	6.3	-0.2	**-8.6**	-1.7	-3.5	1.4	1.7	1.0	1.4
67.0		Rank	2	10	2	**1**	**1**	15	24	7	33	**59**	47	54	9	3	15	4
50.7		Z-score	1.7	1.0	**2.1**	**2.5**	**2.4**	0.8	0.3	1.4	-0.1	**-2.3**	-0.7	-1.3	1.1	1.6	0.7	1.5
		warmest year	2003	1960	1995	**2010**	**2010**	1963	1986	1986	2005	2000	2010	2005	1997	1968	1960	2010
		coldest year	1982	1989	1978	1982	1974	1983	1984	1983	1993	**2011**	1984	1993	1978	1973	1983	1983
Ilulissat	1873	Anomaly	2.8	1.9	5.2	3.3	6.2	4.6	5.5	5.5	2.2	-5.7	-1.3	-1.6	0.0	2.2	0.0	0.7
69.2		Rank	2	24	3	**1**	3	24	24	7	56	127	108	109	37	2	47	17
51.1		Z-score	**2.2**	1.0	**2.4**	**2.8**	**2.1**	1.1	1.0	1.6	0.3	-1.6	-0.7	-0.7	0.6	**2.3**	0.4	1.4
		warmest year	1915	1960	1878	**2010**	1978	1929	1986	1929	1916	1905	1933	1932	1997	1960	1960	1960
		coldest year	1884	1874	1986	1884	1898	1983	1984	1884	1993	1896	1875	1887	1918	1972	1884	1972
Aasiaat	1951	Anomaly	**2.6**	2.2	3.6	2.8	6.0	6.5	7.3	6.7	3.2	-4.6	-0.6	-0.7	1.1	2.3	1.8	1.7
68.7		Rank	**1**	4	**1**	**1**	2	5	5	3	14	57	43	41	12	2	4	2
52.8		Z-score	**3.1**	1.7	**2.2**	**2.9**	1.9	1.2	1.2	1.7	0.7	-1.6	-0.4	-0.3	1.1	**2.0**	1.6	1.9
		warmest year	**2010**	1960	**2010**	**2010**	1978	1980	1986	2010	2005	2000	2010	2010	2003	1960	1960	1960
		coldest year	1989	1986	1978	1986	1971	1983	1984	1984	1993	1984	1984	1993	1992	1972	1983	1972
Nuuk	1873	Anomaly	**3.1**	3.1	4.7	3.6	5.9	1.7	1.1	2.9	-0.1	-4.7	-0.9	-1.9	0.4	0.8	0.1	0.4
64.2		Rank	**1**	3	2	**1**	**1**	38	61	15	91	137	106	127	55	31	71	43
51.8		Z-score	**2.9**	**2.5**	**2.8**	**3.8**	**2.4**	0.6	0.2	1.2	-0.3	**-2.3**	-0.8	-1.4	0.3	0.9	0.0	0.5
		warmest year	**2010**	1960	1878	**2010**	**2010**	1917	1901	2010	1916	1953	2010	1932	1947	2008	2010	2010
		coldest year	1879	1884	1913	1898	1883	1984	1984	1984	1993	1949	1992	1993	1922	1955	1884	1914
Paamiut	1958	Anomaly	2.0	**3.9**	**5.4**	**3.8**	**6.1**	3.6	1.9	3.9	0.2	-4.0	-1.3	-1.7	-0.2	0.9	0.1	0.3
62.0		Rank	2	**1**	**1**	**1**	**1**	9	22	6	29	52	43	46	23	11	24	18
49.7		Z-score	1.9	**2.6**	**2.8**	**3.4**	**2.3**	1.0	0.3	1.4	0.0	**-2.0**	-0.8	-1.0	0.1	0.9	0.1	0.4
		warmest year	2003	2010	2010	**2010**	2010	2010	1986	2010	2005	2005	2010	2005	1987	1958	2010	2010
		coldest year	1982	1963	1986	1982	1974	1983	1984	1984	1993	1984	1992	1993	1972	1969	1969	1969
Narsarsuaq	1961	Anomaly	**2.5**	3.8	**5.6**	**4.0**	6.9	3.2	2.6	4.3	0.6	-3.6	-1.5	-1.5	0.9	1.1	0.4	0.8
61.2		Rank	**1**	2	**1**	**1**	2	13	19	7	27	47	43	40	11	8	19	7
45.4		Z-score	**2.3**	**2.1**	**2.1**	**3.1**	1.8	0.6	0.3	1.1	0.0	-1.4	-0.8	-0.8	1.0	1.3	0.4	1.2
		warmest year	**2010**	2003	**2010**	**2010**	1978	2003	1986	2010	1962	1998	2010	2010	1991	1991	1987	2003
		coldest year	1969	1963	1982	1963	1974	1983	1984	1984	1995	1990	1992	1989	1992	1969	1983	1983
Quaqortoq	1880	Anomaly	**2.8**	3.2	4.5	3.5	6.0	3.1	1.7	3.7	5.7	-3.7	-1.5	0.2	-0.4	1.2	1.0	0.6
60.7		Rank	**1**	3	**1**	**1**	3	19	46	10	6	126	123	74	90	13	18	37
46.0		Z-score	**2.9**	**2.2**	**2.5**	**3.3**	**2.4**	1.2	0.4	1.6	1.6	-1.9	-1.3	-0.1	-0.4	1.4	1.0	0.7
		warmest year	**2010**	1960	**2010**	**2010**	1978	2010	1901	2010	1932	1881	1935	1932	1929	2003	1960	1929
		coldest year	1969	1884	1920	1898	1914	1983	1883	1884	1882	1984	1992	1989	1922	1969	1884	1884
Danmarkshavn	1949	Anomaly	**1.1**	1.4	-2.7	0.0	2.4	0.7	5.6	3.0	2.3	0.2	1.3	1.3	1.3	-0.2	1.1	0.7
76.8		Rank	9	13	47	27	9	20	3	4	13	16	15	9	6	26	7	5
18.8		Z-score	1.2	0.7	-0.8	0.2	1.0	0.3	**2.2**	1.8	0.9	0.4	0.8	1.1	1.3	0.1	1.3	1.3
		warmest year	2002	2002	1972	2002	1956	1990	2008	2005	1976	2006	1967	1976	2008	1958	2003	2008
		coldest year	1968	1966	1971	1971	1975	1978	1970	1967	1966	1969	1956	1966	2006	1955	1999	1955
Illoqqortoormiut	1948	Anomaly	**1.5**	2.1	-2.0	0.5	3.6	2.1	6.0	4.0	0.9	1.1	0.4	0.8	-0.4	-0.8	0.0	-0.4
70.4		Rank	5	6	44	14	6	13	2	2	15	11	15	14	21	26	14	22
22.0		Z-score	1.7	1.2	-0.4	0.8	1.5	0.9	**2.2**	**2.1**	0.7	0.9	0.9	1.0	0.5	0.5	0.8	0.6
		warmest year	2002	2002	2002	2002	1984	1974	2005	2005	1996	2004	2009	1996	1995	1991	2004	2004
		coldest year	1956	1968	1951	1951	1965	1959	1978	1966	1969	1951	1956	1956	1956	1953	1952	1955
Tasiilaq	1895	Anomaly	**1.9**	2.2	-0.1	1.3	4.3	0.6	3.1	2.8	-2.4	0.8	0.4	-0.4	0.8	0.9	0.4	0.7
65.6		Rank	5	9	44	10	4	43	11	5	98	39	57	74	35	33	34	28
37.6		Z-score	1.7	1.6	0.4	1.4	**2.0**	0.4	1.3	1.7	-1.0	0.5	0.0	-0.3	0.4	0.6	0.6	0.7
		warmest year	1939	1915	2002	1941	1933	1987	1932	1929	1929	1926	1933	1929	1932	1939	2010	2003
		coldest year	1982	1917	1917	1917	1917	1918	1919	1918	1899	1919	1979	1990	1998	1983	1983	1983
Prins Christian Sund	1951	Anomaly	**2.7**	1.9	2.1	**2.2**	**4.9**	1.9	0.9	2.7	-0.3	-1.7	0.3	-0.6	0.2	0.6	0.0	0.3
60.0		Rank	**1**	2	2	**1**	**1**	6	21	2	40	57	20	47	23	12	26	18
43.2		Z-score	**2.6**	**2.0**	1.8	**2.7**	**3.3**	1.2	0.4	**2.0**	-0.3	-1.6	0.3	-0.8	0.4	0.7	0.1	0.5
		warmest year	**2010**	2003	2002	**2010**	2010	2010	2005	2010	2005	2004	2010	2005	2008	2005	2010	2010
		coldest year	1982	1969	1978	1982	1971	1983	1993	1993	1989	1969	1982	1989	1970	1969	1992	1970
Summit	1988	Anomaly	**7.0**	0.0	-0.9	2.1	3.6	-1.6	3.1	**1.8**	-3.4	-1.4	-1.9	-2.3	-0.3	2.0	0.1	0.6
72.6		Rank	2	13	13	4	5	17	7	**6**	19	18	21	22	15	5	12	8
38.5		Z-score	**2.0**	0.0	-0.2	0.9	0.9	-0.4	0.8	**0.6**	-0.8	-0.5	-0.7	-1.0	-0.1	1.2	0.0	0.4
		warmest year	1987	1987	1995	1987	2001	2010	2006	**2010**	2005	1994	2010	2005	2007	2005	1987	2010
		coldest year	2005	1995	2006	2009	1992	1993	2002	1993	1990	1992	1992	1992	2000	1992	1992	1992

*** Winter includes December of previous year**

Upper air temperatures (J. E. Box)

Seasonally-averaged 2011 upper air temperature data available from twice-daily radiosonde observations (Durre et al. 2006) in the vicinity of Greenland (see Table HTC4 for site locations) indicate anomalous tropospheric warmth in summer and winter and mid-tropospheric cold anomalies in spring (Fig. HTC8). The typical asymmetry between the tropospheric and stratospheric anomalies is most evident in winter, when record-setting cold anomalies were observed above 100 hPa. Mid-stratospheric atmospheric mass is low and prone to extremes. The overall warm pattern near the surface at 1000 hPa is consistent with a warming trend prevailing since reliable records began in 1964 and which has been most pronounced since the mid-1980s (Box and Cohen 2006).

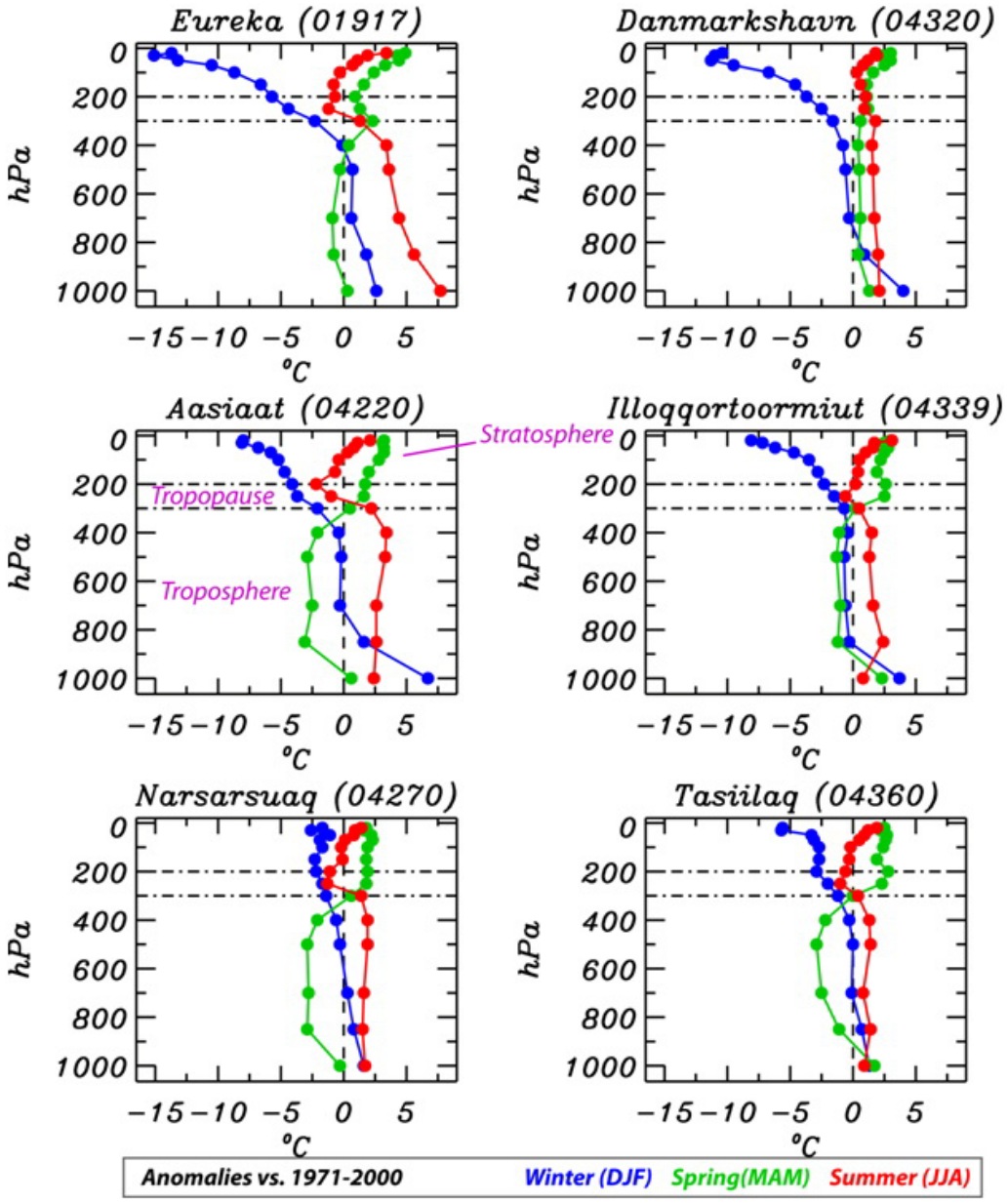

Fig. HTC8. Upper air temperature anomalies relative to the 1981-2010 baseline in winter, spring and summer of 2011.

Atmospheric circulation and air temperature (X. Fettweis)

Summer 2011 was characterized by a constant negative North Atlantic Oscillation (NAO) index for the entire season; a -2.4 standard deviation anomaly in comparison with the 1971-2000 JJA NAO average. Consequently, the 2011 atmospheric flow was characterised by warm air advection from the south along the western coast (Fig. HTC9). The circulation anomaly (Fig. HTC9) caused significant summer temperature departures from normal (Fig. HTC10) and drier conditions than normal at the south of the ice sheet (Fig. HTC11). The effects of the circulation anomaly also extended into the Canadian Arctic Islands, where there were strong positive temperature anomalies and negative glacier mass balances (see the essay on *Glaciers and Ice Caps*).

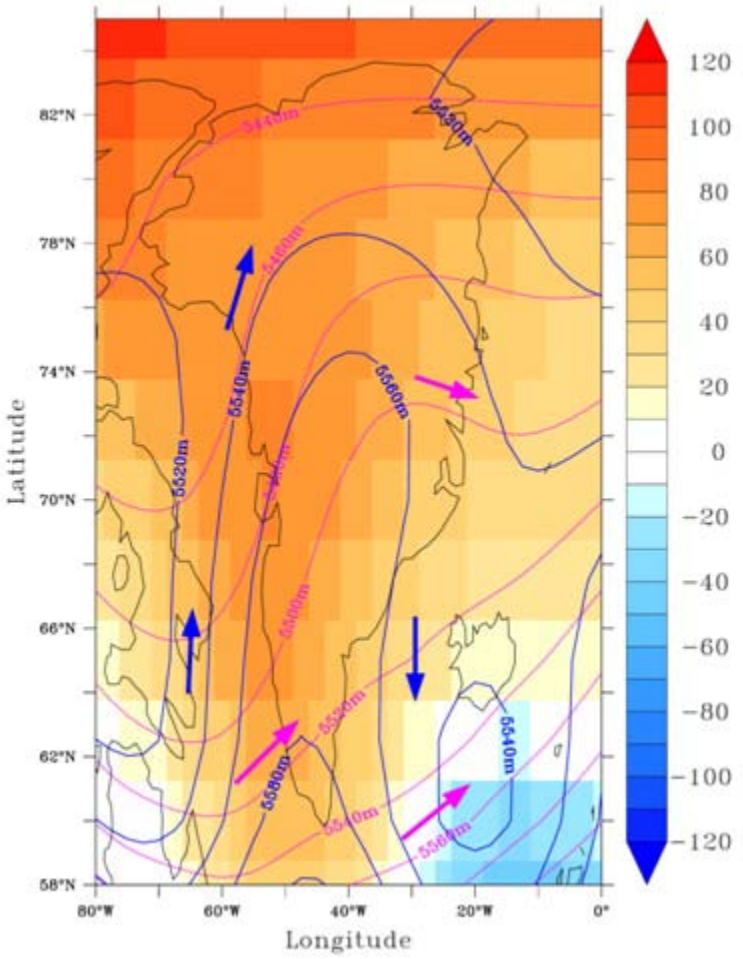

Fig. HTC9. Geopotential height anomalies for summer (JJA) 2011 (referenced to the 1981-2010 mean) at 500 hPa from the NCEP/NCAR Reanalysis. The blue and magenta lines plot the summer (JJA) mean geopotential height at 500 hPa in 2011 and during 1971-2000, respectively. The arrows show the direction of the main air flows.

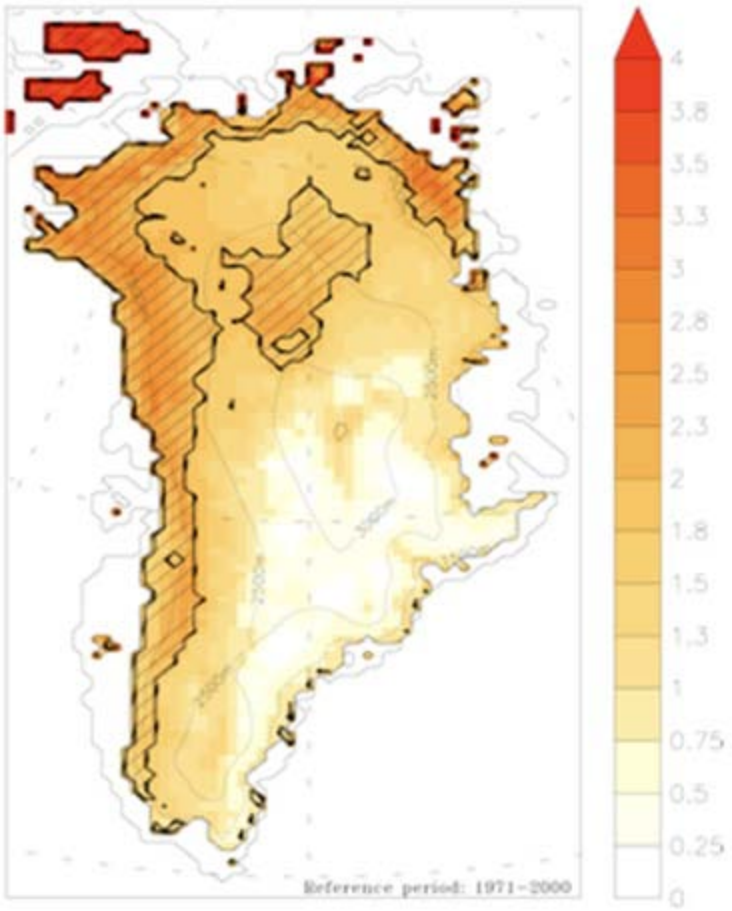

Fig. HTC10. Summer (JJA) mean 2011 near-surface temperature (Kelvin) anomalies simulated by MAR (Fettweis et al., 2011) relative to the period 1981-2010. Areas where temperature anomalies were at least twice the 1981-2010 standard deviation are hatched.

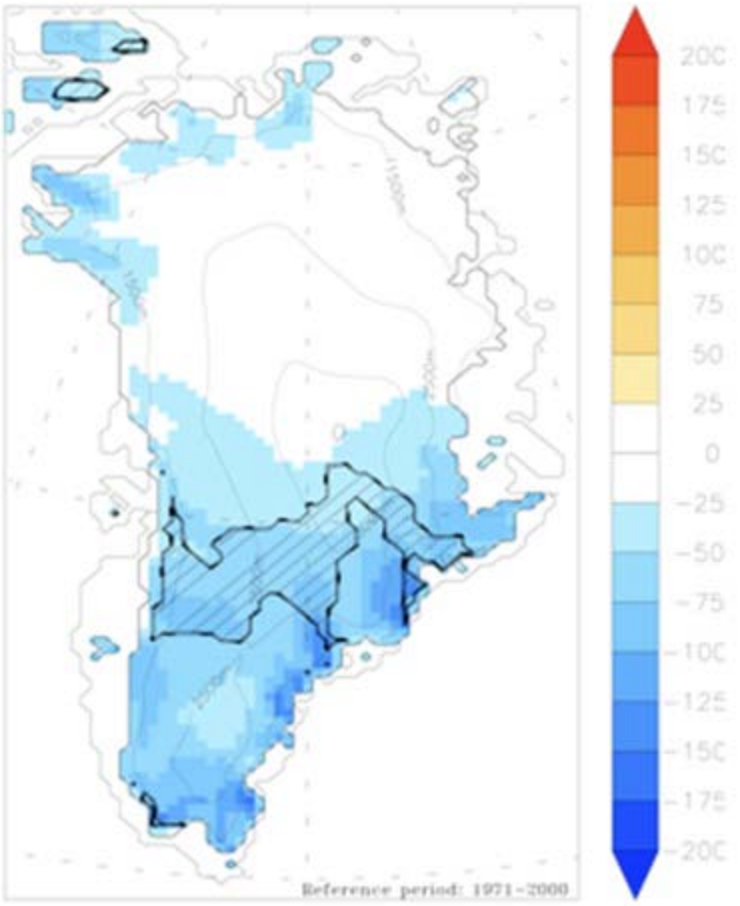

Fig. HTC11. Summer (JJA) snowfall anomaly (mm water equivalence) simulated by MAR (Fettweis et al., 2011) relative to the period 1981-2010. Areas where temperature anomalies were at least twice the 1981-2010 standard deviation are hatched.

Greenland coastal precipitation (S. H. Mernild, J. Cappelen, B. V. Jørgensen, W. H. Lipscomb, J. E. Box, and E. Hanna)

Changes in Greenland precipitation over time are of interest for understanding fluctuations in glacier and ice sheet mass balance and freshwater runoff to the ocean. Long-term changes are difficult to quantify, however, because Greenland meteorological stations are sparsely and non-uniformly distributed. Here, observed precipitation data (uncorrected for gauge catch efficiency and type) from eight DMI (Danish Meteorological Institute; DMI 2000, 2010) synoptic stations are examined, from Kangerlussuaq (continental west) to Qaqortoq in southwest Greenland and from Tasiilaq (maritime east) to Station Nord in the northeast (Table HTC4).

Table HTC4. Greenland station precipitation (uncorrected) anomalies by season for 2011 relative to 1981-2010.

Station (Region), Latitude, Longitude	First year	Statistic	JAN	FEB	MAR	APR	MAY	JUN	JUL	AUG	Winter (DJF)	Spring (MAM)	Summer (JJA)	SEP - AUG
Kangerlussuaq (W)	1976	Anomaly	-7	18	-2	-8	-8	-13	-11	-10	15	-18	-34	-55
67° 01' N		Rank	34	1	25	36	32	34	22	21	4	35	32	34
50° 42' W		Z-score	-1.2	4.5	-0.7	-1.0	-0.9	-1.1	-0.6	-0.5	1.5	-1.3	-1.4	-1.6
		driest year	1990	1989	2006	2011	1995	2000	1999	1977	1990	1995	1980	1980
		wettest year	2000	2011	1991	2005	2005	1994	1997	1991	2004	2005	1983	2005
Nuuk (SW)	1890	Anomaly	17	-4	46	-22	-48	-28	-7	16	51	-24	-21	-116
64° 10' N		Rank	13	37	10	58	99	71	43	38	14	43	58	44
51° 45' W		Z-score	0.5	-0.1	1.4	-0.7	-1.0	-0.8	-0.1	0.3	0.7	-0.4	-0.3	-0.6
		driest year	1939	1933	1909	1902	1911	1913	1933	1966	1939	1930	1903	1949
		wettest year	1953	1890	1968	2006	1928	1979	1983	1984	1954	2005	1915	2005
Narsarsuaq (SW)	1961	Anomaly	-8	-19	-4	-34	-18	-48	-4	19	-14	-56	-33	-208
61° 10' N		Rank	19	24	20	43	27	47	24	17	23	38	35	41
45° 25' W		Z-score	-0.2	-0.3	-0.1	-1	-0.5	-1.3	-0.1	0.4	-0.2	-1.0	-0.5	-1.1
		driest year	1966	2010	1962	1989	1974	2008	1992	1966	1976	1983	1983	1976
		wettest year	1996	1993	1998	1999	1987	1983	1966	1984	1966	1962	2009	1985
Qaqortoq (SW)	1961	Anomaly	-31	-4	-29	-23	-5	-62	-57	23	-25	-56	-97	-293
60° 43' N		Rank	27	13	31	29	14	38	35	13	20	31	33	35
46° 03' W		Z-score	-0.6	-0.1	-0.5	-0.6	-0.1	-1.4	-1.0	0.4	-0.2	-0.7	-1.0	-1.1
		driest year	2004	1982	1994	1989	1985	1974	1992	1980	2010	1985	2010	2010
		wettest year	2005	1993	1983	1975	1987	1997	1982	1984	1992	1983	1984	1996

Station (Region), Latitude, Longitude	First year	Statistic	JAN	FEB	MAR	APR	MAY	JUN	JUL	AUG	Winter (DJF)	Spring (MAM)	Summer (JJA)	SEP - AUG
Tasiilaq (SE)	1898	Anomaly	-24	12	50	53	-26	-31	-14	1	-80	76	-44	-34
65° 36' N		Rank	47	31	19	11	76	108	63	42	67	19	80	53
37° 37' W		Z-score	-0.3	0.2	1.0	1.2	-0.6	-1.1	-0.4	0.0	-0.7	1.1	-0.7	-0.2
		driest year	1948	1957	1940	1950	1941	1991	1954	1943	1931	1915	1924	1931
		wettest year	1972	1932	1964	1909	1903	1953	1901	1947	1972	1964	1901	1903
Illoqqortoormiut (E)§	1950	Anomaly	18	112	4	36	49	3			160	89		
70° 29' N		Rank	13	2	21	5	2	23			2	3		
21° 57' W		Z-score	0.4	3.1	0.2	1.7	4.1	0.2			1.7	2.5		
		driest year	1955	1965	1992	1988	1958	1982	2001	1977	1986	1953	1950	1952
		wettest year	2008	1982	1976	2004	1970	1953	1970	1982	2008	1976	1969	2008
Danmarkshavn (NE)	1949	Anomaly	0	5	24	17	5	-5	-11	27	-6	46	11	36
76° 46' N		Rank	16	14	3	7	8	56	39	4	23	1	13	10
18° 40' W		Z-score	0.0	0.4	1.8	1.3	1.0	-0.8	-0.7	1.6	-0.2	2.4	0.4	0.6
		driest year	1975	2010	1962	1962	1997	2011	2010	1973	1951	1962	2010	1951
		wettest year	2006	2008	1982	2006	2009	1954	1986	1990	2006	2011	1998	2006
Station Nord (NE)	1961	Anomaly	-5	-1	9	0	4	-4	4	18	34	23	36	134
81° 36' N		Rank	16	14	5	14	9	19	10	6	11	11	9	12
16° 39' W		Z-score	-0.3	-0.1	0.5	0.0	0.3	-0.4	0.2	1.1	1.1	0.5	1.1	1.2
		driest year	1997	1994	1986	1986	1980	1990	1993	1988	1988	2006	1996	2006
		wettest year	2006	2010	2010	2010	1988	1994	1995	1999	2010	2010	1995	2010

§Anomalies are in mm water equivalent (w.e.), with respect to the 1981-2010 base period. No precipitation data exist from July and August 2011 for Illoqqortoormiut. In cases when the monthly precipitation is zero for two or more months, the next highest year is mentioned in the table. Bold values indicate values that meet or exceed 2 standard deviations from the base period. Red characters indicate record-setting values. The winter values include December from the previous year.

In 2011, a clear pattern of below-average annual (September through August) precipitation is evident at the west, southwest and southeast stations, with the largest anomalies in the south (above one standard deviation). In east and northeast Greenland, precipitation was above average. Overall, precipitation in 2011 was less extreme than in 2010, when annual precipitation reached a record low since BR 1961 in Qaqortoq and a record high since 1961 at Station Nord. No annual precipitation records were set in 2011. Remarkable extremes occurred; Kangerlussuaq had the wettest February and driest April on record (RB 1976) and Danmarkshavn had the wettest spring (March to May) and the driest June on record (RB 1949).

Surface melting (T. Mote and M. Tedesco)

Greenland ice sheet surface and near-surface melt above ~1% liquid water content is estimated from thresholds in 19 GHz horizontally-polarized brightness temperatures measured by the spaceborne SSM/I instrument (Mote and Anderson, 2005). These data indicated that the melt area for the period June through August 2011 ranked the third greatest since 1979, after 2007 and 2010 in that order. The years were ranked based on the seasonal melt departure (SMD), the sum of the daily melt extent anomalies over each summer (Mote 2007). These annual ranking are sensitive to the length of the selected season. Expanding the season from 15 May to 15 September drops 2011 to the 6th most extensive melt year, following 2010, 2007, 2002, 1998, and 2005, in that order. More extensive than average melt was evident from early June through early August 2011 (Fig. HTC12). An average of 31% of the ice sheet area was melting during June through August 2011, compared to 33% in 2007 and 32% in 2010. No other year since 1979 had an average greater than 30%; the 1981-2010 average was 24.1%.

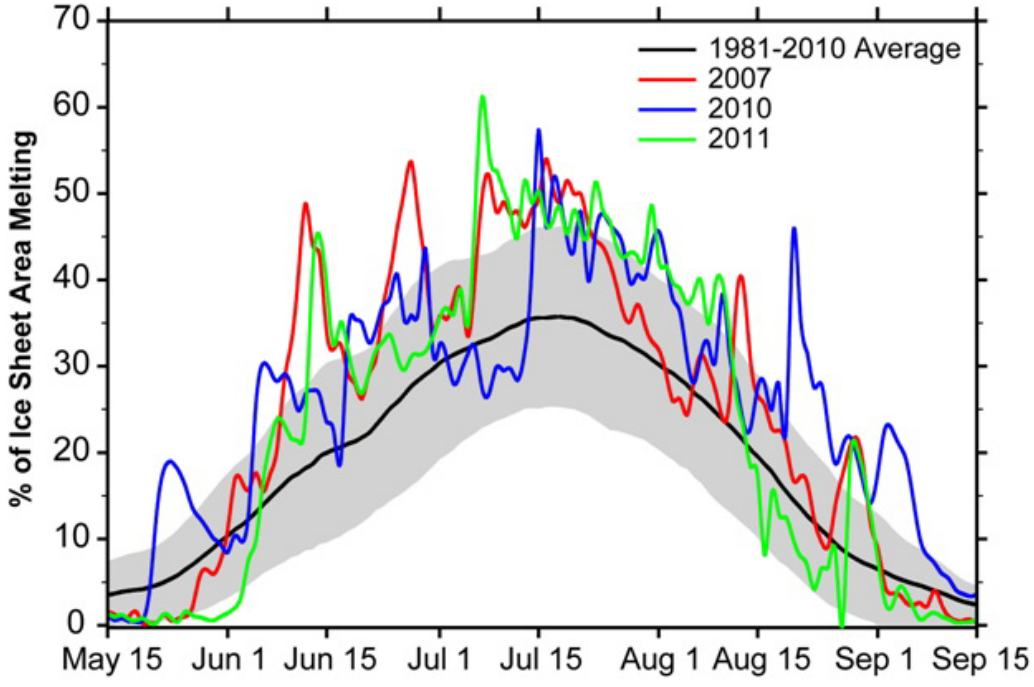

Fig. HTC12. Fractional area (%) of the Greenland Ice Sheet identified as melting from SSM/I. The standard deviation of the 1981-2010 period is shaded.

Melting in Greenland in 2011 was still above the 1979-2010 average and was exceptionally high over the western mid-elevations. The number of melting days in 2011, estimated from spaceborne microwave observations using the approach in (Tedesco, 2007), did not break the previous record set in 2010. Year 2011 is 6th for melting, after 2010, 2007, 1998, 2002, 2005. The updated trend for the area of the ice sheet subject to melting is 16,800 km^2 per year, close to the trend estimated with 2010 of 17,202 km^2 per year. The 2011 departure of the number of melting days from the 1979-2010 baseline is illustrated in Fig. HTC13. In 2011, melting at high elevations (above 2500 m) was ~1 standard deviation above the 1979-2010 average (versus the ~2 standard deviations of 2010). Melting in 2011 was above average over most of Greenland, with large positive anomalies (e.g., longer melting with respect to the average) occurring especially in the west and northwest, with melting lasting up to ~30 days longer than the average.

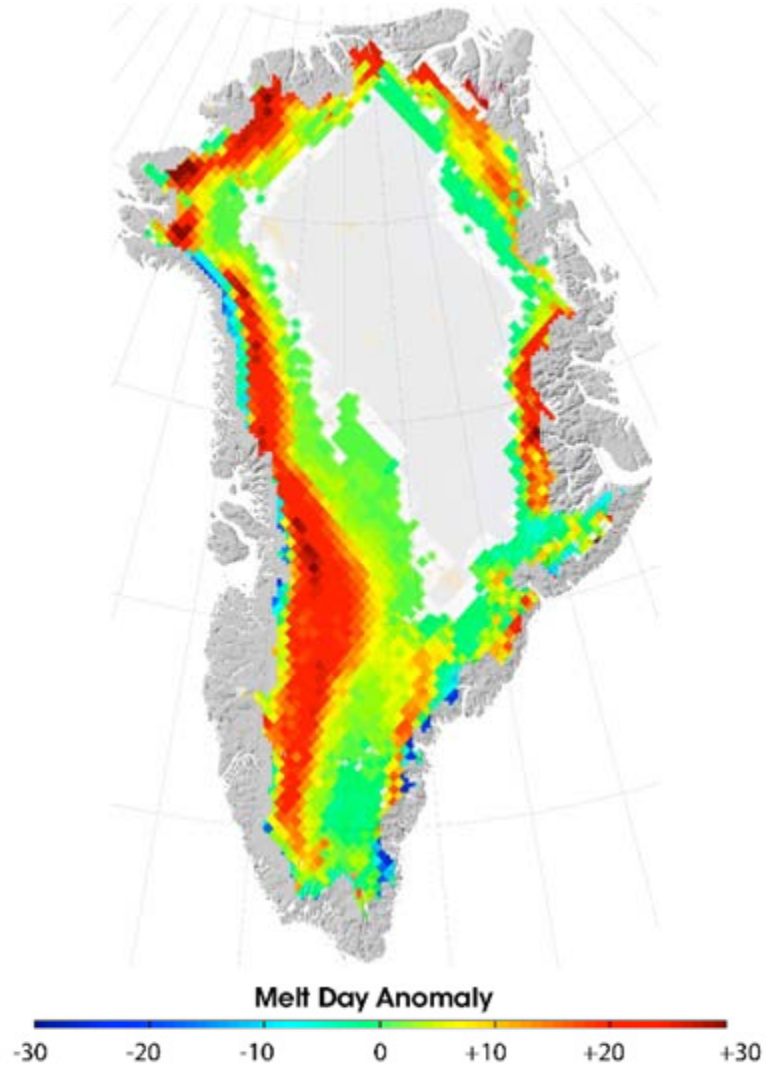

Fig. HTC13. Melting degree day anomaly in 2011 relative to the 1979-2010 baseline.

Albedo (J. E. Box and D. K. Hall)

A dominant source of energy for melting is absorbed solar irradiance, which depends on the surface solar reflectivity from ~0.3 μm to ~4 μm in wavelength, known as the *albedo*. Freshly fallen snow under clear skies has an albedo of ~0.84 (Konzelmann and Ohmura, 1995). Over time, and with increasing temperature, snow grain size increases as crystals metamorphose and grow (Wiscombe and Warren, 1980; Dozier et al., 1981; Warren, 1982) resulting in a decrease in albedo. Melting snow albedo can have values of 0.74 (see measurement summary in Patterson, 1994). Impurity-rich ice sheet albedo retrievals from the MODIS sensor on the NASA Terra platform (the MOD10A1 product; Klein and Stroeve, 2002) can be as low as 0.31 averaged over 5 x 5 km areas, in agreement with the value recommended by Cuffey and Patterson (2011).

Negative albedo anomalies are widespread over the ice sheet during the 2011 melt period. Figure HTC14 illustrates the 2011 anomalies for summer (June-August), when solar irradiance is highest and the albedo is lowest in magnitude. The albedo anomaly is much larger over the regions where darker bare ice is exposed after the previous winter's snow accumulation has ablated. Fig. HTC15 illustrates the significant albedo decline for the ice sheet.

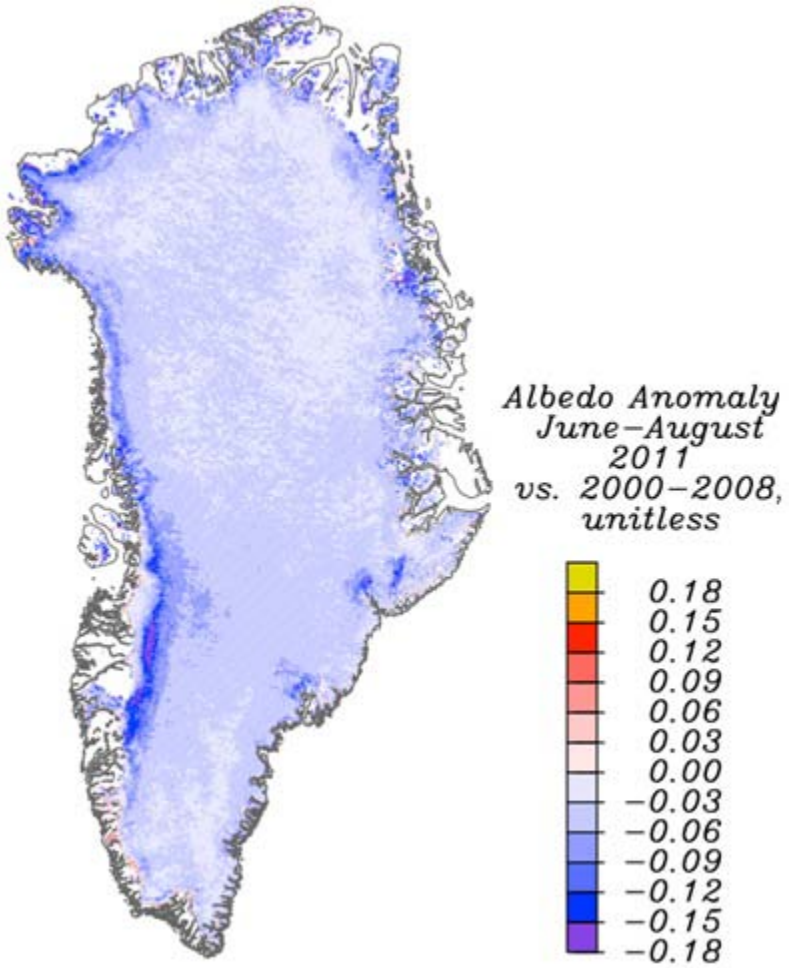

Fig. HTC14. Summer (JJA) albedo anomaly in 2011 relative to the 2000-2008 period.

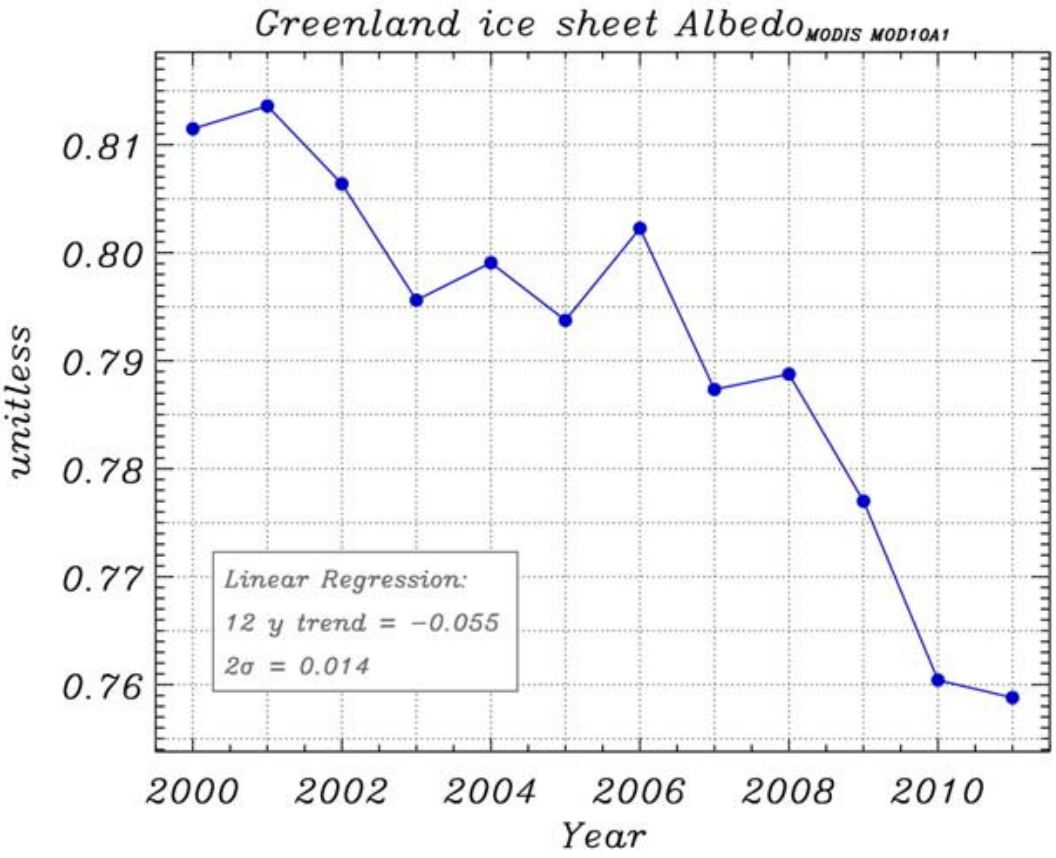

Fig. HTC15. Greenland ice sheet albedo from MODIS (Moderate Resolution Imaging Spectroradiometer) observations, 2000-2011.

Surface mass balance along the K-Transect (R. S. W. van de Wal and X. Fettweis)

The 150 km long K-Transect is located near Kangerlussuaq at 67°N between 340 m and 1500 m above sea level (a.s.l.) on the western flank of the ice sheet (van de Wal et al. 2005). Along the K-transect the surface mass balance (the balance between snowfall (positive mass) and melt water runoff (negative mass) during 2010-2011 was less negative than the previous record-breaking year (2008-2009). Remarkably, only at the two highest sites was the mass balance exceptionally negative like the previous year (2009-2010) (Fig. HTC16). The latter is in agreement with preliminary regional atmosphere simulations. This implies that the weighted-average mass balance over the last year is the second lowest mass balance in 21 years. Sites S8 and S9, the two highest sites in the ablation area, account for approximately 50% of the weighted-average mass balance of the entire transect. The strong ablation just below the equilibrium line in the last two years is likely related to the limited snowfall during the preceding winters.

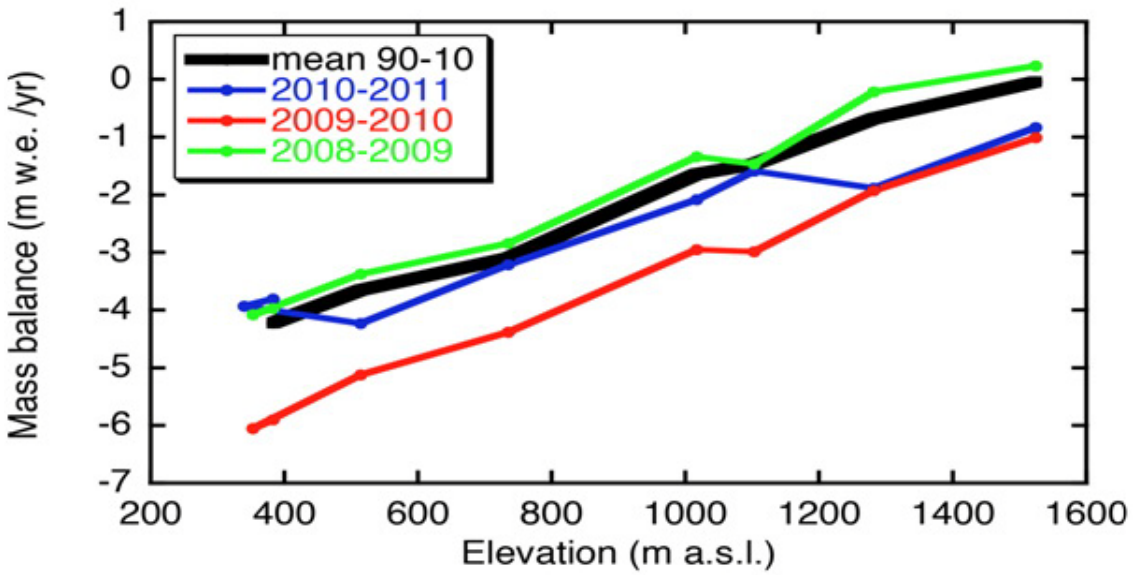

Fig. HTC16. Water equivalent (w.e.) surface mass balance as a function of elevation along the K-Transect during 2010-11, 2009-10 and 2008-09 and for the 20-year average (1990-2010).

Figure HTC17 illustrates the cumulative surface mass balance around the equilibrium line altitude at 1500 m. a.s.l. From a slightly positive value at the end of the 1990s there has been a change to a clearly negative value, suggesting an upward migration of the equilibrium line altitude. The equilibrium line elevation at the end of summer 2011 is estimated to be 1720 m. a.s.l. Low accumulation rates are followed by stronger ablation rates in summer 2007 and 2010. This is likely also to be the case in 2011, though the accumulation record of 2010-2011 is not yet available.

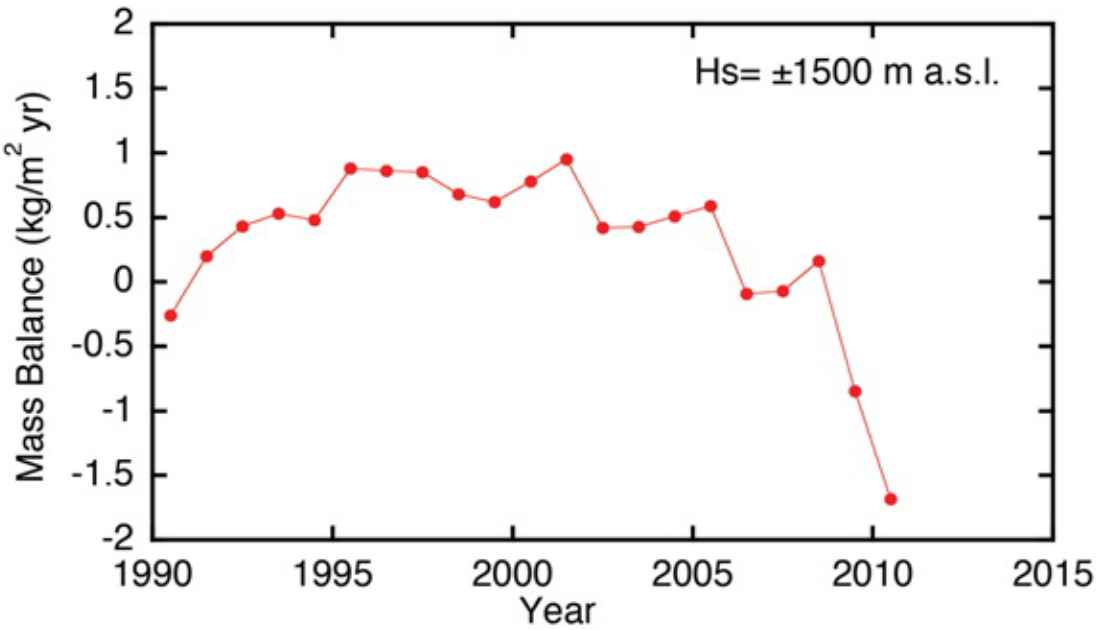

Fig. HTC17. The cumulative mass balance in the vicinity of the equilibrium line altitude (67°N, 50°W) along the K-Transect.

Surface mass balance from MAR simulations (X. Fettweis)

The observationally-constrained Modèle Atmosphérique Régional (MAR) (Fettweis et al., 2011) is coupled with a one-dimensional multi-layered energy balance snow model (Gallée and Schayes 1994; Lefebre et al. 2003) to simulate surface mass balance over the ice sheet. The skill of MAR has been demonstrated by Fettweis (2007) and Tedesco et al. (2011). The past 51 years of surface mass balance (SMB) components are illustrated in Fig. HTC18. The positive meltwater runoff anomaly in 2011 (Table HTC5) results from a conjunction of warmer conditions along the western coast resulting from anomalies in general circulation and drier conditions (mainly at the south of the ice sheet) allowing low albedo values (enhancing the melt) to be maintained through the whole summer. Although the melt season started late in 2011, at the beginning of June, the dry and warm conditions caused record bare ice exposure, which enhanced the melt. Moreover, at the south of the ice sheet, lower winter accumulation than normal allowed the earlier appearance of the bare ice in the ablation zone. Consequently, the SMB rate simulated by MAR from Sep 2010 to Aug 2011 (Table HTC5) is the second lowest in 50 years after 2010.

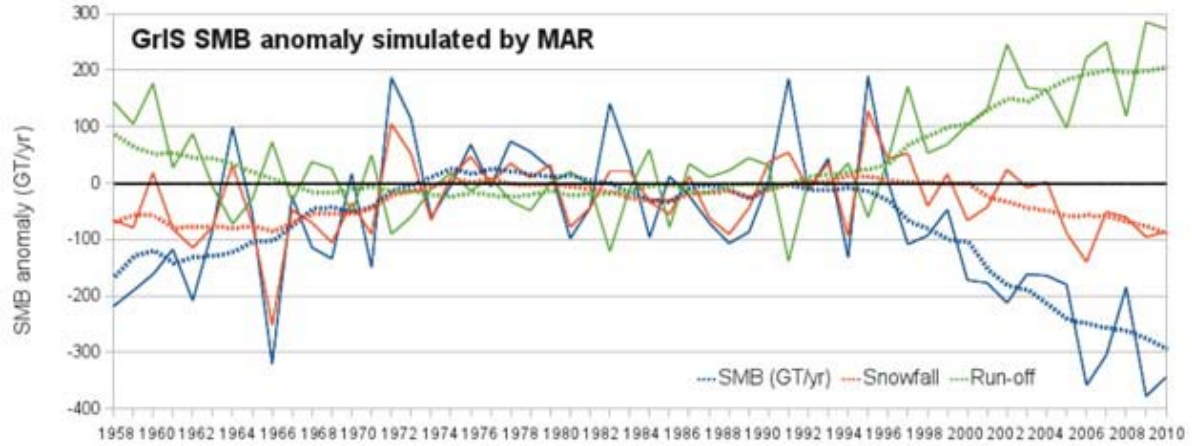

Fig. HTC18. Greenland ice sheet surface mass balance (GrIS SMB) anomalies in Gt/yr simulated by MAR (Modèle Atmosphérique Régional) relative to 1971-2000.

Table HTC5. Surface mass balance (SMB), snowfall and runoff anomalies in 2011 relative to the 1971-2000 base period from MAR.

	SMB	Snowfall	Runoff
Gt/year	-344.3	-86.3	-273.1
Normalized value	-3.6	-1.5	4.4

Greenland mass changes from GRACE (J. Wahr)

GRACE satellite gravity solutions (Velicogna and Wahr 2006) are used to estimate monthly changes in the total mass of the Greenland ice sheet (Fig. HTC19). From the end of April 2010 through the end of April 2011, which roughly corresponds to the period between the beginning of the 2010 and 2011 melt seasons, the ice sheet cumulative loss was -430 Gt, 70% (or 2 standard deviations) larger than the 2003-09 average annual loss rate of -250 Gt y^{-1}. This

2010/2011 mass loss is equivalent to a eustatic sea level rise contribution of 1.1 mm, and is the largest annual loss rate for Greenland in the GRACE record (2002-present), 180 Gt more negative than the 2003-09 average. 2005-2006 had almost as much mass loss as 2010-2011, when evaluated between April/May points. Using GRACE data, Rignot et al. (2011) find an acceleration of Greenland ice sheet mass budget deficit during 1979-2010, in close agreement with an independent mass balance model.

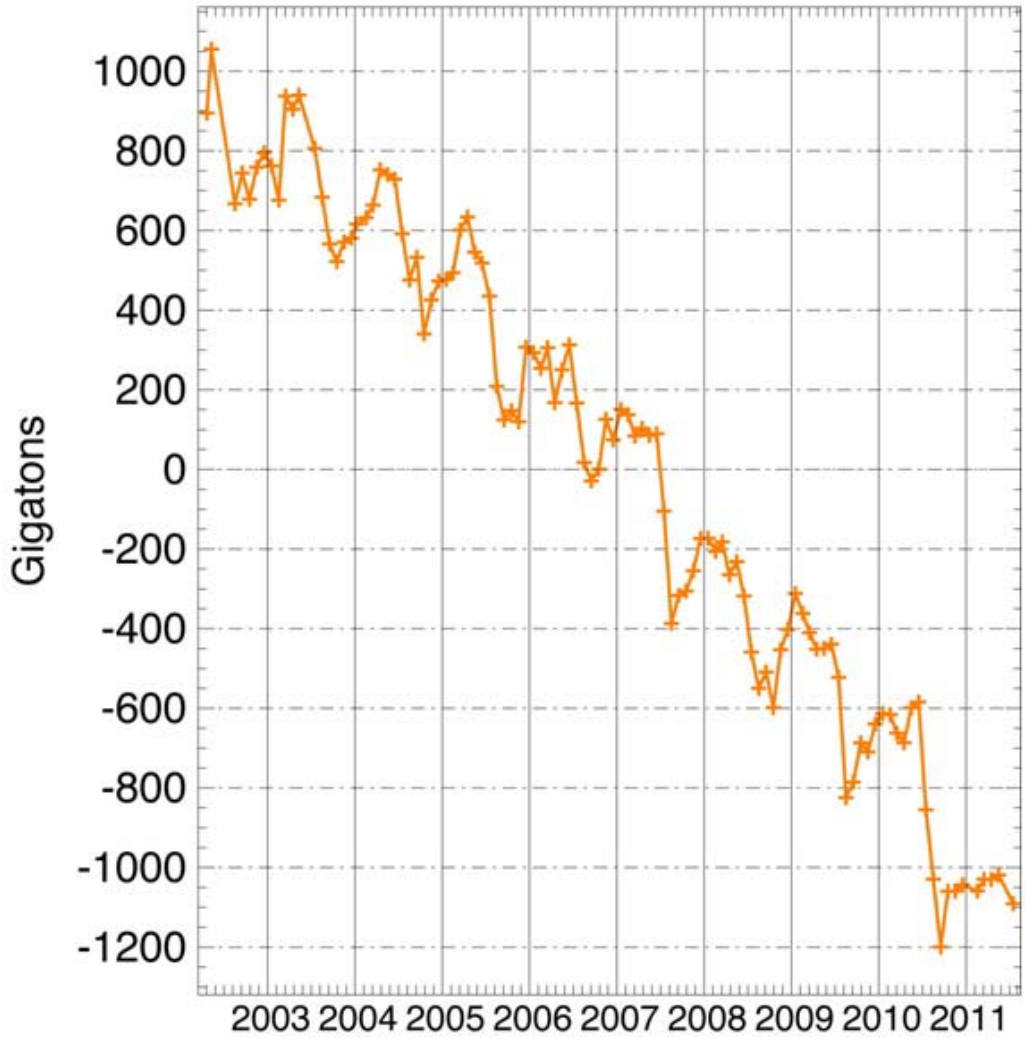

Fig. HTC19. Monthly unsmoothed values of the total mass (in Gigatons, Gt), of the Greenland ice sheet from GRACE. On the horizontal axis, each year begins on 1 January. Each small + symbol is a monthly value.

Marine-terminating glacier area changes (J. E. Box, D. Decker, C. Chen)

Marine-terminating glaciers are of particular interest because they represent the outlets through which the inland ice can move most quickly and in the largest quantities out to the ocean. Iceberg calving from these glaciers represents an area reduction that can be balanced by

forward motion of the ice by flow. Changes at the fronts of marine-terminating outlet glaciers cause flow speed variations by modulating the balance of driving and resistive stresses (Meier and Post, 1987; Joughin et al. 2008). Generally, retreat leads to flow acceleration and, in turn, mass loss from the ice sheet, which contributes to sea level rise.

Daily surveys using cloud-free MODIS visible imagery (Box and Decker 2011; http://bprc.osu.edu/MODIS/) indicate that in the year prior to end of the 2011 melt season, marine-terminating glaciers collectively lost an area of 45 km^2. This is 84 km^2 smaller than the average annual loss rate of the previous 10 years (124 km^2 yr^{-1}) (Fig. HTC20). Glacier area change measurements from the 1980s and 1990s (Howat and Eddy 2011) indicate an increased rate of ice area loss in the most recent decade.

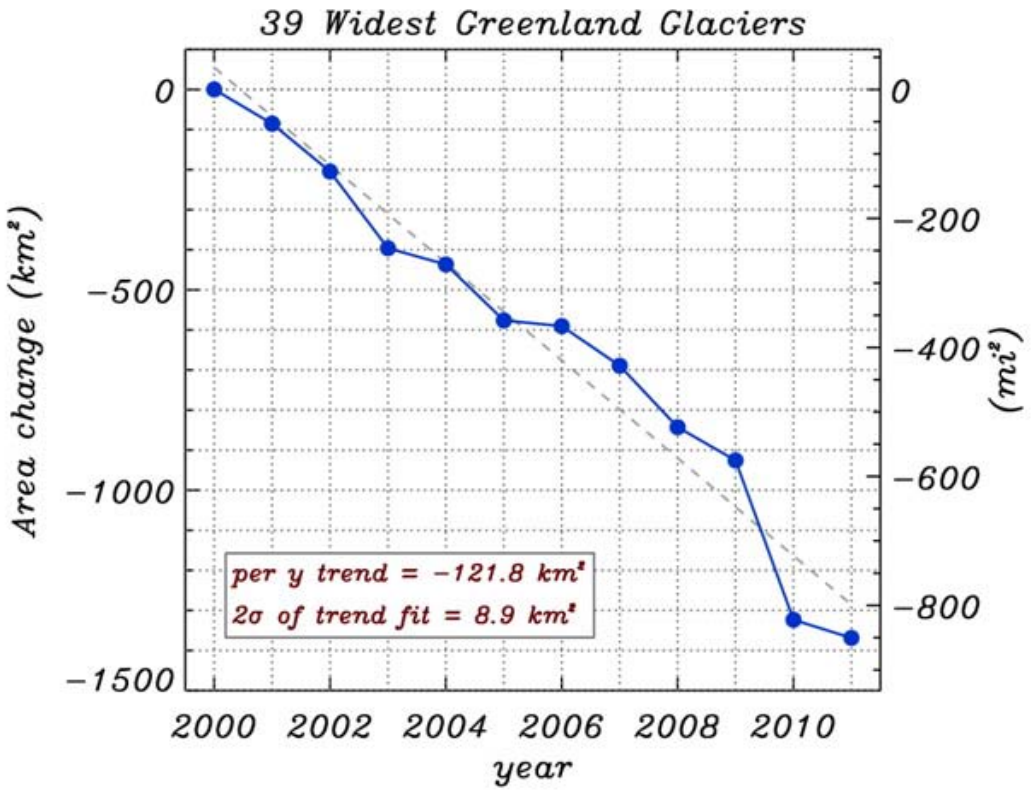

Fig. HTC20. Cumulative net annual area change for the 39 widest marine-terminating glaciers of the Greenland ice sheet (after Box and Decker, 2011). The dashed line is a least-squares regression line.

While the overall area change was negative for 2011, 9 of 39 glaciers grew in area relative to the end of the 2010 melt season. These nine include some of the most productive marine-terminating glaciers, in terms of ice volume discharge. The top ice area gainers included Petermann glacier (+13 km^2), which lost ~275 km^2 in August 2010, Helheim glacier (+8 km^2) and the "79" glacier (+7 km^2). One of the most productive east Greenland glaciers, Kangerdlugssauq, increased by +6 km^2.

The four glaciers with the largest ice loss were: Humboldt (-20 km^2), Zachariae (-19 km^2), Steenstrup (-15 km^2) and Jakobshavn (-9 km^2). According to the linear regression fit in Fig. HTC20, the average annual loss rate for the 39 Greenland glaciers in the past 11 years is 122

km^2 $year^{-1}$. Since 2000, the net area change of the 39 widest marine-terminating glaciers is -1369 km^2, nearly 16 times the size of Manhattan Island, New York.

Mittivakkat Gletscher: The longest-observed mountain glacier in Greenland (S. H. Mernild, N. T. Knudsen and E. Hanna)

Mittivakkat Gletscher in southeast Greenland (17.6 km^2; 65° 41' N, 37° 48' W) has been surveyed for surface mass balance and glacier front fluctuations since 1995 and 1931, respectively (Knudsen and Hasholt 2002, Mernild et al. 2011). The glacier terminus (at the center line) retreated about 22 m (Fig. HTC21) in 2011, 12 m less than the observed record of 34 m in 2010, and approximately 1,600 m in total since the maximum Little Ice Age extension around 1900 and by approximately 1,300 m since 1931. In 2011, net ablation was recorded at all elevations between the summit (930 m a.s.l.) and the terminus (180 m a.s.l.), indicating that the ELA for Mittivakkat was above 930 m a.s.l., and 200 m above the average since mass balance observations began. The total 2011 mass budget loss was 2.45 m water equivalent (w.e.), 0.29 m w.e. higher than the observed record loss in 2010 and significantly greater than the 16-yr average loss of 0.97±0.19 m w.e. yr^{-1} (Fig. HTC22).

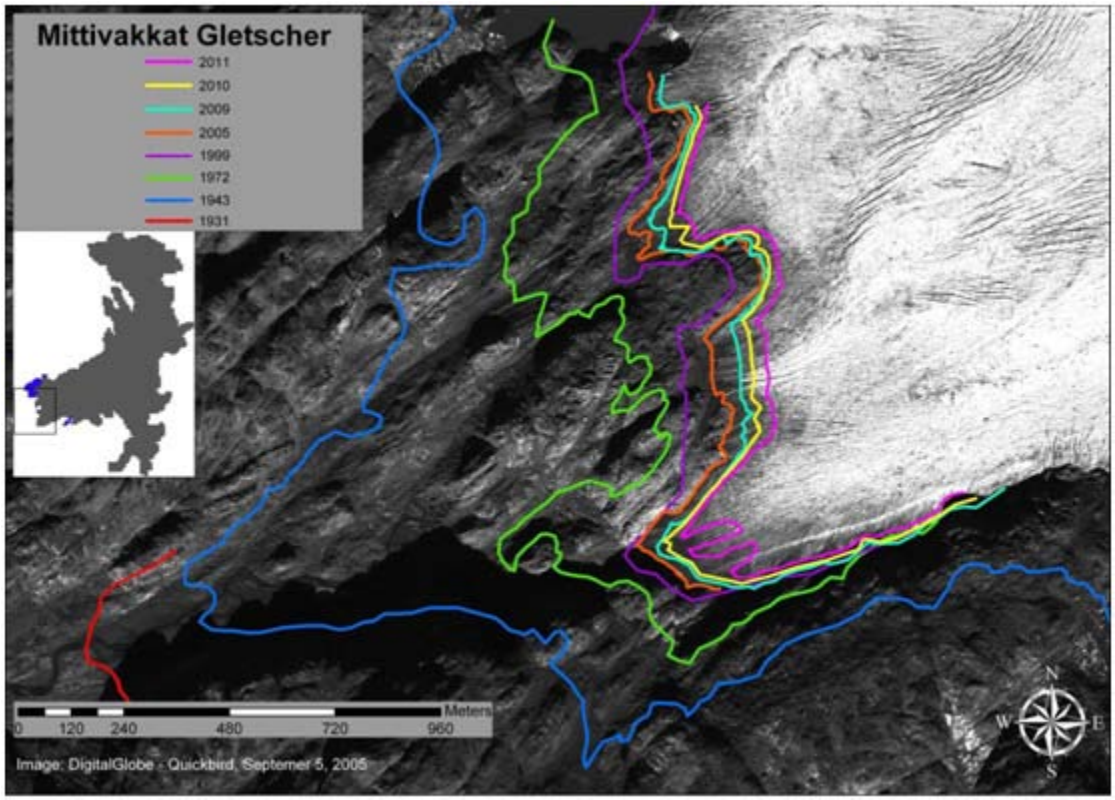

Fig. HTC21. The location of the Mittivakkat Gletscher margin delineated as thick lines for 1931, 1943, 1972, 1999, 2005, 2009, 2010, and 2011 (pink). The 1931, 1943, and 1972 margins were estimated from aerial photographs, the 1999 margin from Landsat 5, and the 2005 margin from Quickbird. The more recent 2009, 2010, and 2011 margins were obtained from topographic surveys (Kern Theodolite observations) and GPS measurements. The Mittivakkat Gletscher outline is shown at left with a black square indicating the photographic area (background photograph: DigitalGlobe, Quickbird 2005 and updated from Mernild et al. 2011).

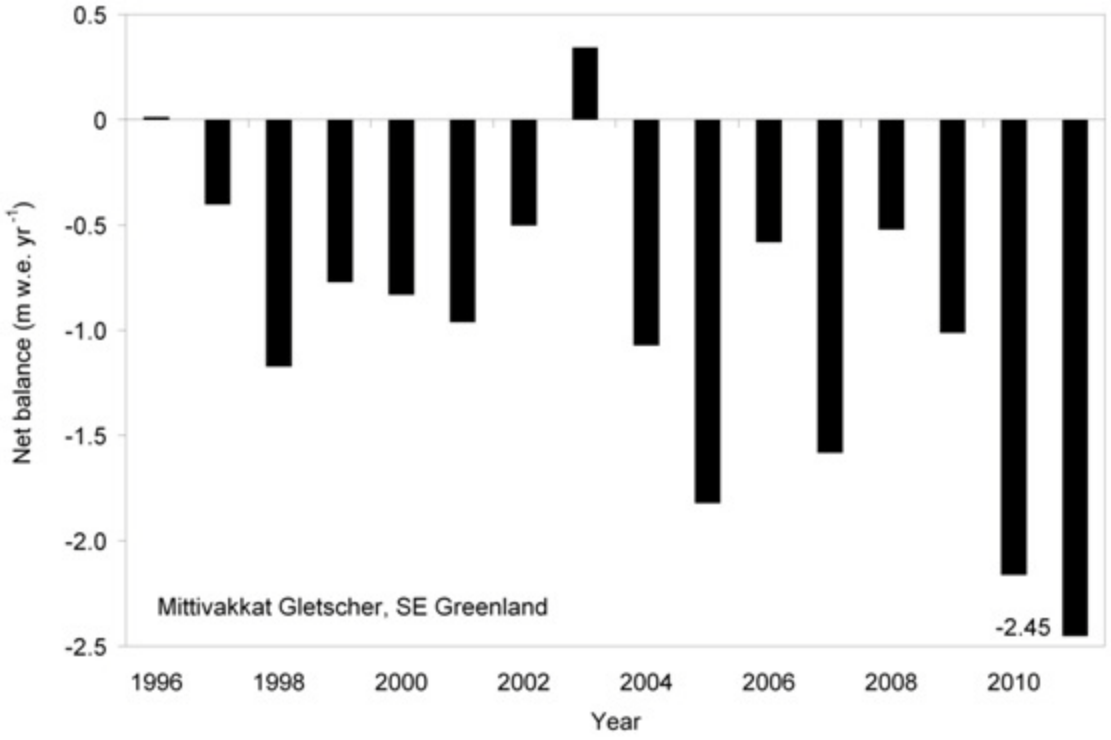

Fig. HTC22. Observed annual water equivalent (w.e.) mass balance of the Mittivakkat Gletscher, southeast Greenland, from 1995 to 2011 (updated from Mernild et al. 2011).

References

Box, J. E., and A. E. Cohen, 2006: Upper-air temperatures around Greenland: 1964-2005, Geophys. Res. Lett., 33, L12706, doi:10.1029/2006GL025723.

Box, J.E. and D.T. Decker, 2011: Analysis of Greenland marine-terminating glacier area changes: 2000-2010, Annals of Glaciology, 52(59) 91-98.

Cuffey, K.M. and W.S.B. Paterson. 2010. The Physics of Glaciers, 4th ed. Elsevier. 693 pp.

Durre, I., R. S. Vose, and D. B. Wuertz, 2006: Overview of the Integrated Global Radiosonde Archive, J. Clim., 19, 53- 68.

DMI, 2000. Technical Report 00-18. The Observed Climate of Greenland, 1958-99 - with Climatological Standard Normals, 1961-90, ed. J. Cappelen, B.V. Jørgensen, E. V. Laursen, L.S. Stannius, and R. S. Thomsen. Ministry of Transport, Denmark.

DMI, 2011. Technical Report 11-05. DMI Monthly Climate Data Collection 1768-2010, Denmark, The Faroe Islands and Greenland, ed. J. Cappelen. Ministry of Climate and Energy, Denmark.

Dozier, J., Schneider, S. R., & McGinnis, D. F. 1981. Effect Of Grain-Size And Snowpack Water Equivalence On Visible And Near-Infrared Satellite-Observations Of Snow. Water Resources Research, 17(4), 1213-1221. doi: 10.1029/WR017i004p01213.

Fettweis, X., Tedesco, M., van den Broeke, M., and Ettema, J.: Melting trends over the Greenland ice sheet (1958-2009) from spaceborne microwave data and regional climate models, The Cryosphere, 5, 359-375, doi:10.5194/tc-5-359-2011.

Gallée, H. and Schayes, G. 1994. Development of a three-dimensional meso-primitive equations model, Mon. Weather Rev., 122, 671-685.

Howat, I.M. and A. Eddy, in press, Multidecadal retreat of Greenland's marine-terminating glaciers, Journal of Glaciology.

Joughin, I., I. Howat, R. B. Alley, G. Ekstrom, M. Fahnestock, T. Moon, M. Nettles, M. Truffer, and V. C. Tsai (2008), Ice-front variation and tidewater behavior on Helheim and Kangerdlugssuaq Glaciers, Greenland, J. Geophys. Res., 113, F01004, doi:10.1029/2007JF000837.

Knudsen, N. T. and B. Hasholt 2004. Mass balance observations at Mittivakkat Glacier, southeast Greenland 1995-2002, Nord. Hydrol. 35, 381-390.

Konzelmann, T., & Ohmura, A. (1995). Radiative Fluxes And Their Impact On The Energy-Balance Of The Greenland Ice-Sheet. Journal of Glaciology, 41(139), 490-502.

Lefebre, F., Gallée, H., van Ypersele, J. P., & Greuell, W. 2003. Modeling of snow and ice melt at ETH Camp (West Greenland): A study of surface albedo. Journal of Geophysical Research-Atmospheres, 108(D8). doi: 4231 10.1029/2001jd001160.

Meier, M.F. and A. Post. 1987. Fast tidewater glaciers. J. Geophys. Res., 92(B9), 9051-9058.

Mernild, S. H., N. T. Knudsen, W. H. Lipscomb, J. C. Yde, J. K. Malmros, B. H. Jakobsen, and B. Hasholt 2011. Increasing mass loss from Greenland's Mittivakkat Gletscher. The Cryosphere, 5, 341-348, doi:10.5194/tc-5-341-2011.

Mote, T.L., and M.R. Anderson, 1995: Variations in Melt on the Greenland Ice Sheet Based on Passive Microwave Measurements. J. Glaciol., 41, 51-60.

Mote, T. L., 2007: Greenland surface melt trends 1973-2007: Evidence of a large increase in 2007. Geophys. Res. Lett., 34, L22507, doi:10.1029/2007GL031976.

Tedesco , M. , X. Fettweis, M. R. van den Broeke, R. S. W. van de Wal, C. J. P. P. Smeets, W. J. van de Berg, M. C. Serreze and J. E. Box. 2011. The role of albedo and accumulation in the 2010 melting record in Greenland, Environ. Res. Lett. 6 014005.

Tedesco M., X. Fettweis, M. R. van den Broeke, R. S. W. van de Wal, C. J. P. P. Smeets, W. J. van de Berg, M. C. Serreze, and J. E. Box , Record summer melt in Greenland in 2010 , EOS AGU, Volume 92, Number 15, 12 April 2011.

Tedesco, M., Snowmelt detection over the Greenland ice sheet from SSM/I brightness temperature daily variations, Geophys. Res. Lett., 34, L02504,doi:10.1029/2006GL028466, January 2007.

Warren, S. G. (1982). Optical-Properties of Snow. Reviews of Geophysics, 20(1), 67-89. doi: 10.1029/RG020i001p00067.

Wiscombe, W. J., & Warren, S. G. (1980). A Model For The Spectral Albedo Of Snow.1. Pure Snow. Journal of the Atmospheric Sciences, 37(12), 2712-2733.

van de Wal, R. S. W., W. Greuell, M. R. van den Broeke, C.H. Reijmer and J. Oerlemans: Surface mass-balance observations and automatic weather station data along a transect near Kangerlussuaq, West Greenland, Annals of Glaciology, 42, 311-316, 2005.

Permafrost

V. E. Romanovsky[1], S. L. Smith[2], H. H. Christiansen[3], N. I. Shiklomanov[4], D. S. Drozdov[5], N. G. Oberman[6], A. L. Kholodov[1], S. S. Marchenko[1]

[1]Geophysical Institute, University of Alaska Fairbanks, Fairbanks, Alaska, USA
[2]Geological Survey of Canada, Natural Resources Canada, Ottawa, Ontario, Canada
[3]Geology Department, University Centre in Svalbard, UNIS, Norway
and Department of Geosciences, University of Oslo, Norway
[4]Department of Geography, George Washington University, Washington, DC, USA
[5]Earth Cryosphere Institute, Tyumen, Russia
[6]MIRECO Mining Company, Syktyvkar, Russia

November 28, 2011

Highlights

- In 2011, new record high temperatures at 20 m depth were recorded at all permafrost observatories on the North Slope of Alaska, where measurements began in the late 1970s.
- During the last fifteen years, active-layer thickness has increased in the Russian European North, northern East Siberia, Chukotka, Svalbard and Greenland.
- Active-layer thickness on the Alaskan North Slope and in the western Canadian Arctic was relatively stable during 1995-2008.

The most direct indicators of permafrost stability and changes in permafrost state are the permafrost temperature and the active layer thickness (ALT). Permafrost temperature measured at the depth where the seasonal variations in ground temperature cease to exist is best to use as an indicator of long-term change. This depth varies from a few meters in warm, ice-rich permafrost to 20 m and more in cold permafrost and in bedrock (Smith et al. 2010; Romanovsky et al. 2010a). However, if continuous year-around temperature measurements are available, the mean annual ground temperature (MAGT) at any depth within the upper 15 m can be used as a proxy of the permafrost temperature. The recently concluded International Polar Year (IPY 2007-2009) resulted in significant enhancement of the permafrost observing system in the Arctic; there are now ~575 boreholes (Fig. HTC23; Brown et al. 2010; Romanovsky et al. 2010a). A borehole inventory, including mean annual ground temperatures for most of these boreholes, is available online (http://nsidc.org/data/g02190.html).

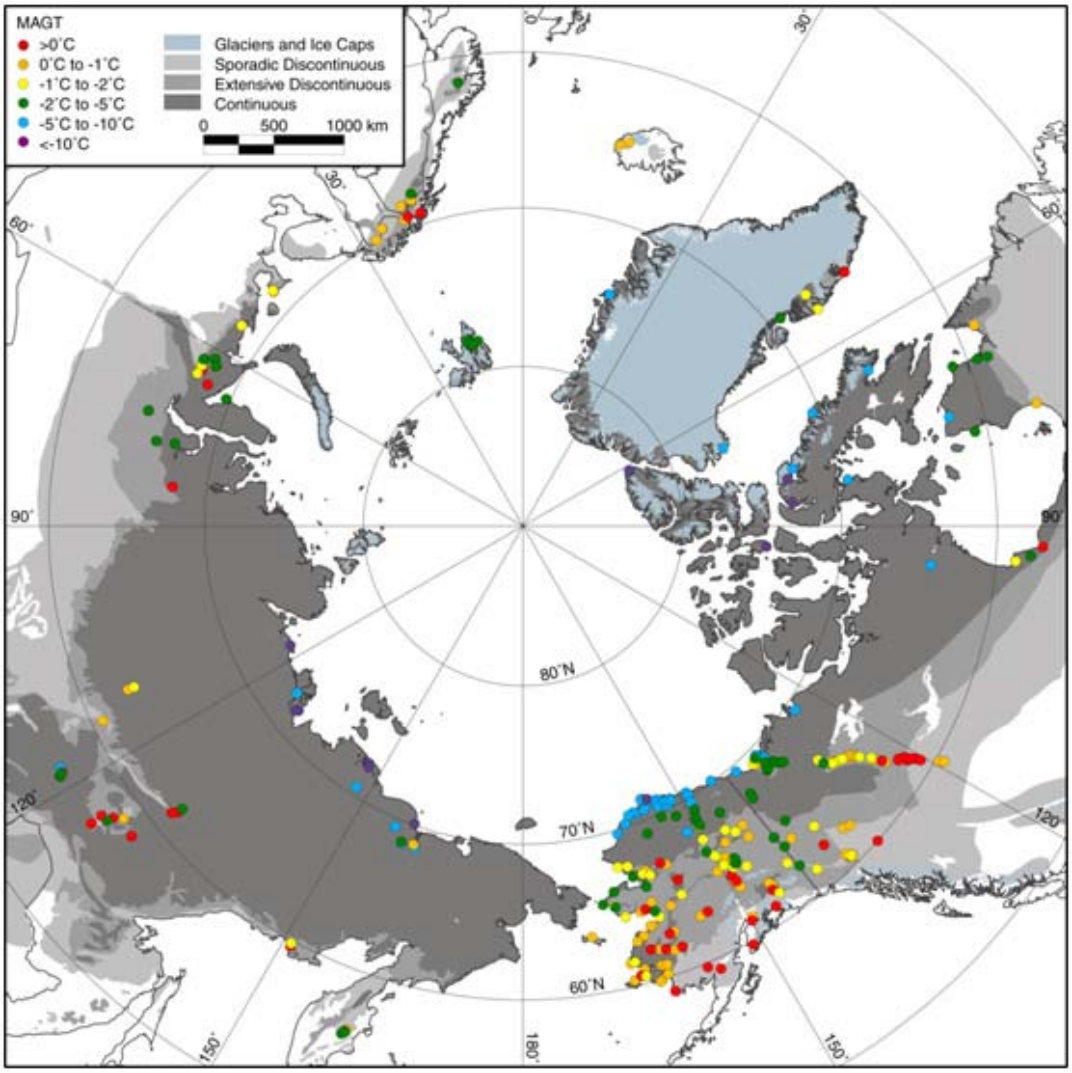

Fig. HTC23. Circum-Arctic snapshot of mean annual ground temperature (MAGT) in permafrost during the International Polar Year (2007-2009; from Romanovsky et al. 2010).

Permafrost temperatures in the Arctic and sub-Arctic lowlands generally follow a latitudinal gradient, decreasing northward. Higher ground temperatures are found in the southern discontinuous zone, where MAGT is above 0°C at many locations (Fig. HTC23). The temperature of warm permafrost in the discontinuous zone generally falls within a narrow range, with MAGT at most sites being > -2°C (Christiansen et al. 2010; Romanovsky et al. 2010a; Smith et al. 2010) (Fig. HTC24). Temperatures as low as -3°C or even -4°C, however, may be observed in some specific ecological or topographic conditions (Jorgenson et al. 2010). A greater range in MAGT occurs within the continuous permafrost zone, from >-1°C at some locations to as low as -15°C (Christiansen et al. 2010; Romanovsky et al. 2010a; Romanovsky et al. 2010b; Smith et al. 2010). MAGT > 0°C is observed at some locations near the southern boundary of the continuous zone (Fig. HTC23), which may indicate that this boundary is shifting northward (Romanovsky et al. 2010b). Permafrost temperatures <-10°C are presently found only in the Canadian Arctic Archipelago (Smith et al. 2010) and near the Arctic coast in Siberia.

Systematic observations of permafrost temperature in Alaska, Canada and Russia since the middle of the 20th Century provide several decades of continuous data from several sites. The data allow assessment of changes in permafrost temperatures on a decadal time scale. A general increase in permafrost temperatures is observed during the last several decades in Alaska (Romanovsky et al. 2007; Osterkamp 2008; Smith et al. 2010; Romanovsky et al. 2010a), northwest Canada (Smith et al. 2010) and Siberia (Oberman 2008; Drozdov et al. 2008; Romanovsky et al. 2010b).

At most Alaskan permafrost observatories there was substantial warming during the 1980s and especially in the 1990s (Fig. HTC24). The magnitude and nature of the warming varies between locations, but is typically from 0.5°C to 2°C at the depth of zero seasonal temperature variations over this 20 year period (Osterkamp 2008). However, during the 2000s, permafrost temperature has been relatively stable on the North Slope of Alaska (Smith et al. 2010) (Fig. HTC24a), and there has been a slight decrease (by as much as 0.3°C) at some locations in Interior Alaska during the last three years (Fig. HTC24b). During the last decade, continuous warming has been observed only at near-coastal sites, where there has also been an increase in "greenness" of tundra vegetation (see the essay on *Vegetation*) and the area of open ocean in summer (see the essay on *Sea Ice*). The latest data may indicate that the observed warming trend along the coast has begun to propagate south towards the northern foothills of the Brooks Range, where a noticeable warming in the upper 20 m of permafrost has become evident since 2008 (Romanovsky et al. 2011). In 2011, new record high temperatures at 20 m depth were measured at all permafrost observatories on the North Slope of Alaska, where measurements began in the late 1970s (Fig. HTC24a). These distinct patterns of permafrost warming on the North Slope and a slight cooling in Interior Alaska are in good agreement with the Arctic/sub-Arctic air temperature differences described in the essay on Temperature and Clouds. These patterns may also be a result of differences in snow distribution (see the essay on *Snow*).

a.

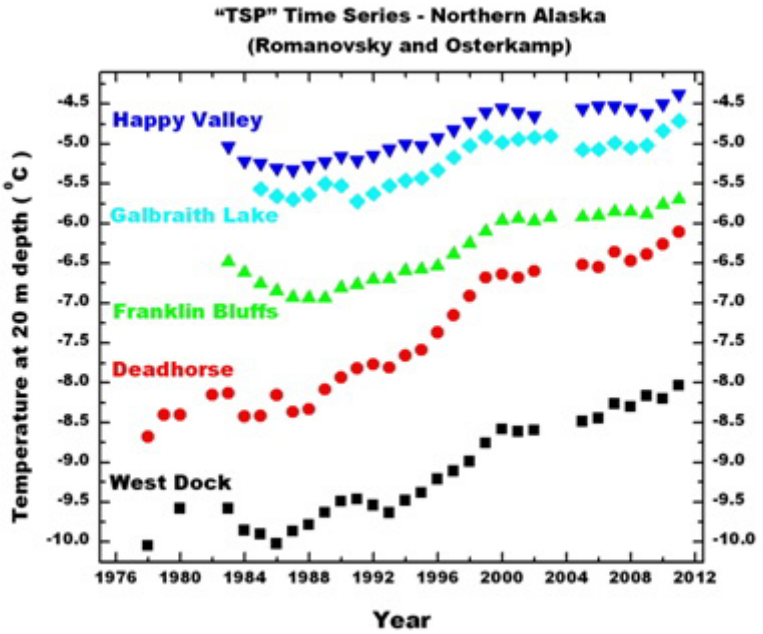

b.

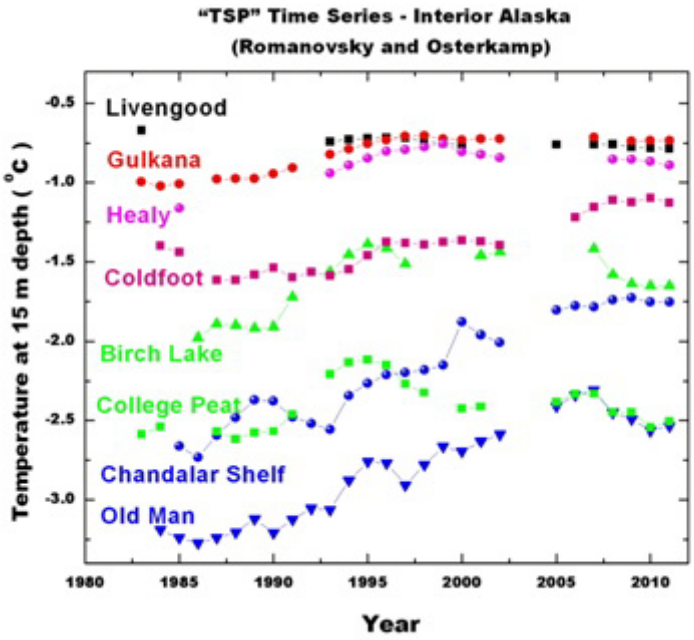

c.

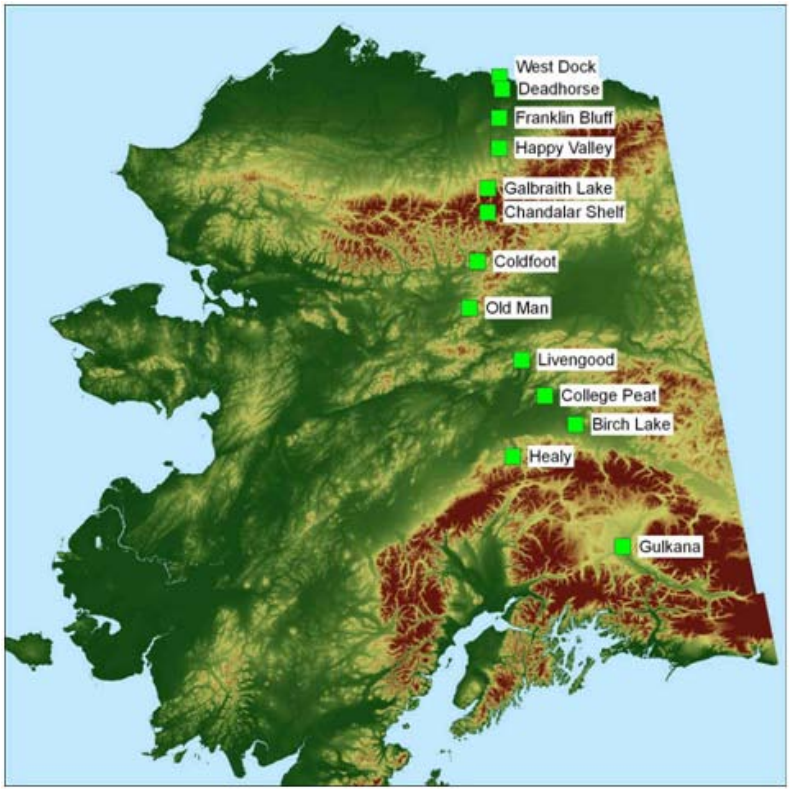

Fig. HTC24. Time series of permafrost temperature measured at 20 m below the surface at locations (a, top) from north to south across the North Slope of Alaska in the continuous permafrost zone, and (b, middle) in Interior Alaska. Note the higher permafrost temperatures in Interior Alaska (b) than on the North Slope (a) The locations of sites named in (a) and (b) are shown in the map (c, bottom).

A similar permafrost temperature increase during the last 40 years was estimated for colder permafrost in northwest Canada (Burn and Kokelj 2009). In the discontinuous zone of western Canada, the increase in permafrost temperature has been smaller (Fig. HTC25a), with negligible change in recent years (Smith et al. 2010). In the eastern and high Canadian Arctic, greater warming has been observed, and since 2000 there has been a steady increase in permafrost temperature (Fig. HTC25b).

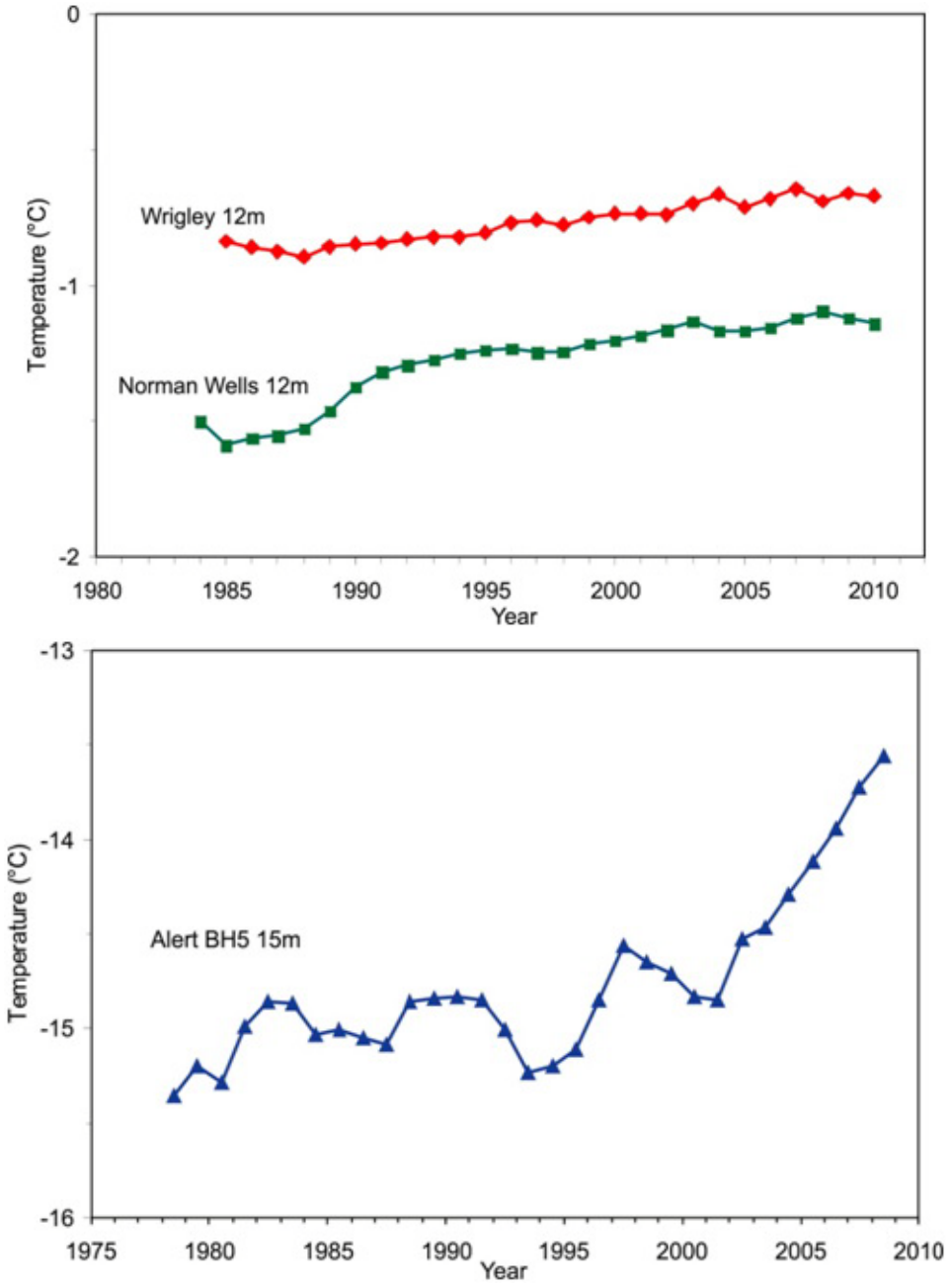

Fig. HTC25. Time series of mean annual permafrost temperatures at (top) 12 m depth at two sites in the discontinuous permafrost zone of the central Mackenzie Valley, Northwest Territories Canada and (bottom) 15 m depth at CFS Alert, Nunavut, Canada (updated from Smith et al. 2010). The method described in Throop et al. (2010) was used to address gaps in the data record and produce a standardized record of mean annual ground temperature.

Permafrost temperature has increased by 1°C to 2°C in northern Russia during the last 30 to 35 years (Drozdov et al. 2008; Oberman, 2008; Romanovsky et al. 2010b). An especially noticeable temperature increase was observed during the late 2000s in the Russian Arctic, where the mean annual temperature at 15 m depth increased by >0.35°C in the Tiksi area and by 0.3°C at 10 m depth in the European North of Russia during 2006-2009. However, relatively low air temperatures during summer 2009 and the following winter interrupted this warming trend at many locations in the Russian Arctic, especially in the western sector. A common feature at Alaskan, Canadian and Russian sites is more significant warming in relatively cold permafrost than in warm permafrost in the same geographical area (Romanovsky et al. 2010a).

Unlike the rest of the Northern Hemisphere, the Nordic area, including Greenland, does not have comparable long-term permafrost temperature data. The few sustained permafrost monitoring sites have significantly shorter records that begin at the end of the 1990s. However, these also show a recent decadal warming of 0.04 to 0.07°C/yr in the highlands of southern Norway, northern Sweden and Svalbard, with the largest warming in Svalbard and in northern Scandinavia (Isaksen et al. 2007; Christiansen et al. 2010).

Long-term observations of the changes in active-layer thickness (ALT) are less conclusive. The active layer is a layer of earth materials between the ground surface and permafrost that freezes and thaws on an annual basis. Thaw depth observations exhibit substantial inter-annual fluctuations, primarily in response to variations in summer air temperature (e.g. Smith et al. 2009; Popova and Shmakin, 2009) (see the essay on *Temperature and Clouds*). Decadal trends in ALT vary by region. A progressive increase in ALT has been observed in some Nordic countries, e.g., in the Abisko area of Sweden since the 1970s, with an accelerated rate after 1995, resulting in disappearance of permafrost in several mire landscapes (e.g. Åkerman and Johansson 2008, Callaghan et al. 2010). This increase in thaw propagation ceased during 2007-2010, coincident with drier summer conditions (Christiansen et al. 2010). Increases in ALT since the late 1990s have been observed on Svalbard and Greenland, but these are not spatially and temporarily uniform (Christiansen et al. 2010).

Increase in ALT over the last fifteen years has been observed in the Russian European North (Mazhitova, 2008), in the north of East Siberia (Fyodorov-Davydov et al. 2008), and in Chukotka (Zamolodchikov, 2008). Active-layer trends are different for North American sites, where a progressive increase of ALT is evident only at sites in Interior Alaska, where the maximum ALT for the 18 year observation period occurred in 2007. Active-layer thickness on the North Slope of Alaska is relatively stable, without pronounced trends during 1995-2008 (Streletskiy et al. 2008: Shiklomanov et al. 2010). Similar results are reported from the Western Canadian Arctic. Smith et al. (2009) found no definite trend in the Mackenzie Valley during the last 15 years, with some decrease in ALT following a maximum in 1998. Although an 8 cm increase in thaw depth was observed between 1983 and 2008 in the northern Mackenzie region, shallower thaw has been observed since 1998 (Burn and Kokelj 2009). In the eastern Canadian Arctic, ALT increased since the mid-1990s, with the largest increase occurring in bedrock of the discontinuous permafrost zone (Smith et al. 2010).

The last 30 years of ground warming have resulted in the thawing of permafrost in areas of discontinuous permafrost in Russia (Oberman 2008; Romanovsky et al. 2010b). This is evidenced by changes in the depth and number of taliks (a sub-surface layer of year-round unfrozen ground within permafrost), especially in sandy and sandy loam sediments compared to clay. A massive development of new closed taliks in the southern continuous permafrost zone, resulting from increased snow cover and warming permafrost, was responsible for the observed northward movement of the boundary between continuous and discontinuous permafrost by

several tens of kilometers (Oberman and Shesler 2009; Romanovsky et al. 2010b). The frequently-reported long-term permafrost thawing in the Central Yakutian area around the city of Yakutsk are directly related to natural (forest fire) or anthropogenic (agricultural activities, construction sites) disturbances (Fedorov and Konstantinov 2008) and are not significantly correlated with climate (Romanovsky et al. 2010b).

References

Åkerman, H. J., and M. Johansson, 2008: Thawing permafrost and thicker active layers in sub-arctic Sweden. Permafrost and Periglacial Processes, 19, 279-292. doi:10.1002/ppp.626.

Brown J., Kholodov A., Romanovsky V., Yoshikava K., Smith S., Christiansen H., Viera G., and J. Noetzli, 2010: The Thermal State of Permafrost: the IPY-IPA snapshot (2007-2009), In Proceedings of the 63rd Canadian geotechnical conference & 6th Canadian permafrost conference, Calgary, Canada, September 12-16, 6 pp.

Burn C. R., and S. V. Kokelj, 2009: The environment and permafrost of the Mackenzie Delta area, Permafrost and Periglacial Processes, 20(2), 83-105.

Callaghan, T. V., F. Bergholm, T. R. Christensen, C. Jonasson, U. Kokfelt, and M. Johansson, 2010: A new climate era in the sub-Arctic: Accelerating climate changes and multiple impacts, Geophys. Res. Lett., 37, L14705, doi:10.1029/2009GL042064.

Christiansen, H.H., B. Etzelmüller, K. Isaksen, H. Juliussen, H. Farbrot, O. Humlum, M. Johansson, T. Ingeman-Nielsen, L. Kristensen, J. Hjort, P. Holmlund, A. B. K. Sannel, C. Sigsgaard, H. J. Åkerman, N. Foged, L. H. Blikra, M. A. Pernosky, and R. Ødegård, 2010: The Thermal State of Permafrost in the Nordic area during the International Polar Year, Permafrost and Periglacial Processes, 21, 156-181, DOI: 10.1002/ppp.687.

Drozdov, D. S., G. V. Malkova, and V. P. Melnikov, 2008: Recent Advances in Russian Geocryological Research: A Contribution to the International Polar Year, In Proceedings of the Ninth International Conference on Permafrost, June 29-July 3, Fairbanks, Alaska, 2008, Vol. 1, 379-384.

Fedorov A.N., and P.Y. Konstantinov, 2008: Recent changes in ground temperature and the effect on permafrost landscapes in Central Yakutia, In: Proceedings Ninth International Conference on Permafrost, Edited by D. L. Kane and K. M. Hinkel. Fairbanks. Institute of Northern Engineering, University of Alaska Fairbanks, June 29-July 3, Fairbanks, Alaska, Vol.1, 433-438.

Fyodorov-Davydov, D.G., A. L. Kholodov, V. E. Ostroumov, G. N. Kraev, V. A. Sorokovikov, S. P. Davydov, and A. A. Merekalova, 2008: Seasonal Thaw of Soils in the North Yakutian Ecosystems. Proceedings of the 9th International Conference on Permafrost, Institute of Northern Engineering, University of Alaska, Fairbanks, Vol. 1, 481-486.

Isaksen, K., J. L. Sollid, P. Holmlund, and C. Harris, 2007: Recent warming of mountain permafrost in Svalbard and Scandinavia. Journal of Geophysical Research, 112, F02S04, doi: 0.1029/2006JF000522.

Jorgenson, M. T, V. E. Romanovsky, J. Harden, Y. L. Shur, J. O'Donnell, T. Schuur, and M. Kanevskiy, 2010: Resilience and vulnerability of permafrost to climate change, Canadian Journal of Forest Research, 40, 1219-1236.

Mazhitova G.G., 2008: Soil temperature regimes in the discontinuous permafrost zone in the East European Russian Arctic. Eurasian Soil Science Vol.41, N. 1, 48-62.

Oberman, N. G., 2008: Contemporary Permafrost Degradation of Northern European Russia, In Proceedings of the Ninth International Conference on Permafrost, June 29-July 3, Fairbanks, Alaska, 2008, Vol. 2, 1305-1310.

Oberman, N.G., and I.G. Shesler, 2009: Observed and projected changes in permafrost conditions within the European North-East of the Russian Federation, Problemy Severa I Arctiki Rossiiskoy Federacii (Problems and Challenges of the North and the Arctic of the Russian Federation), Vol. 9, 96-106 (in Russian).

Osterkamp, T.E., 2008: Thermal State of Permafrost in Alaska During the Fourth Quarter of the Twentieth Century (Plenary Paper), In Proceedings of the Ninth International Conference on Permafrost, June 29-July 3, Fairbanks, Alaska, 2008, Vol. 2, 1333-1338.

Popova, V. V., and Shmakin, A. B., 2009: The influence of seasonal climatic parameters on the permafrost thermal regime, West Siberia, Russia. Permafrost and Periglacial Processes, 20, 41-56. doi:10.1002/ppp.640.

Romanovsky, V. E., S. Gruber, A. Instanes, H. Jin, S. S. Marchenko, S.L. Smith, D. Trombotto, and K. M. Walter, 2007: Frozen Ground, Chapter 7, In: Global Outlook for Ice and Snow, Earthprint, UNEP/GRID, Arendal, Norway, pp. 181-200.

Romanovsky, V. E., S. L. Smith, and H. H. Christiansen, 2010a: Permafrost Thermal State in the Polar Northern Hemisphere during the International Polar Year 2007-2009: a synthesis. Permafrost and Periglacial Processes, 21,106-116.

Romanovsky, V. E., D. S. Drozdov, N. G. Oberman, G. V. Malkova, A. L. Kholodov, S. S. Marchenko, N. G. Moskalenko, D. O. Sergeev, N. G. Ukraintseva, A. A. Abramov, D. A. Gilichinsky, and A. A. Vasiliev, 2010b: Thermal State of Permafrost in Russia. Permafrost and Periglacial Processes, 21,136-155.

Romanovsky, V., N. Oberman, D. Drozdov, G. Malkova , A. Kholodov, S. Marchenko, 2011: Permafrost, [in "State of the Climate in 2010"]. Bull. Amer. Meteor. Soc., 92 (6), S152-S153.

Shiklomanov, N. I., D. A. Streletskiy, F. E. Nelson, R. D. Hollister, V. E. Romanovsky, C. E. Tweedie, J. G. Bockheim, and J. Brown, 2010: Decadal variations of active-layer thickness in moisture-controlled landscapes, Barrow, Alaska, J. Geophys. Res., 115, G00I04, doi:10.1029/2009JG001248.

Smith, S. L., S. A. Wolfe, D. W. Riseborough, and F. M. Nixon, 2009: Active-layer characteristics and summer climatic indices, Mackenzie Valley, Northwest Territories, Canada. Permafrost and Periglacial Processes, 20, 201-220. doi:10.1002/ppp.651.

Smith, S. L., V. E. Romanovsky, A. G. Lewkowicz, C. R. Burn, M. Allard, G. D. Clow, K. Yoshikawa, and J. Throop, 2010: Thermal State of Permafrost in North America - A Contribution to the International Polar Year. Permafrost and Periglacial Processes, 21,117-135.

Streletskiy D. A, N. I. Shiklomanov, F. E. Nelson, and A. E. Klene, 2008: 13 Years of Observations at Alaskan CALM Sites: Long-term Active Layer and Ground Surface Temperature Trends in Ninth International Conference on Permafrost, edited by D.L. Kane and K.M. Hinkel, pp 1727-1732, Institute of Northern Engineering, University of Alaska Fairbanks: Fairbanks Alaska.

Throop, J. L., S. L. Smith, and A. G. Lewkowicz, 2010: Observed recent changes in climate and permafrost temperatures at four sites in northern Canada. In GEO2010, 63rd Canadian Geotechnical Conference and the 6th Canadian Permafrost Conference. Calgary, Sept 2010. GEO2010 Calgary Organizing Committee, pp. 1265-1272.

Zamolodchikov D., 2008: Recent climate and active layer changes in Northeast Russia: regional output of Circumpolar Active Layer Monitoring (CALM). Proceedings of the 9th International Conference on Permafrost, Institute of Northern Engineering, University of Alaska, Fairbanks, Vol. 2, 2021-2027.

Lake Ice

C. Duguay, L. Brown, K.-K. Kang, H. Kheyrollah Pour

Interdisciplinary Centre on Climate Change and
Department of Geography & Environmental Management
University of Waterloo, Canada

November 14, 2011

Highlights

- Ice cover duration in 2010-2011 was comparable to that of 2009-2010 for North America and much of eastern Siberia, but longer by 2-3 weeks for most parts of northern Europe.
- Ice cover duration was shorter by as much as 4-5 weeks in 2010-2011 compared to the 1997-2010 average for the eastern Canadian Arctic.

Lake ice is a sensitive indicator of climate variability and change. Lake ice phenology, which encompasses freeze-up (ice-on) and break-up (ice-off) dates, and ice cover duration, is largely influenced by air temperature changes and is, therefore, a robust indicator of regional climate conditions (e.g. Duguay et al., 2006; Kouraev et al., 2007; Latifovic and Pouliot, 2007).

The analysis of ground-based observational records has provided evidence of later freeze-up (ice-on) and earlier break-up (ice-off) dates over the Northern Hemisphere, particularly during the second half of the 20th century (e.g., Brown and Duguay, 2010). In the last 20 years, however, ground-based lake ice networks have been eroded to the point where they can no longer provide the quality of observations necessary for climate monitoring. Satellite remote sensing is the most logical means for establishing an Arctic-wide lake ice observational network.

In this first report on the state of Arctic lake ice cover, ice phenology dates (freeze-up/ice-on and break-up/ice-off dates) and ice cover duration derived from two satellite-based products are documented for the 2010-2011 ice season and compared to average conditions for the length of the available satellite historical records. The NOAA Interactive Multisensor Snow and Ice Mapping System (IMS) 4 km resolution grid daily product was used to analyze Arctic-wide ice conditions from the largest lakes since its availability in 2004 (Fig. HTC26). The IMS incorporates a wide variety of satellite imagery (AVHRR, GOES, SSMI, etc.) as well as derived mapped products (USAF Snow/Ice Analysis, AMSU, etc.) and surface observations (see Helfrich et al., 2007 for details). Ice-on and ice-off dates as well as ice duration could be derived at the pixel level from this product. Freeze-up (break-up) dates and ice-on (ice-off) dates have the same meaning in this report.

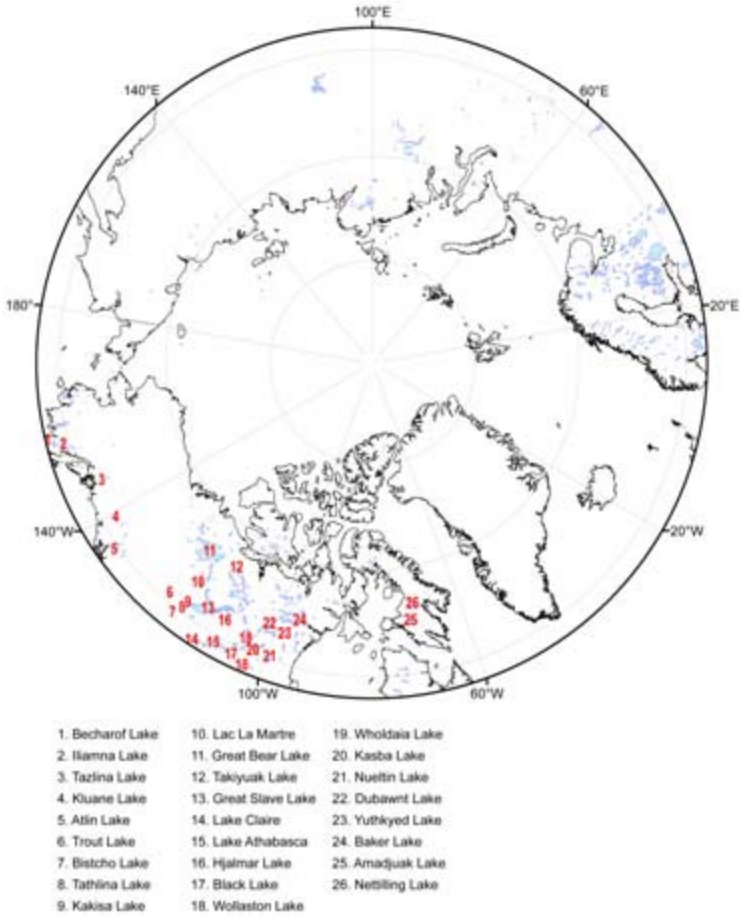

Fig. HTC26. Location of lakes from IMS 4-km (in blue) and CIS data sets (numbered in red, 1-26). IMS (Interactive Multisensor Snow and Ice Mapping System) and CIS (Canadian Ice Service) data go back as far as 2004 and 1997, respectively.

Weekly ice-cover observations from the Canadian Ice Service (CIS) for 26 of the largest lakes across northern Canada and Alaska were also analyzed, starting with the first reported ice season (1997-1998) (Fig. HTC26). Ice analysts at the CIS determine a single lake-wide ice fraction value in tenths (ranging from 0 [open water] to 10 [complete ice cover]) once per week week from the visual interpretation of NOAA AVHRR and Radarsat ScanSAR images. Complete freeze over (CFO) and water clear of ice (WCI) dates can be derived from this product with about a one-week accuracy. CFO is determined as the date when the ice fraction changes from 9 to 10 and remains at this value for the entire winter period, while WCI is determined as the date when the lake-ice fraction passes from 1 to 0. Lake-wide ice cover duration corresponds to the number of days between CFO and WCI within an ice season.

Freeze-up period

Analysis of IMS data shows that freeze-up in ice season 2010-2011 was close to the 2004-2010 mean, with a few lakes showing either later or earlier dates (±10-20 days) in much of North America and eastern Siberia (Fig. HTC27). There are no regions showing a clear temporal coherence, except for northern Quebec (10-20 days later), Baffin Island (10-20 days earlier) and northern/eastern Europe (20-40 days earlier). Similar differences are observed when ice

seasons 2010-2011 and 2009-2010 are compared. There are relatively no differences in freeze-up dates for most regions of the Arctic, with the exception of the Hudson Bay region and Baffin Island in North America (up to 4 weeks later) and northern/eastern Europe (up to 4 weeks earlier). The penetration of cold air from the Arctic into Europe (see the essay on *Temperature and Clouds*) is the most plausible explanation for the earlier freeze-up of the 2010-2011 ice season.

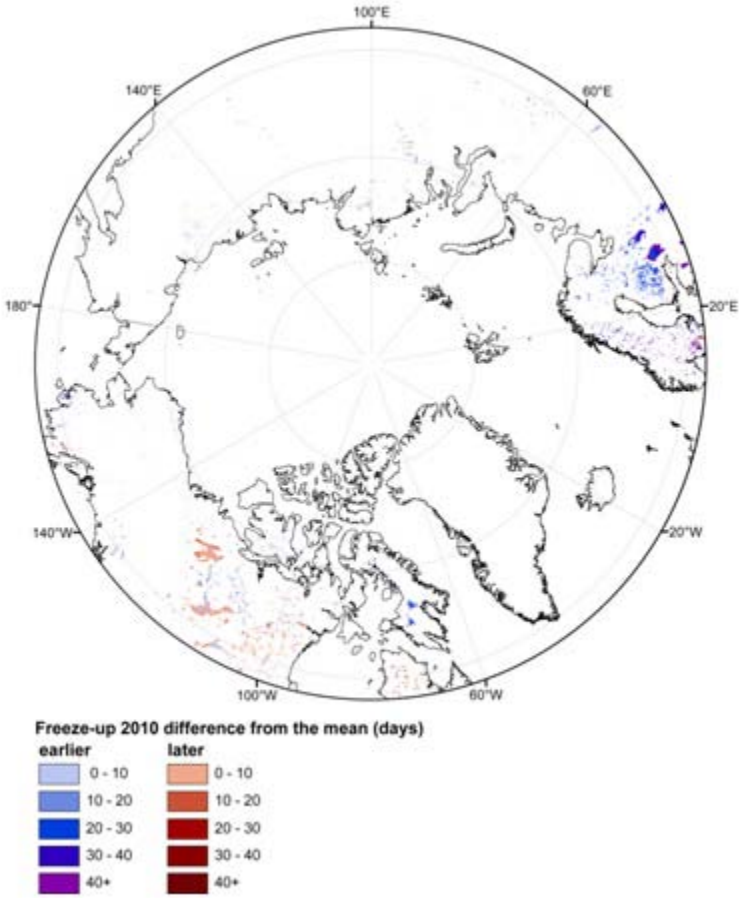

Fig. HTC27. Difference in number of days between freeze-up dates of 2010 and mean (2004-2009). Source IMS 4-km data.

The longer time series of weekly CIS observations over Canada/Alaska reveals that, in contrast to the 1997-2010/1998-2010 mean conditions, CFO of ice season 2010-2011 was later by 1 week on average (± 2 weeks; 18 lakes) but with 3 lakes in the central sector of the Canadian Arctic (Great Bear Lake, Great Slave Lake and Hjalmar Lake) displaying earlier CFO by as much as 3 weeks (Fig. HTC28). A combination of factors, including lake size, break-up dates of the previous spring, and colder open water season temperatures (reduced heat storage) may explain the earlier CFO in 2010-2011.

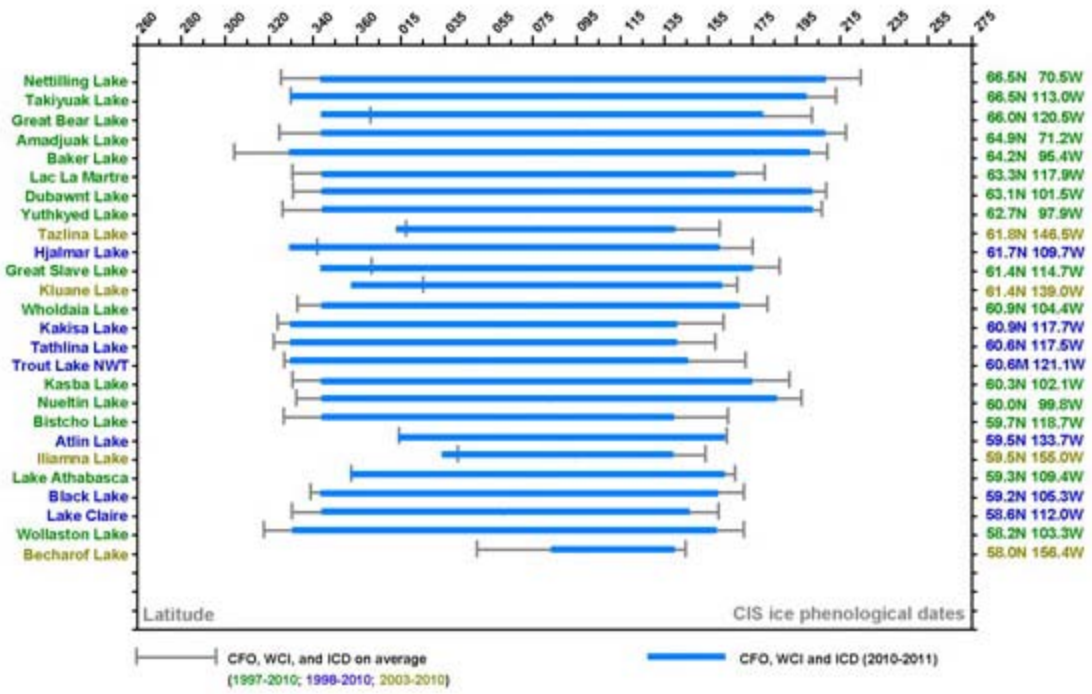

Fig. HTC28. Dates of complete freeze over (CFO) and water clear of ice (WCI) derived from CIS database for mean periods (1997-2010, 1998-2010, 2003-2010) compared to ice season 2010-2011 (light blue). The length of the horizontal bars indicates ice cover duration (ICD).

Break-up period

Break-up dates of ice season 2010-2011 derived from IMS are on average close to those of the 2004-2010 mean period but with some regional differences (Fig. HTC29), being especially highly variable (low coherence) in central Canada (±10-20 days). A large number of lakes in northern Europe (northern portion) and eastern Siberia experienced earlier break-up (10-20 days), while for much of eastern Europe and the southern portion of northern Europe break-up dates were 10-30 days later. The colder climate conditions of winter 2010-2011 in this sector, which led to earlier freeze-up, likely promoted thicker ice conditions (not verified) and, as a consequence, in combination with colder early spring temperatures, delayed ice break-up (see the essay on *Temperature and Clouds*). Break-up dates are generally comparable between ice seasons 2010-2011 and 2009-2010 for all regions, excluding eastern Europe and eastern Siberia, where they occurred 2-4 weeks later and earlier, respectively. The impact of earlier/later break-up dates on July lake surface temperatures (LSTs) derived from MODIS using the method described in Kheyrollah Pour et al. (in review) is illustrated in Fig. HTC30. For eastern Siberia, mean monthly LSTs in July 2011 were 3-4°C warmer than in 2010 (Fig. HTC30a), while they were as cold by the same amount in eastern Europe (Fig. HTC30b). The earlier break-up of 2011 in eastern Siberia is consistent with the record low June snow cover extent over Eurasia (see the essay on *Snow*).

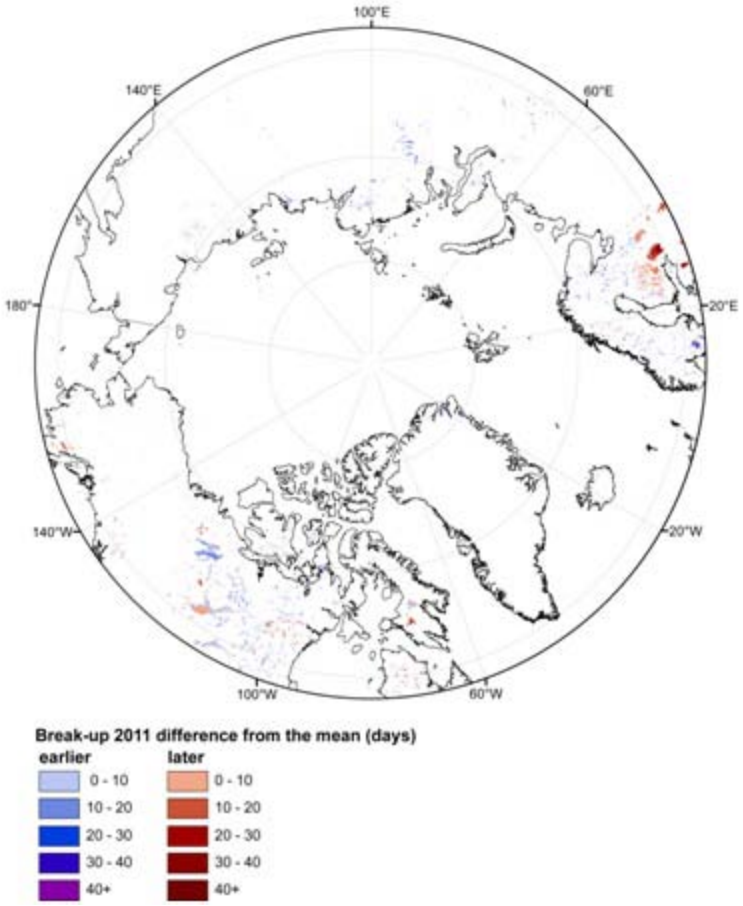

Fig. HTC29. Difference in number of days between break-up dates of 2011 and mean (2004-2010). Source: IMS 4-km data.

a.

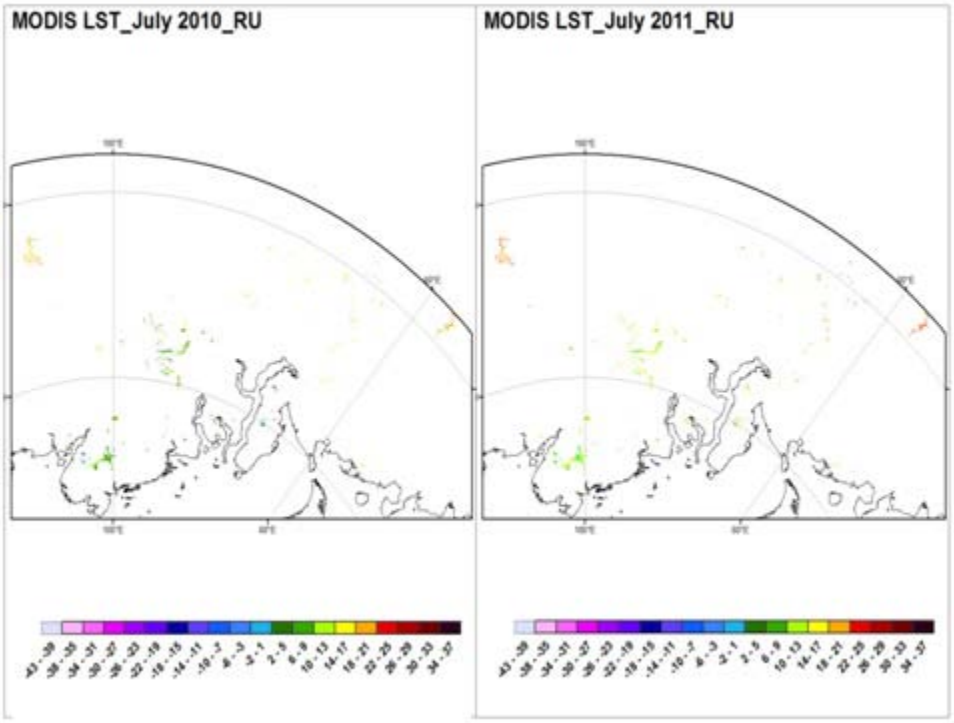

b.

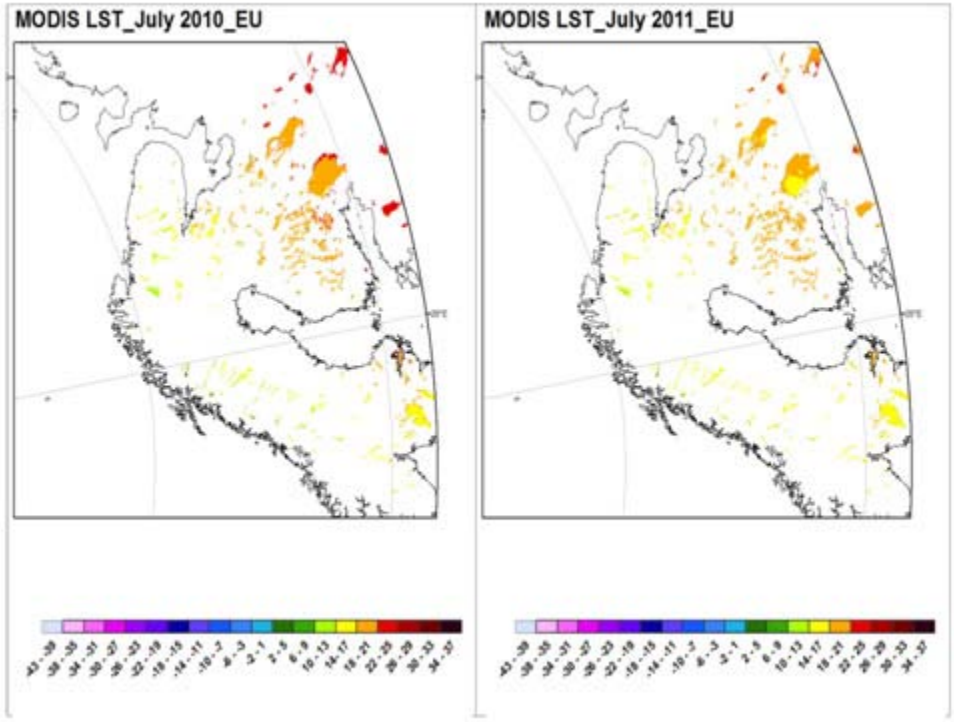

Fig. HTC30. Monthly lake surface temperature derived from combined MODIS Aqua/Terra data (Kheyrollah Pour et al., in review) for July 2010 and 2011 centered on (a) eastern Siberia and (b) northern/eastern Europe.

The CIS time series reveals earlier WCI in 2011 compared to 1997-2010/1998-2010 mean conditions for all 22 lakes analyzed over Canada/Alaska (Fig. HTC28). WCI occurred 12 days earlier (range 1-24 days) on average. For lakes with a shorter historical series (starting in 2003), WCI was still earlier in 2011 by the same number of days on average compared to the 2003-2010 mean. These results suggest a continued trend in earlier break-up dates across the Canadian Arctic first documented by Duguay et al. (2006) with ground-based observations (1966-1995) and extended from the analysis of NOAA AVHRR satellite observations (1985-2004) by Latifovic and Pouliot (2007).

Ice cover duration

When comparing the 2010-2011 ice season against the mean for 2004-2010 from IMS, the net effect of earlier/later freeze-up and earlier/later break-up results in ice cover duration (ICD) being generally shorter by about 2 weeks in central and eastern Arctic Canada, with the exception of lakes on Baffin Island and western Canada/Alaska (longer by 2-3 weeks). ICD was also shorter in eastern Siberia by 2-3 weeks and longer in northern/eastern Europe by as much as 4-6 weeks (Fig. HTC 31). The combination of earlier freeze-up and later break-up due to colder winter/early spring climate conditions explains the longer ICD over Europe. The last two ice seasons (2010-2011 and 2009-2010), however, experienced comparable ICD length for Arctic North America and most of eastern Siberia, and somewhat longer in 2010-2011 for most parts of Europe (2-3 weeks).

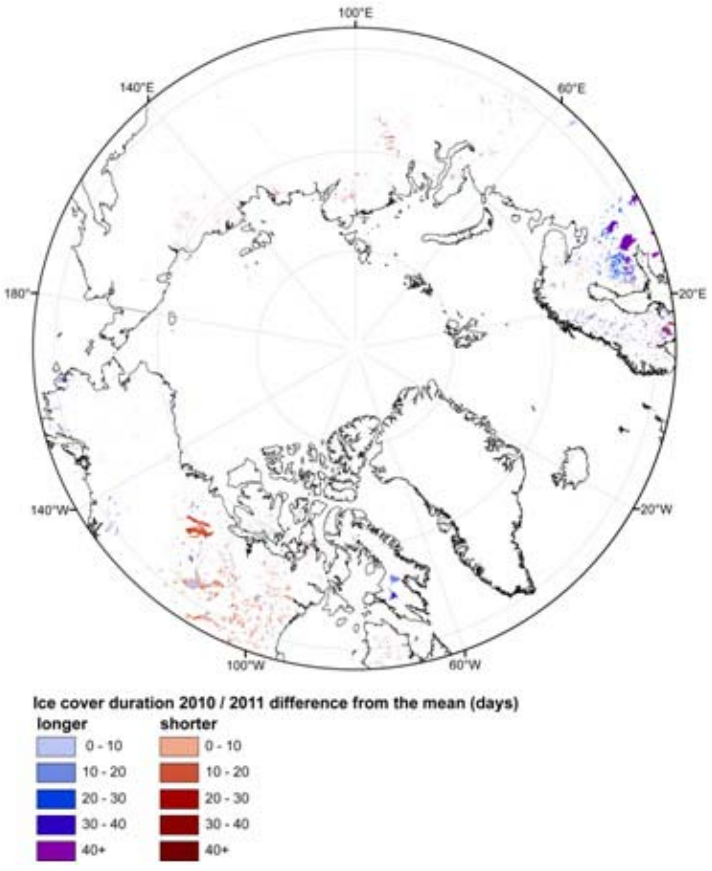

Fig. HTC31. Difference in number of days between ice cover duration of 2010-2011 and the mean for 2004-2010. Source IMS 4-km data.

Comparing the CIS mean (1997-2010/1998-2010) against 2010-2011 reveals a shorter ICD by 2-3 weeks for the majority of lakes with some of the strongest changes (about 30 fewer days) observed on Baffin Island and western Hudson Bay (Fig. HTC28). Only 2 lakes of the full 14-year series, Great Bear Lake and Great Slave Lake in the central region, show a slightly longer ICD (1 week).

References

Brown L. C. and C.R. Duguay. 2010. The response and role of ice cover in lake-climate interactions. Progress in Physical Geography, 34(5): 671-704.

Duguay, C.R., T.D. Prowse, B.R. Bonsal, R.D. Brown, M.P. Lacroix, and P. Ménard. 2006. Recent trends in Canadian lake ice cover. Hydrological Processes. 20: 781-801.

Helfrich, S. R., D. McNamara, B.H. Ramsay, T. Baldwin, and T. Kasheta. 2007. Enhancements to, and forthcoming developments in the Interactive Multisensor Snow and Ice Mapping System (IMS). Hydrological Processes. 21: 1576-1586.

Kheyrollah Pour, H., C.R. Duguay, A. Martynov, and L.C. Brown. In review. Simulation of surface temperature and ice cover of large northern lakes with 1-D models: A comparison with MODIS satellite data and in situ measurements. Tellus Series A: Dynamic Meteorology and Oceanography.

Kouraev, A. V., S.V. Semovski, M.N. Shimaraev, N.M. Mognard, B. Légresy, and F. Remy. 2007. Observations of Lake Baikal ice from satellite altimetry and radiometry. Remote Sensing of Environment. 108: 240-253.

Latifovic, R. and D. Pouliot. 2007. Analysis of climate change impacts on lake ice phenology in Canada using the historical satellite data record. Remote Sensing of Environment. 106: 492-508, 2007.

River Discharge

A. I. Shiklomanov and R. B. Lammers

Water Systems Analysis Group
Institute for the Study of Earth, Oceans, and Space
University of New Hampshire, Durham, NH 03824

November 15, 2011

Highlights

- Total annual discharge, 1813 km^3/year, in 2010 from the six largest Eurasian rivers (Sev. Dvina, Pechora, Ob, Yenisey, Lena and Kolyma) flowing into the Arctic Ocean was very close to the 1936-2009 long-term mean of 1808 km^3/year.
- Mean annual discharge, 514 km^3/year, in 2010 from the four large North American Arctic rivers (Mackenzie, Yukon, Back and Peel) was ~3% lower than the long-term mean (529 km^3/year).

River flow is an integrated characteristic that reflects numerous environmental processes at play in the upstream drainage area. River discharge also plays a significant role in the fresh-water budget of the Arctic, accounting for about 2/3 of the freshwater flux to the Arctic Ocean. Ocean salinity and sea ice formation are, in turn, critically affected by this river input. Changes in the freshwater flux to the Arctic Ocean can exert significant control over global ocean circulation by influencing North Atlantic deep water formation (Rahmstorf, 2002).

River discharge to the Arctic Ocean from Eurasia during 1936-2010 increased at a rate of 2.9±0.5 km^3/year (Fig. HTC32). The most significant positive trend (12 km^3/year) for the six largest Eurasian rivers (Sev. Dvina, Pechora, Ob, Yenisey, Lena and Kolyma) occurred during the last 24 years (1987-2009) (Shiklomanov and Lammers, 2009). Total annual discharge from the six largest Eurasian rivers flowing to the Arctic Ocean in 2010 was 1813 km^3/year, which was very close to the 1936-2009 long-term mean of 1808 km^3/year. Based on Environment Canada and USGS data the mean annual discharge in 2010 from the four large North American Arctic rivers (Mackenzie, Yukon, Back and Peel) was 514 km^3/year or ~3% lower than the long-term mean (529 km^3/year) (Fig. HTC32).

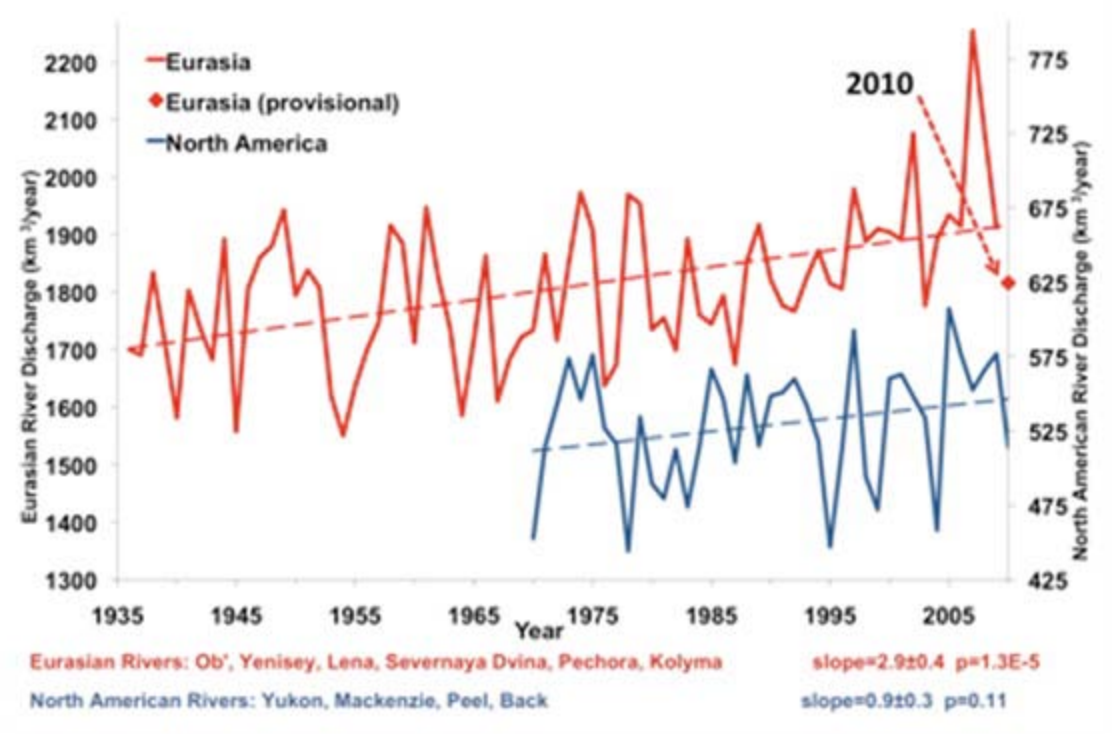

Fig. HTC32. Total annual discharge to the Arctic Ocean from the six largest rivers in the Eurasian pan-Arctic for the observational period 1936-2009 (updated from Shiklomanov and Lammers, 2009) (red line) and from the four largest North American Arctic rivers during 1970-2010 (blue line). The least squares linear trends are shown as dashed lines. Red diamond shows provisional estimate of Eurasian discharge for 2010.

The Yenisey is the only large river in the Arctic drainage with significantly higher (6%) discharge in 2010 than the long-term mean. However, taking into account the large reservoir capacity and the potential for perennial storage regulation, the high discharge in the Yenisey could be partly due to reservoir regulation (Shiklomanov and Lammers, 2009). Discharge in 2010 in the Yukon, Pechora, Severnaya Dvina and Kolyma rivers was 5-15% lower than the long-term mean and the discharge of the Lena, Ob and Mackenzie basins were close (± 2%) to the long-term mean values (Fig. HTC33).

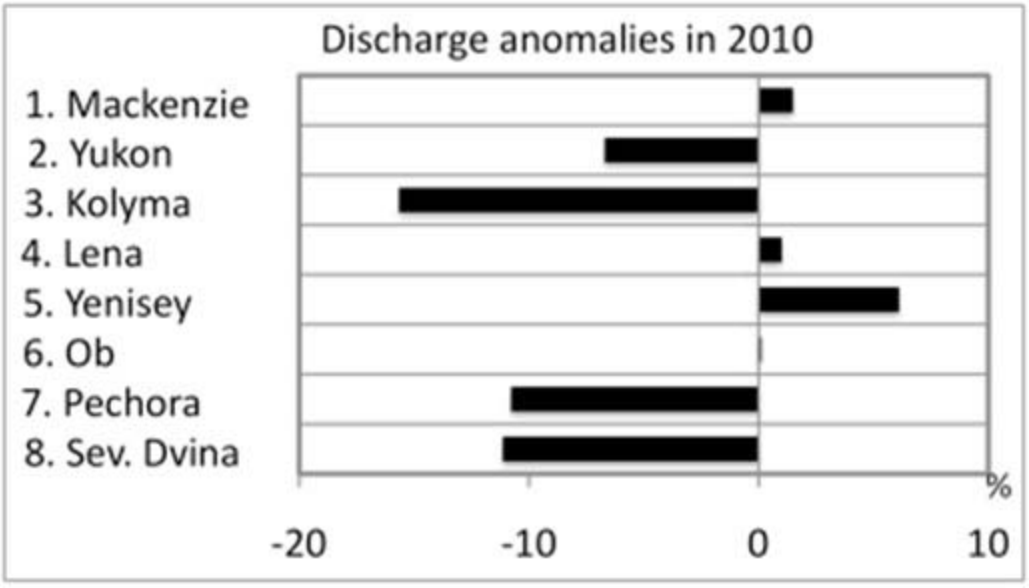

Fig. HTC33. Annual discharge anomalies (%) for 2010 relative to the long-term mean for the largest Arctic rivers. Provisional observational data were used for Eurasian rivers.

Officially distributed river discharge data are usually processed and published with some delay, from 1 year for the USA and Canada to several years in Russia. This is related to (1) more complicated conditions for discharge computation in cold regions with a lengthy period of ice cover (Shiklomanov et. al. 2006), and (2) restrictive access to historical hydrological information in Russia. Driven by the need for more timely information to detect and diagnose changing hydrological conditions, techniques have been developed to estimate river discharge for large Arctic rivers in near real-time using operational stage observations, air temperature and river ice data. These provisional discharge estimates have been used to estimate river flux to the Arctic Ocean until 2010 and showed very small uncertainty against officially released historical data. Currently, the collection of these data is not supported and we applied a less accurate approach based on re-analysis data coupled with hydrological modeling to estimate river discharge. It is worth noting that the absence of real-time hydrological monitoring has caused significant deterioration in the reliability of Arctic river discharge estimates.

Simulated total river runoff for January to July 2011 accumulated across the eight largest Arctic river basins (Mackenzie, Yukon, Kolyma, Lena, Yenisey, Ob, Pechora, Sev. Dvina) is derived from the UNH Water Balance and Water Transport Model (WBMPlus) (Wisser et al, 2010). This model is forced with meteorological information from the Modern-Era Retrospective analysis for Research and Applications (MERRA) for the period from January 1979 to July 2011 to estimate river runoff and discharge across the pan-Arctic drainage basin. The results suggest that total river runoff for January to July 2011, averaged across 8 major Arctic river basins, was 24 mm (or ~17%) lower than the long-term mean observed during 1979-2010 (Fig. HTC34 upper panel). Most runoff during January-July is formed from snowmelt. This is reflected in the comparison of snow water capacity for April 2011, when snow storage is typically close to maximum, with the long-term mean for 1979-2010 from MERRA. The comparison shows 17 mm (water equivalent) less snow in 2011 across all 8 basins (Fig. HTC34 lower panel), consistent with our discharge estimates. Driest conditions in 2011 were seen in the northern Ob, middle Yenisey and southern Lena basins. All rivers except Kolyma show negative discharge anomalies in 2011 from -1% for the Mackenzie to -22% for the Lena (Fig. HTC35).

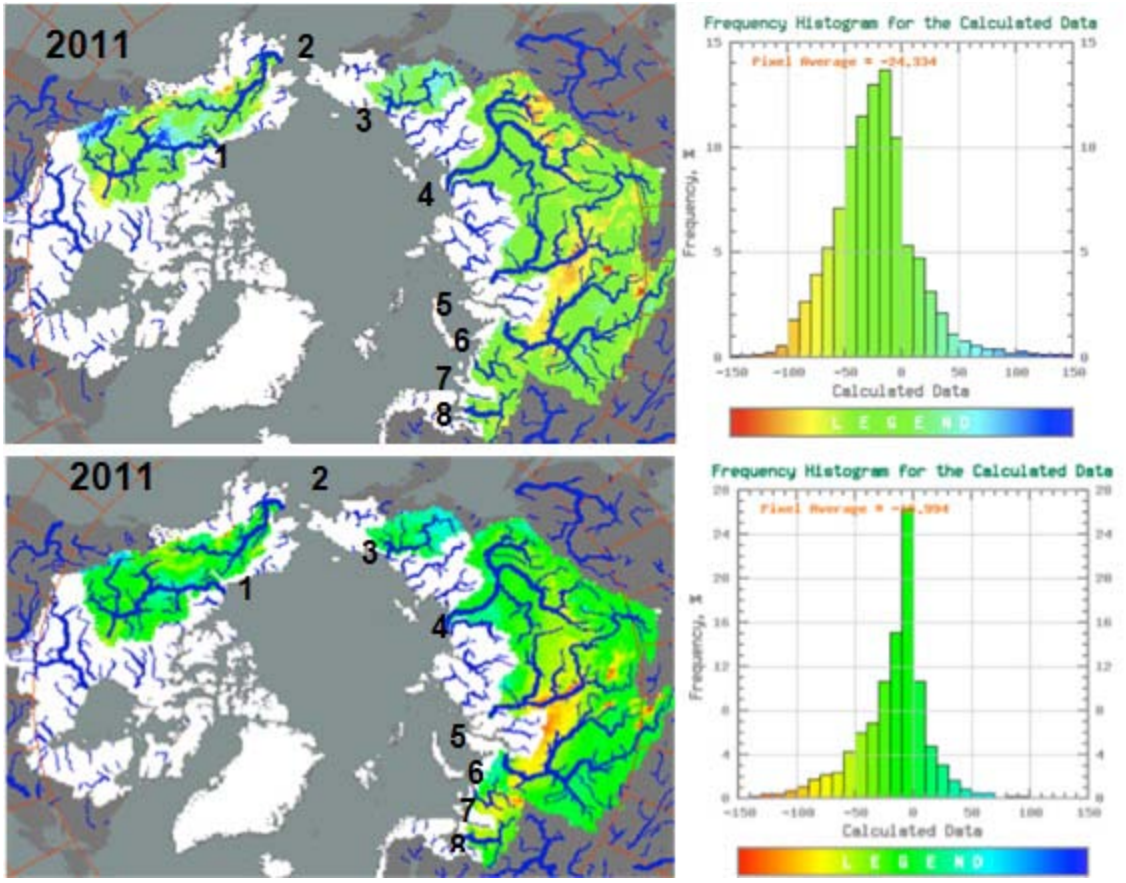

Fig. HTC34. Deviation of total runoff (in mm) for January-July, 2011 (upper panel) from the long-term mean for 1979-2010 evaluated with hydrological model simulations using MERRA data and deviation of mean monthly snow water equivalent (in mm) for April, 2011 (lower panel) from long-term mean over 1976-2010 based on MERRA data. Numbers show rivers: 1-Mackenzie; 2-Yukon; 3-Kolyma; 4-Lena; 5-Yenisey; 6-Ob; 7-Pechora; 8-Sev. Dvina.

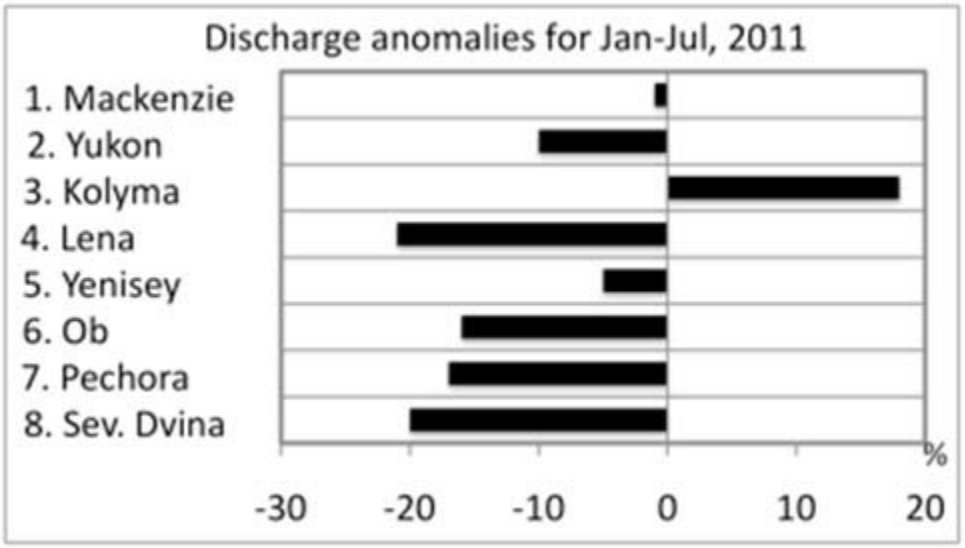

Fig. HTC35. Anomalies of mean river discharge (%) during January-July, 2011 relative to the long-term mean for 1979-2010.

We understand that uncertainty of these discharge estimates varies significantly from one watershed to another. Analysis of correlation between simulated and observed discharge for 1979-2010 showed correlations 0.8 and higher for Mackenzie, Lena and Kolyma, 0.6-0.7 for Pechora, Sev. Dvina and Yukon, 0.5 for Ob and 0.3 for Yenisey. Thus our discharge estimates for Yenisey and Ob are much less confident than for other rivers. However, based on information from ROSHYDROMET our preliminary conclusion is that the 2011 spring floods in Siberia and northern European Russia were normal or less than normal. Maximum spring peak flow, which describes the timing of flow, was observed 7-20 days earlier than the long-term mean in Siberia. For the downstream gauge, Yenisey - Igarka, it was the second earliest spring flood during the 1936-2011 observational period (Fig. HTC36). These results are consistent with analysis of trends showing earlier spring flood timing for multiple gauges across Eurasian pan-Arctic (Shiklomanov et al. 2007) and with the record-setting early spring snowmelt across Eurasia (see Fig. HTC3b in the essay on *Snow*).

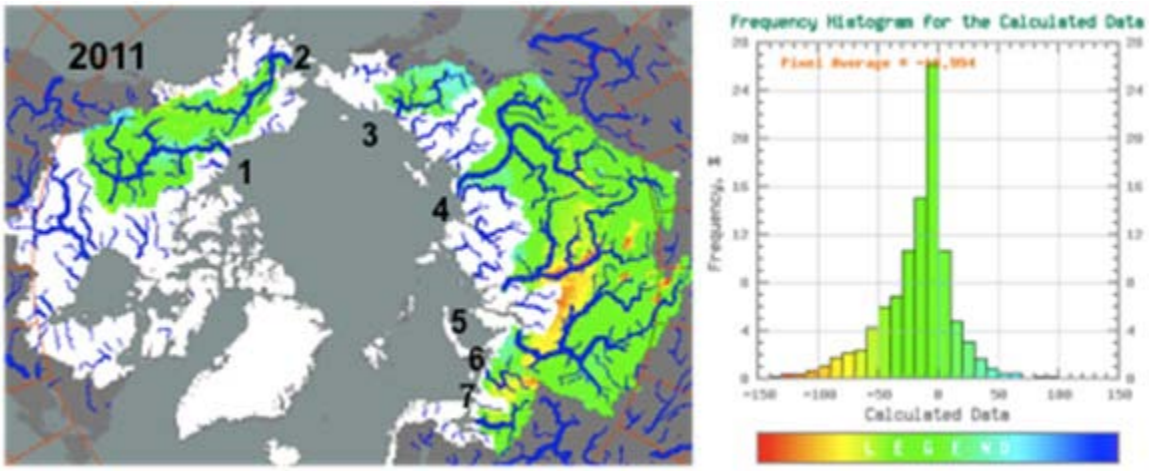

Fig. HTC36. Deviation of mean monthly snow water equivalent (in mm) for April, 2011 from the long-term mean for 1976-2010 based on MERRA data. Numbers show rivers: 1-Mackenzie; 2-Yukon; 3-Kolyma; 4-Lena; 5-Yenisey; 6-Ob; 7-Pechora; 8-Sev. Dvina.

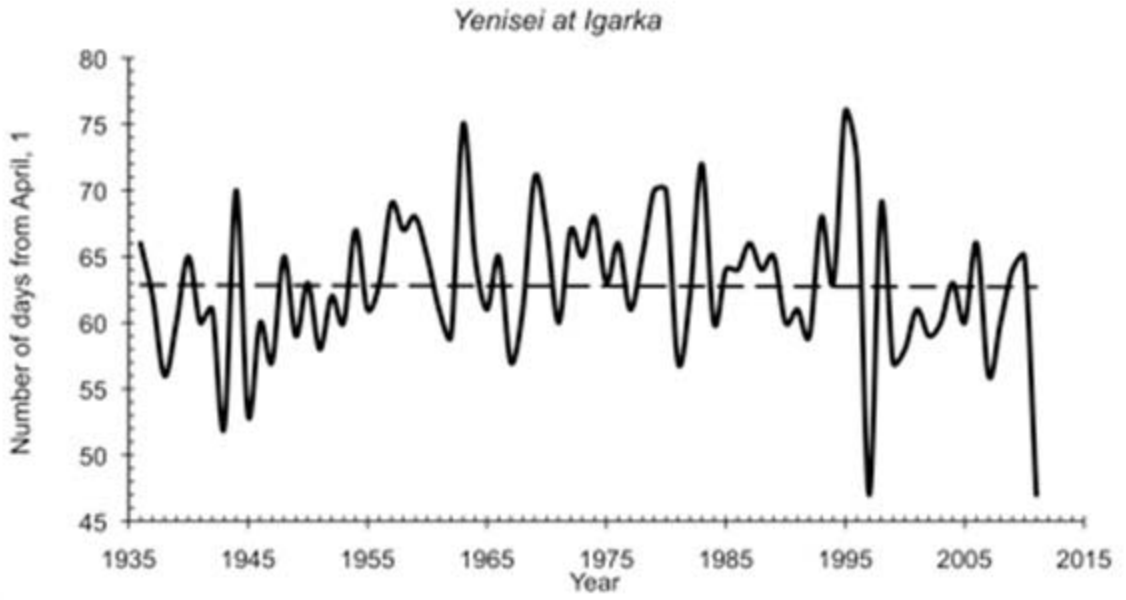

Fig. HTC37. Long-term variability of date of spring peak discharge for Yenisey - Igarka plotted as number of days from April 1. In 2011 the flood peak was the second earliest on record.

References

Bosilovich Michael G., Junye Chen, Franklin R. Robertson, Robert F. Adler. (2008), Evaluation of Global Precipitation in Reanalyses. Journal of Applied Meteorology and Climatology 47:9, 2279-2299.

Rahmstorf, S. (2002), Ocean circulation and climate during the past 120,000 years. Nature 419, 207-214.

Rawlins, M.A., Lammers, R.B., Frolking, S., Vörösmarty, C.J. (2006), Simulated Runoff and Evapotranspiration across Alaska: Model Sensitivity to Climate and Land Cover Drivers, Earth Interactions, 10, doi: 10.1175/EI182.1.

Rienecker, M.M.. M.J. Suarez, R. Todling, J. Bacmeister, L. Takacs, H.-C. Liu, W. Gu, M. Sienkiewicz, R.D. Koster, R. Gelaro, and I. Stajner, (2008), The GEOS-5 Data Assimilation System - Documentation of Versions 5.0.1 and 5.1.0. NASA GSFC Technical Report Series on Global Modeling and Data Assimilation. NASA/TM-2007-104606, 27, 95pp.

Shiklomanov A. I. and Lammers R. B., 2009: Record Russian river discharge in 2007 and the limits of analysis. Environ. Res. Lett. 4 045015 (9pp). doi: 10.1088/1748-9326/4/4/045015.

Shiklomanov, A. I., R. B. Lammers, M. A. Rawlins, L. C. Smith, and T. M. Pavelsky, (2007), Temporal and spatial variations in maximum river discharge from a new Russian data set, J. Geophys. Res, 112, G04S53, doi:10.1029/2006JG000352.

Wisser, D., B. M. Fekete, C. J. Vörösmarty, and A. H. Schumann (2010): Reconstructing 20th century global hydrography: a contribution to the Global Terrestrial Network- Hydrology (GTN-H), Hydrology and Earth System Science, 14, 1-24.

River Biogeochemistry

R. M. Holmes[1], J. W. McClelland[2], B. J. Peterson[3], P. A. Raymond[4], S. E. Tank[3], A. V. Zhulidov[5]

[1]Woods Hole Research Center, Falmouth, MA
[2]University of Texas at Austin, Marine Science Institute, Port Aransas, TX
[3]Marine Biological Laboratory, Woods Hole, MA
[4]Yale University, New Haven, CT
[5]South Russia Center for Preparation and Implementation of International Projects, Rostov-on-Don, Russia

November 15, 2011

Highlights

- In 2010, dissolved organic carbon (DOC) flux from five of the Arctic's six largest rivers (Yenisey, Lena, Kolyma, Yukon, Mackenzie, but not the Ob') was less than the 2003-2009 average.
- Combined DOC flux from the six largest rivers peaked in 2007 but has been lower each year since then, closely tracking the trend in their combined river discharge.

In addition to transporting freshwater to the Arctic Ocean (see the essay on *River Discharge*), arctic rivers transport and process a large range of natural and anthropogenic compounds. For the 2011 Arctic Report Card, we focus on dissolved organic carbon (DOC) export from the watersheds of the six largest arctic rivers, which combined cover 11.3 x 10^6 km^2 or 67% of the pan-Arctic watershed (Fig. HTC38). DOC is the dominant form of organic carbon transported by arctic rivers, its flux is expected to change as the Arctic continues to warm, and it can be an important energy source to the microbial food web and tracer in the Arctic Ocean. In future years we will consider fluxes of additional compounds as well as biogeochemical processing within river systems.

Fig. HTC38. Map of the 16.8 x 10^6 km^2 pan-Arctic watershed and the watersheds of the six largest arctic rivers. Together, these six watersheds cover 11.3 x 10^6 km^2 or 67% of the pan-Arctic watershed. The red dots show the water sampling locations of the Arctic Great Rivers Observatory (www.arcticgreatrivers.org) and the red line shows the boundary of the pan-Arctic watershed.

Several recent papers have investigated DOC flux in arctic rivers (Cooper et al. 2005, Raymond et al. 2007, Cooper et al. 2008, Holmes et al. 2011). However, none of these papers have addressed inter-annual trends. Therefore, using DOC concentration data from the Arctic Great Rivers Observatory (www.arcticgreatrivers.org) and daily discharge from Arctic-RIMS (http://rims.unh.edu) and other sources as outlined in Holmes et al. (2011), we calculated annual DOC fluxes for the six largest arctic rivers from 2003 to 2010. We used the USGS LOADEST program (Runkel et al. 2004) to calculate DOC fluxes based on discharge-concentration relationships for each river. Inter-annual variability in DOC flux is assumed to be a function of differing annual quantity and seasonal distribution of discharge, not differing discharge-concentration relationships over the 8-year period we consider. This assumption is supported by the absence of clear trends in discharge-concentration relationships among years within any single river (Fig. HTC39).

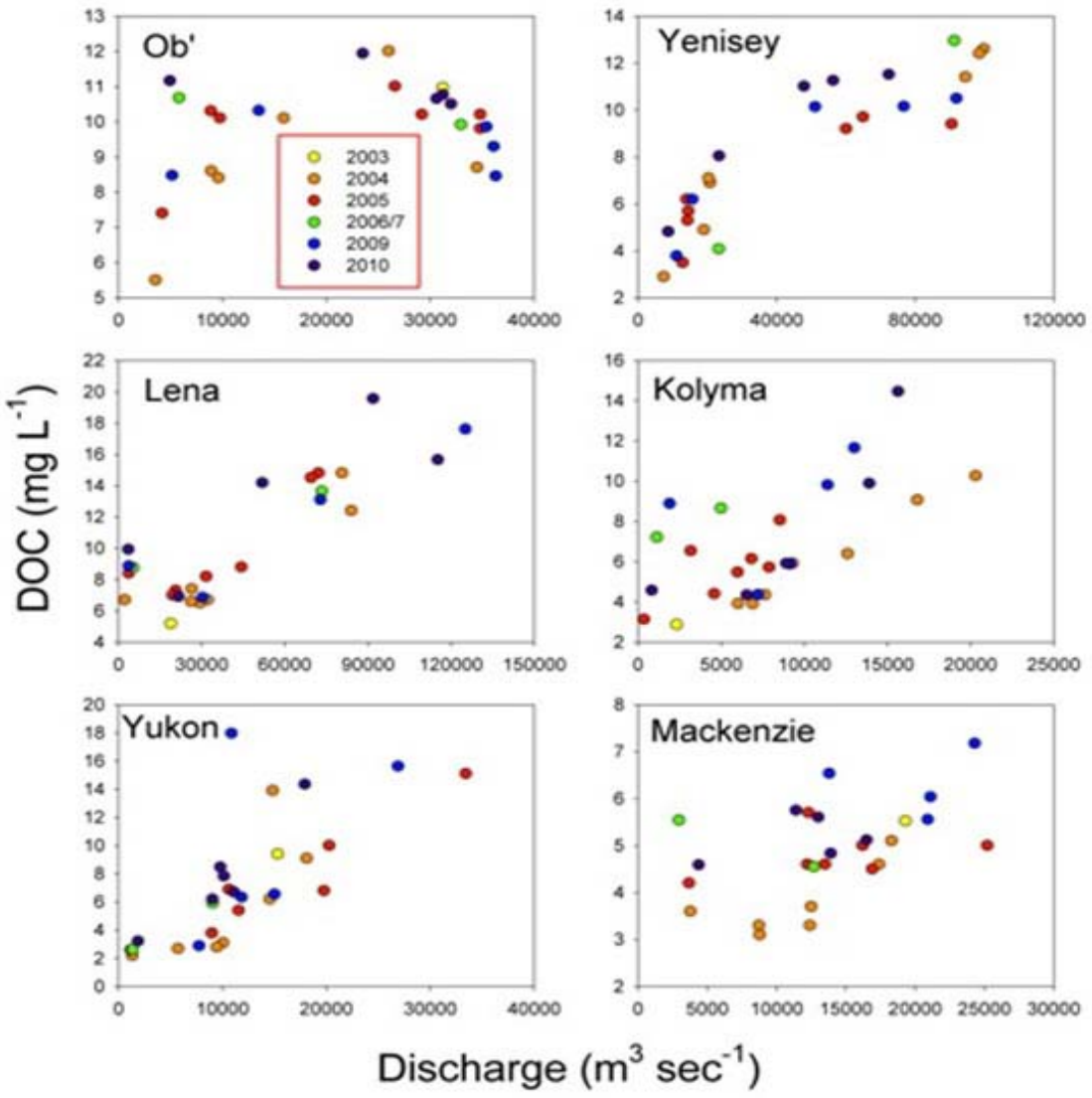

Fig. HTC39. Discharge-DOC concentration relationships for the six largest arctic rivers. Each point represents a single day when a DOC sample was collected. Though the relationships differ substantially among rivers, there are no clear trends across years within individual rivers.

In 2010, calculated DOC flux from the six largest arctic rivers ranged from 0.6 Tg in the Kolyma River to 5.3 Tg in the Lena River (Fig. HTC40). DOC flux in 2010 was less than the 2003-2009 average for the Yenisey, Lena, Kolyma, Yukon, and Mackenzie rivers, but not the Ob'.

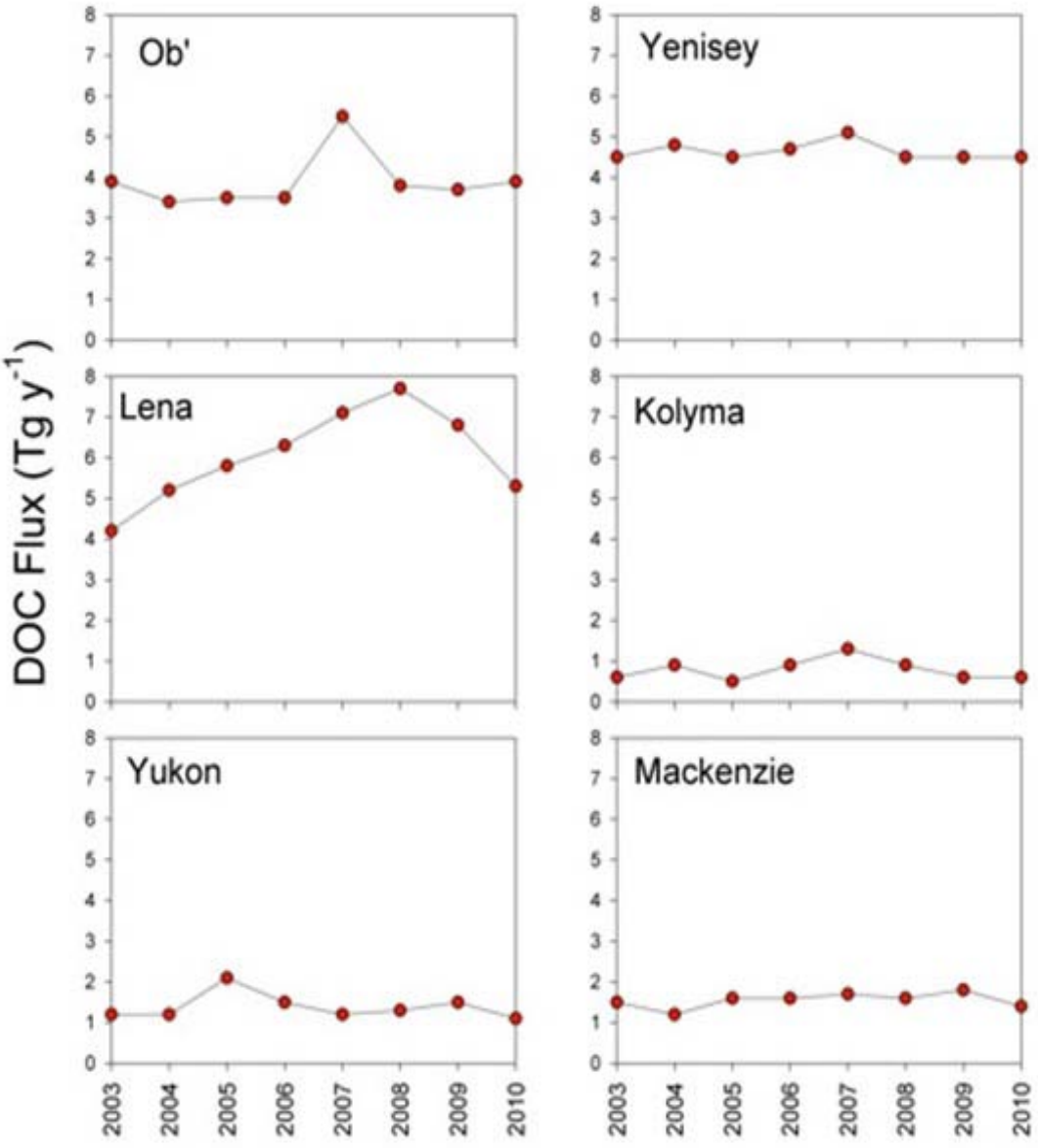

Fig. HTC40. Annual fluxes of DOC for the 2003-2010 period for the Ob', Yenisey, Lena, Kolyma, Yukon and Mackenzie rivers.

Combined DOC flux from the six largest arctic rivers declined for the fourth straight year in 2010, closely following the pattern of their combined discharge (Fig. HTC41). Though there are clear indications of increasing arctic river discharge during the past several decades (Peterson et al. 2002; McClelland et al. 2006; Déry et al. 2009; and see the essay on *River Discharge*), over sub-decadal periods long-term trends are obscured by high inter-annual variability and multiyear oscillations. Indeed, the combined discharge of the six largest arctic rivers increased each year between 2003 and 2007 but has decreased each year since 2007 (Fig. HTC41). Because DOC export is strongly influenced by variations in river discharge, detection of long-term trends in DOC flux requires observations over multiple years. Lack of DOC data for this set of rivers prior to ~10 years ago hinders detection of long-term trends in DOC flux, such as might be associated with the multi-decadal increase in discharge or changing discharge-concentration

relationships linked to permafrost thaw, changing vegetation, altered fire regimes, or direct human impacts on hydrology such as dams. However, ongoing data collection efforts will facilitate detection and attribution of future changes.

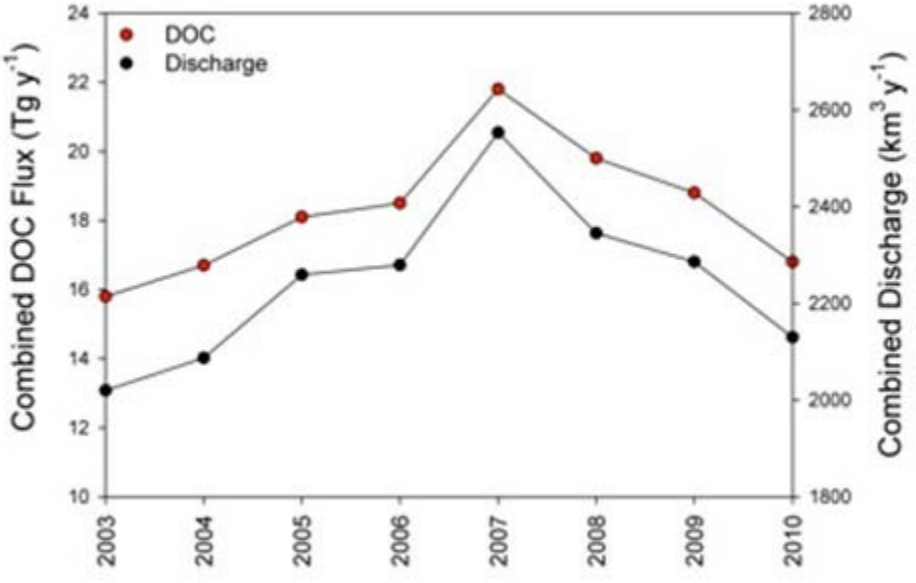

Fig. HTC41. Combined annual DOC flux (red dots) and discharge (black dots) for the six largest arctic rivers.

References

Cooper, L., R. Benner, J. McClelland, B. Peterson, R. Holmes, R. Raymond, D. Hansell, J. Grebmeier, and L. Codispoti. 2005. Linkages among runoff, dissolved organic carbon, and the stable oxygen isotope composition of seawater and other water mass indicators in the Arctic Ocean. Journal of Geophysical Research 110:G02013, doi:1029/2005JG000031.

Cooper, L. W., J. W. McClelland, R. M. Holmes, P. A. Raymond, J. J. Gibson, C. K. Guay, B.J. Peterson. 2008. Flow-weighted values of runoff tracers (δ18O, DOC, Ba, alkalinity) from the six largest arctic rivers. Geophysical Research Letters, L18606, doi:10.1029/2008GL035007.

Déry, S. J., M. A. Hernandez-Henriquez, J. E. Burford, and E. F. Wood. 2009. Observational evidence of an intensifying hydrological cycle in northern Canada. Geophysical Research Letters 36:L13402, doi:13410.11029/12009GL038852.

Holmes, R. M., J. W. McClelland, B. J. Peterson, S. E. Tank, E. Bulygina, T. I. Eglinton, V. V. Gordeev, T. Y. Gurtovaya, P. A. Raymond, D. J. Repeta, R. Staples, R. G. Striegl, A. V. Zhulidov, and S. A. Zimov. 2011. Seasonal and annual fluxes of nutrients and organic matter from large rivers to the Arctic Ocean and surrounding seas. Estuaries and Coasts, DOI 10.10007/s12237-011-9386-6.

McClelland, J. W., S. J. Dery, B. J. Peterson, R. M. Holmes, and E. F. Wood. 2006. A pan-arctic evaluation of changes in river discharge during the latter half of the 20th century. Geophysical Research Letters 33:L06715, doi:06710.01029/02006GL025753.

Peterson, B. J., R. M. Holmes, J. W. McClelland, C. J. Vorosmarty, R. B. Lammers, A. I. Shiklomanov, I. A. Shiklomanov, and S. Rahmstorf. 2002. Increasing river discharge to the Arctic Ocean. Science 298:2171-2173.

Raymond, P. A., J. W. McClelland, R. M. Holmes, A. V. Zhulidov, K. Mull, B. J. Peterson, R. G. Striegl, G. R. Aiken, and T. Y. Gurtovaya. 2007. Flux and age of dissolved organic carbon exported to the Arctic Ocean: A carbon isotopic study of the five largest arctic rivers. Global Biogeochemical Cycles 21:GB4011, doi:4010.1029/2007GB002934.

Runkel, R. L., C. G. Crawford, and T. A. Cohn. 2004. Load Estimator (LOADEST): A FORTRAN Program for Estimating Constituent Loads in Streams and Rivers. Page 69 p. U.S. Geological Survey Techniques and Methods Book 4.